THE PROPERTIES AND PERFORMANCE OF HIGH STRENGTH SILICA FUME CONCRETE

Peter Arnold Claisse

Submitted in accordance with the requirements for the degree PhD.

The University of Leeds Department of Civil Engineering

October 1988

ABSTRACT

Silica fume (SF) has been used as a partial replacement for cement in concrete and experiments have been carried out to measure the durability of the mixes. The SF mixes were made with 20% SF replacement of cement and water/cement (w/c) ratios of 0.3 and 0.46. Three different curing conditions were used to simulate different site conditions and tests were carried out at 3, 28 and 90 days after casting. The following properties were measured for the two SF mixes and the two control (OPC) mixes for each of the ages and curing conditions: corrosion rate of embedded steel by linear polarisation, electrical resistivity, carbonation depth, water vapour permeability, chloride permeability, oxygen permeability and porosity from helium and mercury intrusion. Samples were also investigated by thermogravimetric analysis.

The resulting data matrix was analysed by using the method of analysis of variance to quantify the effect of the SF on the properties tested and their sensitivity to age and curing. It was also analysed by multiple regression to identify major effects of one property on another.

It was concluded that SF will reduce the corrosion rate and that the major contributing factor is the substantial increase in resistivity that the SF causes. This increase in resistivity was found to be highly sensitive to cold curing in the short term but this effect was not permanent. The cause of the increase in resistivity is believed to be the depletion of calcium hydroxide which is caused by the pozzolanic activity of the SF. The analysis also indicated that the SF reduces the porosity in the .01-.15μm size range and that this has a major influence on the durability.

LIST OF CONTENTS

(list of contents cont.)

(list of contents cont.)

(list of contents cont.)

(list of contents cont.)

(list of contents cont.)

(list of contents cont.)

List of tables

List of figures

(list of figures cont.)

(list of figures cont.)

(list of figures cont.)

Abbreviations.

ANOVA   Analysis of variance
CC   Curing condition
C   *celsius*
DD   Dry density
Ln   Natural logarithm
Log   Logarithm to base 10
MS   Mild steel
OPC   Ordinary portland cement
RH   Relative humidity
SF   Silica fume
SG   Specific gravity
SRPC   Sulphate resisting portland cement
TG   Thermogravimetric
w/c   water/cement

Definitions

The following definitions will be used to define the Silica Fume (SF) and control (OPC) mixes:

w/c ratio : water/cementitious ratio i.e. water/(cement+SF)

X% SF addition : addition of SF without removing cement from the control mix such that by weight SF/cement=X%

X% SF replacement at a ratio of 1:Y : replacement of cement in the control mix with SF such that by weight (cement removed)/(SF added)=Y and in the SF mix SF/(cement+SF)=X%. If the ratio Y is not specified it is assumed to be unity as in this project where all mixes tested had 20% SF replacement.

The following definitions will be used to define the porosity and related parameters.

Bulk Volume :   The total volume of a sample defined by its outside dimensions.

Skeletal Volume :   The volume of solid matter in a sample excluding all pores.

Porosity :   The volume of the pores as a percentage of the bulk volume.

Specific Gravity (SG):   The mass divided by the skeletal volume.

Dry Density (DD):   The mass divided by the bulk volume.

Notation

Electrical measurements

A	Constant
B, B_1, B_2	Tafel constants
b	constant
C	Capacitance
C_{dl}	Double layer capacitance
C_f	Interface film capacitance
E_0	Rest potential
I	Current through sample
I_a	Anode current
I_{a0}	Anode exchange current
I_c	Cathode current
I_{c0}	Cathode exchange current
I_{cap}	Current through capacitance
I_{cdl}	Current through double layer capacitance
I_{corr}	Corrosion current
I_r	Current through concrete resistance
I_x	Current through polarisation resistance
k	Decay constant
R_c	Concrete resistance
R_f	Interface film resistance
R_P	Polarisation resistance
V	Voltage across sample
V_{a0}	Anode exchange voltage
V_c	Cathode voltage
V_{c0}	Cathode exchange voltage
V_{cdl}	Voltage across double layer capacitance
V_r	Voltage across concrete resistance
ω	Angular velocity $= 2\pi*$frequency

Vapour Transmission

A	Cross section area of sample
C	Steady state mass loss per 100 days (raw data used to calculate permeability)
K	Rate constant for decay (raw data used to calculate k)
k	Rate constant (corrected for vapour pressure drop)

(notation cont.)

M	Mass loss
M_0	Initial additional mass loss (raw data used to calculate intercept)
P_{DIFF}	Vapour pressure drop across sample
t	Time
x	Fraction of initial mass loss which has occured

Oxygen Permeability

A	Cross section area of sample
e	Viscosity
K	Coefficient of permeability
p	Pressure
P_1	Low pressure
P_2	High pressure
Q	Volume per second passing through sample
v	Velocity of gas from high to low pressure
x	Distance from surface of sample

Mercury intrusion

D	Pore diameter
γ	Surface tension
p	Pressure
ϕ	Contact angle

Porosity and related parameters

DD	Dry density of total sample
L_{opc}	Calcium hydroxide measured in OPC sample
L_{sf}	Calcium hydroxide measured in SF sample
L_{use}	Calcium hydroxide used in pozzolanic reaction
SG	Specific gravity of total sample
SG_a	Specific gravity of aggregate
SG_c	Specific gravity of cement
SG_{ca}	Specific gravity of coarse aggregate
SG_{fa}	Specific gravity of fine aggregate
SG_{hc}	Specific gravity of hydrated cement
SG_p	Specific gravity of paste

(notation cont.)

SG_{sp}	Specific gravity of superplasticiser
M	Mass of total sample
M_a	Mass of aggregate
M_{aw}	Mass of absorbed water
M_c	Mass of cement
$M_{c'}$	Mass of unhydrated cement
M_{ca}	Mass of coarse aggregate
M_{dry}	Mass of sample after drying
M_{fa}	Mass of fine aggregate
M_{hc}	Mass of hydrated cement
M_p	Mass of paste
M_{sp}	Mass of superplasticiser
M_w	Initial mass of water in mix
M_{wet}	Mass of sample when mixed
P	Porosity of total sample
V_{wet}	Calculated volume of sample when mixed
WL	Fractional weight loss of total sample
WL_a	Fractional weight loss of aggregate
WL_p	Fractional weight loss of paste

1. Introduction.

1.1 Silica Fume.

1.1.1 Objective and methods.

The aim of this research is to measure the effect of the partial replacement of cement with silica fume (SF) on the durability of concrete structures. The mixes which are investigated have very high strengths, would be expensive to produce, and are intended for special applications where the performance of concrete made with ordinary cement would not be adequate. The majority of the experiments concern the effect of the SF on the rate of corrosion of the reinforcing steel.

The production processes in which the different types of fume are produced are discussed in section 1.1.2. Sections 1.2-1.4 contain a brief review of the literature on the properties of SF concretes and their supply and use. Details of the mixes and curing conditions used in this project are given in chapter 2.

In chapter 3 the results of direct measurements of corrosion rates are presented. The physical properties of a concrete mix which determine the rate at which embedded steel will corrode are the electrical resistivity, the rate of carbonation and the permeability to chlorides, water and oxygen (Arup 1983). Chapters 3-7 contain results from measurements of these properties. The more fundamental measurements such as porosity are in chapters 8-11 and the mechanical properties are in chapter 12. The interpretation of the results from all of the experiments in terms of their effect on the durability of the mixes is analysed statistically in chapter 13.

1.1.2 Production of Silica Fume.

Silica fume is a byproduct of the production of silicon or silicon alloys in submerged arc electric furnaces. The reactions which take place in the furnaces are described by Rath (1983) and produce liquid metal which is drawn off at the bottom of the furnace and the fume which rises to the top. In western countries it has recently become environmentally unacceptable to release the fume into the atmosphere and thus it is collected (Rau and Aitcin 1983). The fume has a very high electrical resistivity so that separation in an electrostatic precipitator is nearly impossible and it is thus trapped in fabric filters. The type of collection system depends on whether a heat recovery system is in use. If it is used the fume is ducted directly into a heat exchanger at about 800° C and at this temperature any carbon is burnt. If a heat recovery system is not used the fume is mixed with air to cool it to about 200°C immediately above the furnace. The residual carbon in fumes from this type of furnace gives them a dark grey or black colour while fumes from plants with heat recovery systems are normally light grey or white.

SF is principally composed of SiO_2. The proportions of other compounds will depend on the type of alloy being produced in the furnace. Alloys containing more than 96% silicon are known as silicon metals and give rise to a fume containing at least 94% SiO_2. The specification for the fume used in this project was a minimum of 85% SiO_2. This may be be derived from the production of ferrosilicons with silicon contents greater than 75%. Hester (1986b) quotes a specification from the U.S. army corps of engineers which requires 85% SiO_2 but also requires that the SF shall be obtained solely from silicon metal production. Other types of fume arise from the production of ferrochromium silicon, silicomanganese and other alloys. Many of these are unsuitable for use in concrete. For example the fume from calcium-silicon production may contain calcium carbide which produces acetylene (an explosive gas) when mixed with water (Aitcin 1983a). A variety of different alloys may be produced in the same furnace so an effective system to prevent cross-contamination of the fumes is essential.

1.2 Literature Review - Properties which were measured in this project.

1.2.1 Introduction.

This part of the literature review is intended to indicate the extent of the published research in areas which are investigated in this project. It may be seen that a large part of the literature has been published since this work was started in 1984. An extensive review of 161 papers on SF including large numbers in Norwegian, Swedish and Danish has been published by Sellevold and Nilsen (1986). Their review concentrates on normal strength mixes in contrast to the special mixes which are the main subject of this project. Any major disagreement with the conclusions of Sellevold and Nilsen has been noted. Where possible results for mixes containing superplasticisers have been considered in preference to those without.

1.2.2 Electrical corrosion measurements.

The use of electrical measurements to assess corrosion rates is discussed in chapter 3. There are four measurements which can be made: linear polarisation resistance, a.c. resistivity, rest potential and anodic d.c. resistivity (potentiostatic polarisation).

Page and Havdahl (1985) have carried out linear polarisation measurements on pastes with w/c ratios of 0.5 and SF replacement levels of 10-30% some of which also had added chlorides. When the chloride was added SF increased the corrosion rates but in the absence of chloride it did not significantly change the rates. It has been shown (Vennesland 1981 and Gjorv 1983) that the addition of SF causes a massive increase in the a.c. resistivity. This means that all electrical measurements must be interpreted with great care because this effect is so great that it may mask other changes. Preece, Arup and Frolund (1983) report that 20% SF replacement caused no significant change in the potentiostatic current when samples were first tested despite the SF samples

having a much lower w/c ratio than the control. However the SF caused a marked decrease in current when the voltage was used to cause the ingress of chloride. Gautefall and Vennesland (1983) tested cracked samples and found that 10% SF addition caused no significant change in the anodic current for w/c=.37 - 1.0.

This data indicates that in the absence of chlorides or carbonation SF has little effect on corrosion rates.

1.2.3 Carbonation.

Vennesland (1981) measured carbonation depths on specimens which had been exposed to ordinary air or 5% CO_2 for just over one year. He measured the depth with phenolphthalein and found the SF caused a very slight decrease of carbonation for 10 and 20% SF additions (w/c=0.45-2.0). Johansen (1981) made observations on similar samples after three years in air and found that the SF caused an increase in depth. Skjolsfold (1986) tested a number of structures with w/c=.55-.8 and found a small increase caused by the SF replacement of about 10% at a ratio of about 1:3. He also found a much greater variation in depth on the SF structures.

All that may be concluded from this data is that at w/c > .5 and replacement ratio > 1 carbonation rates will be greater in SF concretes.

1.2.4 Chloride Permeability.

Wolsiefer (1984) reports that chloride penetration into a concrete with 20% SF addition and w/c=.22 was only 10% as high as the control sample with w/c=.38 in a ponding test. Marusin (1986) immersed samples with w/c=.4 in a sodium chloride solution and found reductions of about 50% in chloride penetration in the SF samples at replacement levels of 10%, 20% and 30%. Vennesland (1981) exposed samples to the sea for 13 months and obtained results which showed some improvement for 10% and 20% SF additions at w/c=2 but no clear trend for w/c=.9 or .45.

Li and Roy (1986), Christensen et.al.(1984) and Gee (1986) all report results from the high voltage test described in chapter 5. They found that the charge passing was often 100 times less for the SF samples. The validity of their assumption that this is a true measure of chloride diffusion is open to doubt and is discussed in chapter 5. The high resistivity noted in 1.2.2 could easily distort these readings.

Several workers have measured diffusion rates through thin discs of paste immersed in $Ca(OH)_2$ solution. 1M NaCl is normally added to the solution on one side of the disc and the chloride level on the other side is monitored. Byfors (1987) found reductions of around 50% at 10% SF and a reduction of 80% at 20% SF for w/c=.4 - .6. Gautefall (1986) observed a similar effect with greater reductions at w/c=.9. Preece (1983) concluded that a 20% SF mix with w/c=.15 was impermeable but had no effective control. Kumar and Roy (1986) used .05M CsCl as a source of chloride and tested a 10% SF mix with w/c=.4 and found a reduction factor of about 10.

The conclusion from all of the data is that SF reduces chloride diffusion and is more

effective at higher concentrations and higher w/c ratio.

1.2.5 Vapour Permeability.

Preece (1983) measured the water vapour diffusion rate through SF paste but unfortunately the control mix had twice the w/c ratio of the SF mix so the results are difficult to evaluate. Had the w/c ratios been the same the results would probably have been comparable for the SF and the control.

1.2.6 Oxygen Permeability.

Vennesland (1981) measured oxygen diffusion by measuring the d.c. resistivity of samples with an applied potential of -950mV (SCE) as described in chapter 3. The SF was not found to cause any overall difference for 10% and 20% additions and w/c=.45-2.0. Nagataki and Ujike (1986) measured the air permeability and found that the SF reduced it at replacement levels of 10-30% and w/c=.4.

1.2.7 Pozzolanic activity.

In a review paper Hjorth (1982) observes that there is a considerable discrepancy in the literature on the rate of pozzolanic activity in SF mixes. This may be caused by the strong temperature dependence as observed in this project (chapter 11). Cheng-yi and Feldman present results for mortar with w/c=.45 and .6 (1985a) and paste with w/c=.25 and .45 (1985b) cured at 21°C. They found that in mixes with 10% SF there was an initial increase in calcium hydroxide percentage but this was less than that for the OPC and after about 7 days it fell. At 180 days it was well below the OPC level but not zero. With 30% SF there was no calcium hydroxide in any mixes after 14 days. They also (Feldman and Cheng-yi 1985a) observe that none remained in any of the SF samples after exposure to sodium chloride solution. Grutzeck et.al.(1982) found no calcium hydroxide after only 7 days for 22% SF addition (w/c=.36) at 45°C. This would be expected from the results in chapter 11of this project but contradicts the conclusion in the review by Sellevold and Nilsen (1986) which states that 24% SF addition is required to react with all of the calcium hydroxide. Meland (1983) stored samples at "room temperature" and found calcium hydroxide remaining with 30% SF at 180 days. Chatterji et.al. (1982) kept some samples at room temperature and some outside (in Norway) and understandably found varying rates of pozzolanic activity.

1.2.8 Pore size distribution.

The pore size distribution of pastes and mortars has been measured by mercury intrusion (see chapter 9 for details of this method). It has been claimed (Feldman 1986b, Cheng-Yi and Feldman 1985c) that the method gives totally misleading readings unless a second intrusion is carried out on each sample. The increased intruded volumes at high pressures on the first intrusion in SF samples is interpreted as breakdown of the divided structure of large pores rather than the usual interpretation

as evidence of fine pores. If interpreted in this way their results indicate that this effect is less important for paste than mortar.

Kumar et.al.(1987) use the value of the median pore radius in the range .002-7.5 μm as a convenient measure of the effect of SF. Increasing temperature and time increase the effect and at 28 days at 60°C the median radius for 10% SF paste is less than 40% of the radius for OPC (w/c=.4). Another method of analysis of intrusion data is to calculate the total intruded volume over ranges of pore radius. This method is sensitive to the choice of range and Tenoutasse and Marion (1987) report a decreased volume in their smallest range which was .05-.006 μm (60 day paste samples at 20°C w/c=.5). The use of the range .01-.003 μm would almost certainly change this observation (see chapter 9 for the basis of selecting this range). Analysis of the range of 1-2 μm shows an increase in pore volume for SF in many results and Buil and Delage (1987) claim to have located these pores using an electron microscope.

Some workers (Feldman and Cheng-Yi 1985b, Hooton 1986) present results with no analysis. As far as can be seen their graphs indicate a reduction in mean pore radius.

The conclusion is that mercury generally penetrates SF mixes at higher pressures than OPC mixes. There is a divergence of opinion on the cause for this.

1.2.9 Mechanical properties.

In a review of internationally available literature on SF Jahren (1983) found that 70% of the papers contained little else but data on mechanical strength. The situation has probably improved (a recent emphasis on freeze/thaw durability has been evident) but there are still a large number of papers on mechanical strength. Many of these papers (e.g. Loland and Hustad 1981b) use the concept of the efficiency factor which is intended to be a measure of the efficiency of the SF in the mix relative to the cement. This may be calculated for any given property but unfortunately different authors have failed to agree a standard method for calculating it. For compressive strengths of grades of concrete in normal use it is often reported at about 4 which neatly coincides with the cost difference of the materials. Jahren (1986) describes the use of efficiency indexes as "meaningless at best, and misleading at worst".

Dingsoyr et.al.(1985) report a variation of up to 30% in the strengths of high strength mortars caused by the use of different aggregates and failure of aggregate was found to be an important factor in this project (see chapter 12).

Low temperatures have been reported to have a greater effect on SF concretes than control mixes at 28 days (Maage 1986 and Jahren 1986) but the long term effect was not investigated. The long term effect of permitting the mix to dry out during curing has been investigated (Johansen 1981, Sellevold and Radjy 1983). SF concretes were found to be more sensitive to this than the OPC mixes.

1.3 Properties which were not measured in this project.

1.3.1.Introduction.

This part of the literature review is intended to assess the conclusions which have been made on some properties which were not measured in this project.

1.3.2 Freeze-thaw durability.

Opshal (1981) tested concretes without air entrainment and concluded that the SF improved the durability. Both Cheng-Yi and Feldman (1985c) and Sorensen (1983) conclude that it is possible to make a durable mix with 10% SF without air entrainment. They all found, however, that using more than 10% SF caused less predictable and generally worse results.

Traetteberg (1980) reported that air entrainment did not affect the SF mixes but this has not been found by other workers. Virtanen (1983) observed that it is necessary to use more air entraining agent in 10% SF mixes to get the same air content but that it greatly improves the durability. Carette and Malhotra (1983a) had great difficulty in entraining air into 20% and 30% SF mixes and found that they were not as durable as the OPC mixes. Malhotra (1986) directly tested the effect of the air entrainment and found that it had a very major effect but again experienced difficulty in entraining air into mixes with 30% SF. Yamato et.al. (1986) found that at w/c=0.25 the difficulty with entraining air was not important as the mix was durable without air entrainment. With increasing w/c ratios the high SF mixes performed steadily worse than the OPC mixes until at w/c=0.45 the 20% SF mix had a durability factor less than half that of the OPC mix. Pigeon et.al. (1986) found 10% SF mixes with w/c=0.5 to be more susceptible to internal cracking but less so to surface scaling.

Aitcin and Vezina (1984) report initial results from a field trial. The major difference between laboratory results and the field trials is that the laboratory mixes generally have SF replacing an equal weight of cement but on site the ratio is about 1:3 in order to enjoy economic benefits from SF. This discrepancy is probably caused by the fact that the researchers are still trying to get SF put to a more appropriate use than cost cutting in standard mixes. The results of Aitcin and Vezina are not conclusive because the SF appeared to stop alkali-silica reaction which was observed in the OPC mix and confused the readings. Aitcin and Pigeon (1986) carried out more extensive field studies and found that the SF was generally performing adequately but they only checked for surface scaling and even then they found great variability.

The conclusion for freeze/thaw durability is that in conditions of severe exposure the use of SF in high concentrations or with high w/c ratios is not advisable.

1.3.3. Sulphate resistance.

Mather (1980) tested mortars with 30% SF replacement and w/c about 0.5 and found that the SF decreased the expansion due to sulphates by several orders of magnitude.

Popvic et.al. (1984) tested mortars with 10% SF addition and w/c=0.6 and measured the loss in flexural strength caused by the sulphate. The SF mix performed better than the control. An attempt by Hooton (1986) to test 20% SF samples failed because they broke up. He attributed this to early dessication. Helland (1986) reports on a 30 year site trial in acid ground water. The OPC control samples disintegrated but the 15% SF samples (w/c=0.62) performed as well as the SRPC samples (w/c=0.5). The conclusion from the above is that SF may be used to prevent sulphate attack.

1.3.4 Alkali silica reaction (ASR).

Asgeirsson (1986) measured mortar bars to ASTM C277 and found that 5% SF addition reduced the expansion to 30% of the control and 10% SF reduced it to 10% of the control using Icelandic aggregate. He also reports that the presence of sea water greatly increased the expansion indicating that the ability to keep sea water out would be highly beneficial. Tests in Yugoslavia by Popvic et.al.(1984) with 17% SF replacement indicate zero expansion. Replacement ratios of 1:1.4 were used in South Africa by Oberholster and Westra (1981) and Davies and Oberholster (1987) and reductions in expansion were found at all replacement levels from 5% to 30% with the 30% being the most effective. Perry and Gillott (1985) in Canada observed delayed expansion with SF. At replacement levels below 20%, however expansion did take place and at an elevated temperature (50° C) the expansion of the 5% SF sample became greater than the control within a year. Kawamura et.al.(1986) found that in Japan the 5% and 10% SF samples expanded more than the control almost immediately. The 20% SF sample did not expand. Field trials carried out in Canada by Aitcin and Regourd (1985) showed no visible damage at 15% SF and above. Silicate gel was identified in samples from the 15% SF mix but not in the 20% and 40% mixes.

The conclusion from the above is that experience in different countries seems to differ but 20% SF or more will prevent ASR.

1.3.5 High pressure water permeability.

Hooton (1986) tested pastes with w/c=0.25 and found the permeability at 0.7 MPa approximately halved at 10% SF and reduced further at 20% SF. Li and Roy (1986) tested a sample with 10% SF and w/c=0.5 at 10 MPa and found that the SF reduced the permeability by three orders of magnitude.

Kohno and Komatsu (1986) tested concrete samples with w/c=.53 at 2 MPa and obtained 50% reductions with 10% SF addition. Hustad and Loland (1981) tested a number of mixes at 4 MPa. At w/c=0.44 they found a small increase in permeability for 10% addition and a small decrease at 20%. At w/c=0.8 they found a decrease of an order of magnitude for 10% and 20% additions and at w/c=2 the decrease was three orders of magnitude.

Maage (1984) tested cores from structures with approximately 10% SF replacement at

a ratio of 1:3. The test pressure was 4MPa. A decrease in permeability was observed but there was very little data for w/c below 0.45.

The conclusion for water permeability is that for dense mixes with w/c about .35 the SF will have little effect. At high w/c it causes a marked improvement.

1.3.6 Creep.

Buil and Acker (1985) tested a single mix with 25% replacement and w/c=0.4. The control mix had no superplasticiser and had w/c=0.43. The compressive strengths were 76MPa for the SF and 53MPa for the OPC. Both samples were tested for creep with an applied load of 10MPa and the deformation of the SF sample was less. The difference was less for sealed samples. The free shrinkage of the SF samples was found to be less and formed a substantially lower proportion of the total creep. Tazawa and Yonekura (1986) tested mixes at 30% replacement and found that in all cases the specific creep of the SF mixes was greater except for a mix with high w/c (0.65) tested in water. They applied the load of 30% of the compressive strength by stressing a tendon through the centre of the sample. No restressing was carried out and loss of prestress was compensated for in the results. The free drying shrinkage of the SF mixes was less than the OPC particularly at high w/c ratios.

This is a difficult experiment to carry out because of the high stresses required to reach 30% of the compressive strengths and no conclusive data has been located.

1.4 The supply and use of silica fume.

1.4.1 Transportation and storage.

The economics of the production of silicon alloys depend heavily on cheap energy and the process is therefore not viable in the U.K. All of the fume used in this country is therefore imported and the cost of transport forms a major part of the selling price.

In its raw form SF is a very fine powder with a bulk density of 150-250 Kg/m^3 (approximately a quarter of the density of OPC). This is the form in which it was used in this project but transport costs are high and the dust may pose a health hazard (Jahr 1979 and 1983). Aitcin (1983b) describes some of the processes which may be used to decrease the volume. The following three types are known to be available in the U.K.:

1. If SF is mixed with an equal weight of water to make a slurry its volume is reduced to 45% of the volume of the powder. Elkem chemicals supply SF from Norway in this form but apart from the obvious cost of transporting the water it also requires continuous agitation to ensure a uniform concentration. "Emsac" is the same slurry with pre-mixed superplasticiser.

2. If compressed air is introduced into the bottom of an SF silo the particles tend to

agglomerate and the density may be increased to about 500 Kg/m^3. Corrocem (Anon 1986a) is a product of this type and also contains Norwegian SF and a superplasticiser.

3. SF from the only ferrosilicon plant in Iceland is formed into micropellets of 0.5-1.0 mm. diameter (Bradley-Williams 1986). These have a bulk density of about 600 Kg/m^3.

ACI committee 226 (1987) compared the three types and show that they all have different advantages for different applications.

1.4.2 Use of SF in concrete.

Aitcin (1983c) gives a historical summary of the introduction of SF concrete. All cement produced in Iceland now contains 7.5% SF in order to combat ASR (Asgeirsson and Gudmundsson 1979). The use of SF in readymixed "normal strength" concrete has been reported in Canada (Skrastins and Zoldners 1983) and in the U.K. (Anon 1986b). The use of this type of mix in building frames has been reported (Anon 1983). All of the reports of the use of "high strength" mixes of the type investigated in this project come from the North America. Holland et.al.(1986) report the use of high strength concrete with w/c=.3 and 15% SF addition to control abrasion damage in the stilling basin of a dam and Radjy et.al.(1986) report further projects such as a flood control channel. Dumbleton (1987 a and b) describes other applications including a tall office block in Canada. Burge (1983a) describes the use of SF to improve the strength of lightweight concrete.

1.4.3 Uniformity of supply.

Regourd (1983) compared the pozzolanic activity of various fumes and found considerable differences. Only one if them, however, had more than 85% SiO$_2$. Reinhold et.al. (1986) tested 19 different fumes with SiO$_2$ contents down to 65% at cement replacement levels of up to 60% but failed to carry out a consistent test regime on all of the samples. Nebsar and Carette (1986) sampled the fume from two furnaces at intervals for 180 days and found standard deviations of 4% and 2% in the SiO$_2$ content from a silicon metal and a ferrosilicon furnace respectively. Pistilli et.al.(1984) collected samples from a plant over 30 days and their results appear to be similar.

2 Mix Design and Curing.

2.1 Mix Design.

2.1.1 Materials.

Silica fume was supplied by Elkem Chemicals from their works in Norway. The colour of the material was black and the specification indicated a minimum 85% content of SiO_2.

Ordinary Portland Cement was used. Initial supplies were from the Blue Circle Tunstead works and later from the Cauldon works.

Quartzitic aggregate from a quarry in Nottinghamshire was used. (Zone 2-3 sand and 5-20mm. coarse aggregate).

Feb SP2 superplasticiser which is made from the salt of napthalene formaldehyde condensate was used.

2.1.2 Mix Design.

The proportions of cement and aggregate in the control mixes were calculated using the minimum porosity method developed by Cabrera (1988). 20% cement replacement was used for the SF mixes. The water/(cement+SF) ratios were derived using the "Cabrera slump" method which is described below. Sufficient superplasticiser was then added to ensure that both the SF and control mixes had slump values which would be acceptable for site placement (about 100mm). Because of the high water demand of the SF this has to be approximately double the maximum recommended dose for ordinary concrete.

The "Cabrera slump".

A modified V.B. remoulding apparatus (Neville 1981) is used for this test. The slump cone is fixed down to the vibrating table by means of two bolts which pass through flanges welded to opposite sides of the cone. The detailed procedure is as follows:

1) Approximately 20 Kg. of the dry mix is placed in a small mixer and sufficient water is added to give it a w/c ratio approximately 0.1 below the anticipated desired value (no plasticiser is used).

2) The concrete is mixed for 2 minutes.

3) The slump cone is filled in 3 layers in the usual way.

4) When the slump cone is full the vibrating table is turned on for 20 seconds and the

distance from the top of the cone to the resulting concrete level at the centre of the cone is then recorded.

4) The sample is returned to the mixer and sufficient water is added to raise the w/c ratio by about 0.05.

5) The concrete is mixed for a further 1 minute and the process is then repeated.

The slump is plotted against the w/c ratio and when about 4 points have been obtained it should be observed to have risen to a maximum and started to fall. If further points are required it is necessary to make a fresh mix. The optimum mix is taken to be at the maximum slump value. For both high and low strength mixes the value chosen was between the optimum values obtained with and without SF The results for the 2 mixes are presented in figures 2.1 and 2.2.

The final mix designs are in table 2.1. The percentages of superplasticiser were calculated from the quantities of solids which form 40% of the total weight of the solution as supplied.

Mix	A	B	C	D
Cement (Kg/m^3)	344	430	252	315
Silica (Kg/m^3)	86	0	63	0
Water/(cem+silica)	.3	.3	.46	.46
Superplasticiser (% of c+s)	1.4	1.4	1.9	1.9
5-20 mm. aggregate /(c+s)	3	3	4	4
Fine aggregate /(c+s)	1.5	1.5	2.3	2.3

Table 2.1 Mix Designs.

Pastes and mortars were made with the same proportions without the aggregates.

2.1.3 Mixing methods.

For all mixes the superplasticiser was mixed with the water before being added to the other components which had already been mixed dry. Concrete samples were generally in batches of 200-300 Kg. Mortar batches less than 10Kg were mixed in a Hobart mixer and those greater than 10Kg in a small concrete mixer. The consistency of the samples when mixed in the Hobart mixer was very variable and for the very liquid ones it was not possible to use the fastest speed because it caused them to be ejected from the mixer. For the less liquid ones the fastest speed was used. Paste samples were mixed in the Hobart mixer but for some samples they were then subjected to high energy mixing in a liquidiser. The liquidiser was evacuated in order

to reduce the amount of entrained air. All of the mixes were mixed in this way for 2 minutes but for mix D some bleeding was still observed so it was necessary to mix it for a further 3 minutes.

2.2 Curing Conditions.

2.2.1 The 3 conditions.

All samples were cast in a laboratory at approximately 20°C and covered and kept there until being struck the next day. Where permitted by the test procedures three different subsequent regimes were used :

Curing Condition 1 (CC1) : Curing in fog room (20°C and 99% RH) until test age.

Curing Condition 2 (CC2) : Treated with Febcure aluminium pigmented curing agent and stored at 20° *C* and 70% RH until 7 days old and then in water at 6°C. After initial trials with a spray the best method of applying the curing agent was found to be a brush. All surfaces of the samples were fully saturated until the surplus ran off but the quantity applied was substantially below the recommended coverage rate (12cc. for a 100mm. cube). This was probably because the coverage rate is intended for application to concrete which has dried in the sun in a hot climate.

Curing Condition 3 (CC3) : Curing in water at 6°C.

These 3 curing conditions are intended to simulate the best, average and worst conditions likely to be found on a reasonably well run site.

2.2.2 Samples for testing.

Mechanical tests were carried out and exposure tests started with samples at 3, 28 and 90 days.

Tests were carried out on samples at each of the 3 test ages for each of the 3 curing conditions, i.e for a total of 9 different sample conditions.
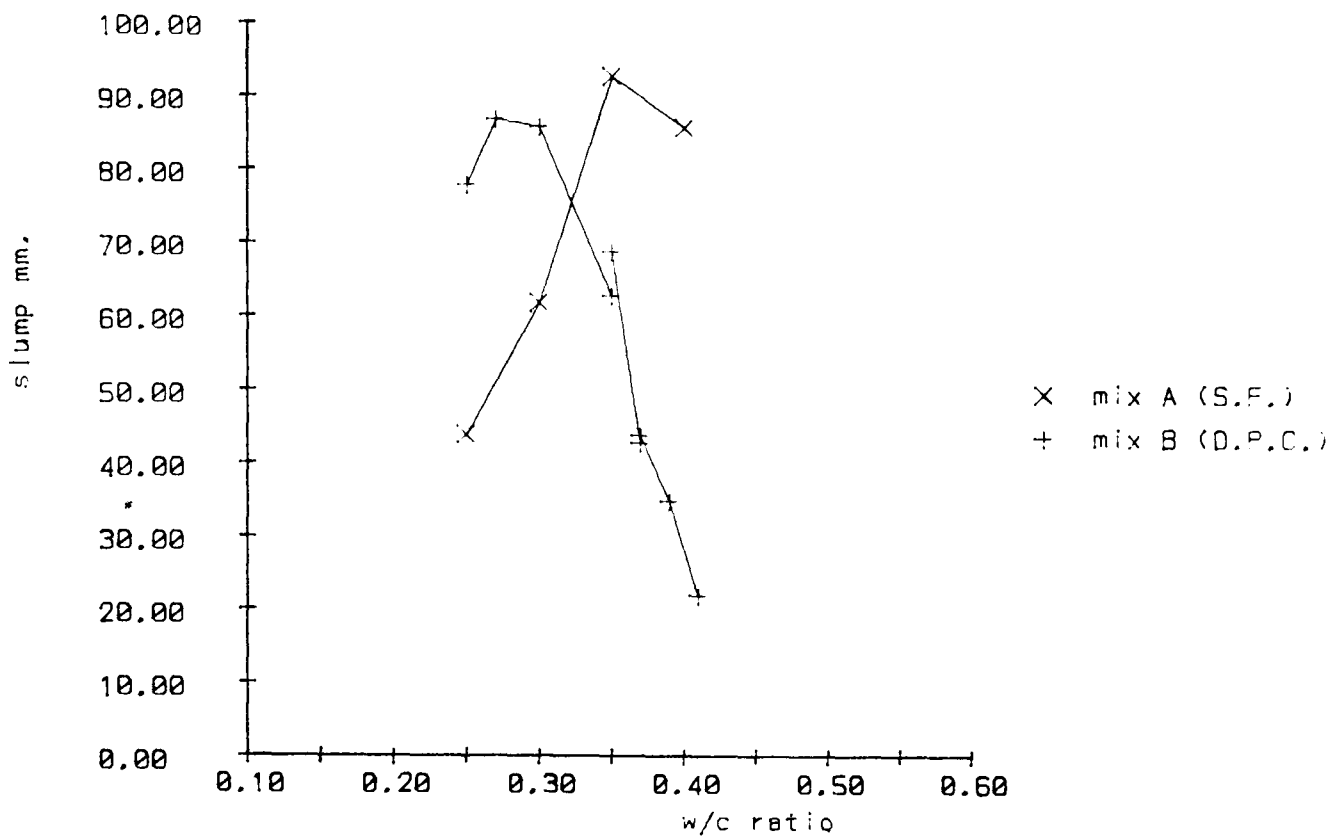
Fig. 2.1 CABRERA SLUMP mixes A and B

× mix A (S.F.)
+ mix B (O.P.C.)
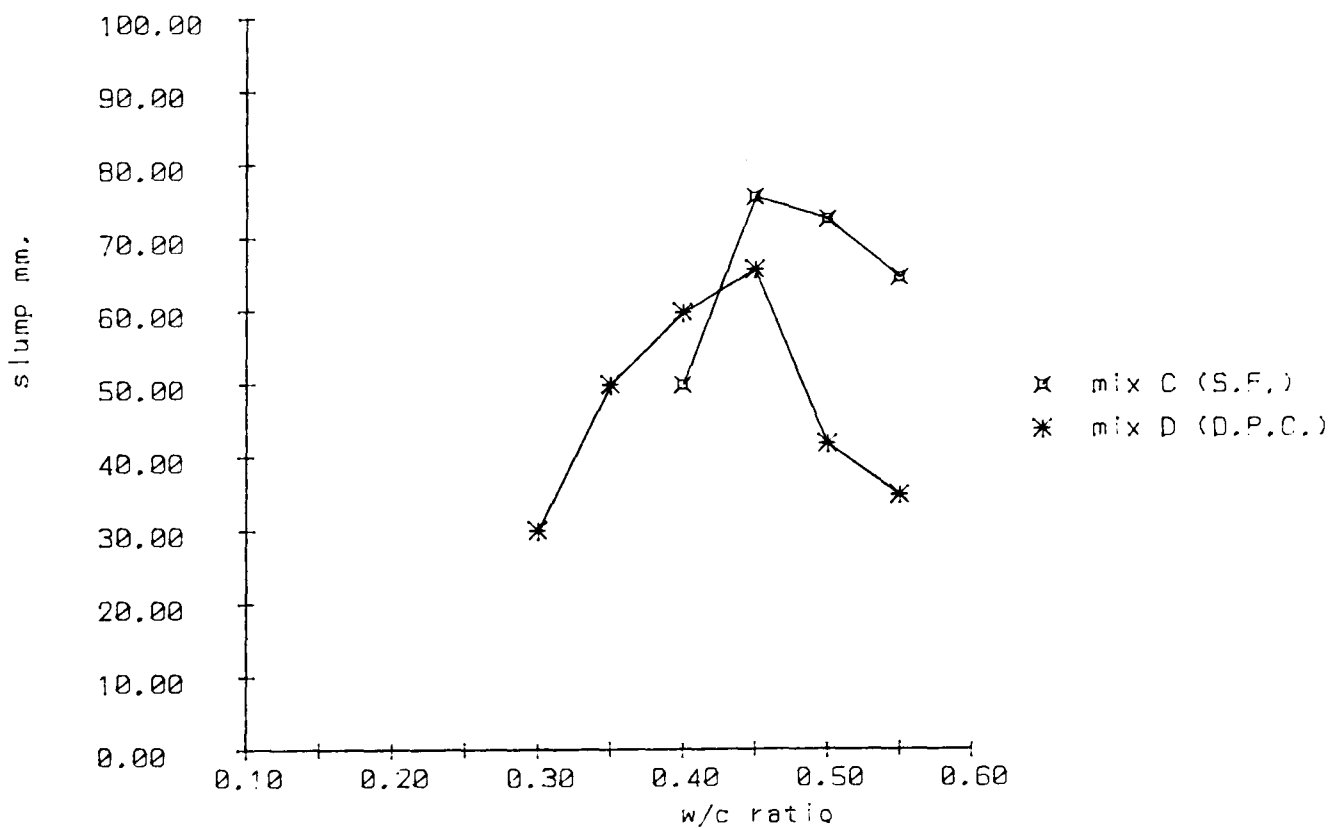
Fig. 2.2 CABRERA SLUMP Mixes C and D

⋈ mix C (S.F.)
∗ mix D (O.P.C.)

In Fig. 2.1 and 2.2 the optimum water cement ratio for a mix is taken to be at the maximum Cabrera Slump. The discontinuity in the line for mix B indicates that a fresh batch was made.

3 Electrical Measurements.

3.1 Introduction.

3.1.1 General.

In this chapter results from the measurement of the properties of electrical circuits passing through steel bars cast into concrete and mortar samples are presented. In order to make an electrical contact to the outer surface of the samples they were partially immersed in a salt solution. This had the important consequence that all of the samples remained saturated. The general arrangement is shown in fig.3.1.

In section 3.2 the linear equivalent circuit for samples at voltages close to their rest potential is discussed. The effect of voltages outside this range is outlined in section 3.3. The external circuits required for measurements and the experimental procedures used are described in sections 3.4 and 3.5 and the results are in section 3.6.

3.1.2 Types of measurement.

There are only two types of measurement which can be made. Either the circuit is left open and the voltage (rest potential) is measured or a voltage is applied and the impedance is measured.

3.1.3 Types of chloride.

In earlier work on chloride induced corrosion such as Ost and Monfore (1966) calcium chloride has been used and Hansson et.al.(1985) have shown it to be more aggressive than sodium chloride. The use of calcium chloride accelerators in reinforced concrete in the U.K. has, however, ceased but the use of sodium chloride for de-icing has clearly not ceased. For this reason sodium chloride has been used for all experiments in this project. Buenfeld and Newman(1984) have shown that other chemicals in sea water have a major effect on the permeability of concrete but the concentration of sodium chloride in the sea is always substantially greater than that of other salts.

3.2 The Equivalent Circuit.

3.2.1 The concept of the linear equivalent circuit.

The simplest way to interpret the results obtained from electrical measurements is by representing them in terms of an assembly of standard linear electrical components in an equivalent circuit. A linear component is one in which the voltage across it is linearly dependent on the current flowing through it (resistors) or the differential of the current (inductors) or the integral of the current (capacitors). It is a mathematical property of the sine function that an addition of two sine waves with different

amplitudes and phases will always give another single sine wave therefore the current flowing through a circuit of linear components under a sinusoidal applied voltage will be sinusoidal. This effect may be shown on phase diagrams (e.g. fig.3.2) where the amplitude of the impedance is represented as a distance from the origin and the phase difference between voltage and current is represented as an angle to the horizontal axis. Any non-linear components in the circuit will mean that the current is not sinusoidal and the impedance cannot be directly represented on a phase diagram. Suitable components for inclusion in the circuit are as follows:

1. Resistances. A typical example is the passage of an ion through a system of open pores in concrete. The velocity (i.e. the current) will be proportional to the applied force (i.e. the voltage).

2. Capacitances. These arise when charge carriers are free to move up to a barrier which they cannot pass. An example occurs at a steel/concrete interface where corrosion is not occuring. If a constant voltage is applied the current will decay to zero as the charge carriers build up a back emf equal to the applied voltage. The current is proportional to the differential of the voltage.

3. Voltage steps. These are theoretical concepts in that they have no internal resistance. However much current flows through them the voltage across them remains the same. The fact that a corroding sample will develop a voltage without an external circuit indicates that there must be a voltage source at the steel/concrete interface (the diffusion potential).

In an equivalent circuit although the sample will clearly not resemble the collection of components which are used to represent it some physical relationships will remain the same. In order to pass through the circuit the current must pass through both the bulk of the concrete and the interface with the steel. Thus the impedances of the concrete and the interface are in series and may be considered separately.

3.2.2 The linear equivalent circuit for concrete.

Before selecting a suitable circuit to use it is necessary to decide on the level of accuracy required. Greater accuracy would require a more complicated circuit. It is known that silica fume replacement causes an increase in resistance of one or two orders of magnitude depending on curing condition (Vennesland 1981). Due to this wide range of resistances an accuracy of around 5% was adequate to differentiate between the samples.

Hammond and Robson (1955) working with samples which contained some moisture, but were not saturated, proposed a capacitance and a resistance in parallel (fig.3.2). The current through this will be comprised of a component through the resistance in phase with the voltage and a component from the capacitance 90° ahead of it. Using the following notation:

C   Capacitance

I_{cap} Current through capacitance

R_c Concrete resistance

I_r Current through resistance

ω Angular velocity=2π*frequency

V   Applied voltage

$$I_r = \frac{V}{R_c} \qquad 1)$$

$$I_{cap} = V\omega C \quad (rms) \qquad (2)$$

The term which is normally used to indicate the relative sizes of the two currents is the power factor which is defined as :

Power loss in resistance / Total power passing through

The power is proportional to the square of the current. Thus:

$$\text{Power factor} = \frac{I_r^2}{I_r^2 + I_{cap}^2} \qquad (3)$$

The conclusion from this is that increasing ω (i.e. increasing the frequency) will increase the relative effect of the capacitance. Hammond and Robson conclude that if the frequency is restricted to 50 Hz the load is almost purely resistive and the power factor approximately one.

Monfore (1968) discussed the possibility of the capacitance being caused by a thin gas film on the surface of the electrode in the solution which would be in series with the resistance. He subsequently chose to use the parallel circuit of Hammond and Robson but in order to avoid the possibility of gas build up it is indicated that it is advisable to keep the voltage low. Monfore's results also show the capacitance to be very low and actually decreasing with increasing input frequency. Whittington et al.(1981) and McCarter et al.(1981) proposed a highly complex circuit to take account of conduction paths through the aggregate but then concluded that they are not significant.

Because the current through the capacitance depends on the differential of the applied voltage an applied square wave will theoretically produce an infinite current. In practice the current will depend on the quality of the apparatus. Despite this Hughes et al (1985) propose a measurement system based on a square wave source. Their final results are within 5% of their measured a.c. resistances.

An example of the correct way of measuring impedance is given by Perez-Pena et al. (1986). They used a proprietary impedance analyser to give an instant readout of the capacitance and resistance at any frequency required. This type of machine was not readily available to the earlier workers. The materials that they tested were, however, very dense and very dry so their observed high capacitances are not relevant to wet

concretes.

The conclusion for these concretes is that at low frequencies and voltages the impedance may be represented with adequate accuracy as a simple resistance.

3.2.3 The linear equivalent circuit for the corroding steel/concrete interface.

It is universally agreed (Arup 1983, Wilkins and Lawrence 1983) that corrosion of steel in concrete depends on two processes which are arranged as in fig. 3.3. The external current I_x is zero when there is no external circuit. This is not a linear equivalent circuit because the two processes are non-linear. Details of the chemical processes are frequently quoted in the literature and show that iron atoms are lost from the steel at the anode and oxygen reduction occurs at the cathode. As the reactions occur electrons are liberated in the steel at the anode and combine at the cathode thus causing current to flow in the direction shown. If both processes are in the same area this is a micro circuit but they can be well separated to give a macro circuit. For example at sea level on a marine structure the cathode may be in the splash zone and the anode below the water level. If a structure is not submerged macro circuits will be severely limited by the connection between the two processes which must pass through the concrete resistance. Linear polarisation measurements are usually only relevant to micro circuits. Macro circuits for testing in this way can, however, be created by cracking the sample e.g. Leeming (1983).

Wilkins and Lawrence (1983) present theoretical voltage current relationships for the separate processes over a range of voltages. The effect of applying higher voltages for the purpose of accelerating or inhibiting corrosion will be discussed later in section 3.3. It is, however, only possible to draw a linear equivalent circuit at voltages close to the rest potential i.e. the potential the system will develop when there is no external current. The full analysis of the circuit near this potential was published by Stern and Geary (1957) and the part of it that is relevant to steel in concrete may be simplified as follows:

Stern and Geary propose that the exponential voltage current relationship which is normal in electrochemical systems applies.

Thus for the anode :

$$I_a = I_{a0} e^{\left[\dfrac{V - V_{a0}}{B_1}\right]} \qquad (4)$$

Where

I_a is the anode current

V is the voltage across the system

B_1 is a constant for all samples

V_{a0} and I_{a0} are constants for the particular sample.

V_{a0} and I_{a0} are called the exchange voltage and current because there is actually a second component to the current:

$$I_{a-} = I_{a0} e^{\left[\frac{V_{a0}-V}{B_1}\right]} \qquad (5)$$

It may be seen that if V is well above V_{a0} this second component is negligible but at $V = V_{a0}$ an equal "exchange" current I_{a0} will flow in each direction.

Thus at the anode :

$$V = V_{a0} + B_1 Log\left[\frac{I_a}{I_{a0}}\right] \qquad (6)$$

Similarly at the cathode :

$$V = V_{c0} - B_2 Log\left[\frac{I_c}{I_{c0}}\right] \qquad (7)$$

At the rest potential E_0

$$I_c = I_a = I_{corr} \text{ (the corrosion current)}$$

Thus :

$$E_0 = V_{a0} + B_1 Log\left[\frac{I_{corr}}{I_{a0}}\right] = V_{c0} - B_2 Log\left[\frac{I_{corr}}{I_{c0}}\right] \qquad (8)$$

Thus subtracting from (6) and (7)

$$V-E_0 = B_1 Log\left[\frac{I_a}{I_{corr}}\right] = -B_2 Log\left[\frac{I_c}{I_{corr}}\right] \qquad (9)$$

But when x is close to 1 : x-1 = Ln[x]

Thus $\qquad$ (x-1)Ln[10] = Log[x]

Thus when I_a and I_c are close to I_{corr}

$$V-E_0 = B_1 Ln [10] * \left[\frac{I_a}{I_{corr}} -1\right] = -B_2 Ln [10] * \left[\frac{I_c}{I_{corr}} -1\right] \qquad (10)$$

With the following definitions:

$$\text{Constant B} = \frac{B_1 B_2}{(B_1 + B_2) Ln [10]} \qquad (11)$$

and

$$\text{Polarisation resistance } R_p = \frac{B}{I_{corr}} \qquad (12)$$

Equation (10) reduces to:

$$\text{External current } I_x = I_a - I_c = \frac{V-E_0}{R_p} \qquad (13)$$

Thus the relationship between voltage V and external current I_x is equivalent to a resistance of value R_p and a voltage step E_0 in series. The purpose of linear polarisation measurements is to measure the resistance R_p and obtain from it the corrosion current I_{corr} and thus the rate of loss of mass from the steel.

The linear effect is shown graphically in fig.3.4 which shows computer plots of two logarithmic functions and their sum. The values of the constants were chosen as typical for the system. In fig.3.5 two different theoretical samples are shown. Both samples have the same voltage current relationship at the cathode but the one with the higher anodic current has a lower rest potential and a lower linear gradient.

3.2.4 The complete linear equivalent circuit.

In sections 3.2.2 and 3.2.3 it was shown that the complete circuit must contain a resistance to represent the bulk concrete in series with another resistance and a voltage step to represent the interface. In order to obtain the rest of the circuit it is necessary to use impedance analysis. In its simplest form this would involve measuring the complex impedance at various frequencies and then testing circuits made up with actual resistors etc. until a similar response was found. The response of circuits is, of course, normally calculated rather than physically measured.

John et.al.(1981) measured the impedance and proposed the circuit shown in fig.3.6 in which the circuit for the interface may be seen to be in parallel with a capacitance (the double layer capacitance). Dawson (1983) reports later work from the same laboratory. In this work the impedance at different frequencies was measured by applying a random (white noise) signal and analysing the input and output by fast Fourier transform. The values of the components were then obtained from further computer analysis. Dawson suggests that the additional components C_f and R_f represent a film which develops on the surface of the steel and is chemically different from the bulk of the concrete. John et.al.(1983) presented an idealised Nyquist impedance plot for this circuit (see fig.3.6). Hope et al (1986) suggested that while this circuit is correct for a non-corroding system the simplified circuit of fig.3.7 may be used for a corroding system.

3.3 The effect of applying higher voltages.

3.3.1 General.

As indicated in 3.2.3 the complete linear equivalent circuit is only valid for applied voltages close to the rest potential. Referring to figs.3.6 and 3.7 the combination of R_p and the voltage step becomes a non-linear impedance but the rest of the circuit remains the same. Outside the linear range of about 50mV but within the Tafel region of about 200 mV the d.c. response is logarithmic. Outside this range saturation polarisation occurs and there is no simple dependence of current on voltage.

3.3.2 Anodic voltages.

If a large anodic voltage is applied the cathodic process will not be significant and the anodic process will be greatly accelerated. Following the method of Preece (1983) an applied potential of +100mV vs. saturated calomel electrode (SCE) was used to accelerate corrosion in this work. Publishing under the name of Hansson (1984) she further suggests that the ingress of chloride ions which is accelerated by the applied voltage will cause a sudden increase in current when the ions reach the embedded steel. Experimental results from this method have been presented by Hansen et.al. (1986). Many workers have measured potentiostatic polarisation curves. In order to measure these the voltage is increased in steps of about 50mV and the current is permitted to stabilize for 1 hour or 1 day and then measured. The conclusion that a lower current measurement indicates a better protected bar is probably more valid for macro corrosion cells where large voltages may occur. If only one voltage is required and its size is not important the potential which developes between mild and stainless steel may be used (Gautefall and Vennesland 1983). The stainless steel may even be fixed to the corroding sample and cast into the concrete with it (Beeby 1985).

3.3.3 Cathodic voltages.

In this instance the cathodic process of oxygen reduction will dominate. Since this is harmless to the steel it is the basis of a system used to protect it (cathodic protection). For this system the voltage must be carefully set because if it is too large other processes which do not occur without an applied voltage will start. The great advantage of this protection system is that it also drives the chloride ions out of the concrete.

Gjorv et.al.(1976) have proposed the use of an applied voltage of -900mV vs. SCE to measure oxygen permeability. Continuous aeration of the solution is recommended.

3.3.4 A.C. voltages.

As would be expected from the linear equivalent circuit the non-linear effects which apply to d.c. at higher voltages do not affect a.c. and the impedance is not greatly changed. Measurements in this project at up to 4 volts did not show any significant change in the resistance. Hansson and Hansson (1983 and 1985) chose to apply low frequency square wave voltages and describe the effect of C_{dl} on this wave form.

3.4 The methods of measurement.

3.4.1 Measurement of impedance.

It is possible to measure the impedance by using a bridge circuit but in this work it was done by simply applying a voltage and measuring the current. The current was measured by measuring the voltage across a resistor (the count resistor) in series with the sample as shown in fig.3.1. It may be seen that if the two voltages are measured to

the same accuracy the accuracy of the system is highest when they are equal i.e. the impedances of the sample and the count resistor are equal.

3.4.2 Linear polarisation measurements.

There are a number of simple d.c. methods for measuring R_p which are possible with a knowledge of the linear equivalent circuit. The procedure for all of them is basically as follows (Fontana and Greene 1967):

1 Let the system seek its rest potential E_0
2 Apply a potential V within 20mV of the rest potential
3 Measure the current flow I_x
4 Calculate $R_p = \dfrac{V - E_0}{I_x}$ from eq.(13)

$$I_{corr} = \frac{B}{R_p} \qquad \text{from eq. (12)}$$

The systems differ in their methods used to correct for the effect for the concrete resistance R_c and the double layer capacitance C_{dl}. There is also some variation in the chosen values for the constant B. This constant may theoretically be obtained by measuring the response in the logarithmic Tafel region outside the linear range but it is usually obtained from measurements of actual mass loss.

The usual way of compensating for the effect of C_{dl} is to introduce a time delay of possibly a few minutes between the application of the voltage and the measurement of current (e.g.Stratfull 1983). Using the circuit in fig.3.7 the rate of decay of the transient may be calculated as follows:

Let

Voltage across $R_c = V_r$
Voltage across $C_{dl} = V_{cdl}$
Current through $C_{dl} = I_{cdl}$
Current through $R_p = I_x$
thus

$$I_{cdl} = C_{dl}\,\frac{dV_{cdl}}{dt} \qquad (14)$$

$$I_x = \frac{V_{cdl} - E_0}{R_p} \qquad (15)$$

The total current through the sample

$$I = I_{cdl} + I_x = C_{dl}\frac{dV_{cdl}}{dt} + \frac{V_{cdl}-E_0}{R_P} = \frac{V_r}{R_c} \qquad (16)$$

The total voltage applied across the sample

$V = V_{cdl} + V_r$ is constant

thus

$$\frac{dV_{cdl}}{dt} = -\frac{dV_r}{dt} = -R_c\frac{dI}{dt} \qquad (17)$$

and

$$I = -C_{dl}R_c\frac{dI}{dt} + \frac{V-IR_c-E_0}{R_P} \qquad (18)$$

This reduces to :

$$I + \frac{1}{k}\frac{dI}{dt} - b = 0 \qquad (19)$$

where

$$k = \frac{R_P+R_c}{C_{dl}R_PR_c} \qquad (20)$$

and

$$b = \frac{V-E_0}{R_P+R_c} \qquad (21)$$

The solution to this is

$$I = Ae^{-kt} + b \qquad (22)$$

The boundary condition is that when the voltage is applied at time t=0

$$V_c = E_0 , \qquad I = \frac{V-E_0}{R_c}$$

thus

$$A = (V-E_0)\left[\frac{1}{R_c} - \frac{1}{R_P+R_c}\right] \qquad (23)$$

From equation (22) it may be seen that with increasing time the current decays to I=b which is the current which would flow if C_{dl} was not in circuit. The initial value $I=(V-E_0)/R_c$ only gives a measure of the concrete resistance and not the polarisation resistance. For constant R_c and C_{dl} a rapidly corroding sample with low R_P will have a high decay constant k. This means that the current will decay faster making the measurement easier. The risk involved in using a delay is that a voltage is being applied during the delay and chemical movements will be caused which may change the anodic exchange current.

Some of the systems of measurement are as follows:

Andrade and Gonzalez (1978) report results obtained using calcium hydroxide solution

in place of the concrete.

In this situation they report that the IR drop (i.e. R_c) was low and make no mention of C_{dl}. Their data fits reasonably well with a value of 26mV for B in corroding samples.

Gonzalez, Vazquez and Andrade (1982) report the use of apparatus which compensates automatically for R_c. Its method of operation is not stated but it is probably the "instant off" method. In this the measurement is made immediately after the voltage is removed. The voltage across R_c goes immediately but that across the rest of the circuit is maintained by the capacitance. In later work (Gonzalez et. al. 1985a) various A.C. impedance systems are reviewed.

Stratfull (1983) gave great detail of a method of measurement to be used on bridge decks. The effect of R_c was overcome by using a biased square wave input which effectively turned the supply off for half of the cycle and the reading was made during this half. A delay of 2.5 minutes was used to permit C_{dl} to equilibrate. Stratfull also suggested that the measurements should be continued into the Tafel region both anodically and cathodically in order to obtain B_1 and B_2 directly and calculate B from equation (11).

Page et al (1985 and 1986) found that R_c could be ignored probably because they made the second connection to the sample by embedding a second electrode in the concrete rather than forming a contact to the surface. Their method of compensating for C_{dl} was to apply a steadily increasing voltage V which increased to 20mV in 2 minutes. This rate is sufficiently slow that the current through C_{dl} which is proportional to dV/dt will be negligible. The value of 26mV was used for B.

In the present work a delay of 30 seconds was used to permit C_{dl} to equilibrate. R_c was measured separately and subtracted.

Measurement of linear polarisation resistance with d.c. requires the use of a potentiostat. This is required because reference electrodes do not work if currents are passed through them. The potentiostat is essentially a power supply which is connected between the sample (the working electrode) and the secondary (auxiliary) electrode which in this case was a length of R6 mild steel rebar extending around the perimeter of the tank immersed in the salt solution. The voltage output from the potentiostat is controlled so that a constant potential difference is maintained between the sample and a reference electrode. The size of this potential difference may either be controlled with a potentiometer control on the potentiostat or by an external input to it. A circuit showing how this may be achieved with an operational amplifier is shown in fig.3.8 and is based on one from Bracher (1983). A Hermes series 10R potentiostat which had terminals for mounting the count resistor on the front of it was used for this work. Fig 3.9 shows the potentiostat circuit indicating its relationship with the linear equivalent circuit of the sample. Count resistors of 10kohms and 100kohms were used.

3.4.3 A.C. resistivity measurements.

If an a.c. voltage is applied C_{dl} will present an impedance which decreases with increasing input frequency. If the effective impedance of the sample is found to be independent of frequency it may be assumed that the impedance of C_{dl} is negligible and R_c is being measured. In the present work 50Hz was used and the results were found to be unchanged at 1kHz. In a less corroding sample where the circuit in fig.3.6 may be more appropriate than that in fig.3.7 the use of values of R_c obtained in this way as a correction factor for linear polarisation could introduce an error because no account is taken of R_f. Fig.3.10 shows the a.c. resistivity measuring circuit. The 100mv supply was obtained by stepping down the mains supply through a variable and then a fixed transformer. For the check of frequency independence a signal generator was used. Count resistors of 150 Ohm and 2000 Ohm were used.

3.4.4 Rest potential measurements.

It may be seen from fig.3.7 that when there is no external circuit the voltage across the whole sample will be equal to the diffusion potential E_0.

A relationship between E_0 and the corrosion rate may be seen from equation 8 :

$$E_0 = V_{c0} - B_2 Log \left[\frac{I_{corr}}{I_{c0}} \right] \qquad (24)$$

If a comparison is made between systems with the same cathode conditions (i.e. the same cathodic exchange currents I_{c0} and V_{c0}) but differing anode conditions and thus different corrosion rates it may be seen that the rest potential will be proportional to the log of the corrosion current.

For these measurements an instrument with a high input impedance (>10Mohm) is required to avoid disturbing the sample. The hand held Fluke instrument which was used for other readings could not be used and the measurements were made with a Jenway PHM6 high impedance voltmeter.

3.4.5 Measurement of current under applied voltage.

In order to measure current the circuit was arranged so that a variable count resistance could be introduced into it without disconnecting the applied voltage. The resistance was then adjusted to give a voltage drop of about 1mV across it and when the circuit had stabilized (approx. 30 seconds) the current was known from the voltage drop across the count resistor and its resistance.

3.4.6 The computer interface.

A computer interface to a BBC microcomputer using an MF1010 interface (Anon 1985c) was used for rest potential and linear polarisation measurements. In order to provide the high impedance mentioned in 3.4.4 all inputs to the interface were put

through operational amplifiers as shown in fig.3.11. The circuit is shown in two separate halves because due to a design fault in the MF1010 it could not all be used at the same time to provide a complete system. (This fault caused an interruption to the output voltage when a reading was taken on any of the inputs). The voltage controlling circuit was used to measure the rest potential and set the offset voltages for some of the samples but it was then necessary to record the current by hand. For measuring current decay the voltage was set manually and the current measuring circuit was used.

3.5 Experimental procedure.

3.5.1 Concrete samples.

Cylindrical samples of concrete containing a 12mm. diameter round bar were prepared as shown in fig. 3.12. The bar was degreased before casting. After curing as described in chapter 2 an electrical connection was made to the top of the bar. In order to make an effective connection with solder it was necessary to heat the end of the bar to the melting point of the solder with a blow lamp so a continuous flow of water across the steel/concrete interface was maintained to prevent de-bonding of the bar in the concrete. The samples were then placed in a tank containing 10% sodium chloride solution at about 20°C with the level of the solution 30mm. below the top of the concrete as shown in fig. 3.12.

Two sets of samples were cast and the following procedures were used:

Set 1 (one sample per condition)

1. Immersion in salt solution
2. Initial measurements: Rest potential, ac resistivity.
3. +100mV applied for 28 days.
4. Measurements at 28 days: Rest potential, ac resistivity.
5. +100mV applied until all samples reached 10 months old (from casting).
6. Measurements: Rest potential, linear polarisation (time delays of 10,20 and 30 second, voltage changes set by computer interface to -10,-5,+5,+10,+30,+50 and +70 mV), ac resistivity.

Set 2 (two samples per condition)

1. Immersion in salt solution.
2. Initial measurements: Rest potential, linear polarisation, ac resistivity, current at +100mV.
3. +100 mV applied for 28 days.
4. Measurements at 28 days: Rest potential, linear polarisation, ac resistivity, current at

+100mV.

note :

1. The linear polarisation for set 2 was measured with a time delay of 30,60 and 90 seconds. The potential change was in the range +10 to +30mV for one sample and -10 to -30mV for the other.

2. There was a delay of 24 hours after disconnecting the +100mV before linear polarisation and rest potential readings.

3. There was a delay of 24 hours after applying the +100mV before measuring the current

3.5.2 Mortar samples.

The cylinders which were used for electrical measurement of carbonation (which is described in chapter 4) were used for this test. (100mm long by 25mm diameter with 100mm long 6mm diameter ms bar on the axis projecting 20mm from one end - immersed in 10% NaCl solution to a depth of 90mm). The carbonation system is described in chapter 3. For each condition two samples were carbonated in the tank and two were kept in the room as controls.

The following procedure was used:

1. Immersion in salt solution on removal from carbonation tank after 28 days of exposure.

2. Measurements at 28 days: Rest potential, linear polarisation and ac resistivity.

3. Left in open circuit in salt solution for 21 days.

4. Measurements at 49 days: Rest potential, linear polarisation and ac resistivity.

note :

The linear polarisation was measured with a time delay of 30,60 and 90 seconds. The potential change was in the range +10 to +30mV for one sample and -10 to -30mV for the other.

3.6 Results.

3.6.1 Linear Polarisation readings.

Fig.3.13 shows the decay of the current for one of the samples over 1.5 hours which shows that waiting for a long time does not achieve a steady state because the corrosion processes are affected by the applied voltage as indicated in 3.2.5. For the analysis the three readings at different times were used and two further values were obtained by fitting an exponential decay function (as eq.(22)) to the three measurements and calculating its value for zero and infinite time. One of the lines on the graph in fig.3.13 is a fit of this type to readings at 10,20 and 30 seconds and the

other is a fit to readings at 30,60 and 90 seconds.

The linear behaviour indicated in eq. (13) is shown for a highly corroding concrete sample from set 1 in fig.3.14 and for an effectively non-corroding one in fig.3.15. It may be seen that the linear relationship holds over a greater range of voltage for the non-corroding sample but the effect of the time delay is much greater for the non-corroding sample. All of the results were investigated to see if there was any systematic difference between the results obtained from polarising anodically and cathodically but none was found.

The results were then plotted on graphs of rest potential against log polarisation resistance which should give a straight line as indicated in equation (24). With the exception of the mortar samples (which had just been introduced into the tank and had not had time to seek their true rest potentials) the correlation coefficients R^2 for the linear relationships were found to be in the range 0.7-0.925 for the 30 second results. For both types of reading (10,20 and 30 second and 30,60 and 90 second) the 30 second correlation coefficient was the best. By calculating the correlation before and after applying the correction for R_c this correction was found to systematically increase R^2. The value of 26mV was used for the constant B. The final values were therefore based on readings taken after a delay of 30 seconds and were averages of anodic and cathodic readings. Gonzalez et.al. (1985b) also recommend a 30 second delay and justify it from an analysis of the equivalent circuit.

3.6.2 Rest potential.

The relationships of rest potential with corrosion current which were discussed in the previous paragraph are shown in figs.3.16-3.19 for the final values of corrosion current. The main set (set 2) may be seen to be an improvement on the set 1 concrete samples (figs.3.16 and 3.17). These graphs would indicate that potential surveys of structures will give a good indication of corrosion. Fig.3.20 shows, however, that carbonation caused a marked increase in potential of mortar samples immediately after placing them in the tank. This phenomenon has been reported previously by Gonzalez et.al.(1983) and Browne et.al.(1983). Gonzalez et. al. consider the situation where the carbonation has reached the steel and show that the consequential reduction in pH would be expected to raise the potential at the interface. Browne et. al. suggest that if the carbonation front has not reached the steel a liquid junction potential will be present between the carbonated and uncarbonated regions due to the increased hydroxyl ion concentration in the uncarbonated region. The junction potential will, however, have a maximum magnitude of 100mV. The effect of the phenomenon is to create difficulties in interpreting potential surveys because a more positive voltage which normally indicates that the structure is in good condition with a low corrosion rate could also indicate the opposite due to extensive carbonation.

3.6.3 A.C. resistance.

Fig 3.21 shows the excellent repeatability of this measurement and fig.3.22 shows the relationship with corrosion current. If independence of voltage is assumed calculation of the resistivity from the resistance for cylindrical samples is relatively simple except for the ends. The inaccuracies caused by the end effects are, however, too great to make useful comparisons with absolute values from other workers.

3.6.4 Current at +100mV.

Fig.3.23 shows the relationship with corrosion current. The correlation between the two measurements indicates that the current at +100mV gives a good measure of the corrosion rate.

3.6.5 Corrosion rates.

The final values for corrosion rates obtained from linear polarisation are shown in figs 3.24-3.29 (all of the results are given in the data tables in Appendix 3). Fig 3.24 shows the results for the concrete samples when first exposed. Apart from the 3 day CC2 samples which had a low corrosion rate because they were dry the expected decrease with increasing age of sample generally occured. The corrosion rates after exposure (fig 3.25) were actually lower for most samples than the rates before exposure. This reduction will have been due to the enhancement of the oxide layer caused by the anodic current. The current only increased for the mix D CC1 and CC2 samples where the chloride had evidently reached the bars. The reason why this increase in current did not occur for mix D from CC3 in not clear. None of the six samples tested from CC3 (2 per age) showed significant increases in corrosion current or current under applied voltage but all twelve samples from CC1 and CC2 showed significant increases in both. Possibly the low temperature curing left the matrix less hydrated and thus more reactive for chloride binding.

In order to check the extent of the protection given to the steel in the SF samples against the effect of the applied voltage by the potential drop across their high concrete resistance the value of this drop was calculated from the known currents and resistivities. The maximum value was only 2 mV for the SF samples but some of the mix D samples with much higher currents had values over 100 mV. No special protection was thus available to the SF samples.

Fig.3.27 shows that the initial rate of corrosion for the mortar control samples was lower for the OPC mixes. This did not occur for the concrete samples (fig.3.24) and may thus have been a result of the OPC mixes drying out to a greater extent than the SF mixes. The initial corrosion rates for the carbonated samples (fig.3.26) show an increased spread in the data but are all greater than the range of OPC readings for the control samples. Fig.3.28 for the carbonated samples and fig.3.29 for the control samples show the combined effect of carbonation and exposure to chlorides. There is a considerable spread in the data which may have been caused by cracking in the

samples before they were placed in the chloride solution. The results are, however, very different from those for the concrete samples where the SF mixes showed the lowest corrosion rates (fig.3.25) and indicate that mix B performs best under these conditions. This apparent loss of benefit from the SF when the samples dry out is discussed further in chapter 14.

3.7 Conclusions.

The interpretation of the results in relation to the effect of the silica fume will be discussed in association with the results from other experiments in chapter 13 and 14. The present conclusions relate to the method only.

1. The results obtained from electrical measurements on a corroding steel/concrete system may be explained by the linear equivalent circuits shown in figs.3.6 or 3.7.

2. The four measurements: Linear polarisation, a.c. resistivity, rest potential, and current at +100mV all give a broadly similar ranking for the mixes but the linear polarisation is considered to be the most important for durability because it is a direct measure of the corrosion rate.

3. The following improvements to the apparatus for further work are suggested:

a) Alterations to make the computer interface fully automatic would improve the accuracy of the results.

b) The installation of a circulating pump would ensure uniform salt concentrations and could be arranged so as to aerate the solution for oxygen permeability measurements.

c) For this work three tanks were used with connecting 25mm.i.d. siphon tubes. These did not prevent the build up of potential differences of up to 100mv. between the tanks which had to be corrected for. The use of a single large tank would prevent this occurring. the potentiostatic polarisation current

d) It has been shown that both R_c (Monfore 1968) and λ (Beeby 1985) are temperature dependent. Although the apparatus is in a basement room and not subject to major variations the temperature of the solution could be recorded.

e) If the bars were accurately machined to size before casting into the concrete the depth of corrosion could be physically measured at the end of the experiment.
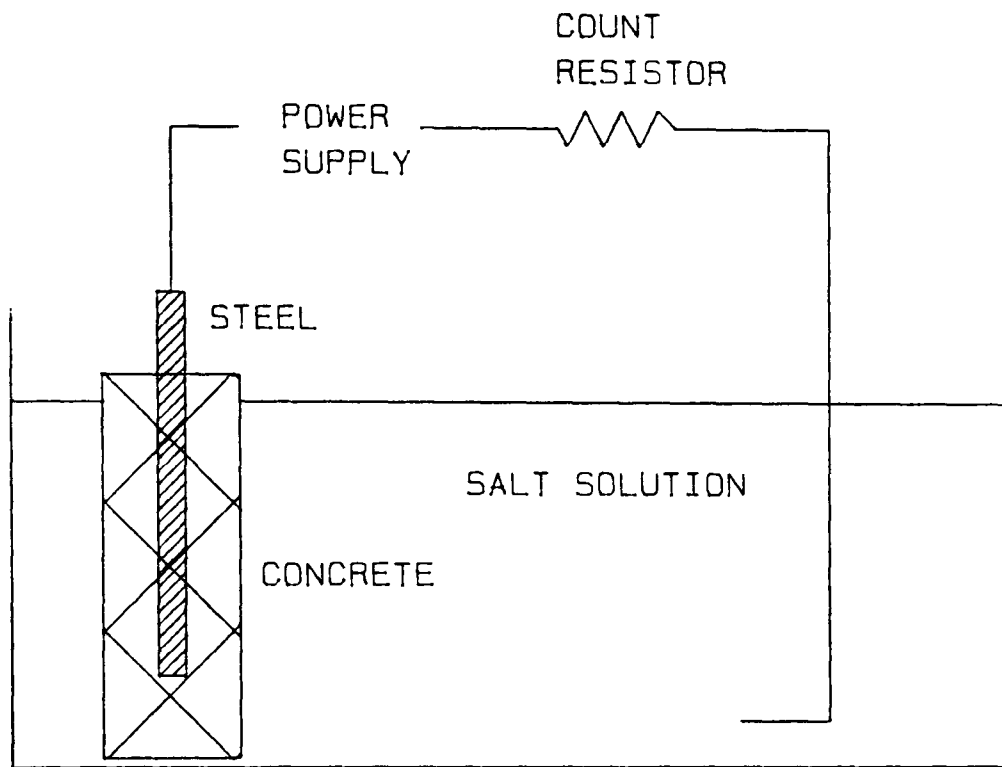
Fig 3.1
BASIC CIRCUIT FOR ELECTRICAL MEAUREMENTS

Current $I=V/R+jVwC$

Impedance $Z=(R-jR^2wC)/I+R^2w^2C^2$

_ _ Locus of points for increasing w
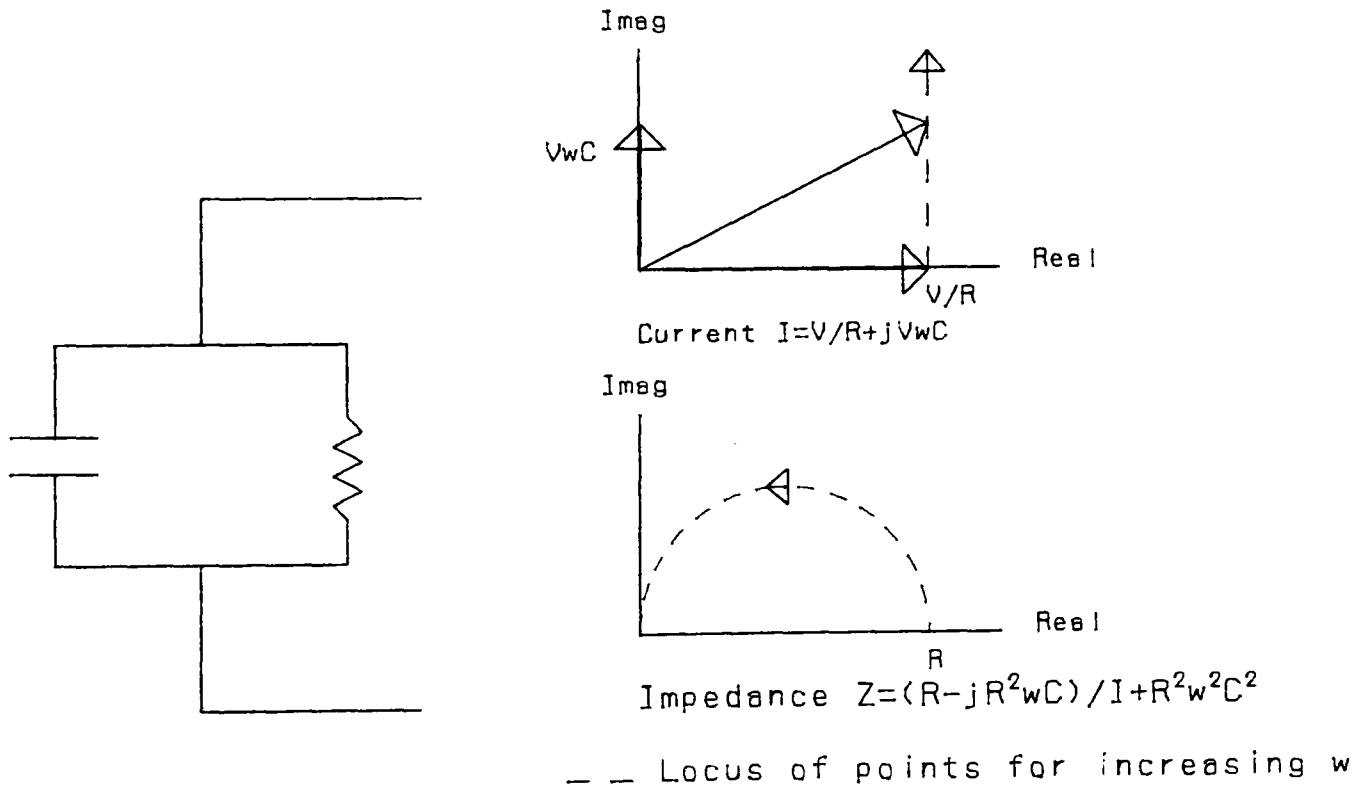
Fig 3.2

EQUIVALENT CIRCUIT FOR CONCRETE AND THE THEORETICAL FREQUENCY RESPONSE
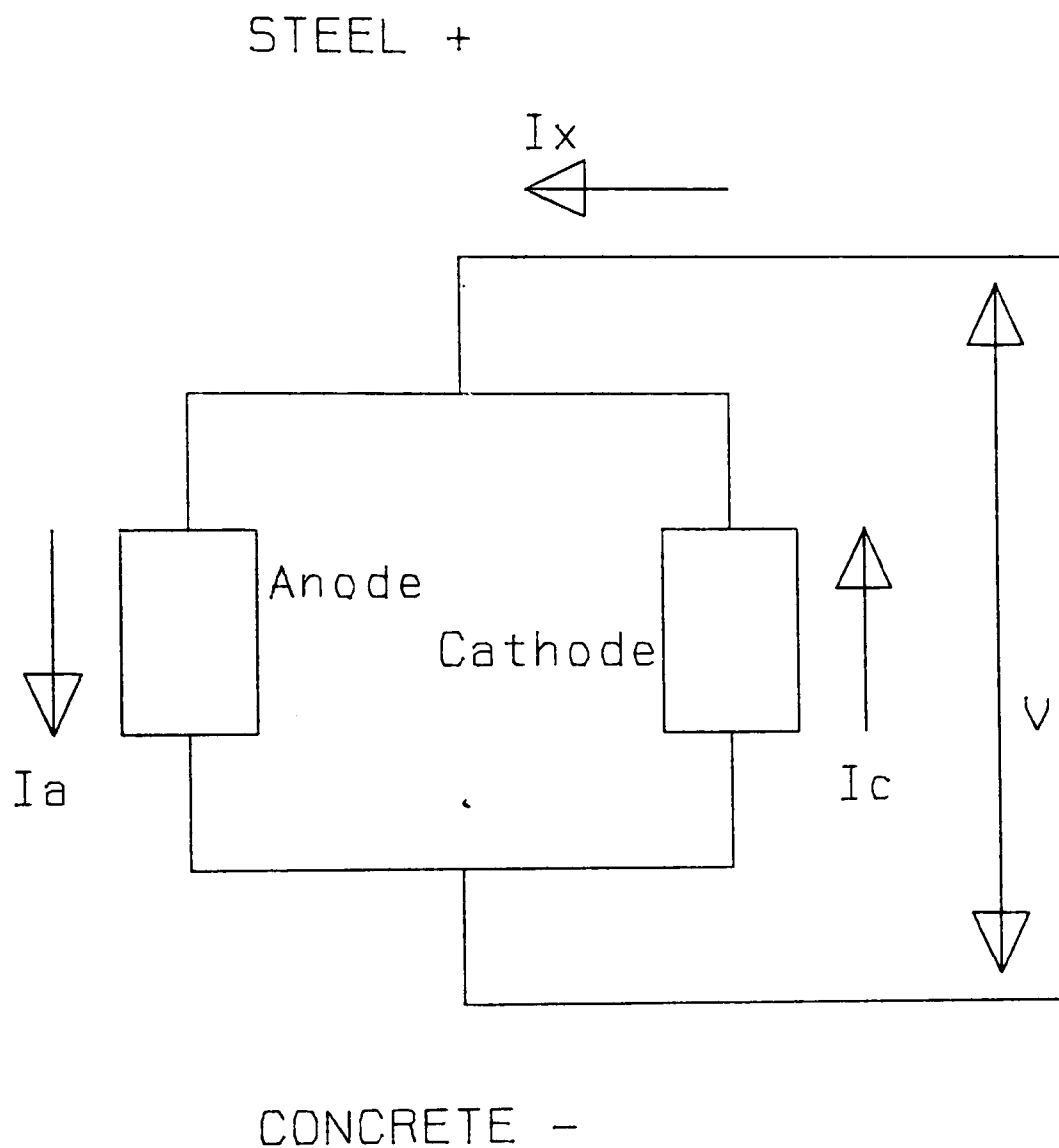
STEEL +

CONCRETE –

Anode $V = Va0 + B1 * LOG(Ia/Ia0)$
Cathode $V = Vc0 - B2 * LOG(Ic/Ic0)$

Fig.3.3 Corroding steel/concrete interface
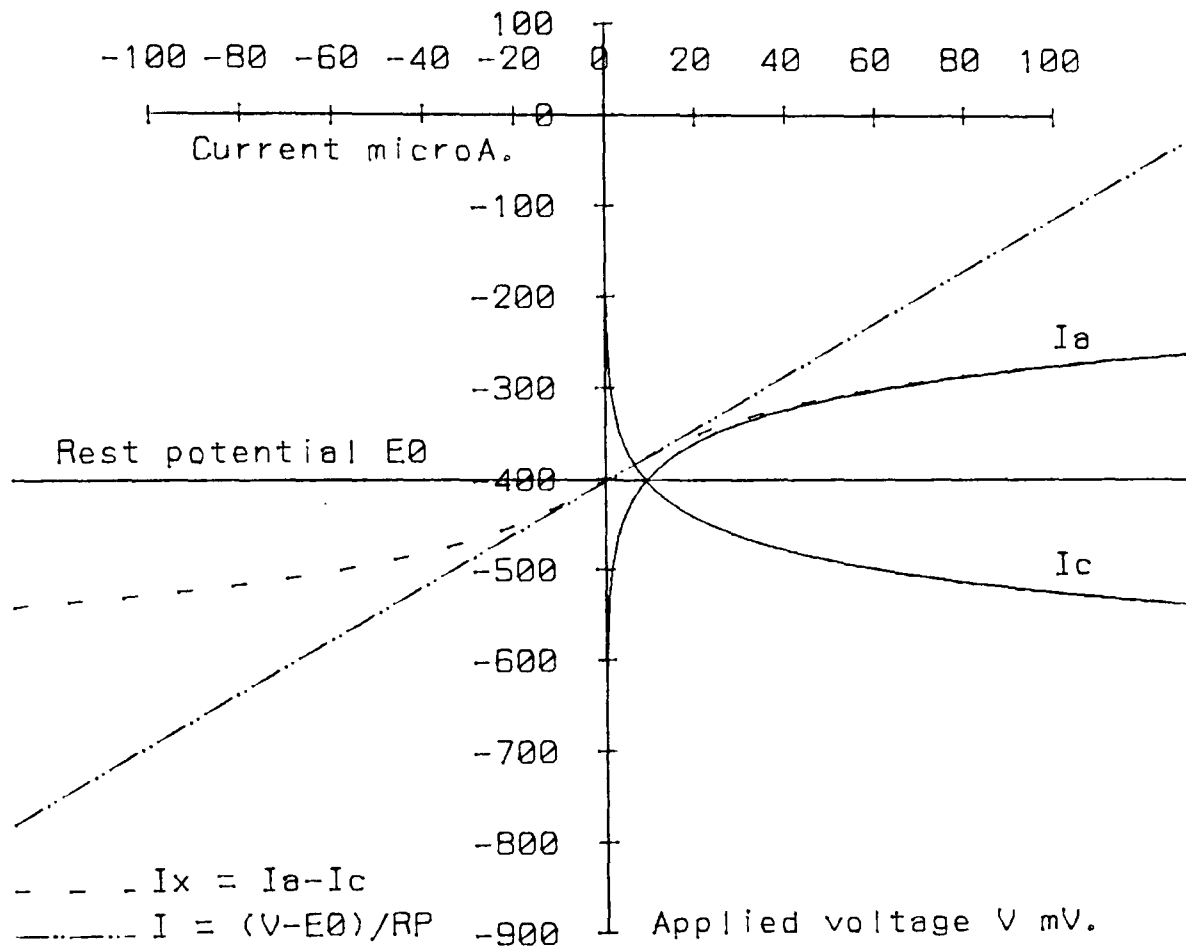
COMBINATION OF ANODIC AND CATHODIC CURRENTS

Fig.3.4
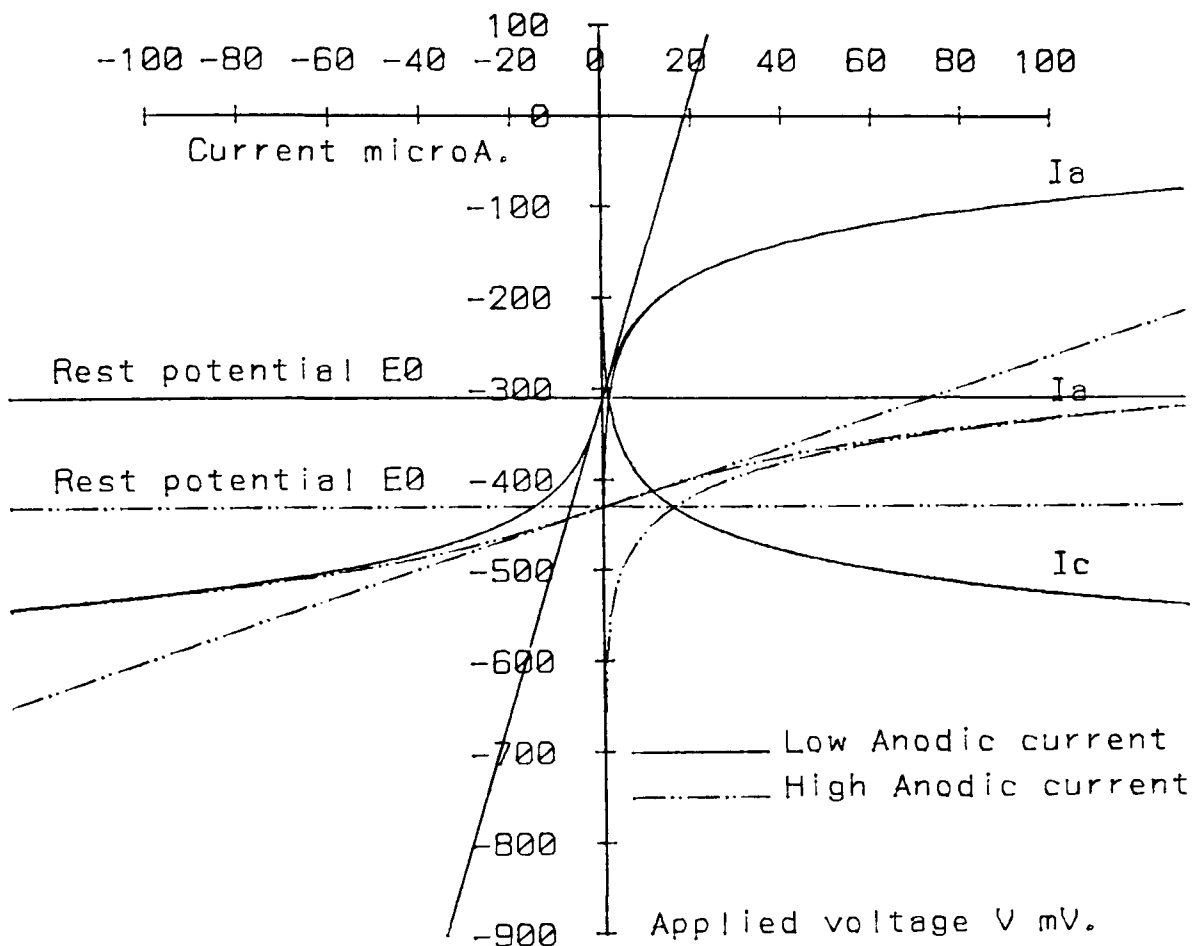
Low Anodic Current
Constant B= 0.02606 V.
Rest potential E0=-0.31000 V.
Corrosion current Icorr=1.56609 microA.
Polarisation resistance RP=0.01664 Ohms.

High Anodic current
Constant B= 0.02606 V.
Rest potential E0=-0.43000 V.
Corrosion current Icorr=15.66094 microA.
Polarisation resistance RP=0.00166 Ohms

EFFECT OF HIGH AND LOW ANODIC CURRENTS

Fig.3.5
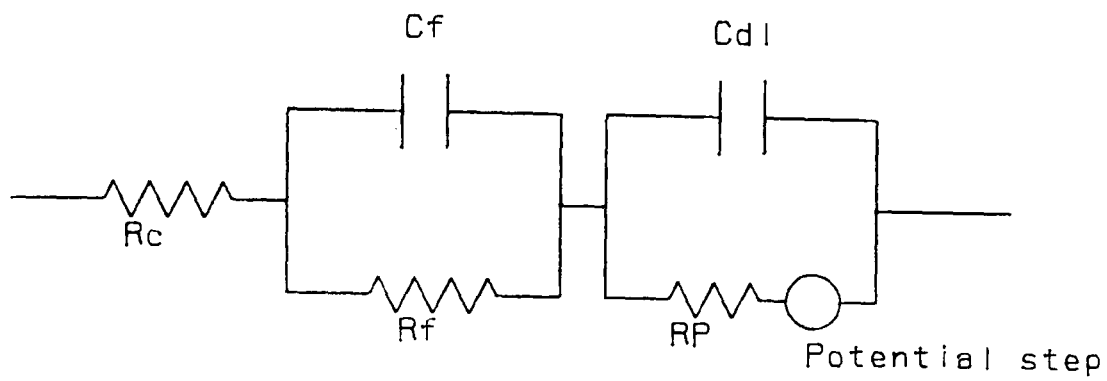
ADAPTED FROM JOHN ET AL (1983)

Fig 3.6a

EQUIVALENT CIRCUIT FOR STEEL IN CONCRETE INCLUDING

COMPONENTS TO REPRESENT THE INTERFACE FILM
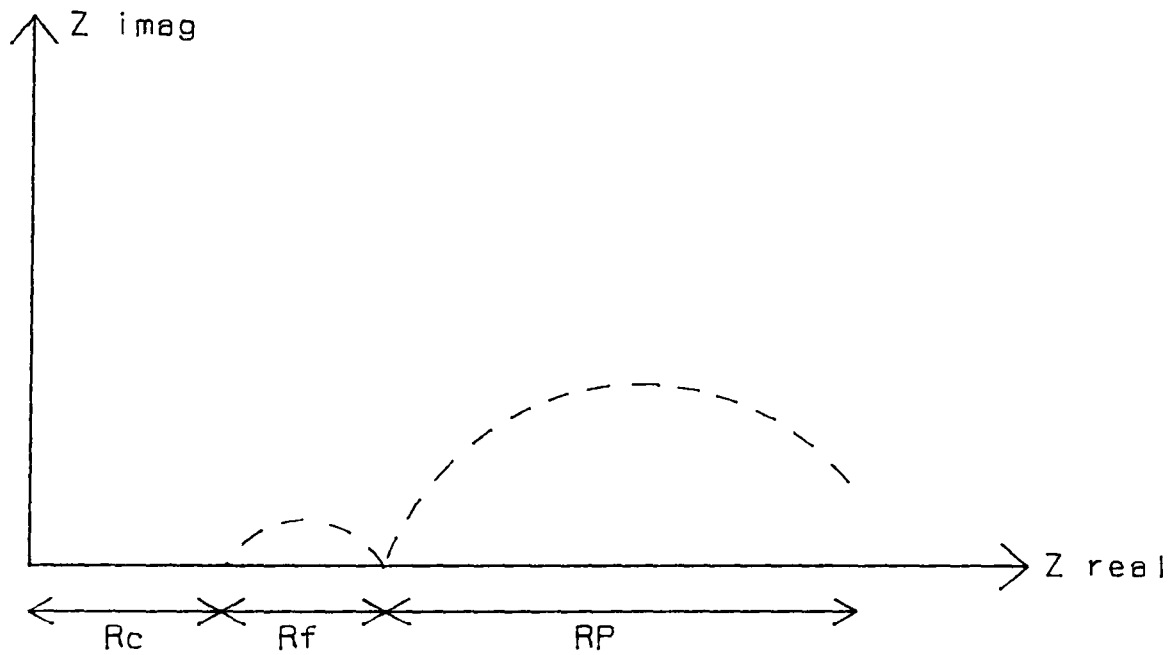
Impedance at different frequencies

After John et al.(1983)

Fig 3.6b
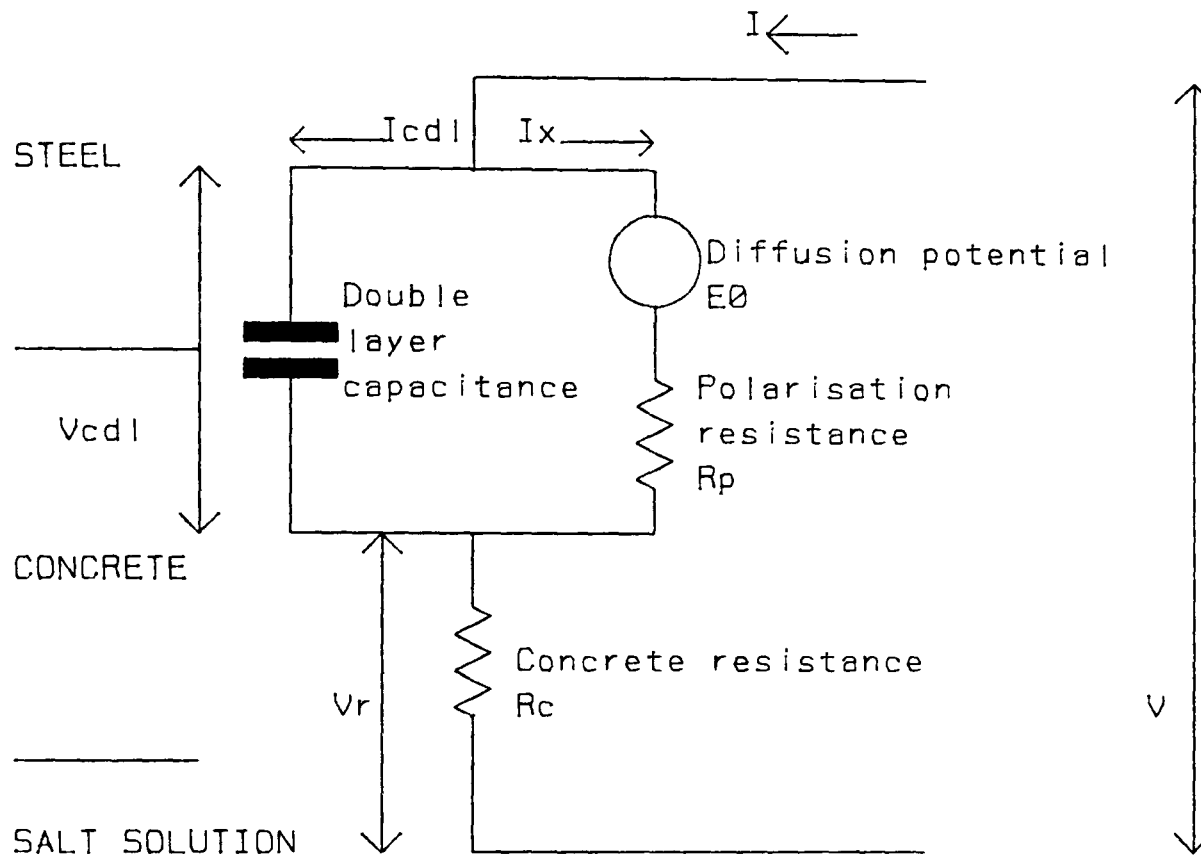
THE EQUIVALENT CIRCUIT OF STEEL IN CONCRETE
USED IN THE ANALYSIS

Fig. 3.7

POTENTIOSTAT

AUXILARY
ELECTRODE

COUNT RESISTOR

POWER
SUPPLY

WORKING
ELECTRODE
(SAMPLE)

INPUT
VOLTAGE   (either internal or external)

REFERENCE
ELECTRODE
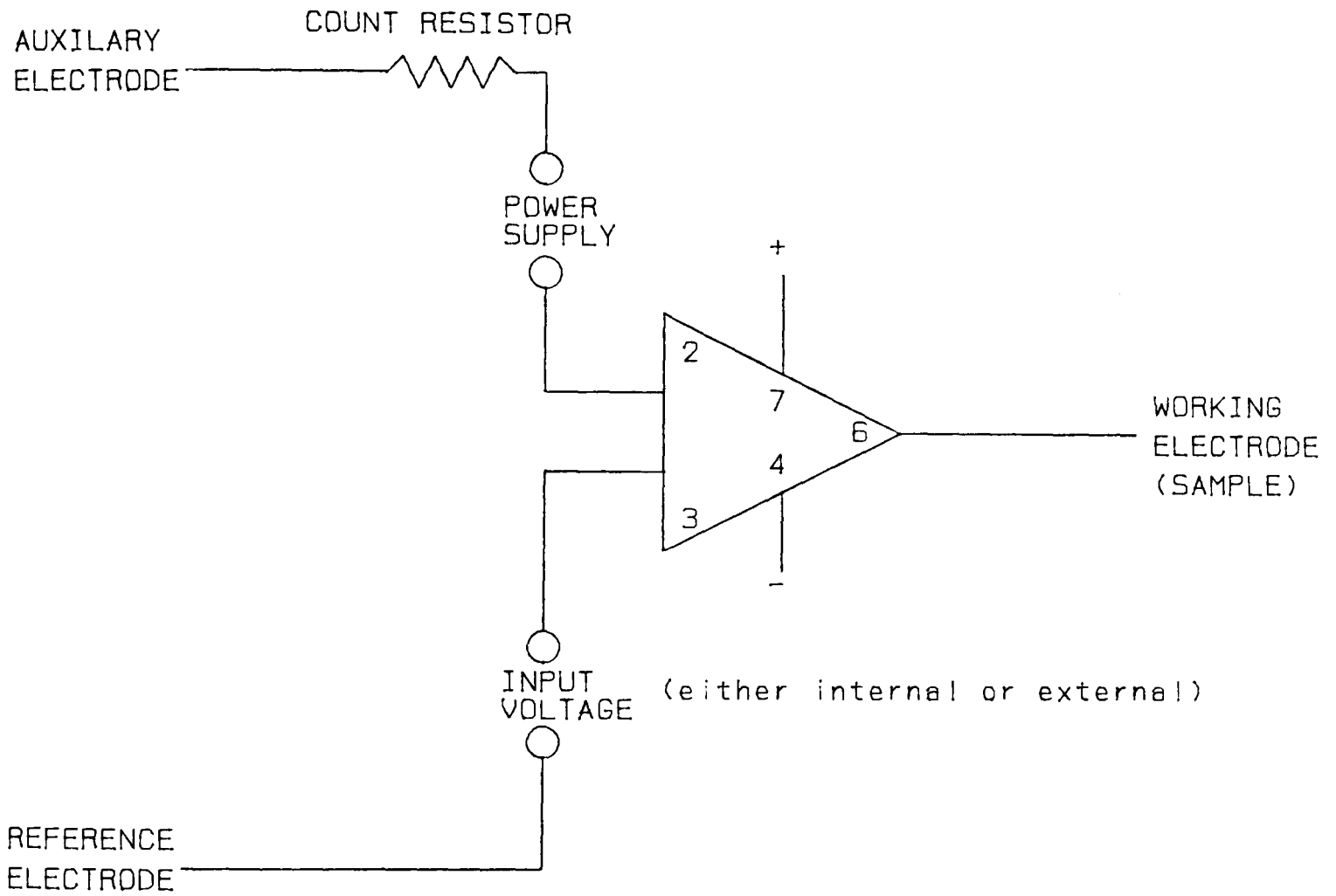
Fig 3.8

An idealised circuit for a basic potentiostat

POTENTIOSTAT

Working   Reference Secondary
Electrode   Electrode Electrode

Count resistor

Corroding
steel
bar

Mild
steel
bar

CONCRETE SAMPLE

Tank

Calomel
Electrode

10% NaCl
Solution
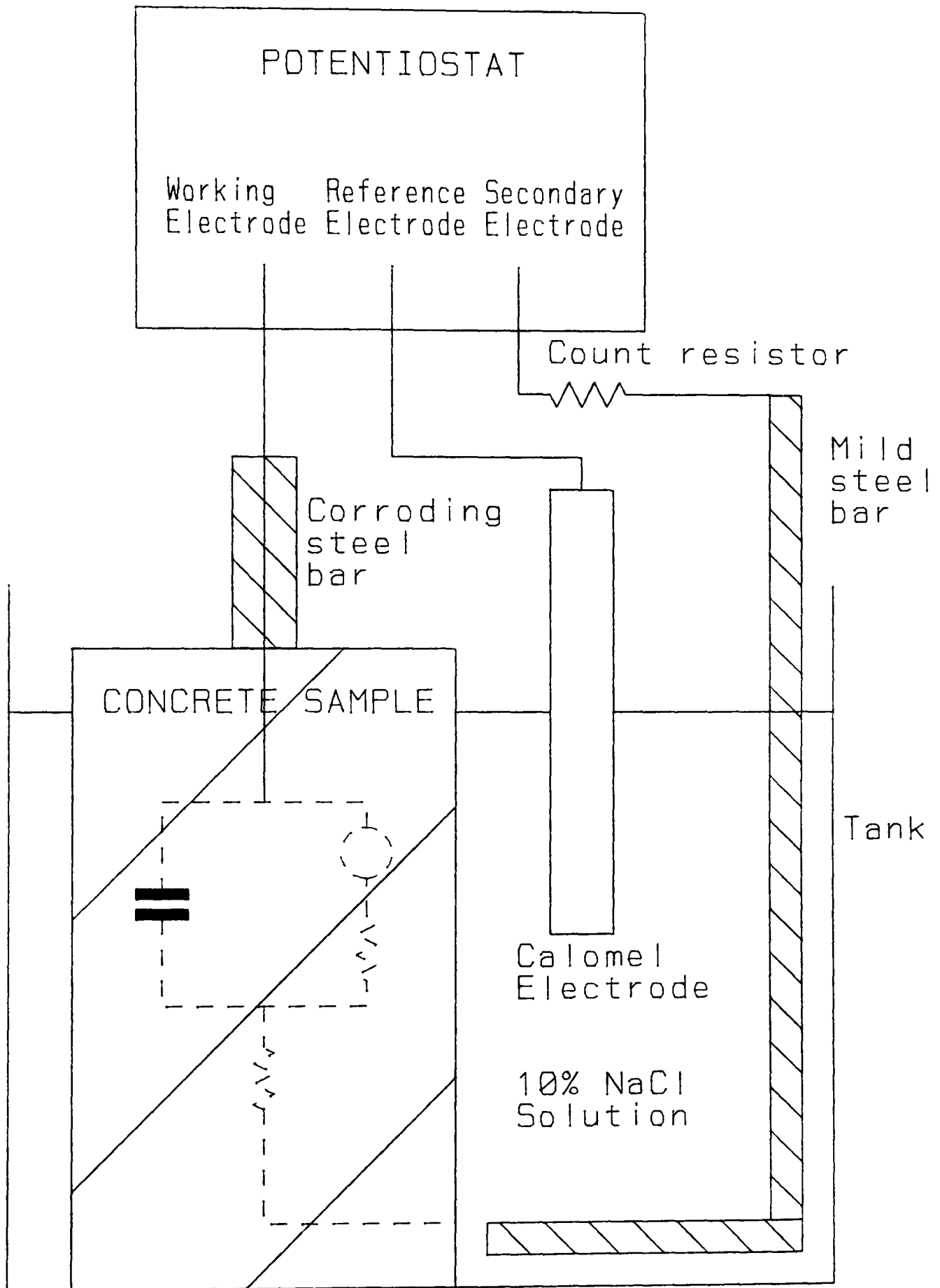
Fig.3.9 POTENTIOSTAT CIRCUIT
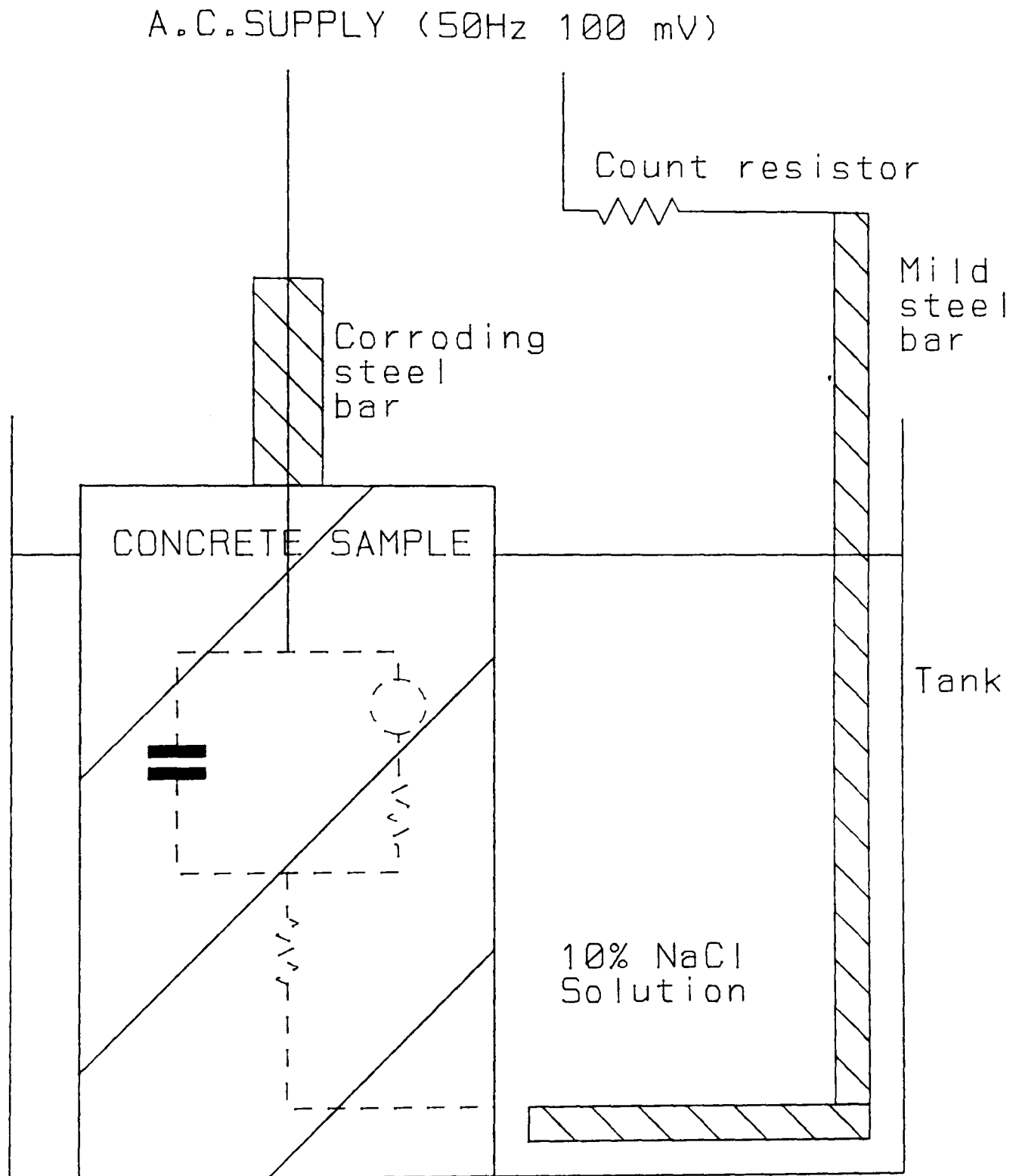
Fig. 3.10 A.C. RESISTIVITY CIRCUIT
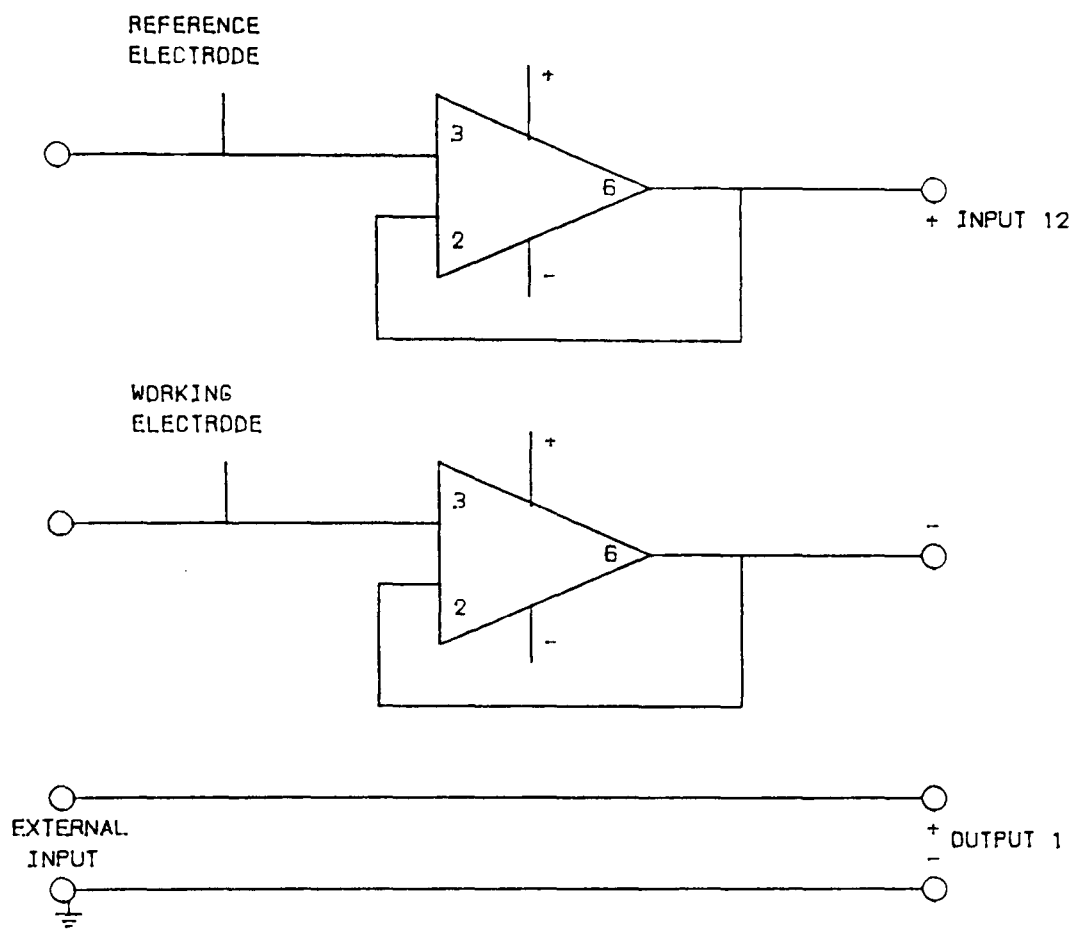
VOLTAGE CONTROLLING CIRCUIT
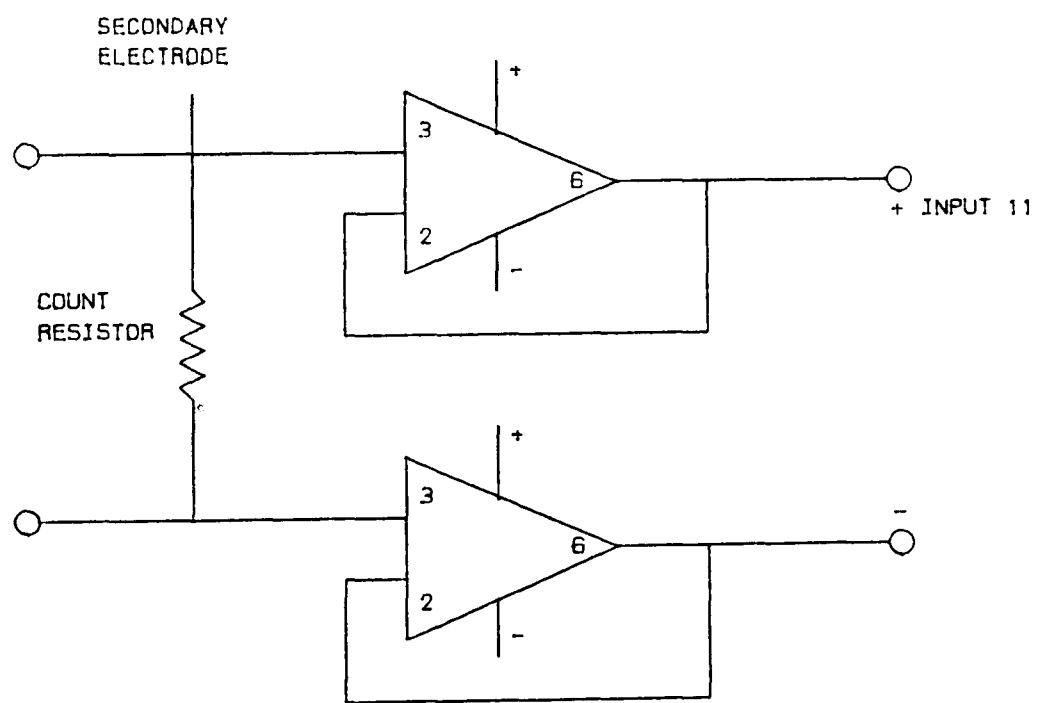
CURRENT MEASURING CIRCUIT

Fig 3.11

CIRCUIT BETWEEN POTENTIOSTAT TERMINALS (SHOWN ON LEFT)

AND MFI COMPUTER INTERFACE (SHOWN ON RIGHT)
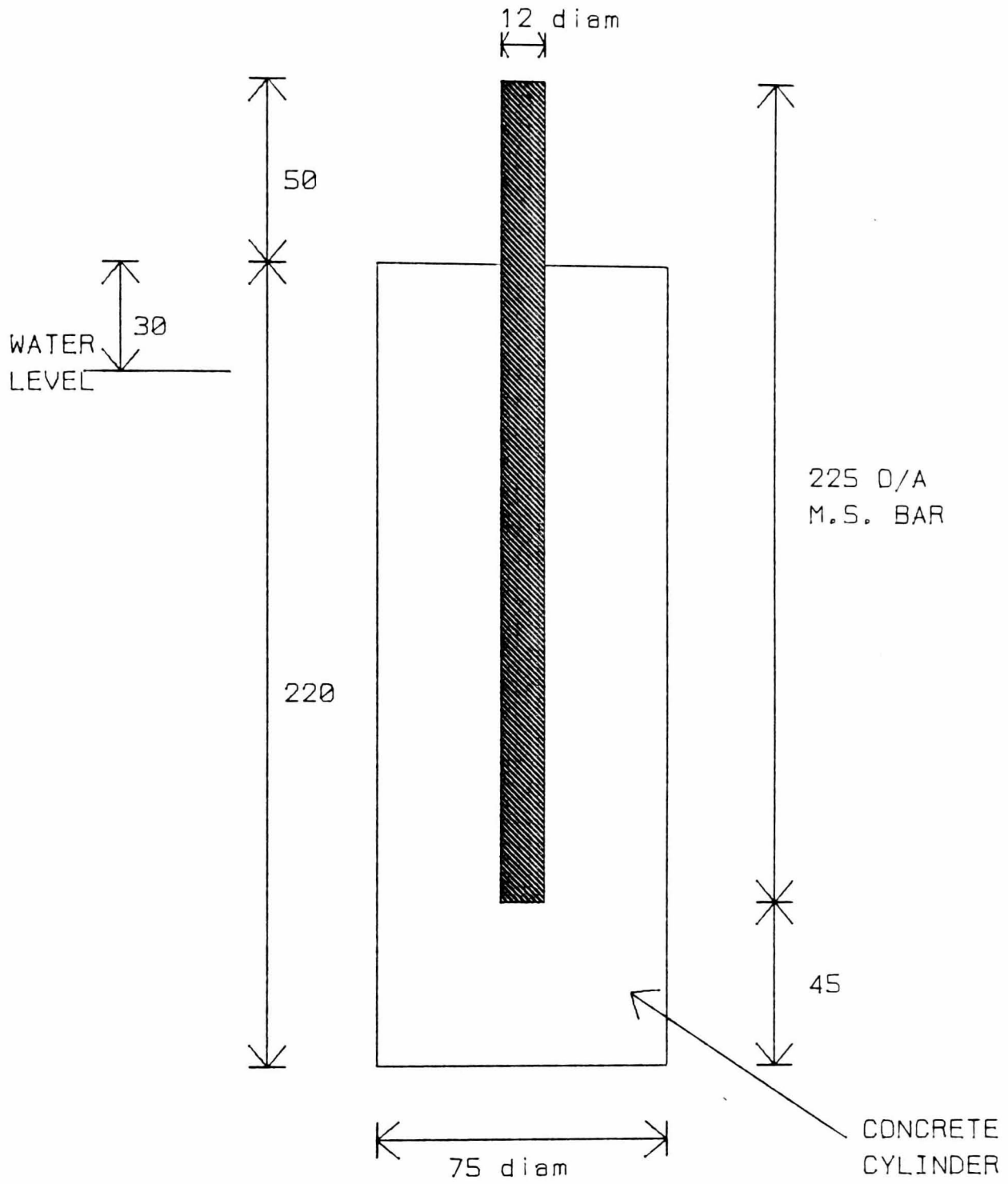
Section through corrosion/resistivity specimen

Fig 3.12
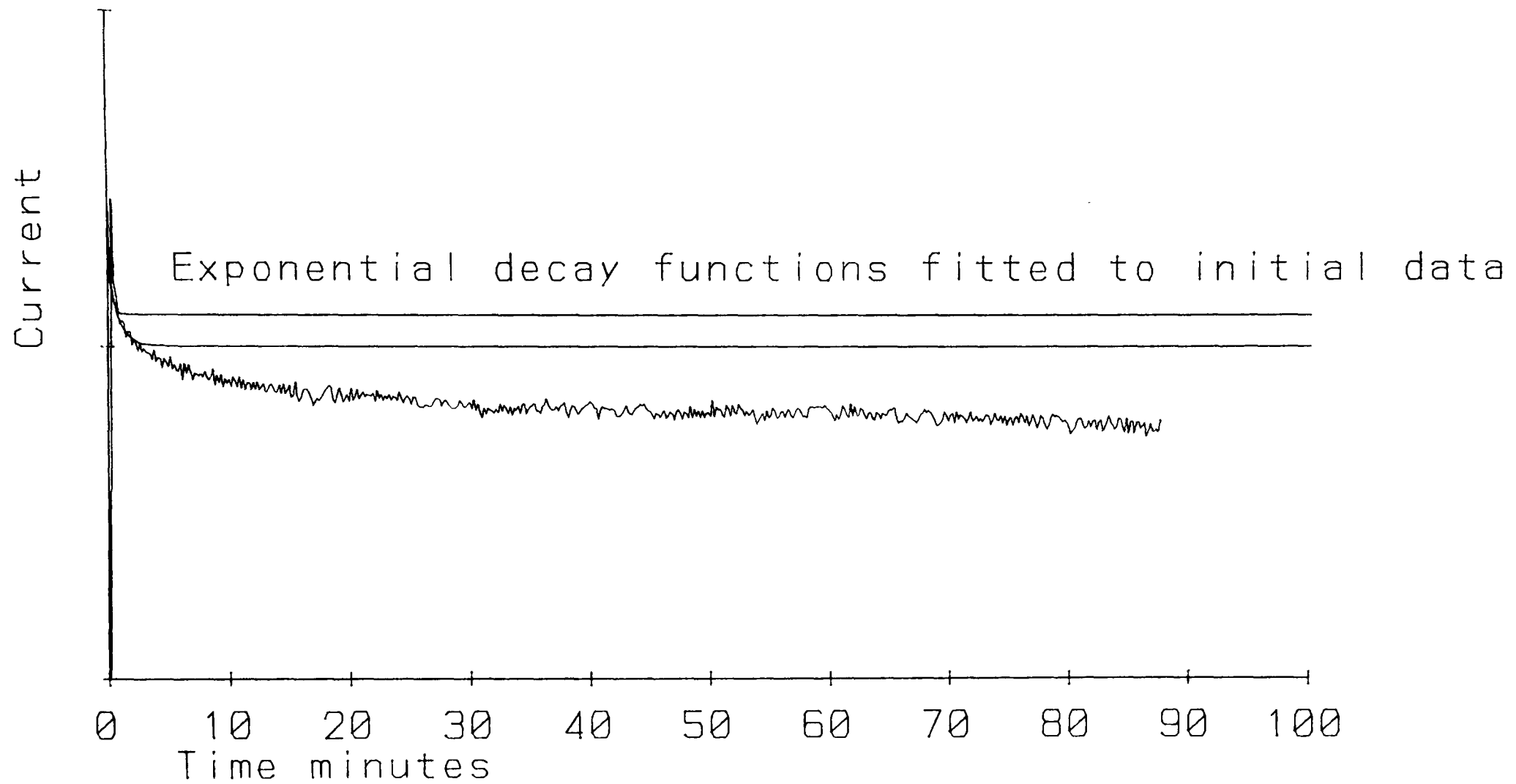
Fig. 3.13 CURRENT DECAY IN LINEAR POLARISATION READING
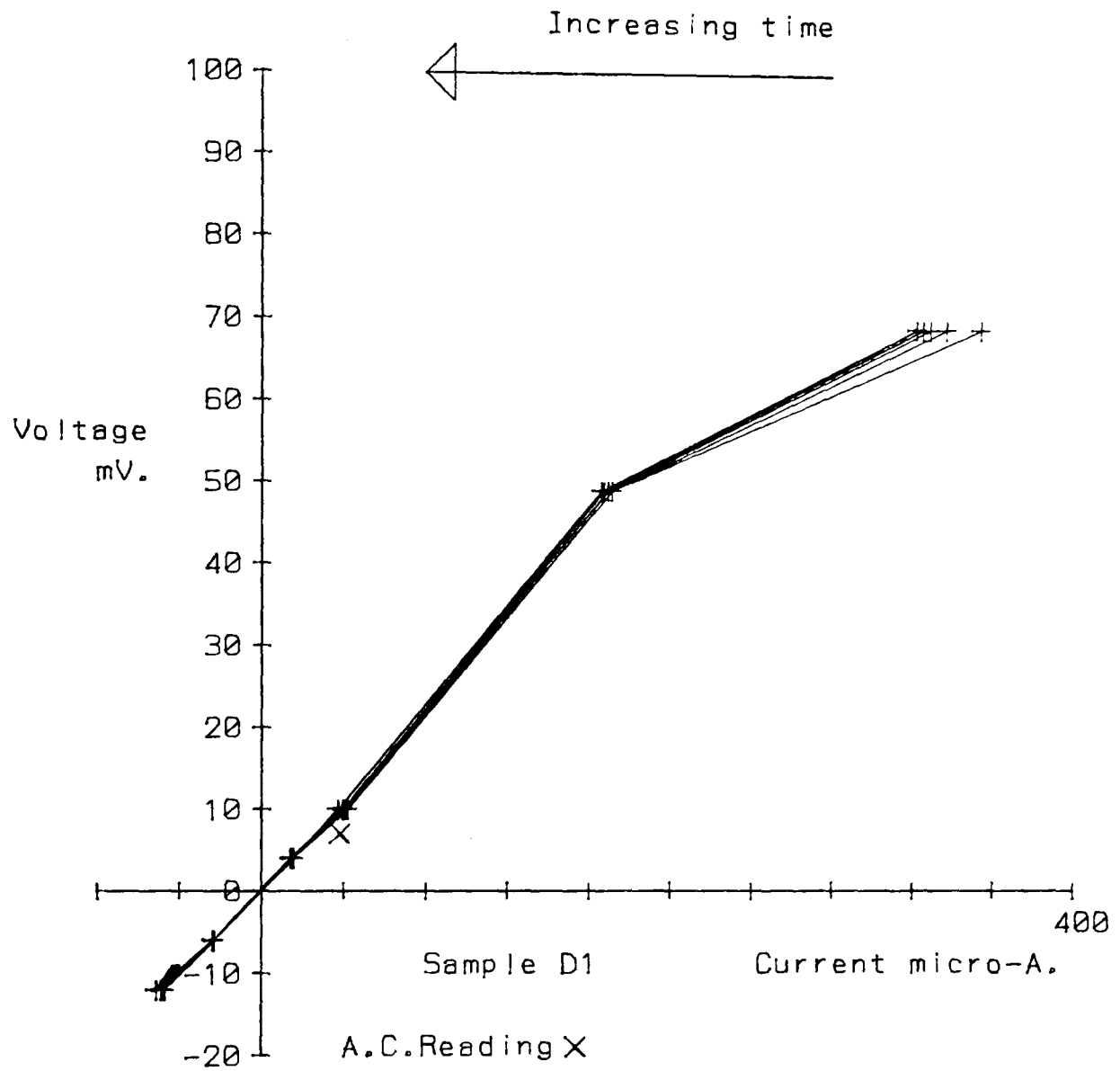
Mix D (O.P.C.,w/c=0.42) the data shows a high corrosion current

Linear polarisation measurements at 10,20 and 30 seconds
and extrapolations to zero and infinite time
Fig. 3.14
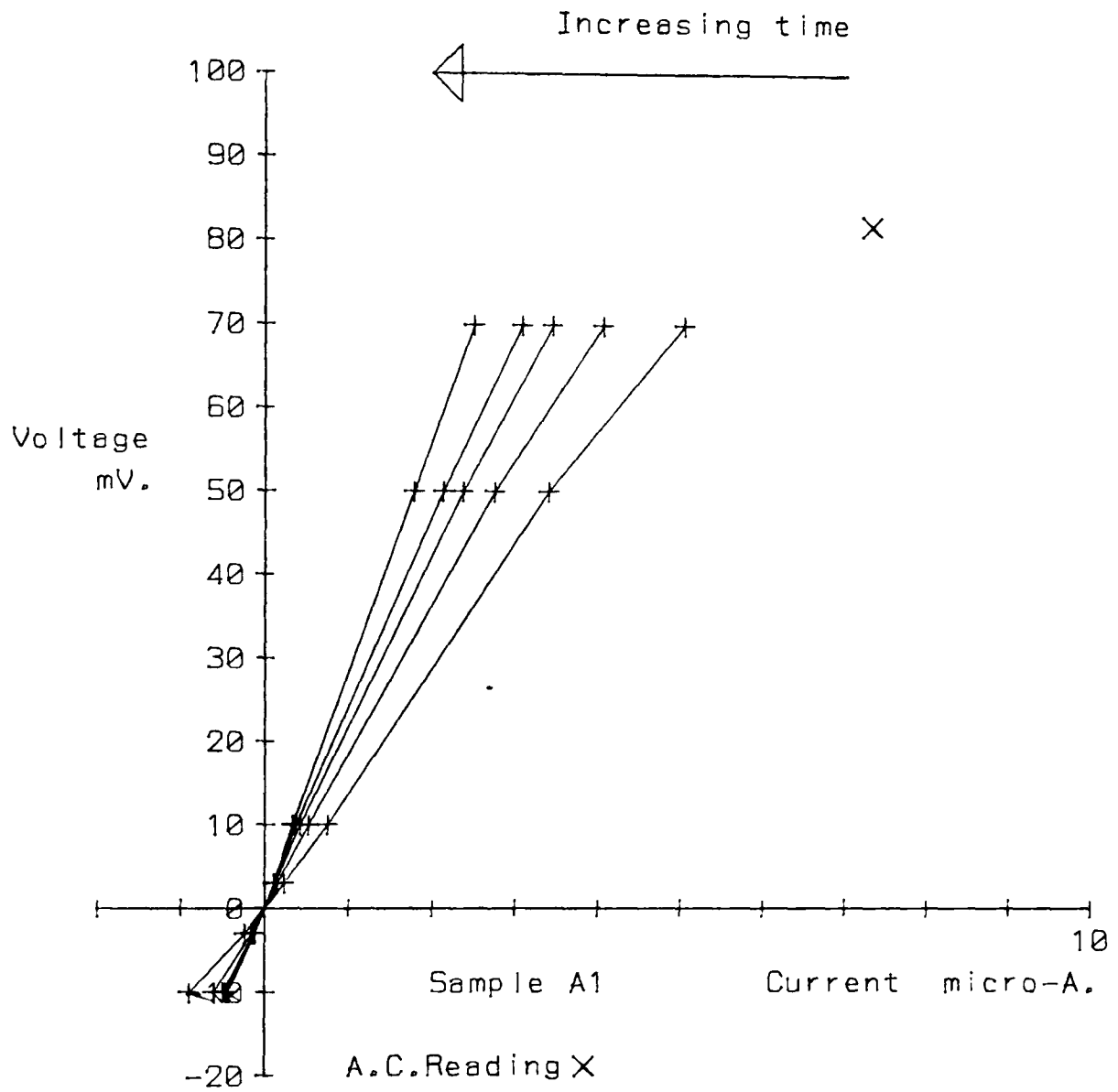
Mix A (S.F.,w/c=0.3) the data shows a low corrosion current

Linear polarisation measurements at 10,20 and 30 seconds
and extrapolations to zero and infinite time
Fig. 3.15
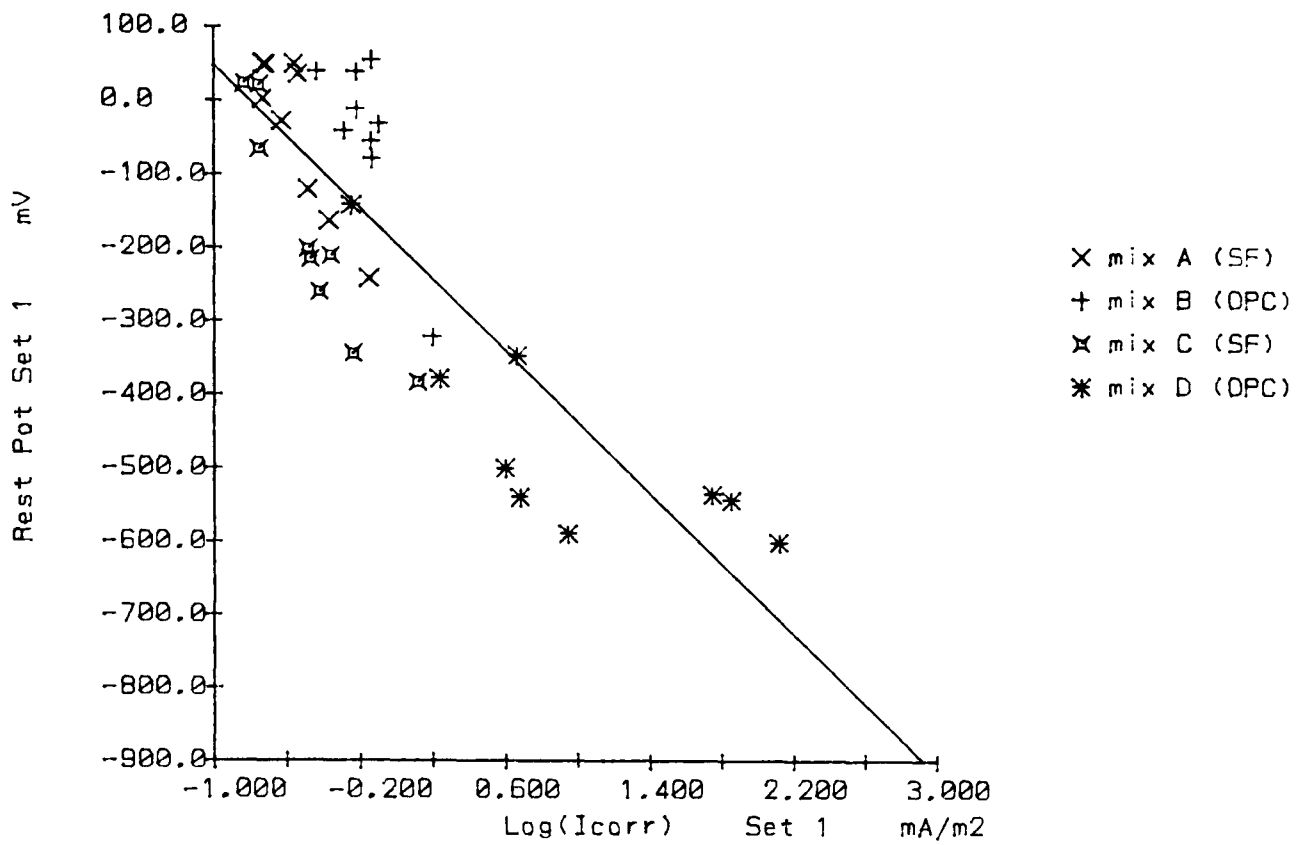
Equation for line : Y=-193.3626834+X*-241.6564922
R squared=0.699

Fig. 3.16 Showing the linear relationship between the rest
potential and the corrosion current for the set 1 samples
after 10 months exposure.
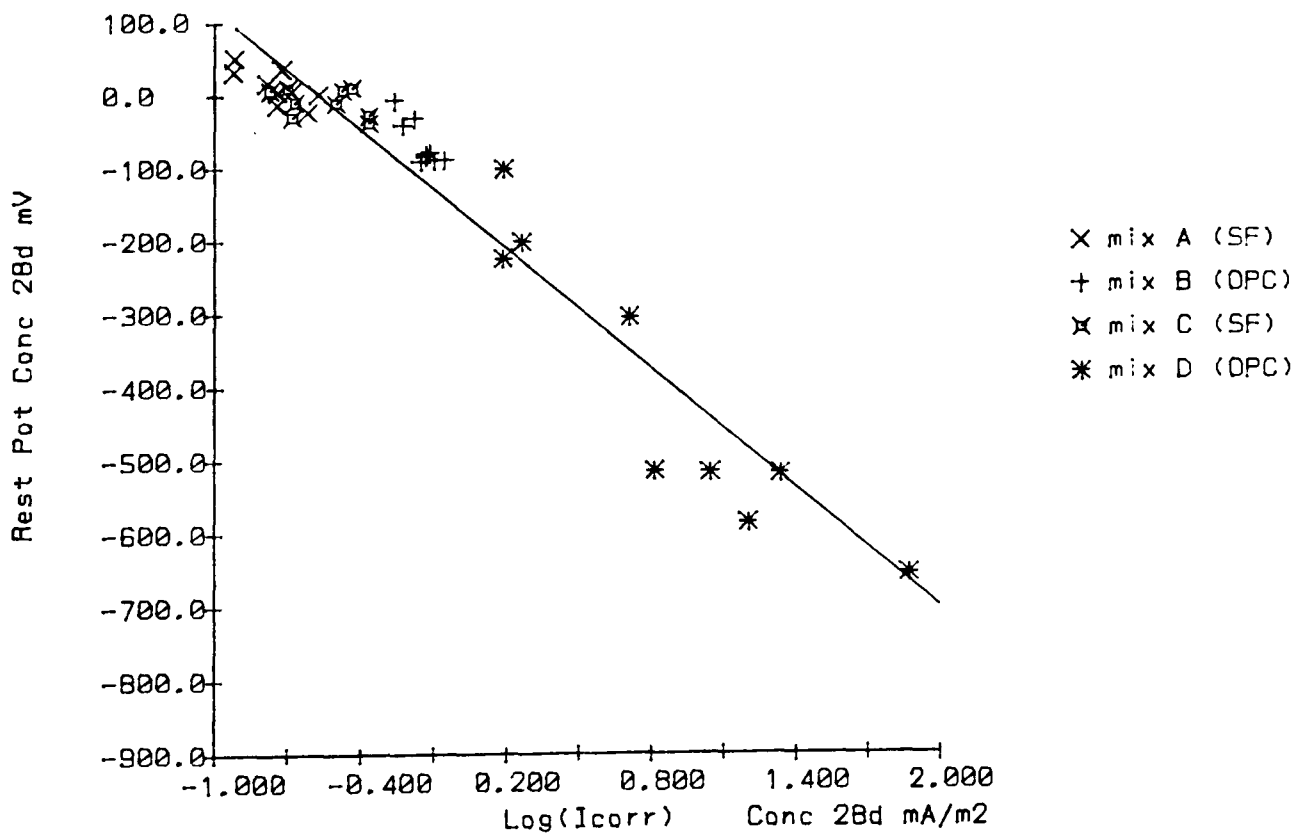
Equation for line : Y=-154.0885724+X*-272.9426489
R squared=0.925

Fig. 3.17 Showing the same relationship as fig.3.16 but for
the set 2 samples after 28 days.

Equation for line : Y=-172.0796592+X*-211.8810974
R squared=0.703
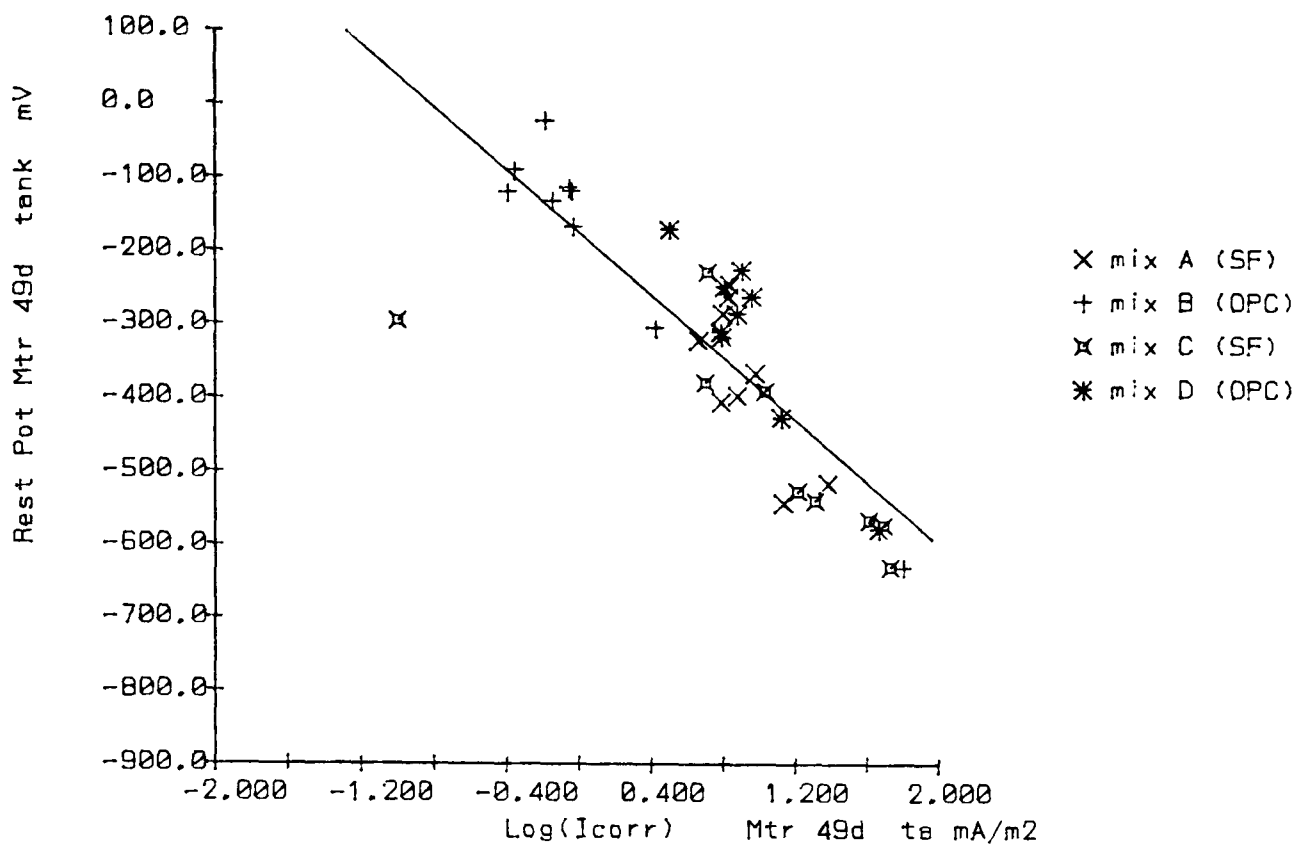
Fig. 3.18 Showing the linear relationship between the rest potential and the log of the corrosion current for the mortar samples which had been carbonated in the tank for 28 days and then exposed to the salt solution for 21 days.

Equation for line : Y=-226.9081637+X*-220.1373242
R squared=0.843
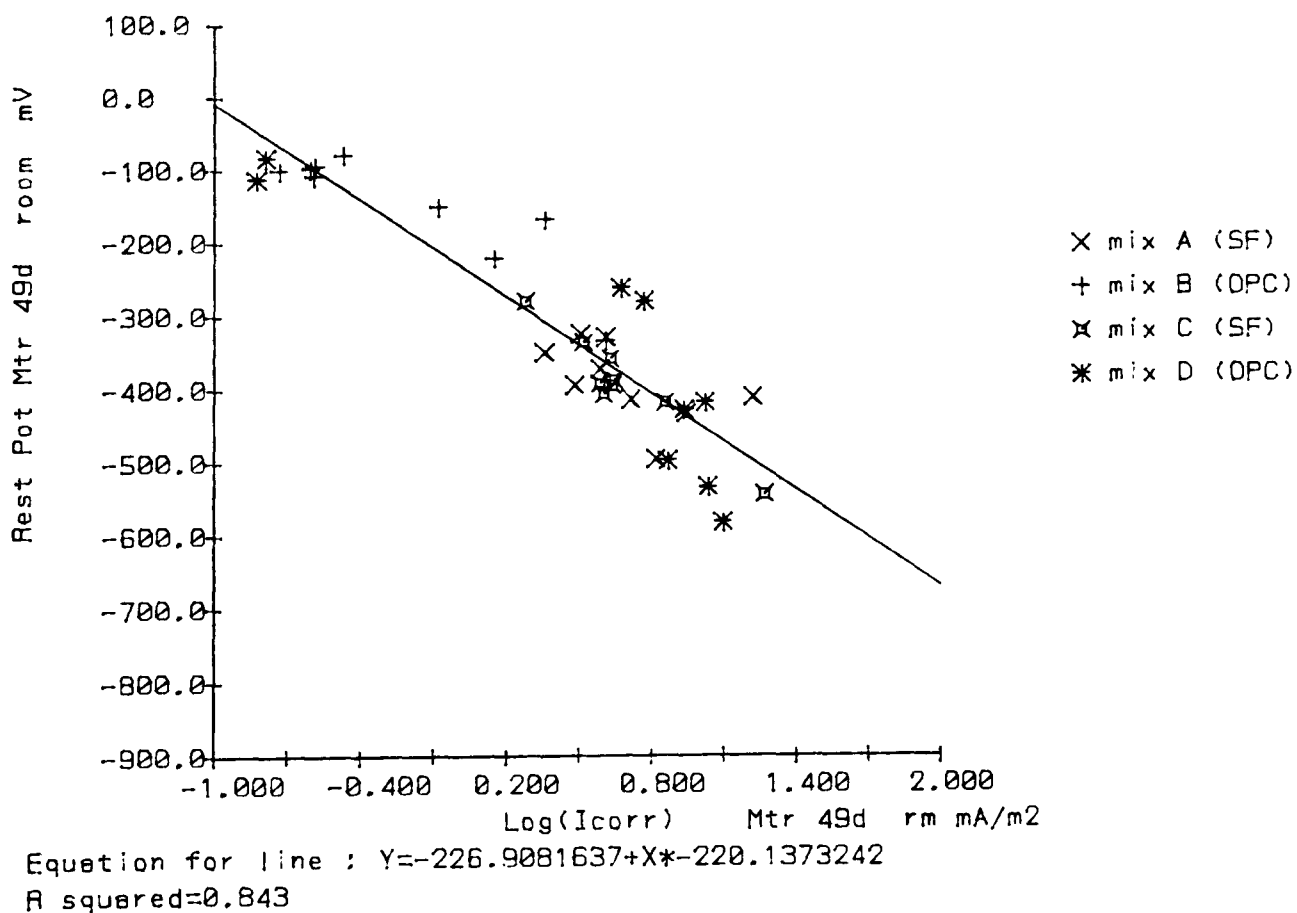
Fig. 3.19 Showing the same relationship as fig 3.18 but for the control mortar samples which were kept in the room while the other samples were in the carbonation tanks.
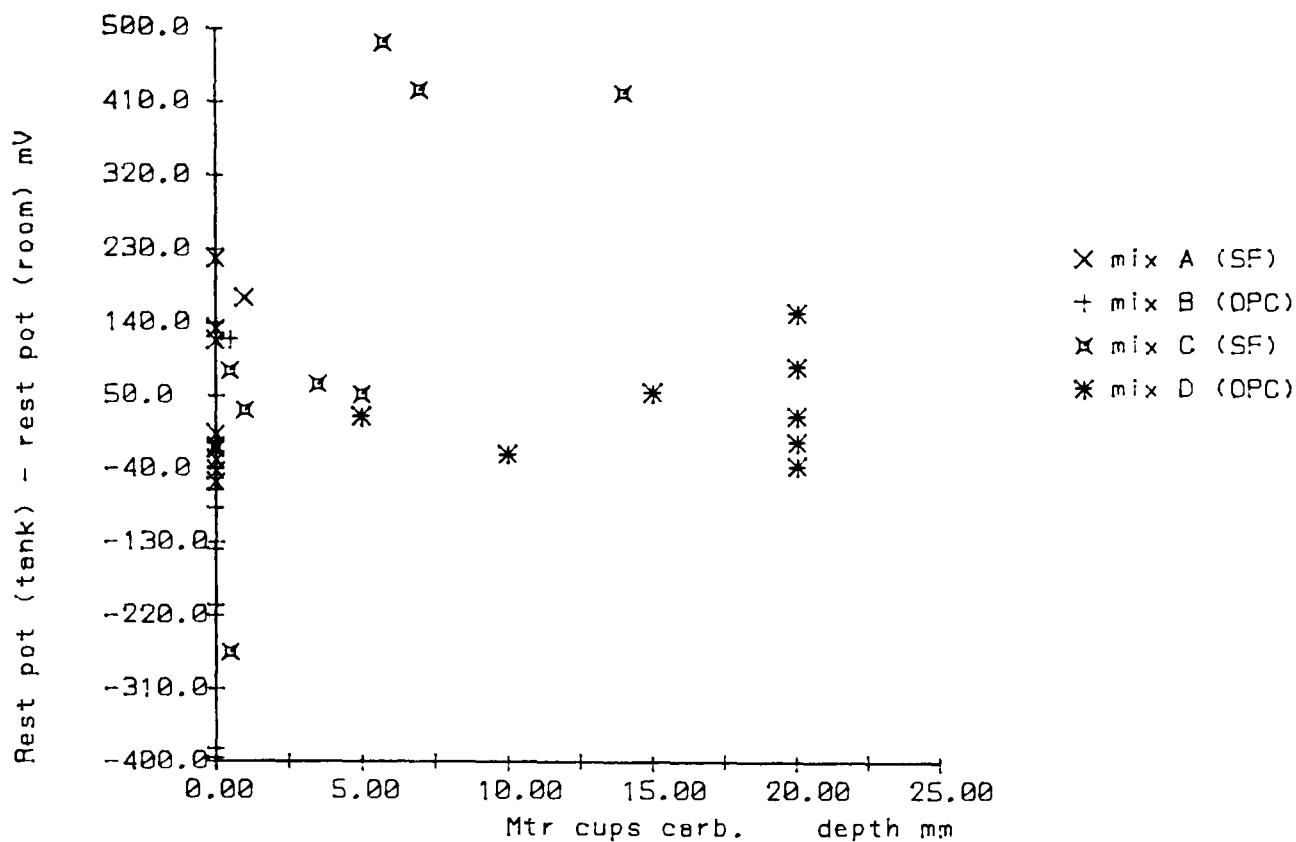
Fig. 3.20 Showing the relationship between the difference in the rest potential caused by carbonation and the carbonation depth measured with phenolphthalein. The rest potentials were measured on initial exposure to solution. Carbonation measurements are described in the next chapter. Carbonation caused an increase of up to 500mV in the rest potential.
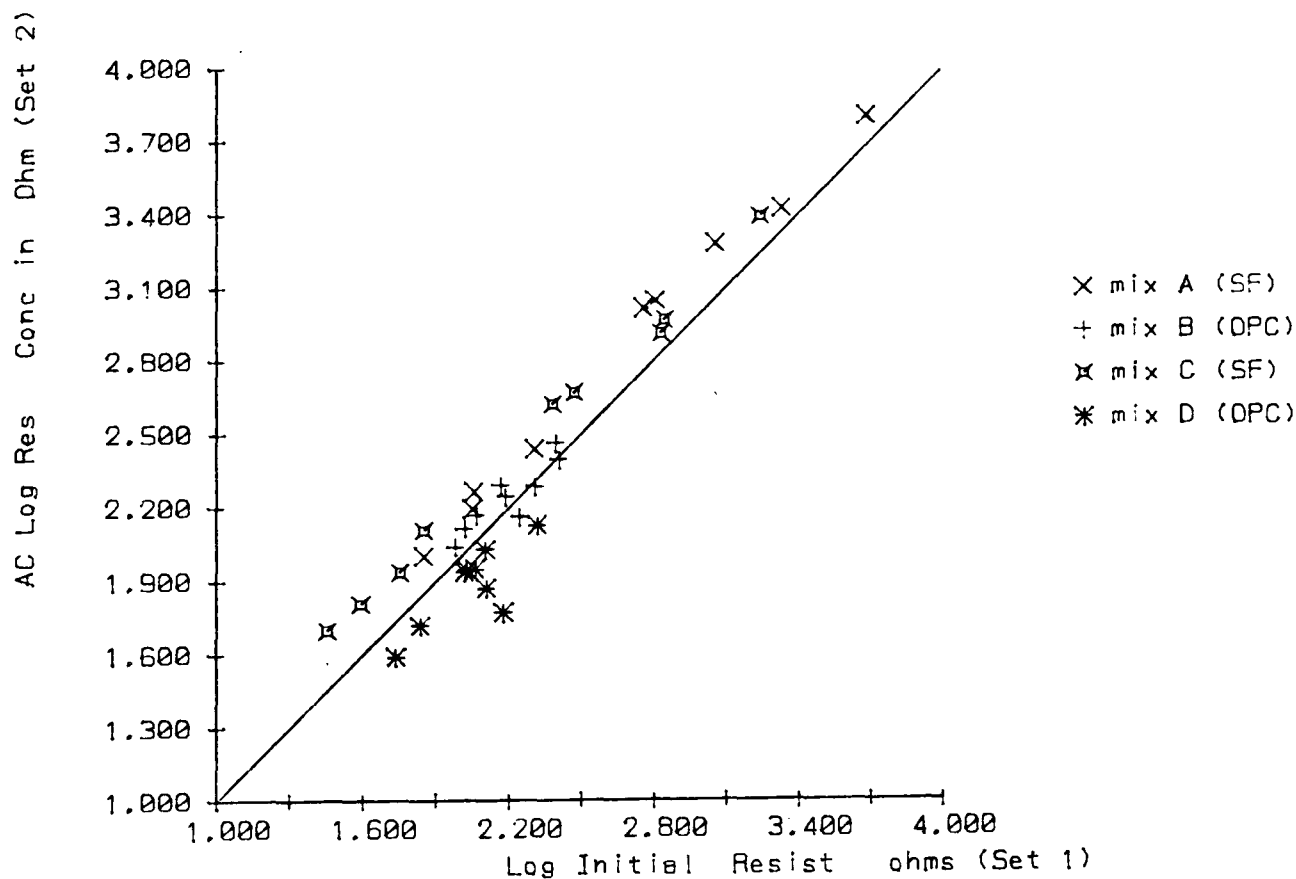
Fig. 3.21 Showing the relationship between the a.c. resistances of the two sets of samples when first exposed to the salt solution. The results show the excellent repeatability of this measurement.
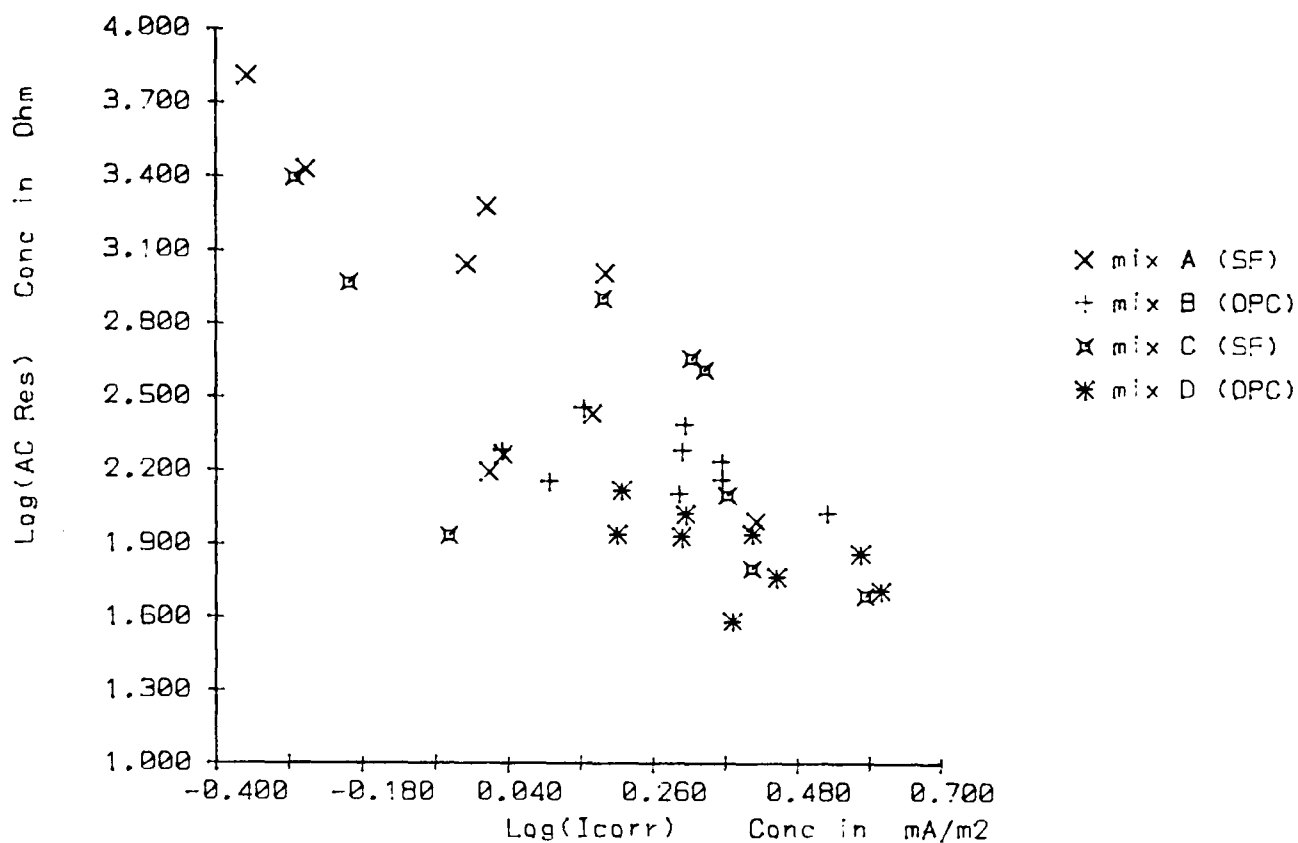
Fig. 3.22 Showing the relationship between the a.c. resistance and the corrosion current fot the set 2 concrete samples on initial exposure to the salt solution. The values for corrosion current had already been corrected for errors to the linear polarisation measurements caused by resistivity so this graph shows resistivity directly reducing the corrosion rate.
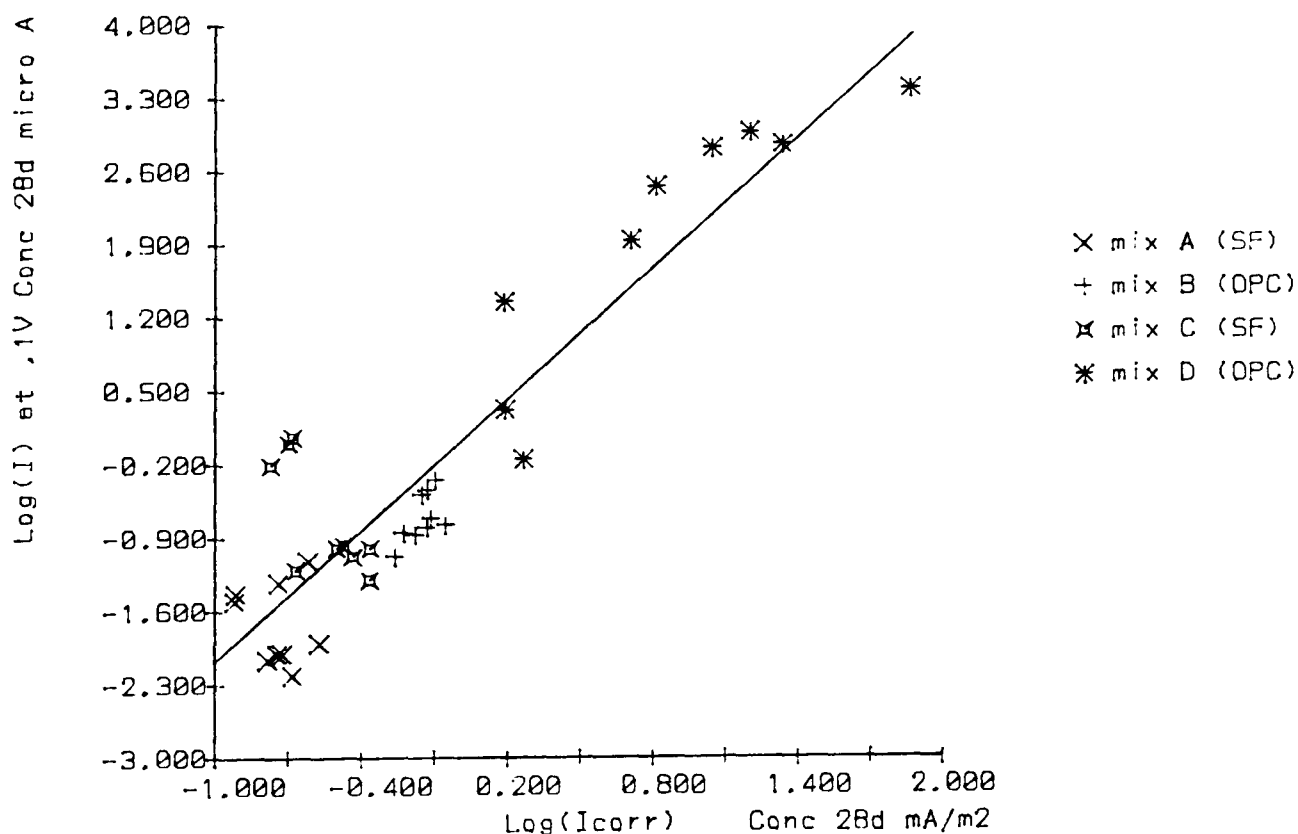
Equation for line : Y=2.223755512E-2+X*2.086281943
R squared=0.840

Fig. 3.23 The relationship between current at +100 mV and corrosion current in open circuit for set 2 concrete samples after 28 days exposure to the solution with the applied anodic voltage. The graph indicates that measuring the current can give a measure of corrosion rate.

Curing Condition 1   Curing Condition 2   Curing Condition 3

X mix A (SF)   + mix B (OPC)   ⋈ mix C (SF)   ✳ mix D (OPC)
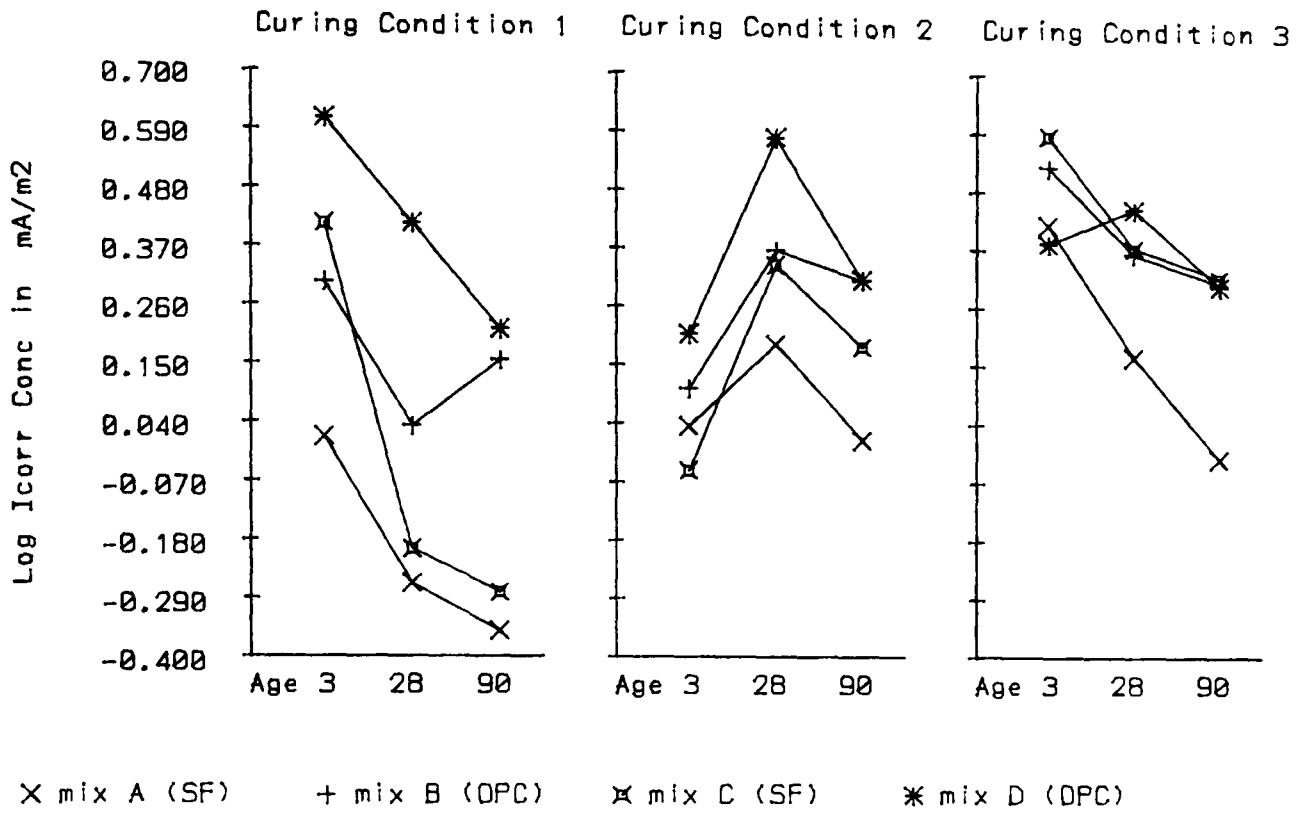
Fig.3.24 Corrosion rate for main (set 2) concrete samples when first exposed to salt solution.

Curing Condition 1   Curing Condition 2   Curing Condition 3

X mix A (SF)   + mix B (OPC)   ⋈ mix C (SF)   ✳ mix D (OPC)
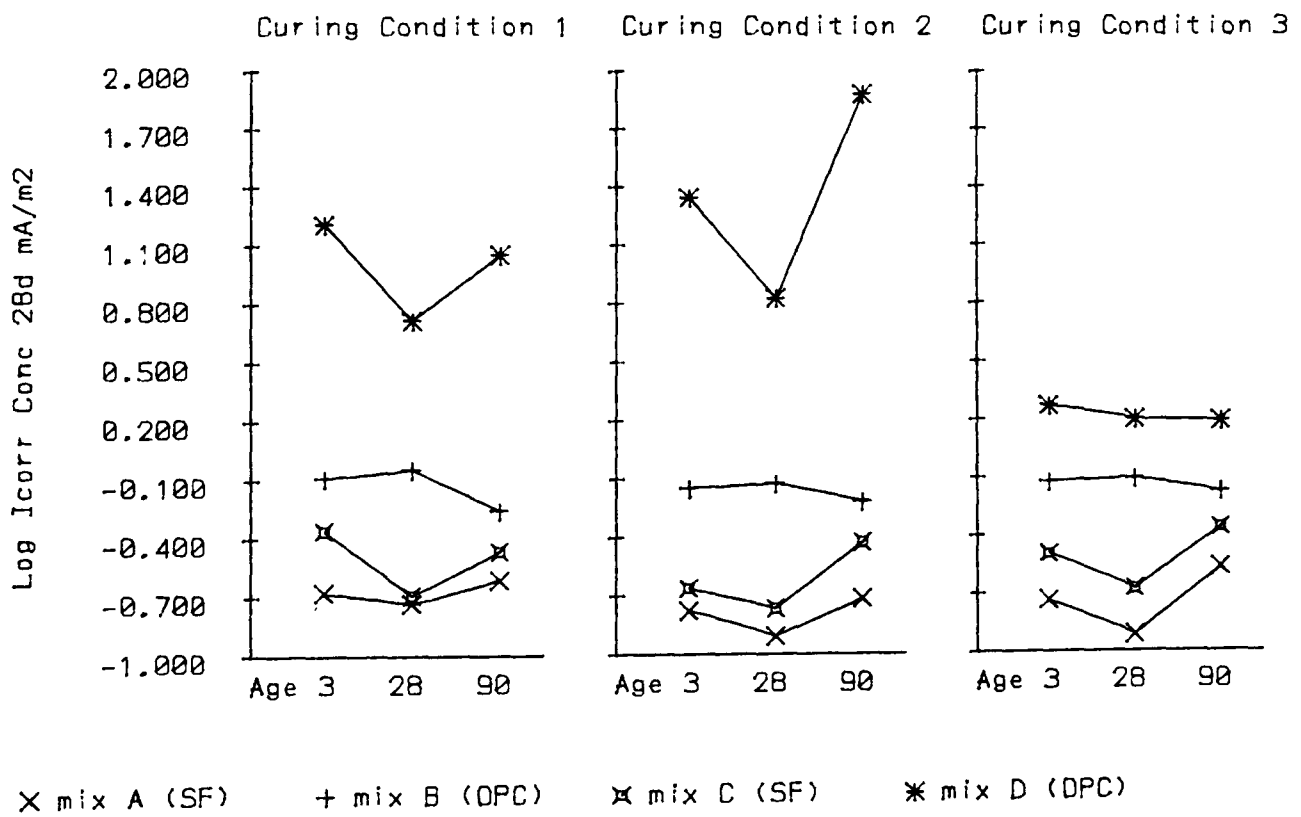
Fig.3.25 Corrosion rate for main (set 2) concrete samples after 28 days exposure to salt solution.

Curing Condition 1   Curing Condition 2   Curing Condition 3

Log Icorr Mtr 28d   ta mA/m2
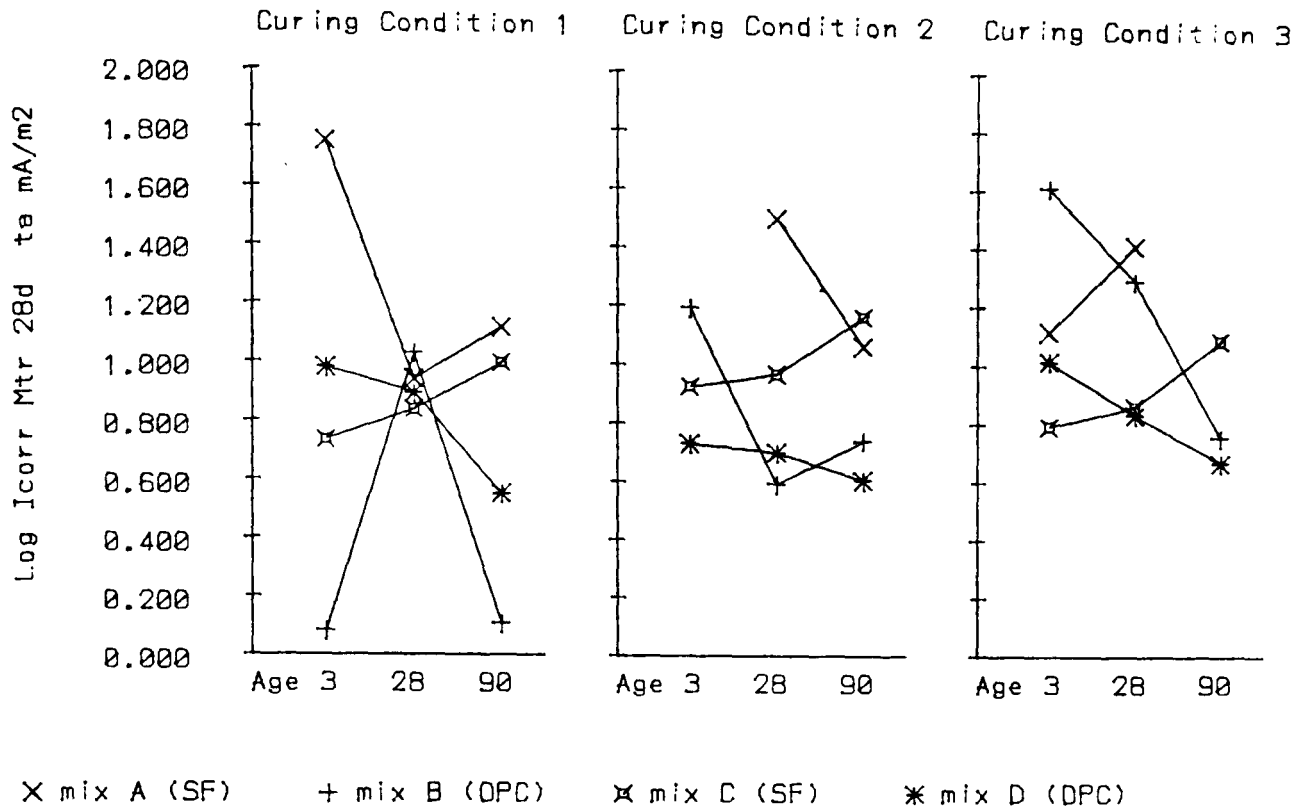
Fig.3.26   Corrosion   current   of   mortar   samples   from
carbonation tank when first exposed to salt solution. Two
mix A values are missing because the applying the correction
for mortar resistance made them negative.

Curing Condition 1   Curing Condition 2   Curing Condition 3

Log Icorr Mtr 28d   rm mA/m2

X mix A (SF)   + mix B (OPC)   ⋈ mix C (SF)   ✻ mix D (OPC)
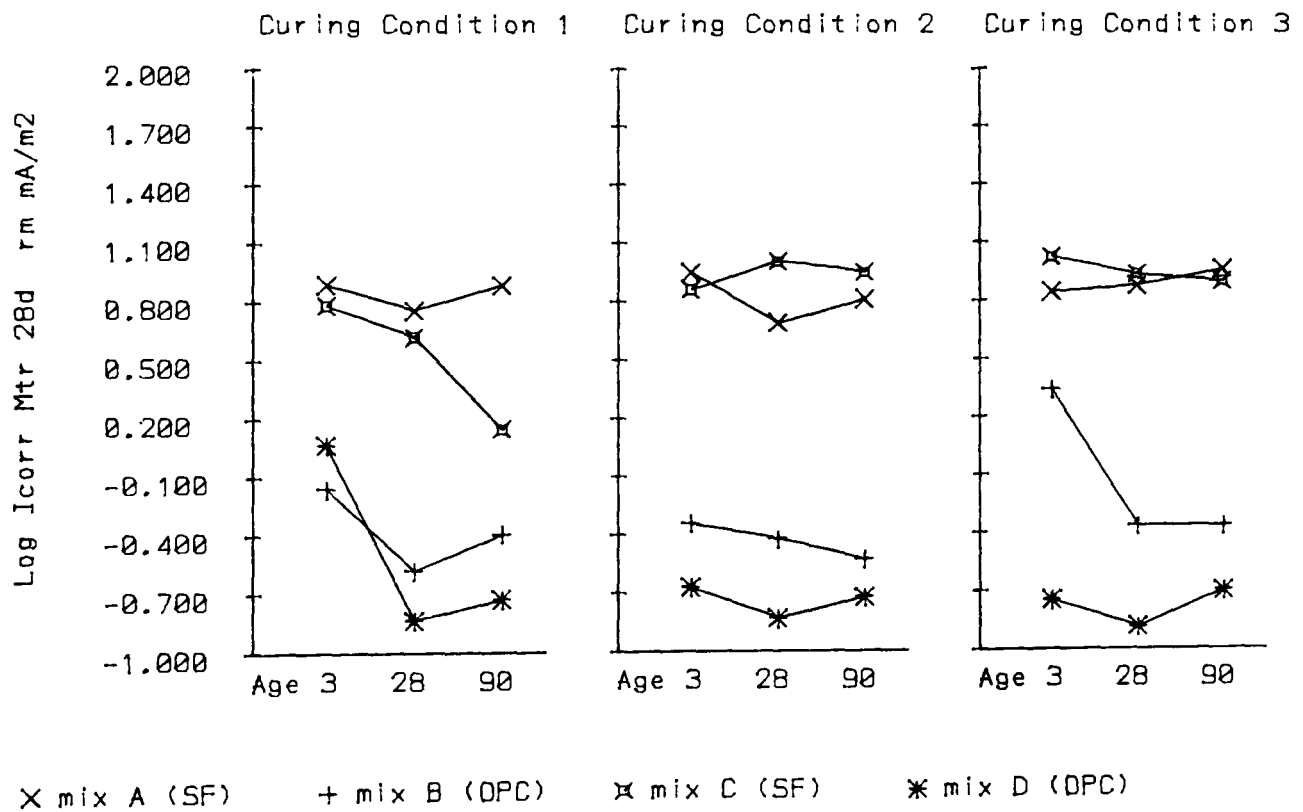
Fig.3.27 Corrosion current of mortar control samples when
first exposed to salt solution.
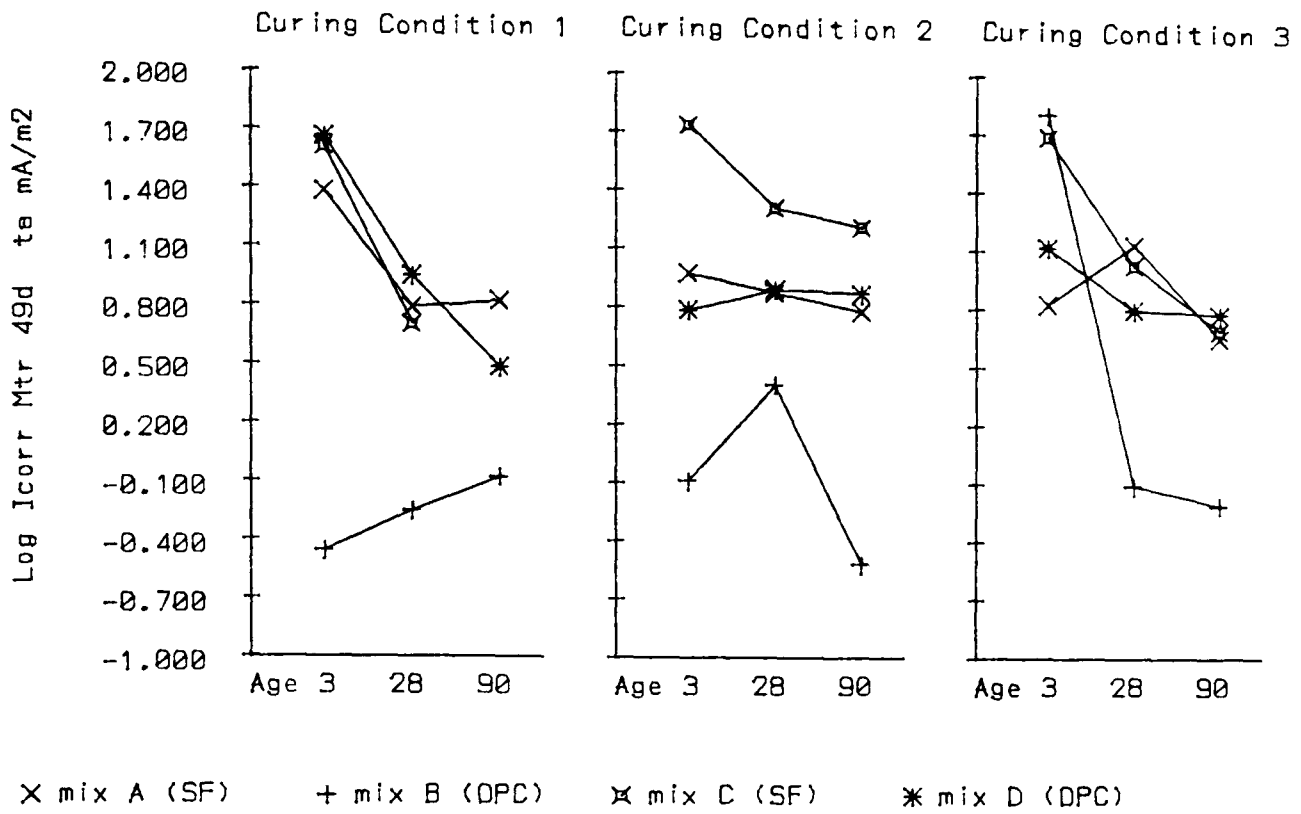
Fig.3.28 Corrosion current of carbonated mortar samples after exposure to salt solution.
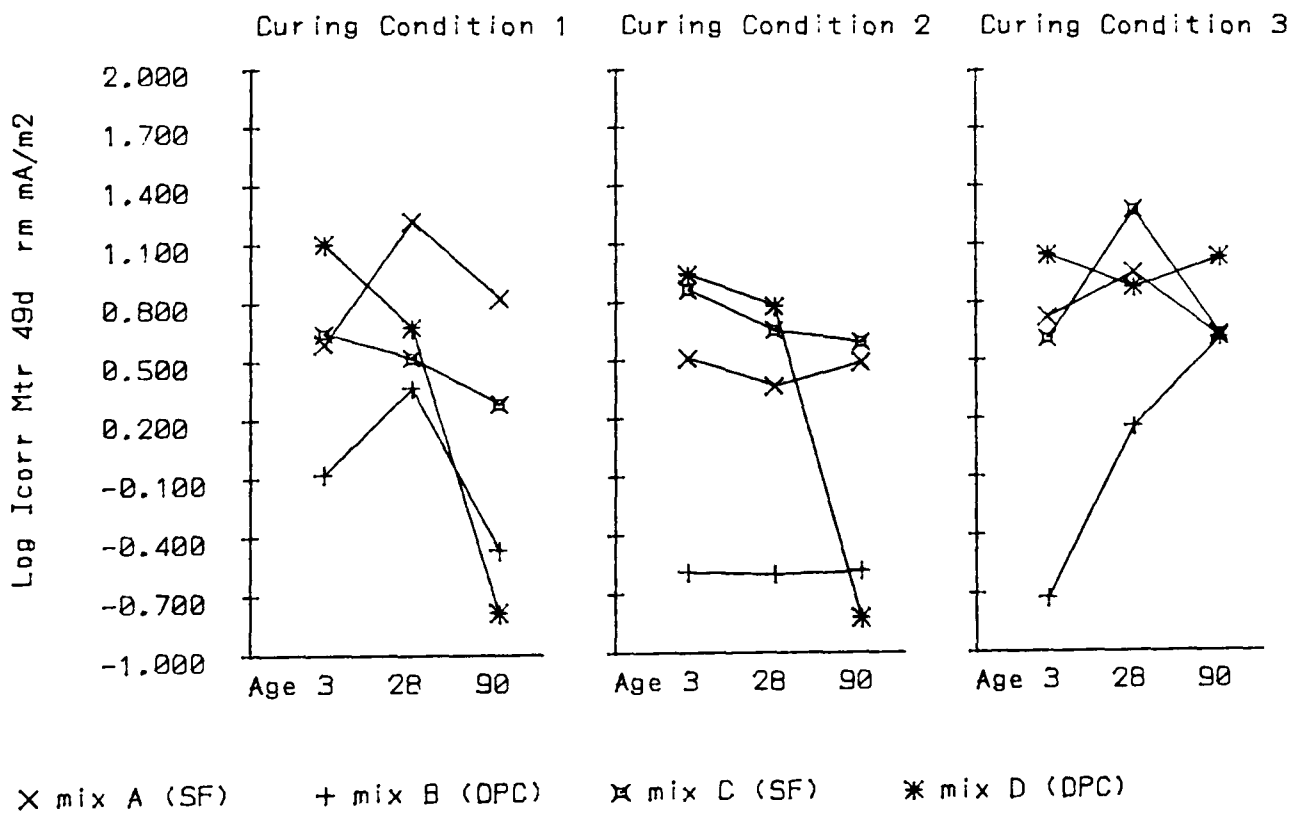
Fig.3.29 Corrosion current of control mortar samples after exposure to salt solution.

4 Carbonation and Drying Shrinkage.

4.1. Apparatus for accelerated carbonation.

4.1.1 The apparatus.

It is known that the rate of carbonation of cementitious materials is strongly dependent on relative humidity (RH) and decreases at very low and very high humidities (Neville 1981). Carbonation is a chemical reaction caused by the ingress of carbon dioxide gas into the sample and will therefore also be dependent on temperature, gas pressure and CO_2 concentration. The apparatus to accelerate carbonation was therefore constructed to expose the samples to an environment where these four variables could be controlled.

The apparatus went through a number of stages of development but since the changes were primarily intended to make it easier to use and more reliable and did not greatly affect the samples it will only be described here in its final form. The original construction was started as part of another project (Cabrera et.al.1985) but the external circuit to condition the gas outside the sample tanks and pump air into the system was introduced as part of this project. The apparatus is shown schematically in fig.4.1. A larger apparatus without the capability to sustain pressure has been described by Dhir et.al.(1985).

4.1.2 Control of relative humidity.

In the apparatus it is at present only possible to lower the humidity, not to raise it. Because water is produced in the carbonation reaction it is necessary to have a relatively powerful de-humidification system. This consists of a pair of heaters rated at 100W and 150W to warm the gas followed by a cold radiator to precipitate the moisture. The cooling system for the cold radiator is similar in mechanism and size to a domestic refrigerator with a compressor. The gas is blown across the cold radiator by a fan and may return through a large bypass pipe. This enables gas to pass across the heater and cold radiator several times before continuing round the circuit. The water is extracted through a drain. The humidity is measured with an electronic probe in one of the sample tanks.

4.1.3 Control of temperature.

The temperature was controlled by keeping the apparatus in a temperature controlled room. The sample tanks were made of aluminium which has a high thermal conductivity and the temperature of the gas was checked with the same probe as the RH. It was not found to be necessary to use the heating and cooling systems in the de-humidifier to control temperature but this is available if required.

4.1.4 Control of pressure.

The system was designed for a safe working pressure of 1 atmosphere above ambient. The pressure vessels containing the samples are substantially built aluminium castings originally made for paint spraying. The humidity control vessel is constructed of welded 6mm. steel plate. The connecting pipes are reinforced 12mm diameter flexible PVC. The pressure is measured with pressure gauges on both sample vessels.

4.1.5 Control of CO_2 content.

A standard cylinder of industrial grade CO_2 is used. In order to achieve 88% concentration used in this project the following procedure was used:

1. Start with apparatus full of air at 1 atmos.(i.e.ambient)

2. Pressurise with CO_2 and mix by running pump to give 50% CO_2 at 2 atmos. (i.e 1 atmos. above ambient)

3. Release through vent to lower pressure to 1 atmos.

4. Repeat stages 2 and 3 to give 75% CO_2 at 1 atmos.

5. Pressurise to give 87.5% CO_2 at 2 atmos.

Small samples may be drawn from the exhaust for testing for CO_2 content with a system that depends on measuring the loss of volume when the gas is exposed to potassium hydroxide which absorbs the CO_2. The concentration may then be adjusted by introducing CO_2 from the cylinder or air with the pump.

4.1.6 Control of the total system.

The system is at present controlled manually but the switching has been collected into a single box in preparation for automatic control. This will include sensors for the four variables and control of the electrical components and the valves. The solenoid cut out is necessary because the pump cannot start under pressure and when left running it would otherwise burn out in the event of a temporary power failure.

4.2 Measurement of strain.

The samples for strain measurement were cast measuring 25mm. square by 200mm. long. Each prism had a set screw with a rounded tip cast in each end as shown in fig. 4.2. The strain of the samples was measured both with a mechanical dial gauge and with an electronic linear displacement transducer. By comparing the strain readings at two different exposure times for each system a better correlation was found for the electronic system (R^2 was .89 compared to .76). For this reason the results from the electronic system were used but both systems are considered to be basically comparable. The improved results from the electronic system were probably due to the better condition of the contacts to the samples. Any small particle of corrosion or dirt on the contacts causes a major error. The electronic system was calibrated from the mechanical gauge with a best line fit to all of the readings and checked with feeler

gauges.

4.3 Measurement of carbonation.

4.3.1 Strain.

Carbonation causes shrinkage in concrete (Neville 1981) and this effect may be used to detect it. Unfortunately drying also causes shrinkage and it is difficult to separate the two effects if they occur at the same time. The carbonation measured from shrinkage is a combined effect of the depth of carbonation and the exact degree of carbonation within the carbonated layer.

4.3.2 Phenolphthalein.

The traditional method of measuring carbonation is by spraying a freshly broken surface with phenolphthalein. This is a simple method to use and specially suited for site measurements (e.g. Smith and Evans 1986). This method gives an indication of the depth of carbonation but no indication of the relative degree of carbonation at a particular point beyond the binary information from the colour change. A particular hazard has been observed when mortar samples are carbonated under pressure in that an area was observed on the mix D samples with small spots of colour about 1mm. across with clear areas between them. At first sight this appears to be uncarbonated (coloured) but comparison with other readings indicate that it is definitely carbonated. This effect is probably caused by CO_2 being forced under pressure down large pores, possibly associated with the aggregate, but not penetrating the areas between them.

4.3.3 Resistivity.

The electrical a.c. resistivity of carbonated samples has been measured (see chapter 3). The ratio of resistivities of carbonated and uncarbonated samples is proposed as a measure of carbonation. The increase in resistivity caused by carbonation has been observed by previous workers (Browne et.al. 1983) and is believed to be a result of the calcium hydroxide being an important agent in the conduction process. Measurements of carbonation in this way would be of the combined effect of depth and degree as with strain measurements.

4.3.4 TG analysis.

The degree of carbonation in samples has been measured by thermogravimetric analysis (see chapter 11 for details). This will give no indication of the area of carbonation just of the degree of carbonation at one point.

4.4. Experimental procedure.

4.4.1 Exposure environments for all samples.

The carbonation tanks were kept at 70% RH, 21°C, one atmosphere pressure above ambient and 88% CO_2. Some samples were also kept in the controlled environment test room outside the tanks where the conditions were identical except for the CO_2 content. Samples kept in the room were used as controls for short term exposure but concrete samples kept in it for one year were tested for carbonation.

4.4.2 Mortar samples (prisms).

Prisms were cast as shown in fig.4.2 for measurement of strain. After curing, the prisms were placed in the test room for 24 hours to dry. They were then placed in the carbonation tanks. The length of the prisms was measured after casting, after curing, after drying, after 4 days of exposure, and after 18 days when the samples were removed from the tanks. When the final measurement was completed the prisms were broken and the depth of carbonation was measured by spraying the broken surfaces with phenolphthalein.

4.4.3 Mortar samples (cylinders).

Cylinders measuring 100mm long by 25 mm diameter were cast with 100mm long by 6m diameter ms bars on the axis projecting 20mm from one end as shown in fig.4.2. After curing and 28 days in the tanks the ac resistivity was measured. 2 cylinders per condition were exposed and 2 more were kept in the test room for control.

4.4.4 Mortar samples (cups).

Two samples per condition were cast in plastic cups and after curing and 28 days in the tanks they were broken and the carbonation depth was measured with phenolphthalein. Due to the geometry of the samples the maximum measurable depth was 20mm.

4.4.5 Concrete samples.

Two 100mm cubes were cast for each condition and after curing they were stored in the test room. After one year of exposure they were broken and the carbonation depth was measured with phenolphthalein. Samples were also drilled from the outer 1mm. and from the centre of one of the cubes and tested by thermogravimetric analysis.

4.5 Results and Discussion.

4.5.1 Drying shrinkage.

The results for strain measured during curing are in fig.4.3, those for the 24 hour drying period are in fig.4.4 and the combined strain during curing and drying is shown in fig.4.5. The anomalous readings (such as that for mix A CC2 age 28 in fig.4.4) were caused by dirt on the contacts as discussed in section 4.2.

The differences between the low w/c ratio mixes (A and B) and the high w/c ratio

mixes (C and D) give rise to two opposing effects. The change in w/c ratio would be expected to cause less shrinkage in mixes A and B but they also have lower aggregate contents which would tend to make them shrink more. Neville (1981) presents data which indicates that the effect of w/c ratio would be slightly greater than the effect of the aggregate so mixes C and D would be expected to shrink slightly more.

In fig.4.3 it may be seen that in wet curing (CC1 and CC3) mixes B and C expanded most. The swelling seems to have been very rapid and did not increase with continued curing after 3 days. In dry curing (CC2) the SF mixes A and C showed greatest shrinkage. The shrinkage of the OPC samples was substantially recovered by 28 days (CC2 samples were placed in water after 7 days) but, assuming that the mix A 28 day reading was not accurate, there is no evidence of the shrinkage of the SF mixes recovering to the same extent. Fig.4.4 shows that the 3 day samples showed greatest shrinkage during drying as expected. The combined effect in fig.4.5 is of interest because the CC2 results give evidence of the SF mixes shrinking more at all ages.

4.5.2 Carbonation.

The shrinkage during carbonation is shown at 4 days in fig.4.6 and at 18 days in fig.4.7. The increase of shrinkage with age is due to the slower drying of the older samples, causing them to dry during exposure, rather than during the 24 hours of drying outside the tanks. The main effect was, however, that the low w/c mixes shrank substantially more than the others. This can be seen for the 18 day results and to a lesser extent for the 4 day results. All of the other measures of carbonation show conclusively that the low w/c mixes carbonated most so the only explanation can be that a drying shrinkage effect has dominated the readings.

The carbonation depth measured with phenolphthalein on the mortar cups is shown in fig.4.8 and its relationship with that measured on the mortar prisms and the concrete cubes is in figs.4.9 and 4.10. These graphs indicate that this measurement is not very repeatable but the repeatability is not any worse between mortar exposed in the tank and concrete exposed in the room than between two sets of mortar samples exposed in tank.

The relationship between the resistivity measurement and the phenolphthalein measurement on the mortar cups and the concrete is shown in figs.4.11 and 4.12. It may be seen that the carbonation causes the resistivity to increase by a factor of up to 10. It is difficult to assess the resistivity measurements from the phenolphthalein results because of the known limitations of the phenolphthalein method.

No relationship was found between the thermogravimetric readings and the other measurements. The ratio of the calcium carbonate to the total of calcium carbonate+calcium hydroxide was calculated to give a measure of the proportion of available hydroxide which had carbonated but still no relationship was found. The results for the inner samples from the centre of the cubes are in fig.4.13 and those for the surface are in fig.4.14. (The calcium hydroxide contents of these samples are

shown with the other thermogravimetric results in figs.11.8 and 11.9). It is of note that in the outer samples (fig.4.14) the carbonate content is highest for mix C (SF) despite the relative lack of calcium hydroxide available for carbonation.

4.6. Conclusions.

1. An apparatus has been constructed which will form the basis of an automatic system for providing a fully controlled environment for accelerated carbonation.

2. In order to measure carbonation strain it would be an advantage to dry the samples in a CO_2 free environment before exposure. Vacuum drying might be a good method for this.

3. Measurements of carbonation with phenolphthalein were not found to be very repeatable.

4. Measurement of resistivity may be a good way to measure carbonation. Further research in this area would be necessary to prove the method. It could be used on site by measuring the resistance between the surface and the reinforcement while carrying out a potential survey. It could indicate areas of carbonation which would be useful when interpreting the survey and assessing the state of the structure.

RADIATOR

VALVE

FAN

CAPILLARY TUBE

COMPRESSOR

ELECTRIC MAINS SUPPLY

SOLENOID CUT OUT

CONTROL BOX

REFRIGERANT CIRCUIT

COOLING

HEATER 1

HEATER 2

DEHUMIDIFIER

DRAIN

PUMP

BYPASS

INLET/ EXHAUST

CIRUIT FOR CO2 & AIR

HUMIDITY/TEMP PROBE

PRESSURE GAUGES

CO2 SUPPLY VIA

PRESSURE REGULATOR

SAMPLE TANK

SAMPLE TANK
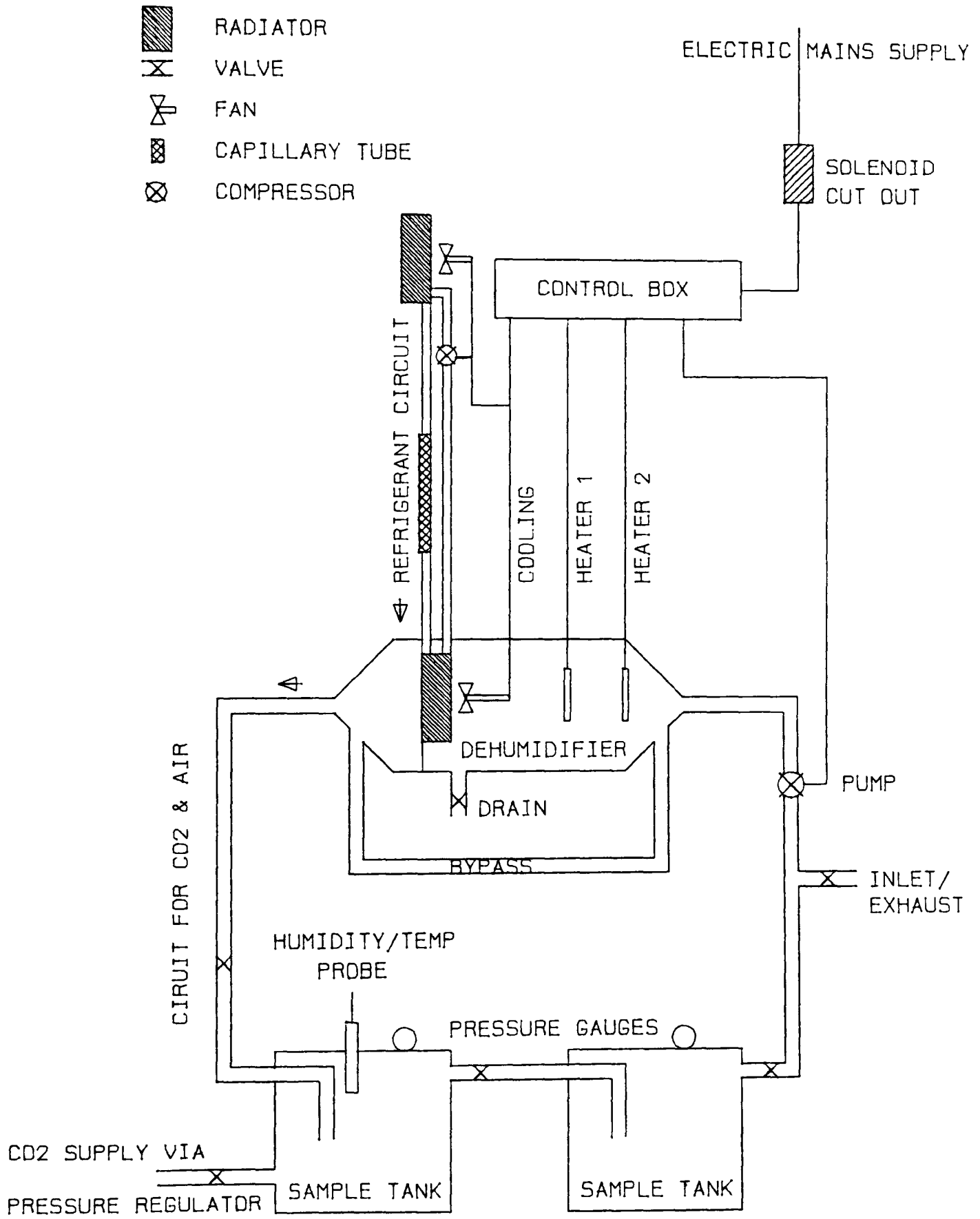
Fig 4.1

Apparatus for accelerated carbonation of paste and morter samples.

200mm

25mm sq.

S/S SET SCREWS

PRISM

6 dia

20

100

20

25 dia
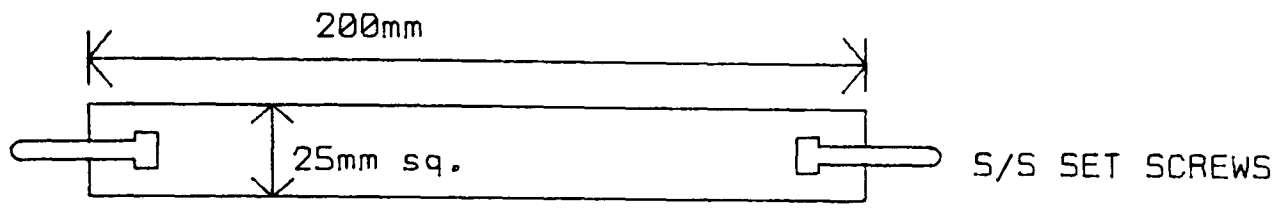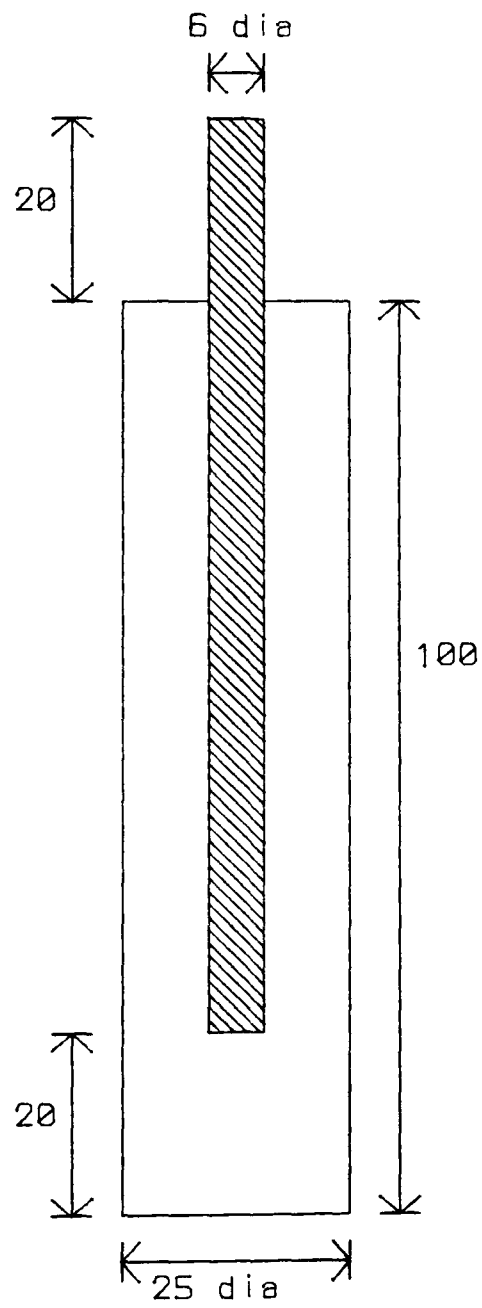
CYLINDER

Fig 4.2 Geometry of carbonation samples
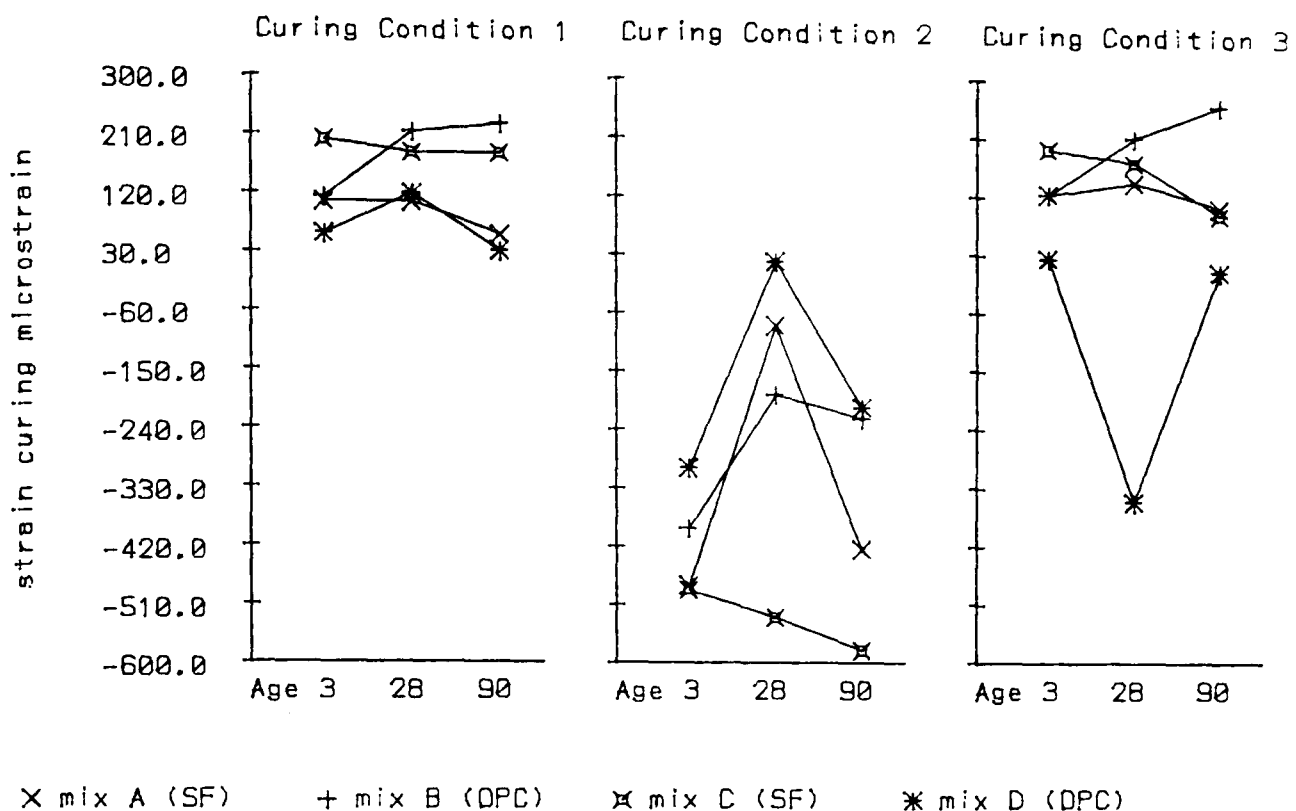
Fig. 4.3 The strain recorded by measuring the mortar prisms with the linear displacement transducer before and after curing. The shrinkage observed for the curing condition 2 samples was caused by the dry curing.
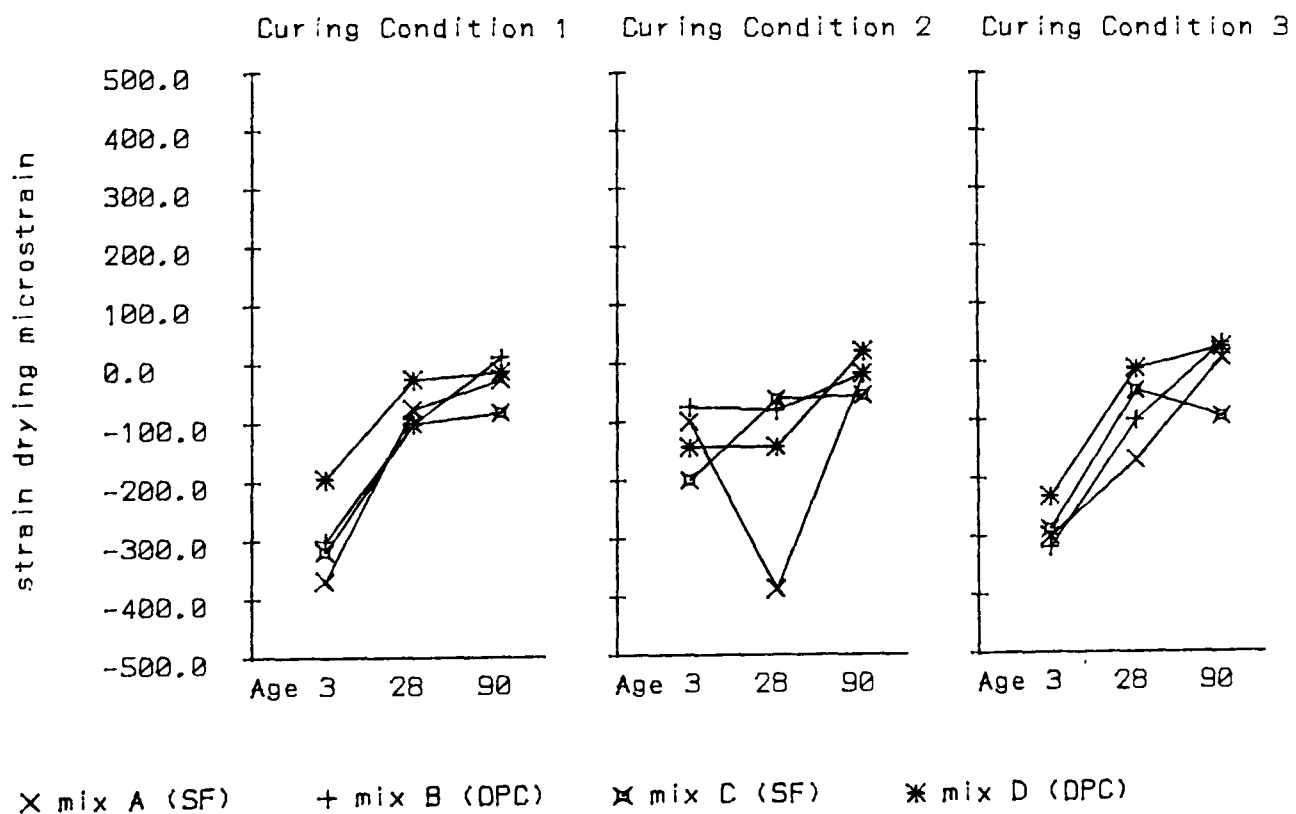
Fig. 4.4 The strain during the 24 hour drying period before exposure to carbon dioxide.
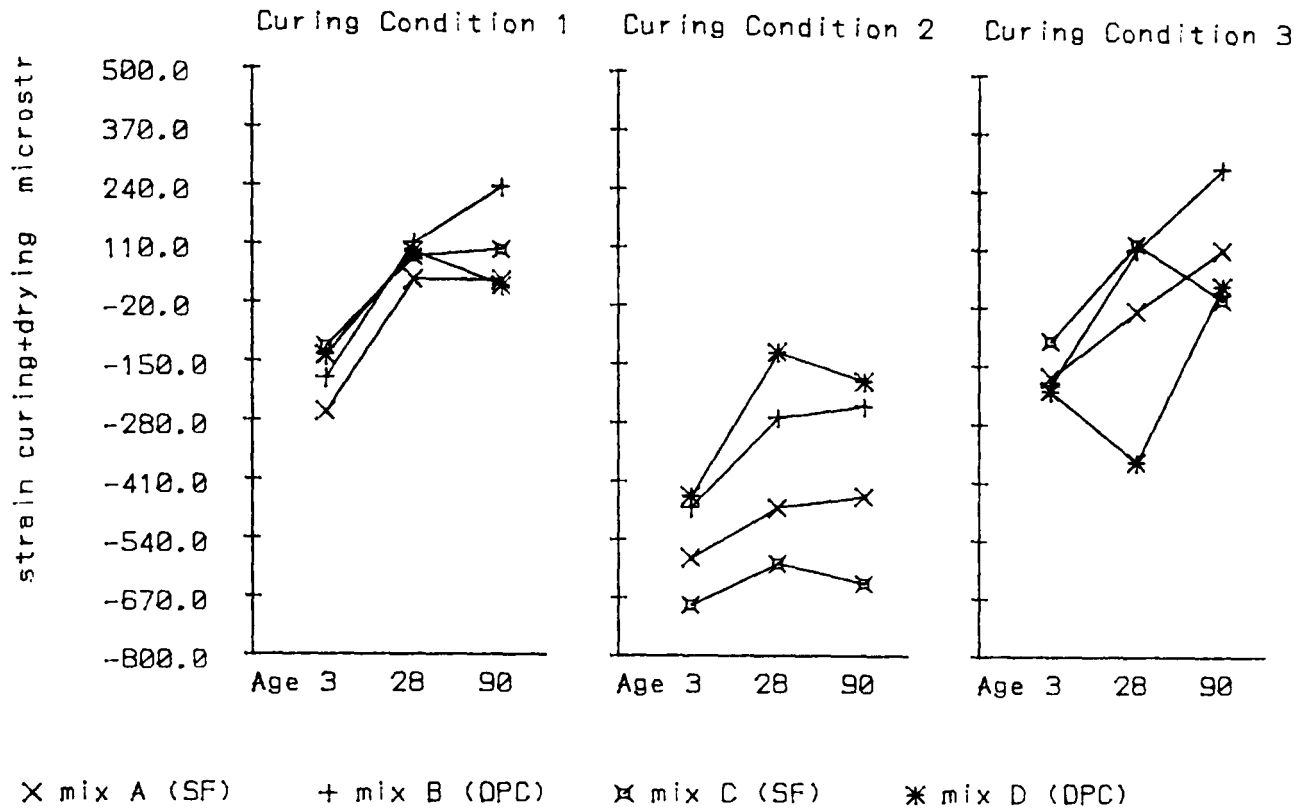
Fig. 4.5 The total of the strain for curing and drying shown in figs.4.3 and 4.4. The SF mixes show greater shrinkage in curing condition 2 indicating a greater sensitivity to dry curing.
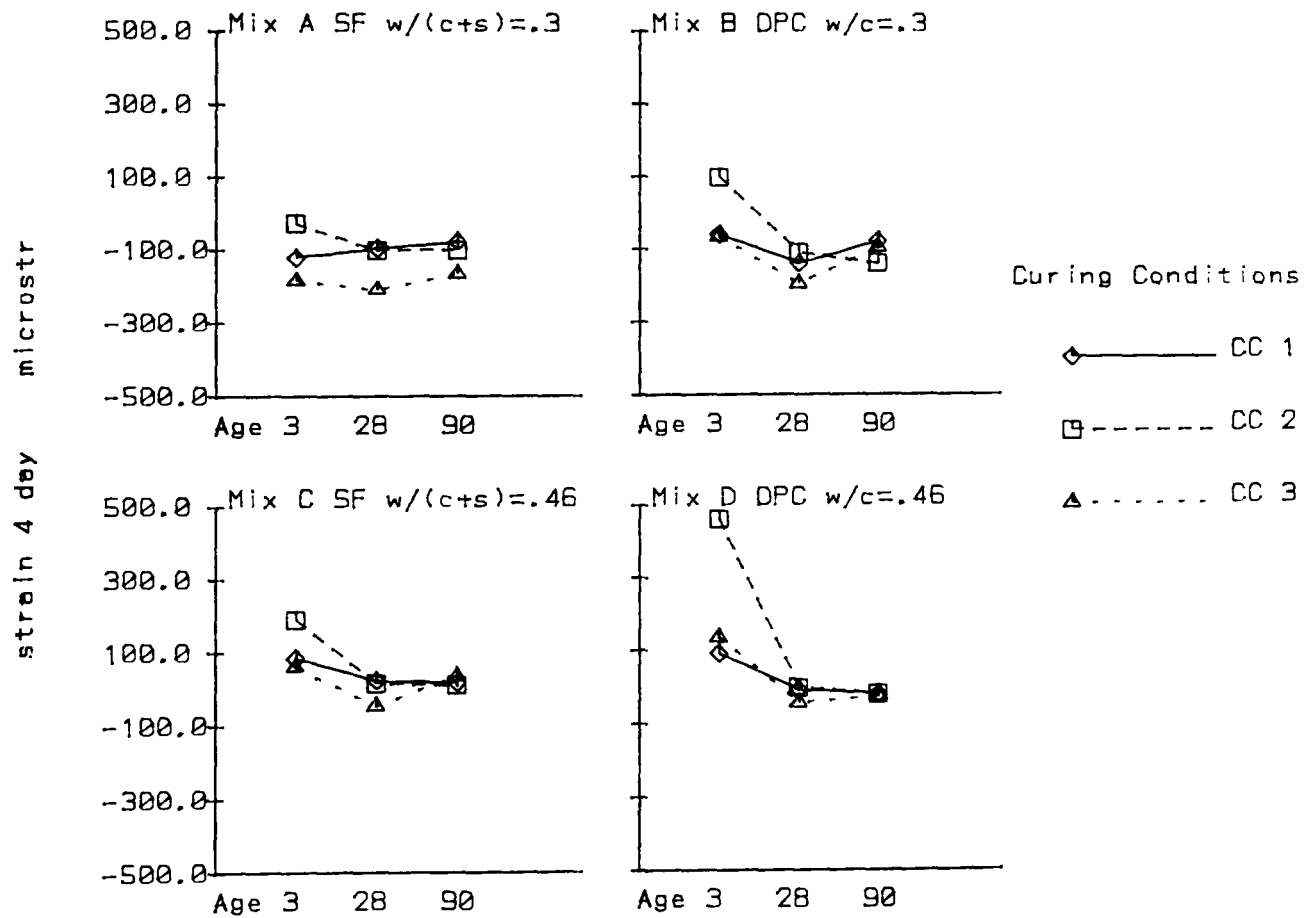
Fig. 4.6 Strain measured during the first four days of carbonation.
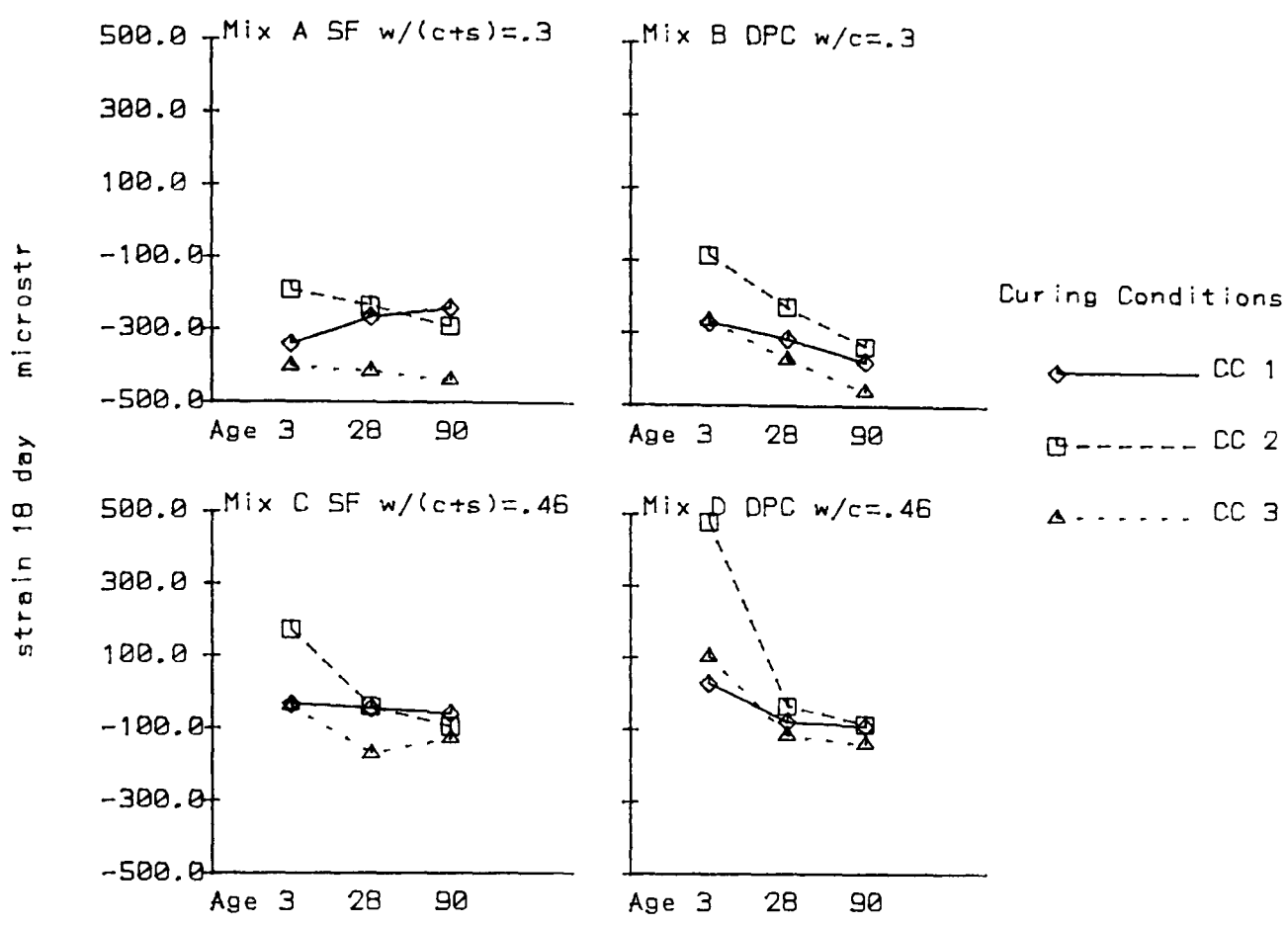
Fig. 4.7 The final results for the strain of the mortar prisms after 18 days of exposure.
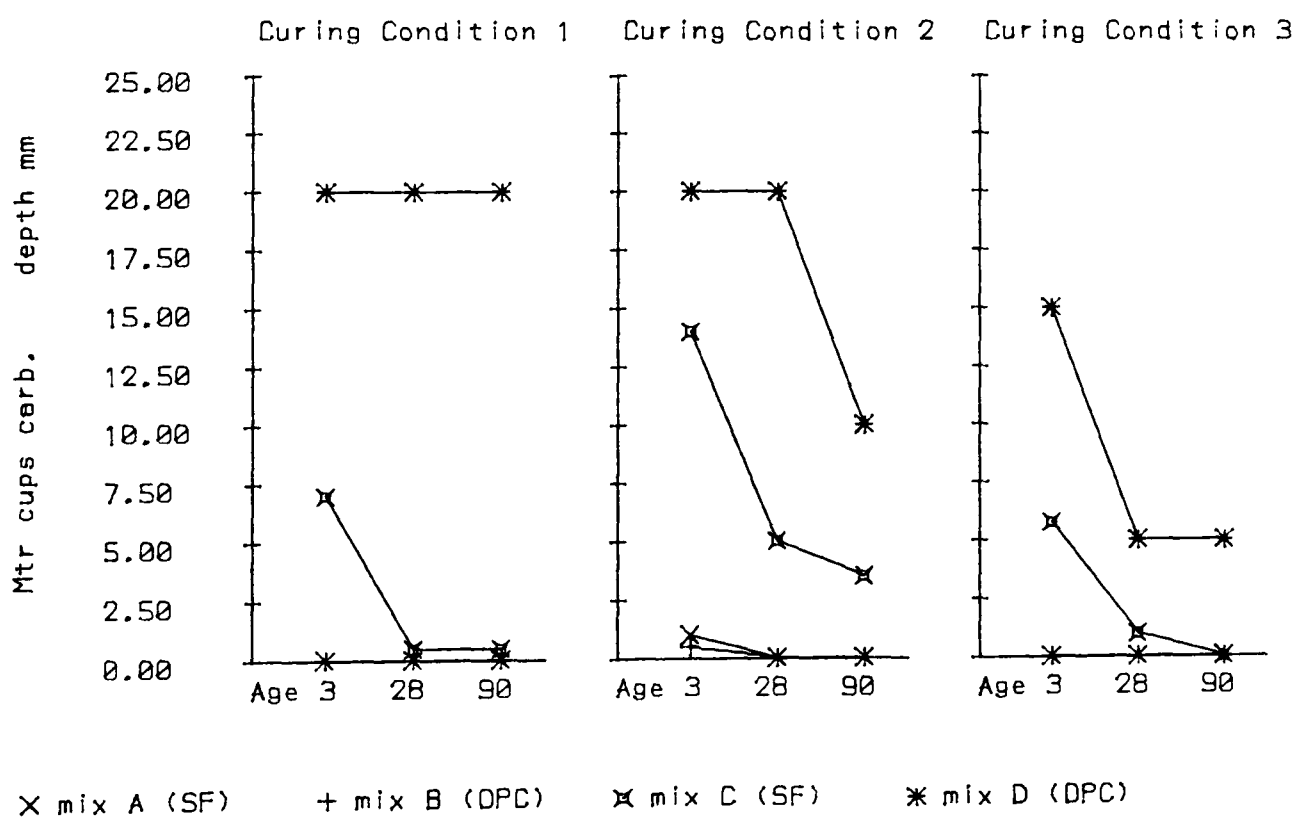
Fig. 4.8 Depth of carbonation of mortar samples measured with phenolphthalein after 28 days carbonation.
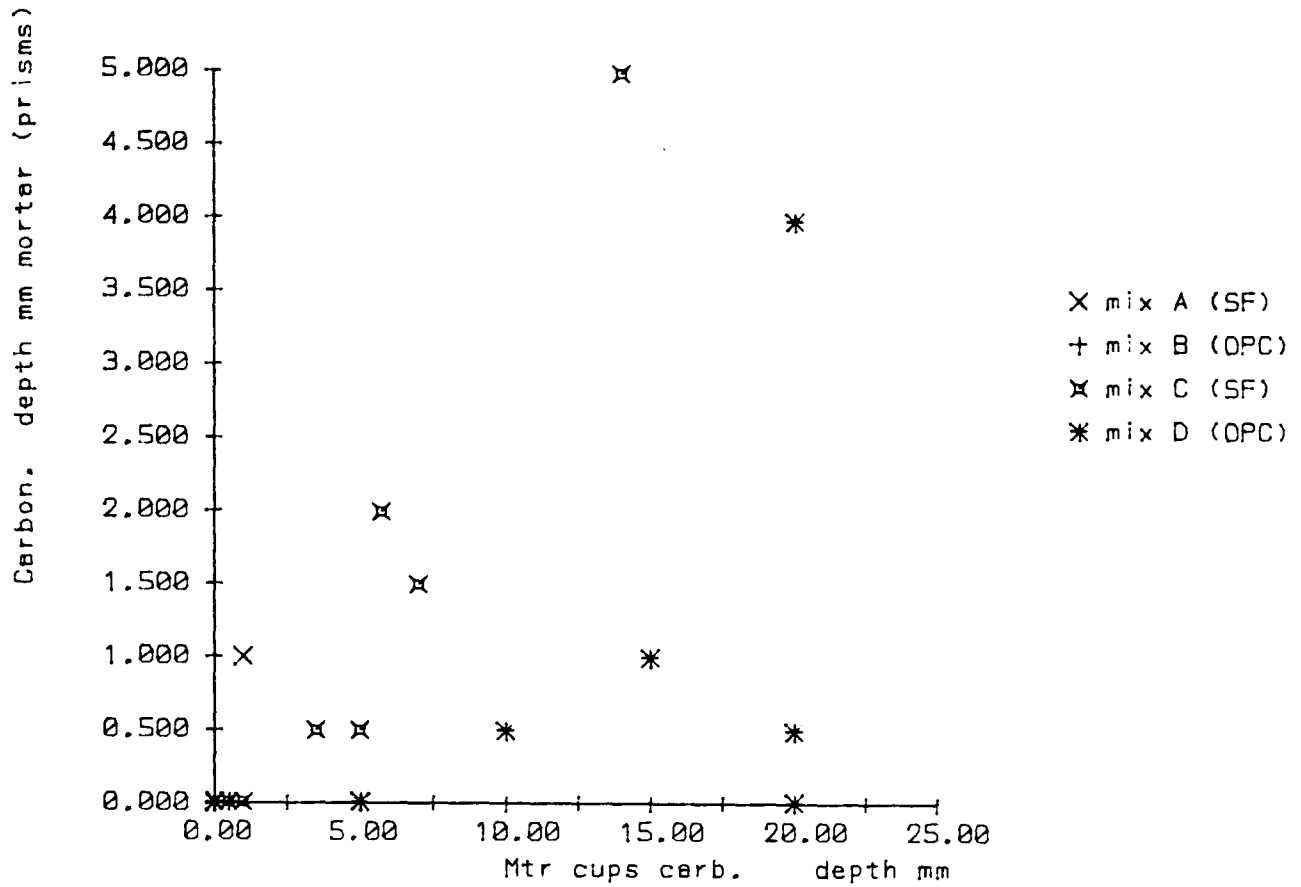
Fig. 4.9 Comparison of two sets of data for carbonation depth measured with phenolphthalein. The prisms were exposed to carbon dioxide for 18 days and the cups for 21 days.
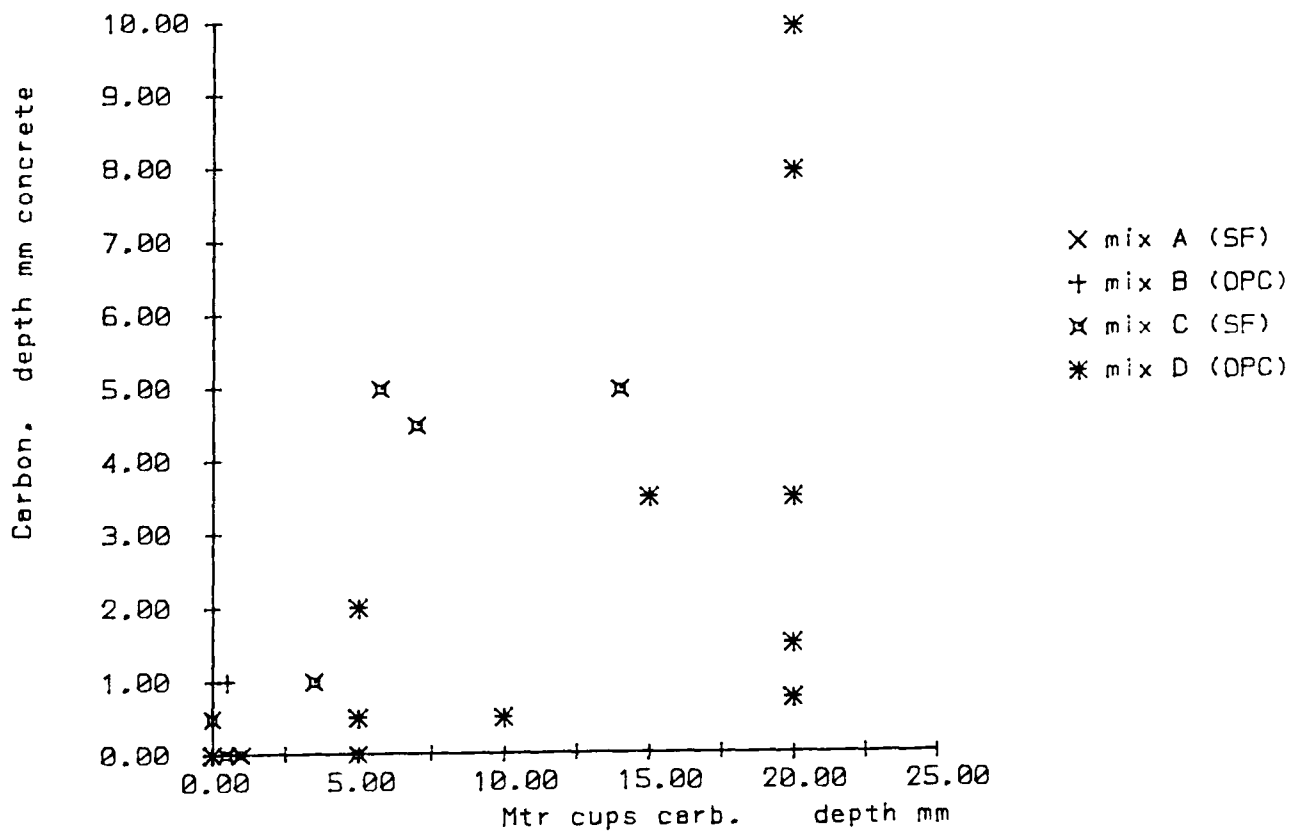
Fig. 4.10 Another comparison of data sets for carbonation depth measured with phenolphthalein. (see fig.4.9 above). The concrete samples were exposed to room air for one year. These two graphs show that this standard method is not very repeatable.
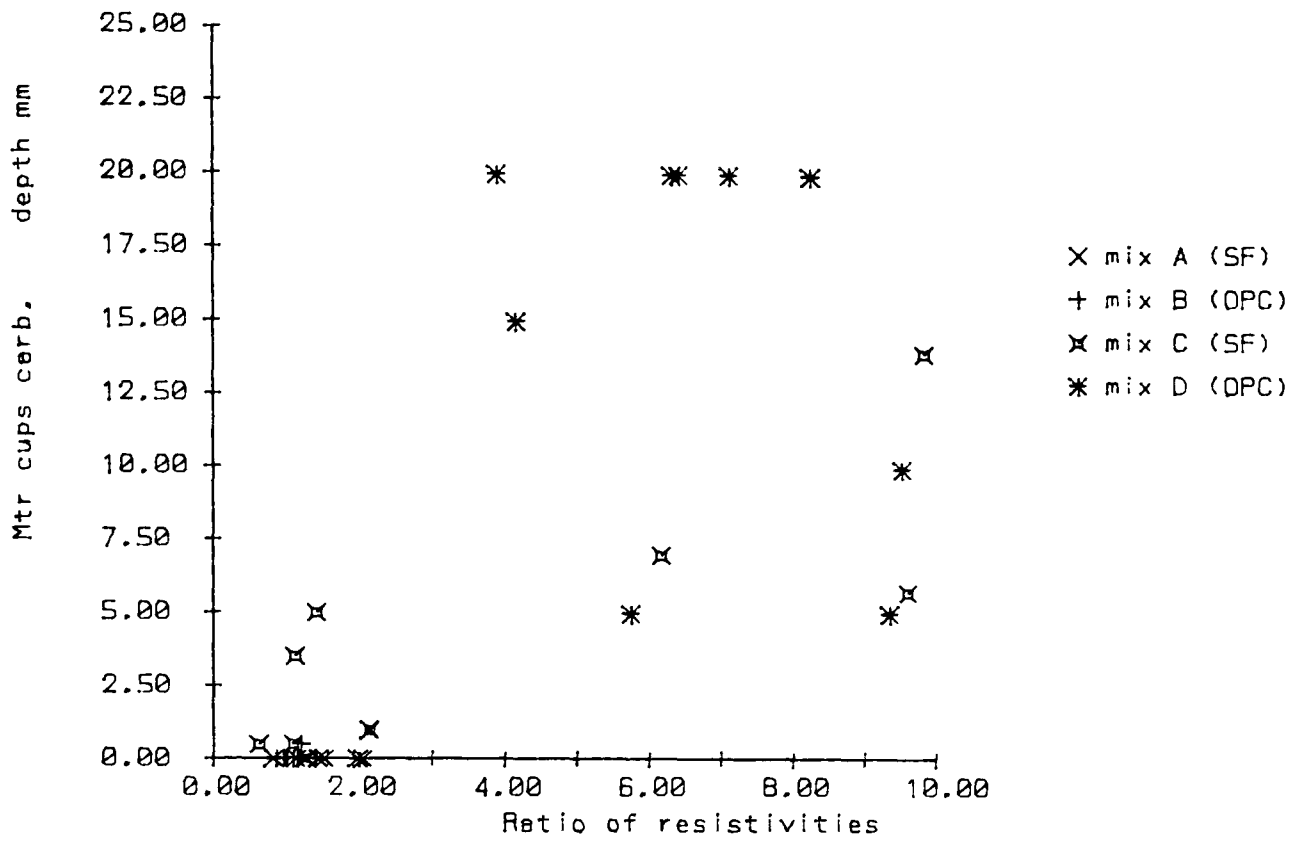
Fig. 4.11 This graph and the one below it test the use of the ratio of the a.c. resistivity of a carbonated sample to that of a similar uncarbonated sample as a measure of carbonation. Depths measured with phenolphthalein are plotted against this parameter.
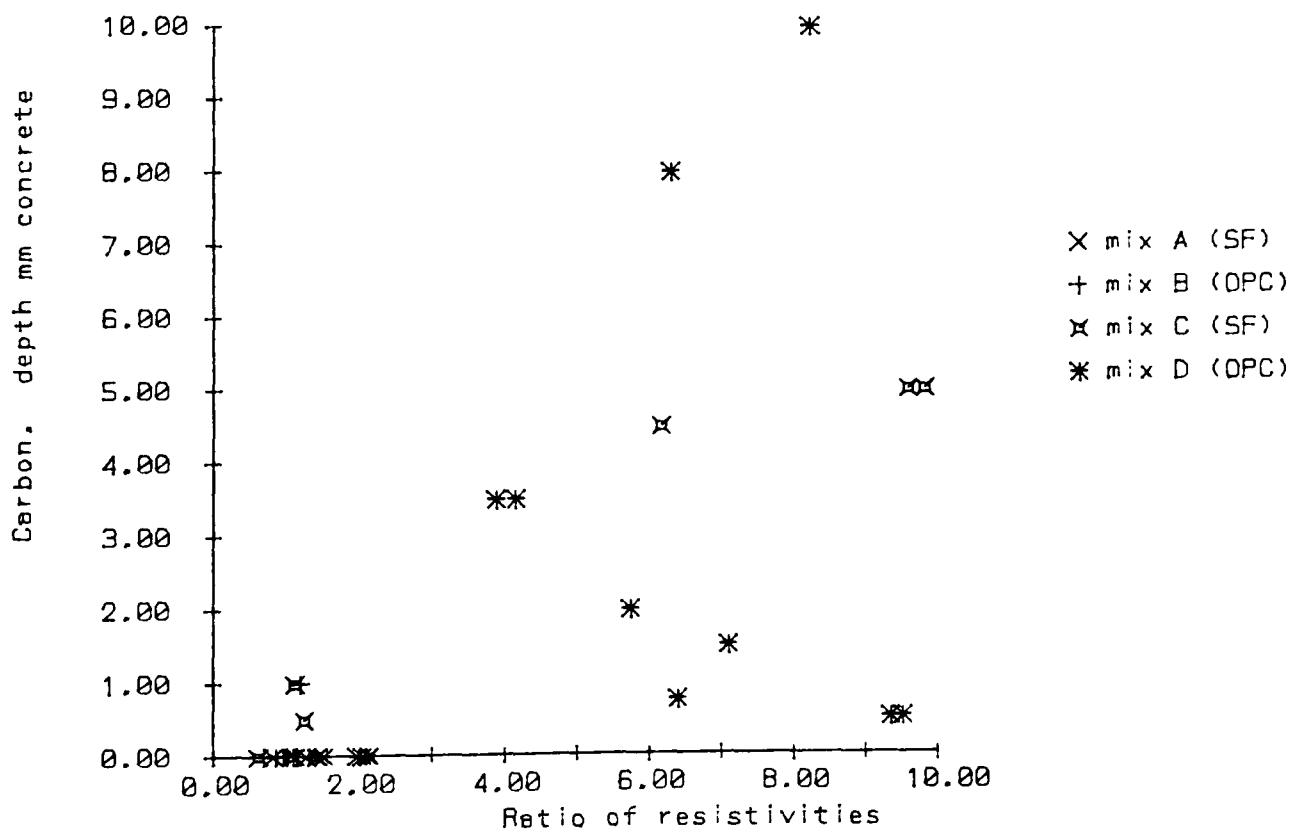
Fig. 4.12 In this graph the correlation of carbonation depth with resistivity ratio is clear despite the fact that the depths were measured on concrete exposed in air while the resistivity ratio was for mortar exposed to carbon dioxide.
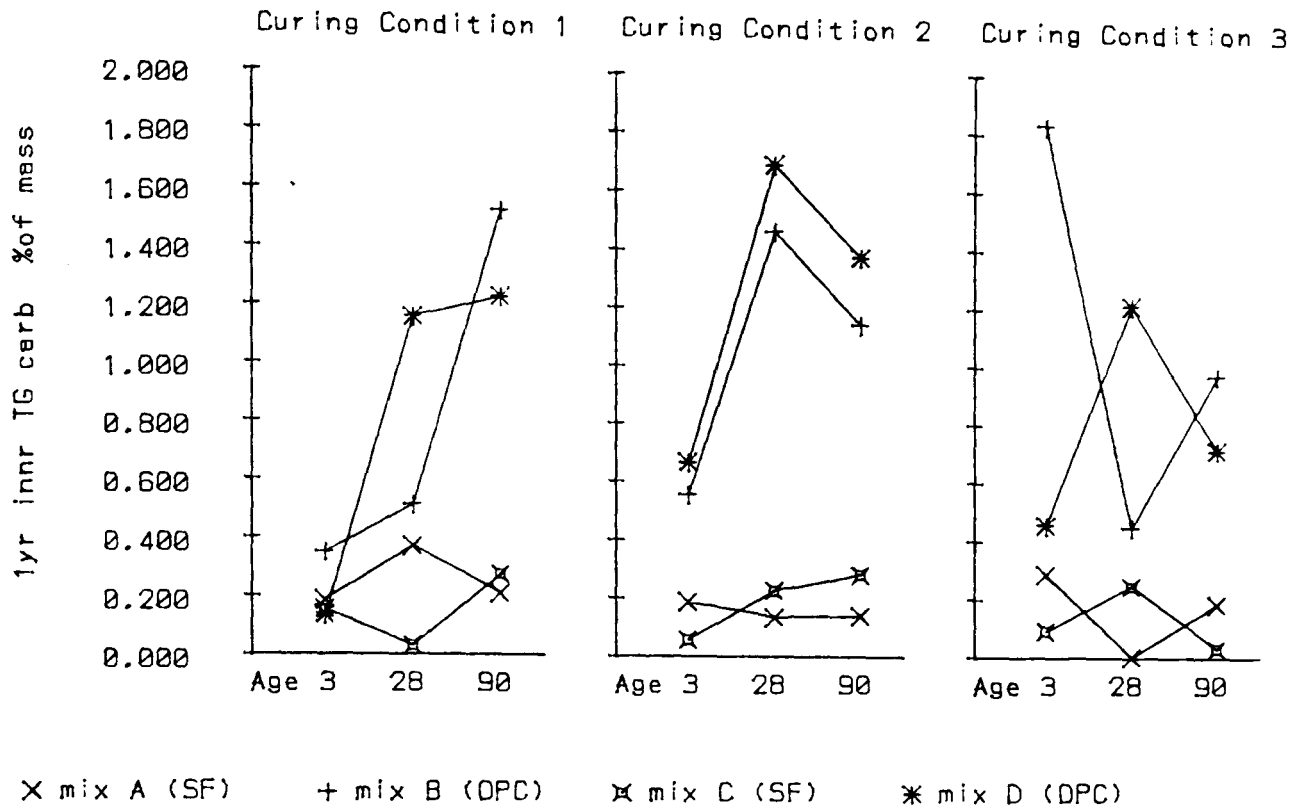
Fig. 4.13 The two graphs on this page show the amounts of calcium carbonate detected by thermogravimetric analysis in samples drilled from concrete cubes after one year exposed to room air. Samples from a freshly broken inner face are shown above and from an outer face below. (note that the scale is different)
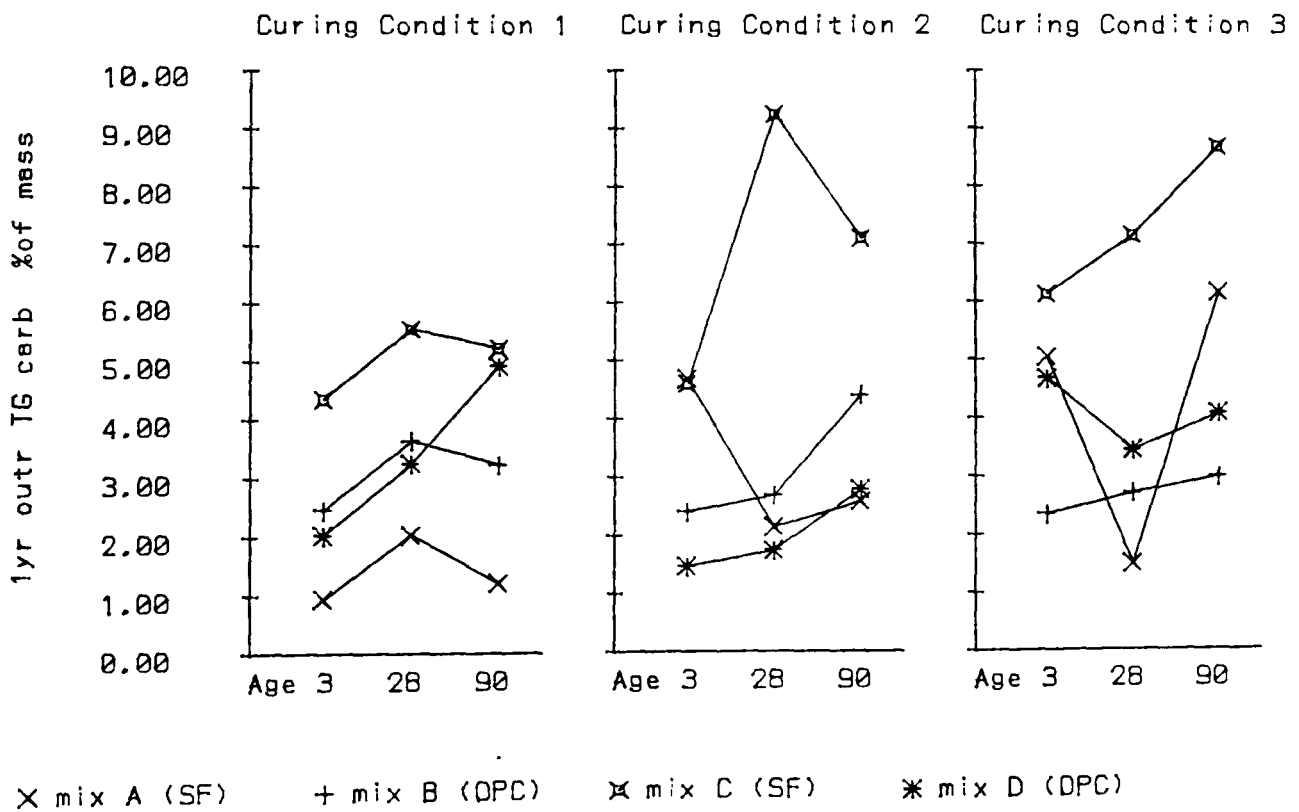
Fig. 4.14 In this graph substantial amounts of carbonate are evident in the SF samples unlike the samples from the inner face (above) where the pozzolanic reaction has consumed all of the lime available to carbonate. (for T.G. method see chapter 11)

5 Chloride transmission.

5.1 Introduction.

Chloride transmission has been measured by two methods which employ different systems both to cause the chloride to move through the samples and to detect it. The first method, which is discussed in section 5.2, only uses gravity to assist the chloride to penetrate the sample and uses analysis of drilled samples to measure penetration. The second method, which is in section 5.3, uses an applied voltage to cause rapid electro-migration and measurement of current to monitor it.

5.2 Gravity Assisted Chloride Diffusion.

5.2.1 Experimental method.

Concrete beams were cast in moulds 500mm long by 100mm square. A rebate 20mm deep by 40mm wide and 300mm long was formed in the top of each beam. After curing, four 32mm. diameter holes were drilled in each beam in the bottom of the rebate just deep enough to form the shape of the tip of the drill (approximately 10mm deep at the centre). A heavy rotary hammer drill was used. The rebate was then filled with saturated sodium chloride solution and the beam was kept at approximately 20°C. After 28 days samples were drilled from the bottom of the holes and tested for acid soluble chloride content by the titration method of BS 1881 (1971) part 6.The depth of drilling for samples was controlled by the drilling time because it was not possible to provide accurate direct control. The exact procedure for sampling was as follows:

1 Remove salt solution and wash off remaining salt with cold water.

2 Wait for concrete to surface dry at room temperature.

3 Drill for 10 seconds and discard dust.

4 Drill for 5 seconds and retain dust as sample 1 (approx 5mm. depth).

5 Drill for 5 seconds and discard dust.

6 Drill for 5 seconds and retain dust as sample 2. (approx. 10mm. depth).

This method produced samples of about 2-4 grammes. Material from the 4 holes in the same beam was mixed to provide sufficient for testing.

5.2.2 Calculation of results.

The depth was calculated by weighing the total amount of material collected. (This method was checked by measuring with a vernier caliper for one third of the samples). The results were calculated by fitting an exponential decay function to the two readings.

It was observed that the predicted concentration was near zero by 20mm depth. The integral was therefore calculated over the range 0-20mm and from it the average

concentraton in that area was obtained.

5.3 High Voltage Chloride Migration.

5.3.1 Experimental method.

Mortar samples were tested for chloride transmission with a voltage of 40 volts applied across them. The diffusion rate was recorded by measuring the current passing. This method is very similar to the FHWA test developed by Whiting (1981). This apparatus was built as part of another project (Lynsdale 1987) but some additions to the software were written as part of this project.

The samples were cast as cylinders 100mm diameter by approximately 55mm long. The apparatus is shown in fig.5.1. At the test age the samples were installed in the test cells with NaCl (30g/L) on the negative side and NaOH (12g/L) on the positive side. Before testing, the 3 day CC2 samples were saturated in water under an applied vacuum for 2 hours, because they were dry. All other samples were wet from curing. A rubber membrane was used to seal the curved surfaces of the samples and at each end this was sealed to the cell with silicon rubber.

The current was recorded by measuring the voltages across 0.1 Ohm shunts in the circuit as shown in fig.5.1. The readings were taken every five minutes with an intelligent analog to digital converter unit which was connected to a BBC microcomputer. The temperature was also recorded with a thermocouple in the sodium chloride. All of the results were written direct to computer disc. The detailed procedure for the apparatus is included as appendix 2.

5.3.2 Calculation of results.

A typical output of the raw data is shown for three samples in fig.5.2. The second trace on the graph shows the temperature. Correction for the effect of temperature on the resistivity has not been applied. If temperature correction was applied it would increase the spread of the readings because the samples with lower resistances generally reached higher temperatures.

The initial current, final current, and total charge passing during the 6 hours of measurement were calculated. The lengths of the samples were measured and a small correction factor was applied to normalise the results to exactly 55mm length, (i.e. if the length of the sample was 56mm. the readings were multiplied by 56/55).

5.4 Results and discussion.

5.4.1 Results.

The development of the chloride concentration and the total charge passing with age at the time of testing is shown in fig.5.3 and fig.5.4. The relationship between the two is shown in fig.5.5. Although the relationship between them which was observed by

Whiting (1981) is confirmed, inspection of the data reveals that the major dependence of charge passing on the age and curing condition of the pozzolanic mixes is not reflected in the chloride sampling results. The results of the two experiments are presented in table A3.5 in appendix 3.

5.4.2 The mechanism of conduction of d.c..

It has been established (Monfore 1968) that conduction is almost all through the pore water, conduction through the cement matrix and aggregate is negligible, (It has been observed by Hansson (1984) that a closed pore structure would allow almost no current). Thus the current at the cathode may be assumed to be largely composed of chloride ions migrating towards the sample. Assuming normal isotope concentrations the ions will have an average mass of 35.5 atomic units i.e. $5.94*10^{-26}$ Kg and one electronic charge i.e. $1.6*10^{-19}$ coulomb. Thus for each Coulomb of charge recorded 0.37 mg of chloride ions will enter the sample.

When the ions have entered the sample the situation becomes more complicated. Each ion will penetrate a given distance and then stop. Whiting (1981) measured the concentrations of chloride in samples after the diffusion test and found that they decay to zero within the thickness of the sample and do not extend to the opposite face. From the point where the chloride ion stops another ion such as a hydroxyl ion must start in order to conduct the electron to the anode.

The precise point at which the ions stop will be dependent on the existing concentration of chloride and other factors such as the ability of the matrix to bind them. If the only factor is the initial concentration the current may be expected to increase linearly with time. (The resistance must be lower in the areas with chloride in them or the ions would go straight through). Whatever the final distribution is it follows that the first ions to enter the sample will initially stop at the surface. Thus the initial current will be dependent on the mobility of the ions already in the sample (primarily hydroxyl ions) and not the chloride ions.

It may be seen from table A3.5 (Appendix 3) that the current flow in the OPC samples increases during the test indicating that the main controlling factor is the extent of the existing penetration into the sample. For the SF samples, however, it decreases indicating a different mechanism. It is proposed that this mechanism is the depletion of hydroxyl ions. This would explain the strong dependence on age and curing condition because the supply of these ions will be reduced with the progress of the pozzolanic reaction. This depletion is purely a property of the electrical test and has no direct connection with the chloride permeability under normal circumstances.

5.5 Conclusions.

Conclusions on the effect of the SF are discussed in association with the results from other experiments in chapters 13 and 14. The risks of drawing conclusions from single experiments are very clearly shown by the results from the high voltage experiment

which actually gave a result for resistivity (see chapter 13).

1 A simple measure of chloride penetration into concrete has been obtained by filling drilled holes with chloride solution and sampling by continuing drilling with the same bit.

2 The results from comparing this test with a rapid chloride determination show that the relationship between charge passing in the FHWA rapid chloride permeability test and chloride penetration into OPC samples does not hold for silica fume samples.

3 The reason for this difference is that the current is controlled by the hydroxide ions in the silica fume samples and by the chloride ions in the OPC samples.

4 A useful addition to the experiment would be to measure the ac resistivity and possibly the rest potential of the cells before and after the test. The correlation of the results with resistivity results from chapter 3 is discussed with other relationships in the conclusions in chapters 13 and 14.
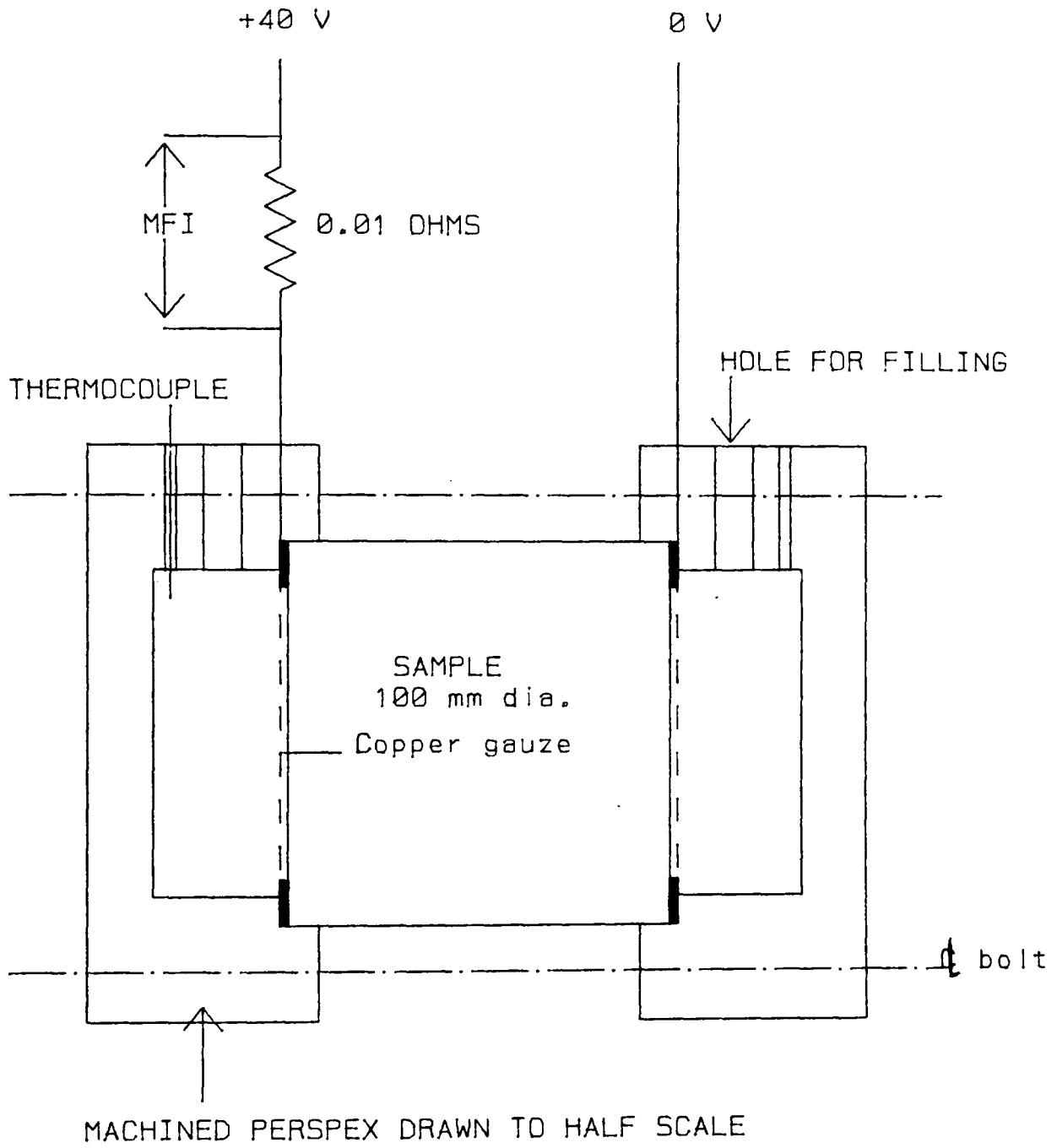
Fig 5.1

SAMPLE HOLDER FOR HIGH VOLTAGE CHLORIDE TRANSMISSION EXPERIMENT

Mix C 28 day

Mix D 28 day
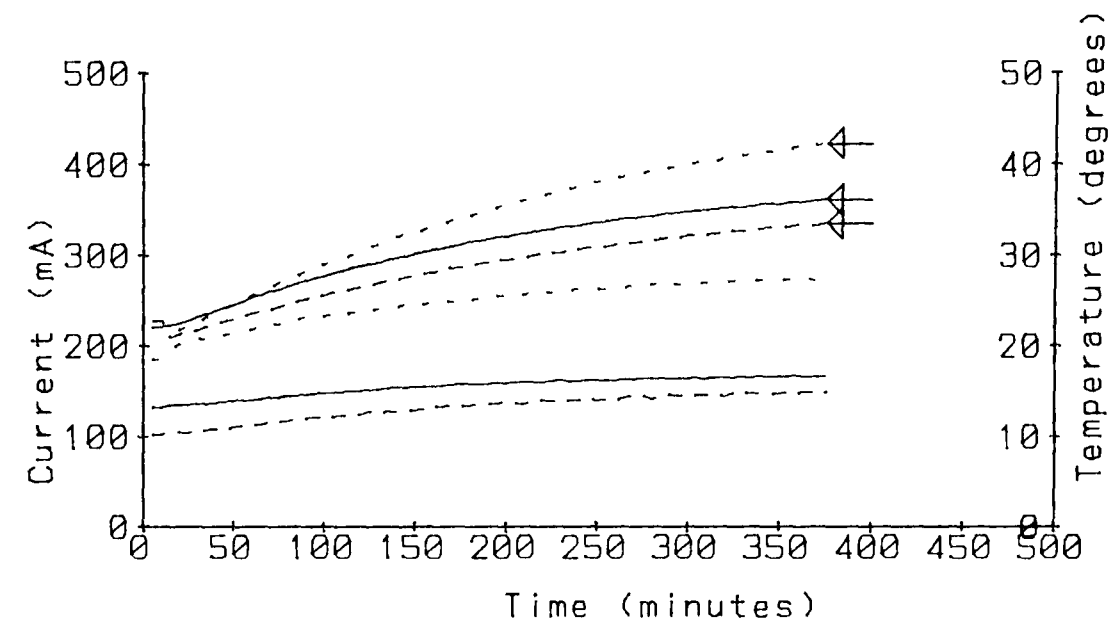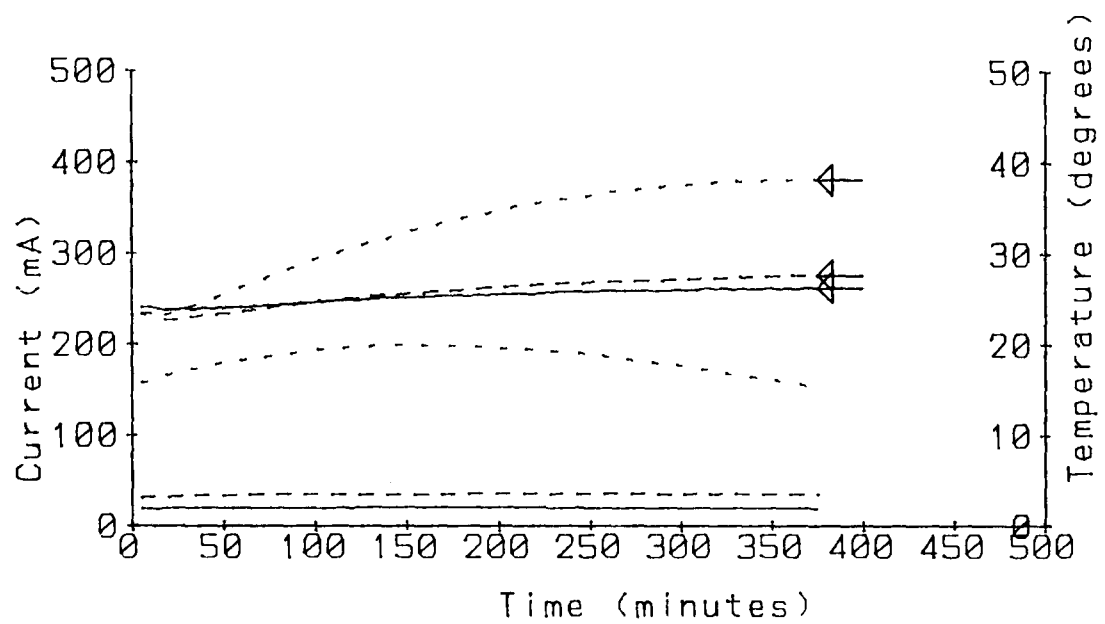
_____CC1   ___CC2   ..._CC3

⊲_Temperature traces

Fig 5.2 Typical outputs from the high voltage chloride apparatus.
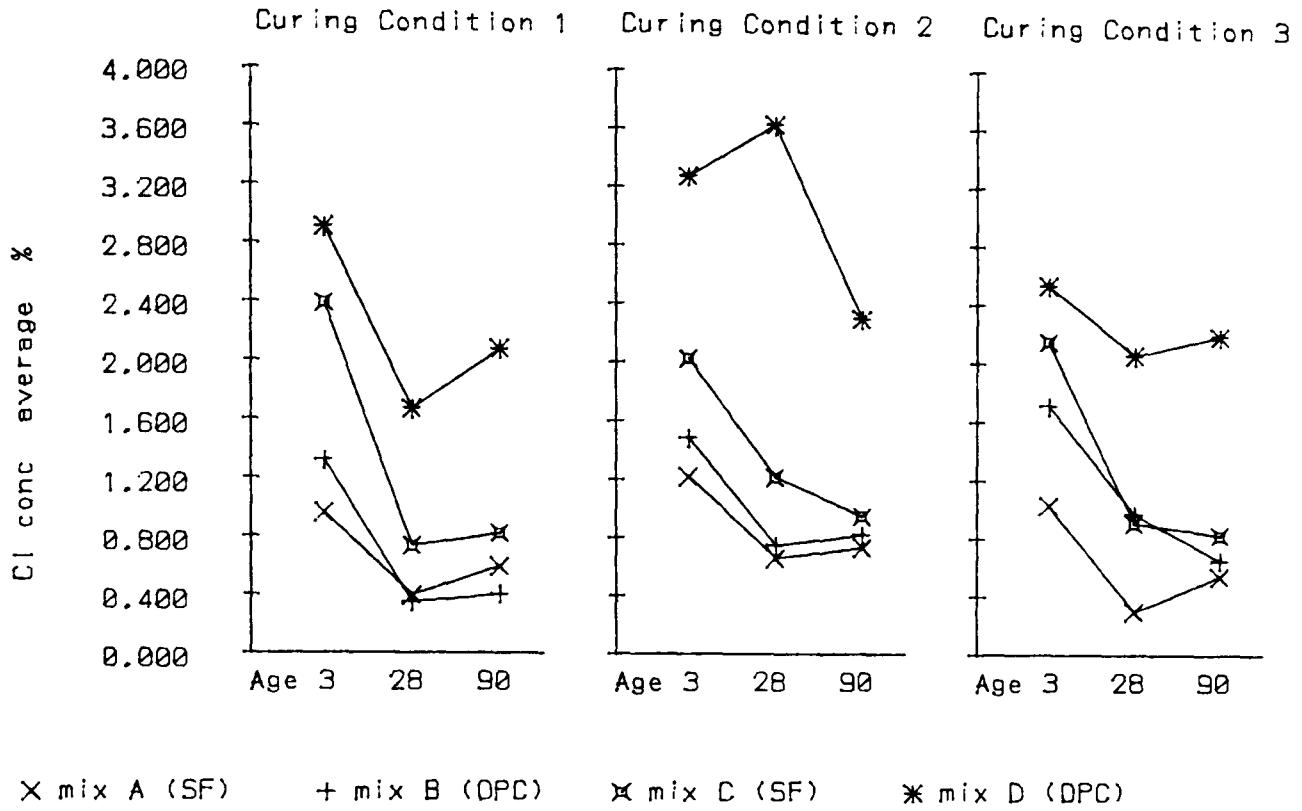
Fig. 5.3 The average chloride concentration in the depth range 0-20mm expressed as a percentage of the weight of cement+SF.
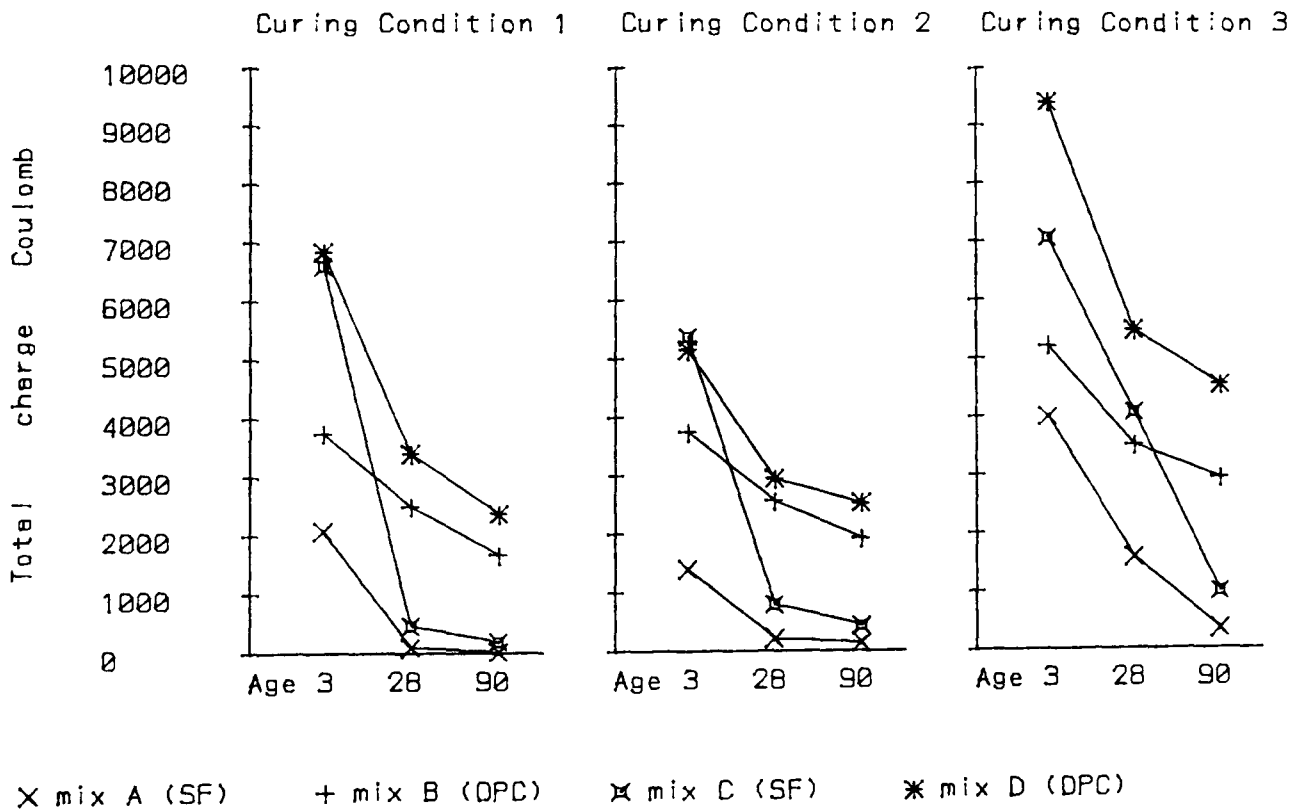
Fig. 5.4 The total charge passing during the six hours of testing with an applied voltage of 40 Volts.
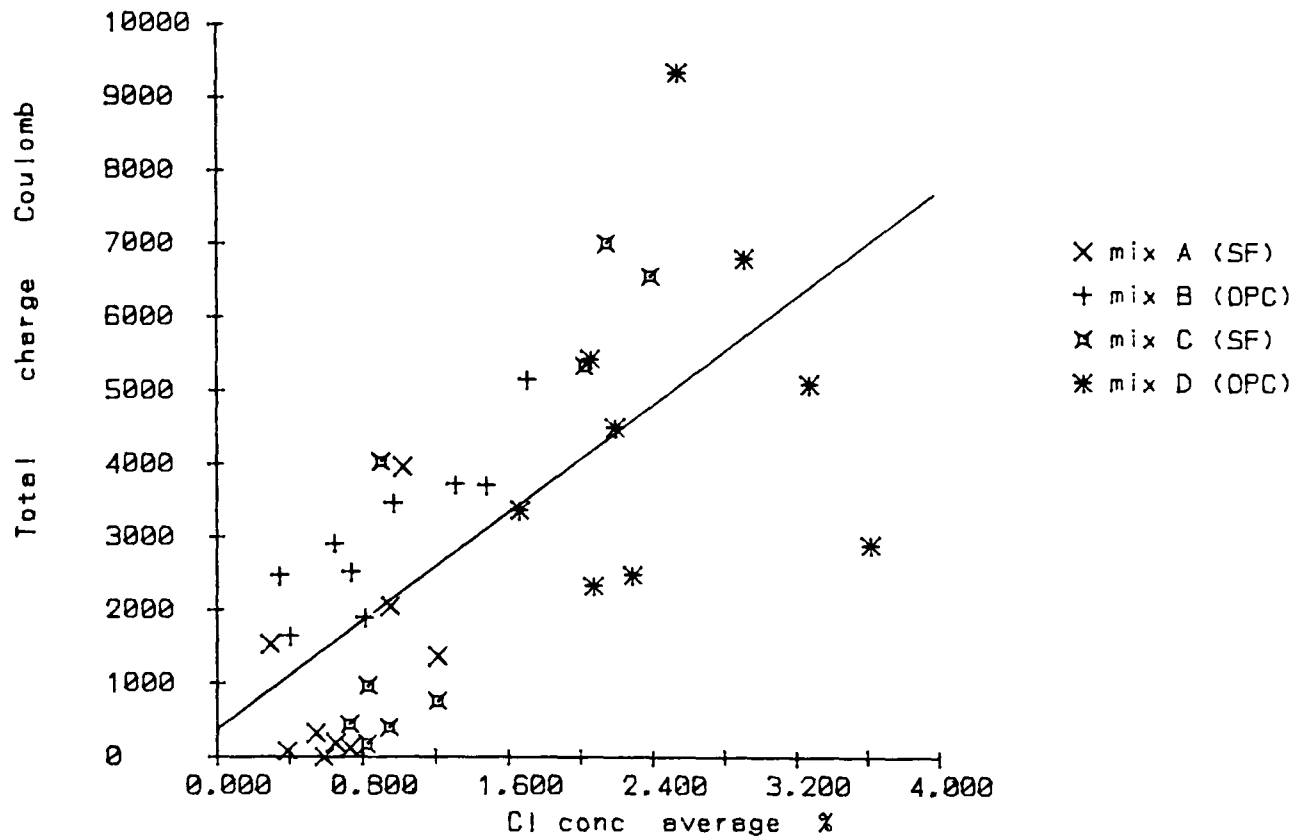
Fig. 5.5 The relationship between the two measurements of chloride transmission. The graph shows total charge passing vs. average chloride content within 20mm of surface expressed as a percentage of total cementitious content.

6 Vapour Transmission.

6.1 Experimental method.

6.1.1 General description.

The vapour transmission rate through paste samples has been measured. The samples were sealed into the top of sample bottles containing water and the rate of transmission of vapour from the inside to a controlled humidity environment outside was measured by measuring the weight loss of the bottles. Two sets of samples were tested: the main set (set 1) which was made with paste mixed in the Hobart mixer in the normal way and a small additional set (set 2) which was made from paste which had been mixed using high energy mixing (see section 2.1). In set 2 some of the bottle tops containing the samples were weighed separately from the bottles.

6.1.2 Procedure - Set 1.

Low energy mixing was used and the samples were cast in 100mm. cube moulds. After 24 hours 25mm. cores were cut from them. At the test age thin discs were cut from the central portion of the cores. The thickness of each disc was measured with a micrometer and all were in the range 3.5-4.7 mm. The discs were the permitted to dry at room temperature for approximately two hours and then set in epoxy resin in holes formed in the lids of 125cc. sample bottles. The bottles were then part filled with de-ionised water and the lids put on them and sealed as shown in fig. 6.1. The effectiveness of the seals was checked by briefly inverting the bottles. The bottles were then placed in trays in large storage bins. Details of the bins are as follows:

BIN 1 : Open to the atmosphere in a room controlled at 70% RH.
BIN 2 : Sealed with a quantity of sodium dichromate in the bottom to give an RH of 55.2%. (Sneck and Oinonen 1970).
BIN 3 : Sealed with a quantity of lithium chloride to give an RH of 12.4%.
All of the bins were kept at 21°C. The RH was checked periodically using an electronic probe.

The transmission rate was measured by weighing the bottles. Two samples were tested for each of the 4 mixes, 3 curing conditions, 3 test ages and 3 bins to give a total of 216 bottles.

6.1.3 Procedure - Set 2.

The purpose of the set 2 samples was to measure the effect of high energy mixing and to measure the weight loss of some samples (i.e. bottle tops) separately from the bottles. In order to remove the tops it was necessary to omit the silicone rubber seal so

additional samples were made to check whether this affected the weight loss. All of the set 2 samples were made using high energy mixing, cured in curing condition one for three days and then tested in bin one. The method of cutting the samples and installing them in the bottle tops was the same as for set 1. Three different types were tested (2 samples per mix of each):

Type 1 As main set (set 1)

Type 2 Silicon rubber seal omitted

Type 3 Seal omitted and tops weighed separately.

6.2 Analysis of the data.

6.2.1 Initial preparation.

The weights of the bottles were initially plotted against time, a typical plot showing 6 bottles is shown in fig.6.2. These plots were used to identify bottles where obvious leakage was causing a wrong result. Out of the total of 216 in set 1 there were 3 of this type and the results from them were not used.

6.2.2 Analysis of the steady state.

The physical interpretation of the steady state is simple. Whatever processes initially change the sample they are bound to reach equilibrium and at this point the rate of transmission will be constant. It was observed that during the first month the rate of weight loss varied but after this it remained almost constant. A straight line was therefore fitted to the data obtained after the first 30 days.

The equation used to describe the process is as follows:

$$M = xM_0 + Ct \qquad (1)$$

Where:

M is the cumulative mass loss until the current time t

x is a function of time which represents the fraction of the initial additional mass loss M_0 which has occurred. When the transmission rate is constant after 30 days x=1.

C is a constant for each sample. After 30 days $C = dM/dt$

Thus after 30 days the linear relationship is:

$$M = M_0 + Ct \qquad (2)$$

The constants M_0 and C were obtained for each sample from the straight line fitting to the data.

6.2.3 The initial processes.

The total effect of the initial processes is measured by M_0. In order to quantify the rate

at which they take place it is necessary to fit a curve to the initial data. The initial mass loss is higher than the steady state. The following two processes contribute to this effect:

1. When the samples were first installed they had a relatively constant moisture content throughout. Whatever the final distribution it was certainly not constant across the thickness of the sample. An increase in moisture content on the wet side would not affect the measured weight but a loss from the dry side would cause a loss of weight. The factors controlling the exact rate of moisture loss are complex because the rate of migration of water will depend on the local humidity gradient and the total amount to be lost from any given depth will depend on the final distribution. As a rough approximation it is, however, reasonable to assume an exponential decay, i.e. the rate of loss will be proportional to the amount remaining to be lost.

2. When the samples were installed they were not fully hydrated. Due to the presence of moisture the hydration will have continued and the hydration products will have formed in previously open pores. The factors controlling the transmission rate are again complex because the rate of hydration will depend on the availability of water and there is also a negative component caused by the loss of water to the reaction. An exponential decay may be very approximately justified by assuming that the rate of hydration depends on the quantity of cement remaining to hydrate and the rate of transmission decreases linearly with the quantity of hydration products present. Thus the rate of hydration will decay exponentially and the rate of transmission will follow it.

If the two processes are assumed to proceed at approximately the same speed they may be represented by a single term to describe the initial additional losses:

$$M_0 \times e^{-Kt}$$

where K is a rate constant to represent the effect of both processes.

thus

$$M = M_0 - M_0 e^{-Kt} + Ct \qquad (3)$$

and

$$Kt = Ln\left[\frac{M_0 - M + Ct}{M_0}\right] \qquad (4)$$

A value for K may be obtained by plotting the right hand side of this equation against time t but it is greatly affected by small deviations from linear behaviour with increasing time. Thus the best fit of the inverse to $1/t$ was used to obtain a value for K. It may be seen from fig 6.2 that this procedure gives a good fit to the data.

Thus for each sample the constant C was used to measure the steady state loss and the

the constants M_0 and k were used for the extent and duration of the initial additional losses.

It would, of course, be possible to obtain the best values of all three constants by fitting equation (3) to the data using multiple regression and avoid the assumption of linearity after 30 days. The accuracy of the method of obtaining the constants in order may, however, be seen to be good from fig.6.2 and it is quick and easy to use.

6.2.4 Results for weight loss.

The results for the steady state loss C for set 1 are presented in figs.6.3-6.5.

Summary of samples tested:

Main set (set 1) :   Low energy mixing

Set 2 Type 1:   Tested as main set (set 1)

Set 2 Type 2:   Silicon rubber seal omitted

Set 2 Type 3:   Seal omitted and tops weighed separately.

LOSS PER 100 DAY (C)

Mix	w/c	main set	Type 1	Type 2	Type 3
A(SF)	.3	0.623	0.674	0.94	1.344
B(OPC)	.3	1.710	1.650	2.262	2.759
C(SF)	.46	2.456	1.487	1.385	1.701
D(OPC)	.46	1.779	4.034	3.970	4.106

INTERCEPT (M_0)

Mix	w/c	main set	Type 1	Type 2	Type 3
A(SF)	.3	0.646	0.319	0.324	0.229
B(OPC)	.3	0.741	0.415	0.378	0.188
C(SF)	.46	1.213	1.426	1.362	1.263
D(OPC)	.46	0.533	1.103	1.021	1.043

RATE CONSTANT (K)

Mix	w/c	main set	Type 1	Type 2	Type 3
A(SF)	.3	0.099	0.161	0.139	0.069
B(OPC)	.3	0.071	0.091	0.088	0.142
C(SF)	.46	0.056	0.136	0.145	0.142
D(OPC)	.46	0.075	0.082	0.078	0.082

WEIGHT LOSS OF SAMPLES (LIDS)

Mix	A	B	C	D
	0.14	0.07	0.12	0.12

Table 6.1   Results for set 2

The results for set 2 and the equivalent samples from set 1 are in table 6.1.
Droplets of water were observed on the underside of the lids after several weeks at low transmission rates. The weight of the lids remained stable after 28 days.

6.3 Calculation of a coefficient.

6.3.1 Effect of sample thickness.

A number of different coefficients have been used for transmission rates. Henry and Kurtz (1963) found the rate of transmission through concrete using the wet cup method (i.e. with water in the bottles as used in this work) to be independent of the sample thickness and used a coefficient which is independent of the thickness. Using the dry cup method (i.e. with dessicant in the bottles) Woodside (1959), Wierig (1965) and Spooner (1983) assume the rate to be proportional to thickness and Mills (1985) derives a dependence on the square of the thickness.

The dependence on thickness in the data was checked by considering each similar pair in set 1. For each pair the percentage difference in thickness and the percentage difference in the constants C, M_0 and K were calculated. No correlation was found between any of the constants and the thickness and it was thus concluded that the rate is independent of thickness. The coefficient used did not, therefore, contain a term for thickness.

6.3.2 Effect of Relative Humidity.

Henry and Kurtz (1963) found some dependence on RH but only after 100 days and Wierig (1965) reports a non-linear dependence. The dependence of the measured weight losses on relative humidity was investigated by checking for a constant ratio between results from the different bins. The target RH for bin 1 was 70% and for bin 2 it was 55.2% and thus a linear dependence of rate on RH would give a ratio of (100-55.2)/(100-70)=1.49

The other ratios are in table 6.2.

	Ratio of RH drop	C ratio	M0 ratio	K ratio
Bin 2/Bin 1	1.49	0.95 (.84)	1.13 (.86)	0.89 (.34)
Bin 3/Bin 1	2.92	1.73 (.83)	1.29 (.76)	1.03 (.06)

Table 6.2 Effect of RH

Figures in brackets after the ratios are the values of R^2 for the relationship.
The relationship with RH is clearly non-linear. In order to provide equal weighting to data from each bin when calculating an average the results were weighted in proportion

to the ratios for C given above.

The permeability was therefore calculated from the average value over six readings of:

$$\frac{C}{A P_{DIFF}} \ Kg/m^2 Pa \ s \qquad (5)$$

where:

C is the rate of mass loss in kg/s

A is the area of the sample in m^2

P_{DIFF} is the vapour pressure drop in Pa.

The initial mass loss (intercept) was calculated from the average of:

$$\frac{M_0}{A P_{DIFF}} \ Kg/m^2 \ Pa \qquad (6)$$

and the rate constant k was calculated from:

$$K \ P_{DIFF} \ Pa/s \qquad (7)$$

The results for the coefficients are shown in figs.6.6-6.8.

6.4 Discussion.

6.4.1 The mechanism of transmission.

The fact that the rate is independent of the sample thickness severely limits the choice of possible mechanisms. The possibility of a continuously changing moisture content across the thickness is ruled out. Bazant and Najjar (1972) observe that the mean free path of a molecule of water vapour at room temperature is many times greater than the size of continuous pores in concrete and Mills (1985) observes that at 96% RH pores with diameters below 35nm. will sustain a meniscus. It may therefore be concluded that, with the exception of an outer surface layer, the pores are all either full of water or vapour at near 100% RH. Wierig (1965) shows experimental readings of the vapour pressure across a wall with RH 95% and 0% on each side and it remains at 95% until the mid-point. He also shows a graph of transmission rate against thickness which indicates that the transmission rate is independent of thickness for thin samples but dependent for thicker ones (more than 10mm. thick for mortar samples). The model proposed above would indicate that keeping one side at 100%RH would extend the range for which the transmission rate is independent of thickness.

Further support for the theory that this is not a vapour diffusion process is gained from the observation of water droplets on the underside of the samples. These droplets will clearly prevent the ingress of any gas or vapour into the sample. Rose (1965) discussed the various degrees of saturation possible in a porous body. He suggests two mechanisms of transmission without full saturation but without a vapour pressure gradient. One takes place when just the necks of the pores are filled with water where vapour condenses on one side of the neck and evaporates from the other. The other

mechanism is surface creep of a fine film of water coating the pore surfaces.

Powers (1960) proposes a mechanism for the loss of water from the dry side. He observes that if it was necessary for water to evaporate from surfaces in the necks of the outer pores as in the "ink bottle" analogy virtually no water would be lost. He therefore proposes a mechanism where the process is controlled by the formation of vapour bubbles in those pores which are of adequate size. This would indicate that the rate would be linearly dependent on porosity. The porosity has been measured in another part of this project and relationships between variables are discussed in chapter 13.

6.4.2 The initial processes.

The results from set 2 given in table 6.1 indicate that the measured loss of weight from the samples formed almost 50% of the total initial loss M_0 in mixes A and B but only a small part in mixes C and D. The relatively small differences between the results for the Type 1 and Type 2 samples indicate the the omission of the silicone rubber seal to enable the tops to be removed did not have a major effect on the observed sample weight loss. This observed loss may only be used to indicate a lower limit of the relative importance of the moisture loss in the total initial weight loss discussed in section 6.2.3. This is because the uptake of water to the wet side including the observed formation of droplets will reduce the observed weight loss. Morrison et.al. (1979) used a method of direct measurement of the uptake of water to the wet side. They had water in direct contact with the wet side but they suggest the the pressures created by the humidity gradient are far greater than the hydraulic pressures so this should have little effect.

6.4.3 High energy mixing.

The effect of high energy mixing may be seen by comparing the first two columns in table 6.1. The steady state weight loss rate C is not greatly changed for mixes A and B but for the mixes with higher w/c ratio it is reduced for the SF mix (C) and increased for the OPC mix (D). The decrease for mix C is probably caused by improved dispersion of the SF. The increase for mix D could be explained by the observation the when only mixed at low energy it lost a large amount of water through bleeding and thus had a higher density.

For mixes A and B the total effect of the initial processes (M_0) is reduced and the rate at which they take place (K) is increased. This could either be caused by faster hydration of a more closed pore system limiting the total water loss. For mixes C and D it should be noted that increasing the straight line gradient C would be expected to decrease M_0 and K (see fig 6.2) and decreasing C will have the reverse effect. The increases in M_0 and K for mix D are therefore significant and could indicate greater moisture loss as a result of reduced loss through bleeding at time of mixing.

6.4.4 The effect of RH.

The effect of the different relative humidities in the bins may be seen from table 6.2. It may be seen that for the bin 1 / bin 2 ratio the ratio for C is less than 1 while the RH drop ratio is greater than 1. This may have been caused by vapour transmission in bin 1 being assisted by air circulation in the room (it was open while the others were sealed). The ratio for C for bin 3 is as expected, a linear dependence on RH was not anticipated. The ratios for K have very low R^2 values indicating no effect of RH on the rate of achieving equilibrium. The reason for the small increases in M_0 in bins 2 and 3 is not known.

6.4.5 The effect of curing.

The effect of age and curing condition on the steady state loss C for set 1 may be seen for each bin in figs.6.3-6.5 and the average in fig.6.6. Extending curing has caused a small reduction in C which is approximately equal for all of the mixes. Different curing conditions have little effect. This indicates that there is sufficient moisture in the samples during testing for hydration to proceed.

6.4.6 The initial mass loss.

Figure 6.7 shows that increasing curing time greatly decreases M_0 (the total effect of the initial processes). Improved curing conditions also decrease it. This is clearly caused by the greater progress of the hydration before the start of the test.

6.4.7 The rate constant.

Figure 6.8 shows the effect of age and curing condition on K (the rate of the initial processes). An increase for longer curing times would be expected from the reductions in M_0.

6.5 Conclusions.

The following conclusions only concern the method and the mechanism of transmission.

1. The rate of transmission of water vapour through paste has been measured using the apparatus shown in fig.6.1.

2. High energy mixing has a major effect on the water vapour transmission rate through paste. This effect is sufficient to change the ranking of the mixes.

3. The transmission rate is independent of sample thickness over the range 3.5-4.7mm. because a major part of the sample is fully saturated during the experiment and the degree of saturation only falls in the surface region.

4. The higher initial weight losses are caused by several processes including movement to moisture equilibrium and continued hydration. Separation of the effect of these by weighing the samples separately is complicated by uptake of water to the wet side of the sample.

5. Wittmann (1987) has measured the streaming potential caused by moisture movement with a basically similar apparatus. He claims that this method could be used in principle to determine the contribution of liquid water to the moisture transmission. It might also separate out the initial effects and would make a useful addition to the experiment.

25mm

LID →

EPOXY RESIN

PASTE
SPECIMEM

SILICON RUBBER SEAL

← SAMPLE BOTTLE

WATER

LEVEL
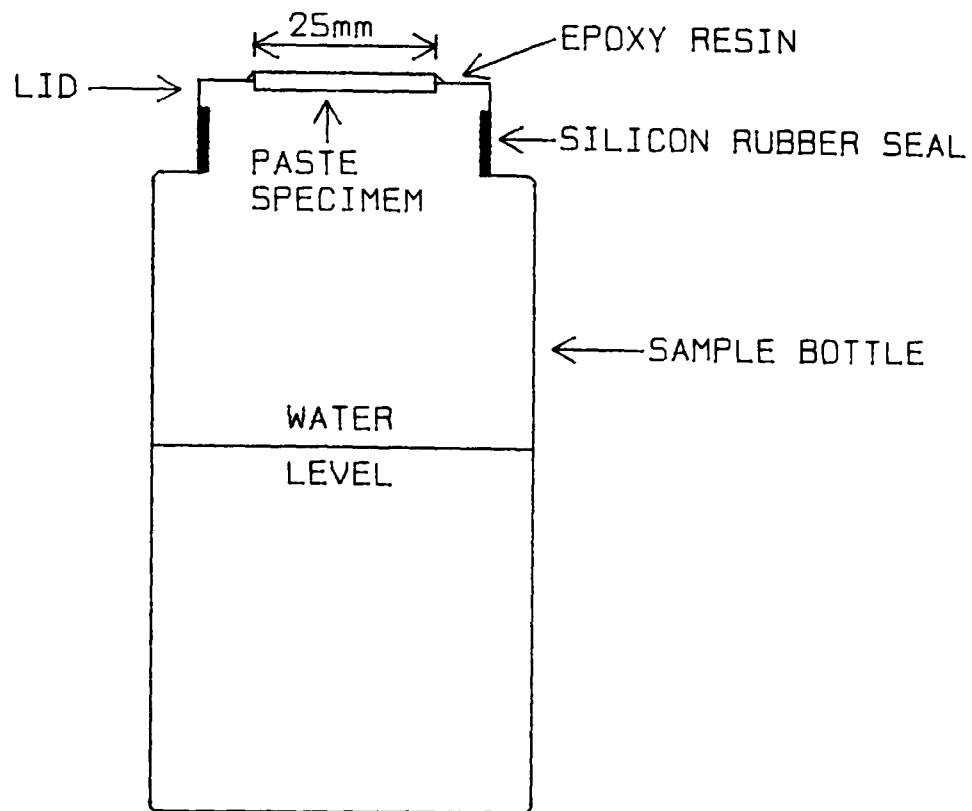
DETAIL OF BOTTLE FOR VAPOUR TRANSMISSION MEASUREMENT

Fig 6.1a

ADHESIVE TAPE SEAL

LID

P.V.C.BIN →

POSITION OF HUMIDITY
PROBE WHEN IN USE (HOLE
SEALED AT OTHER TIMES)

TYPICAL
BOTTLE
POSITIONS

SALT SPREAD
LOOSE IN BIN

TIMBERS TO KEEP
TRAY CLEAR OF SALT
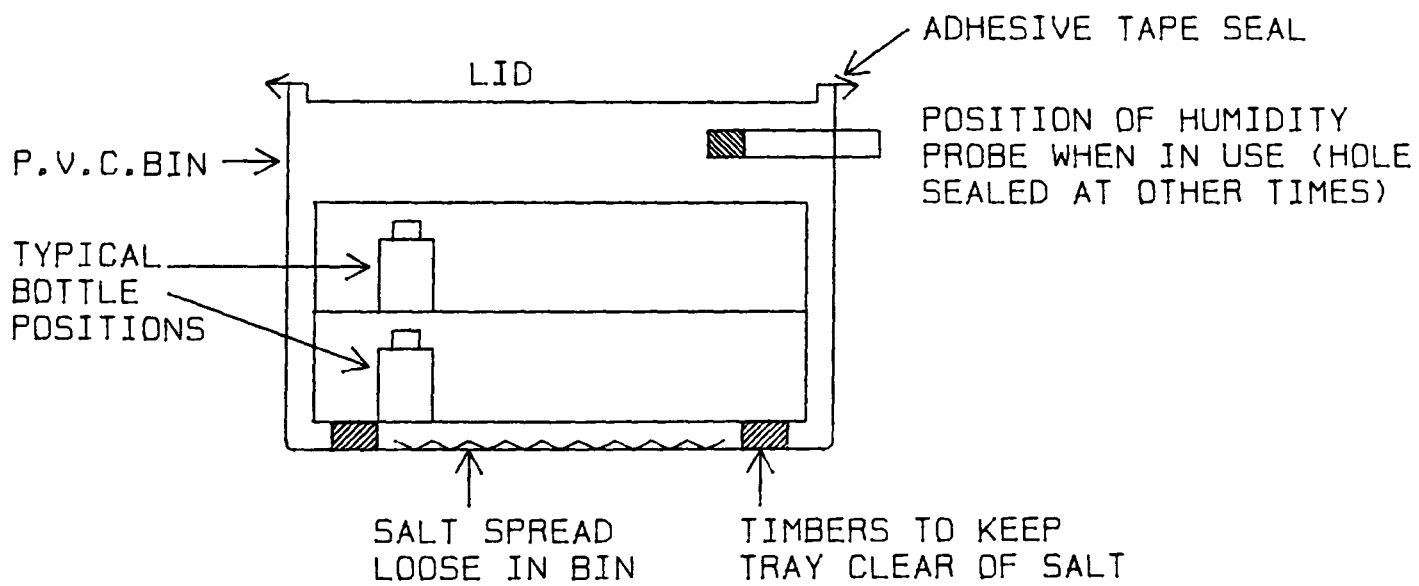
G.A. OF BIN

Fig 6.1b
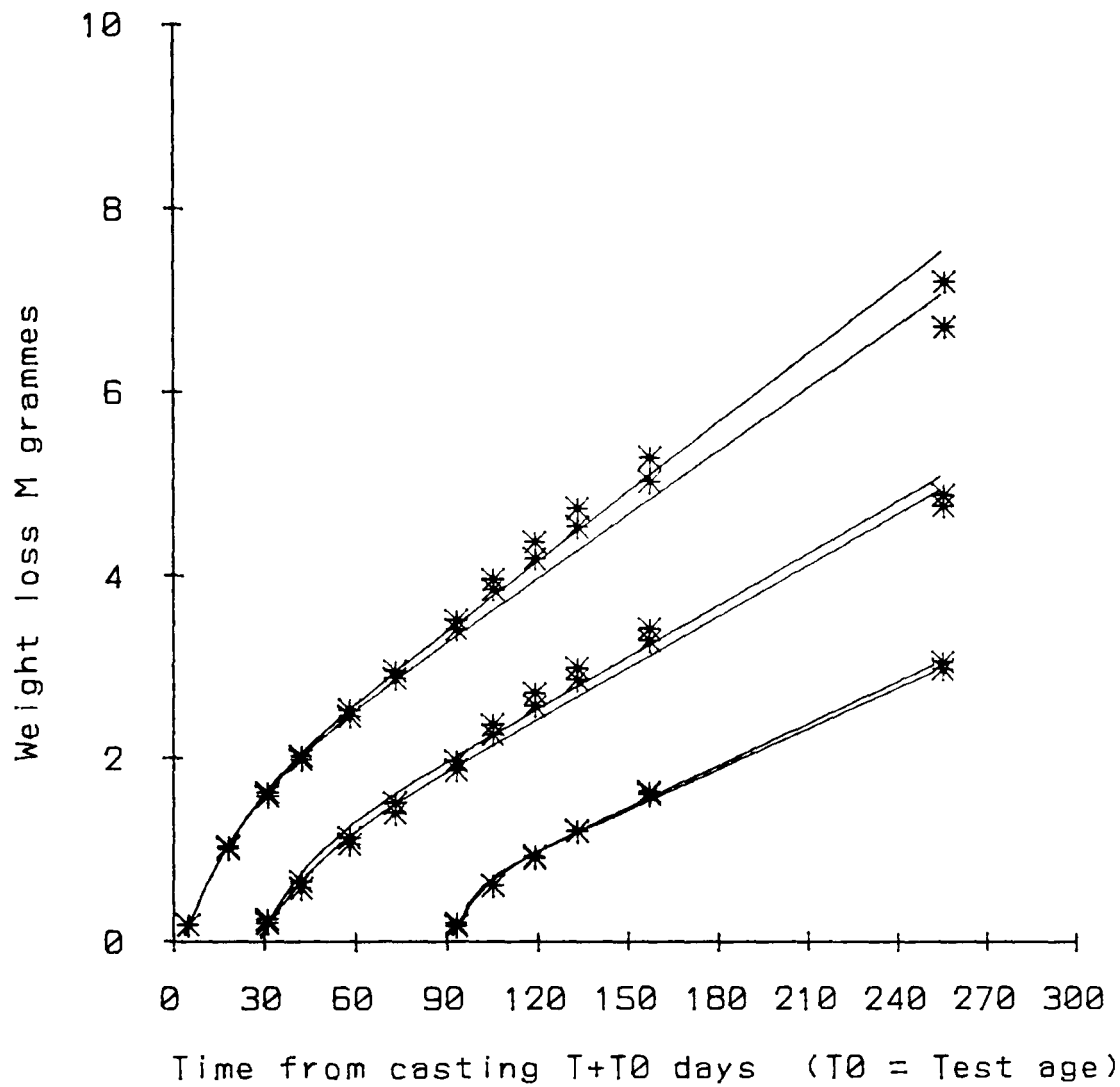
Mix C Bin 1 CC 1

Equation for lines is M = M0 - M0*exp(-KT) + C*T

Test age 3.000 Sample 1.000 C=0.026 M0=1.186 K=0.056
Test age 3.000 Sample 2.000 C=0.024 M0=1.240 K=0.055
Test age 28.000 Sample 1.000 C=0.019 M0=0.784 K=0.067
Test age 28.000 Sample 2.000 C=0.019 M0=0.689 K=0.061
Test age 90.000 Sample 1.000 C=0.016 M0=0.545 K=0.131
Test age 90.000 Sample 2.000 C=0.015 M0=0.547 K=0.155

Fig 6.2 Typical outputs for vapour transmission
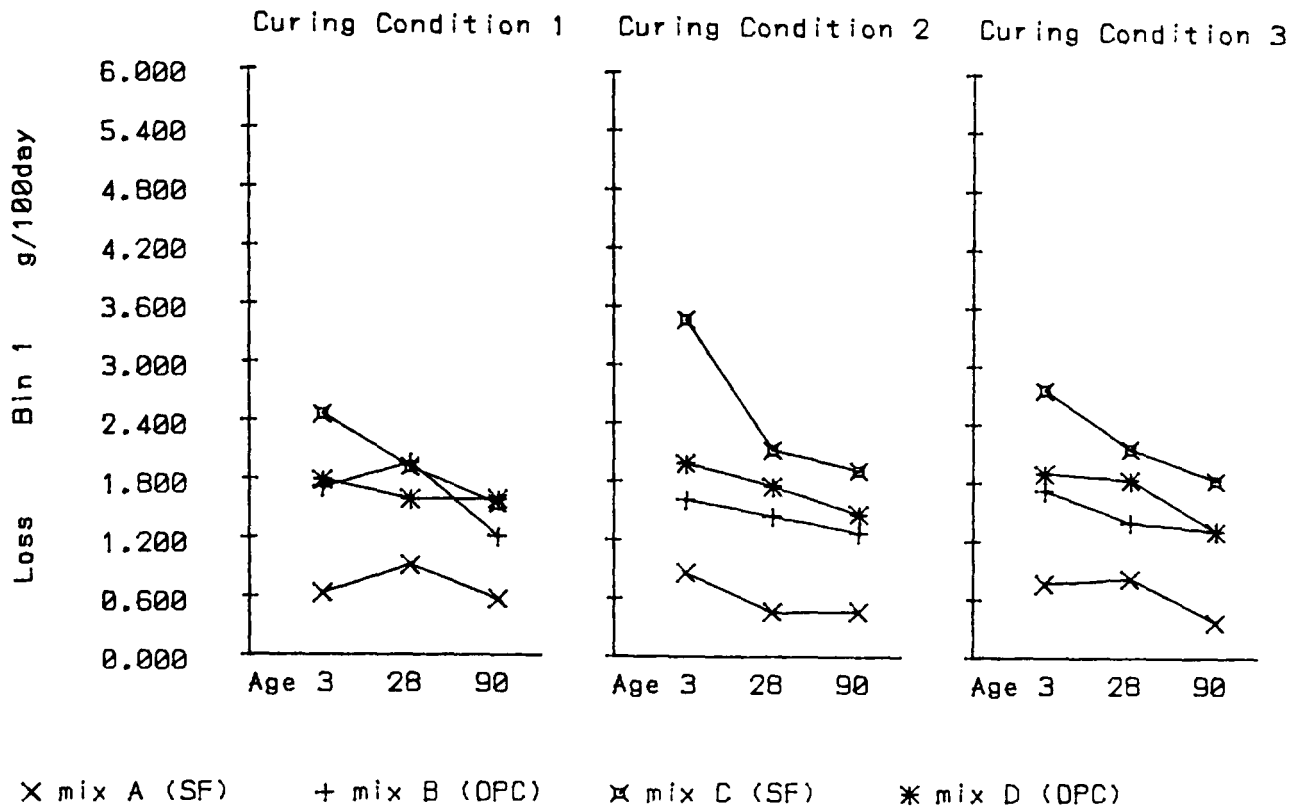
Fig. 6.3 Weight loss from the bottles in bin 1 (open to the room at 70% RH).
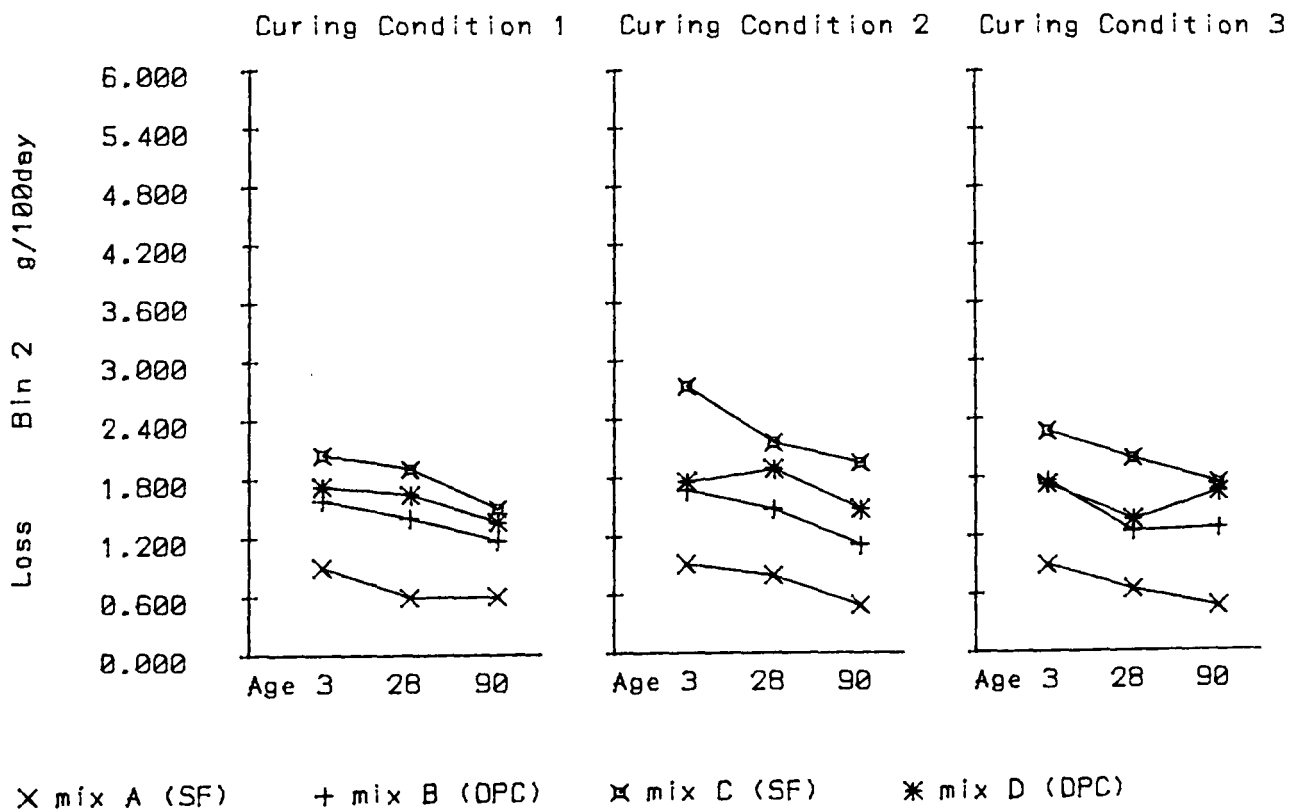
Fig. 6.4 Weight loss from the bottles in bin 2 (sealed with a quantity of sodium dichromate to give 55.2% RH) The results in figs. 6.3-6.5 are for the main set with low energy mixing. High energy mixing reverses the ranking of mixes C and D.
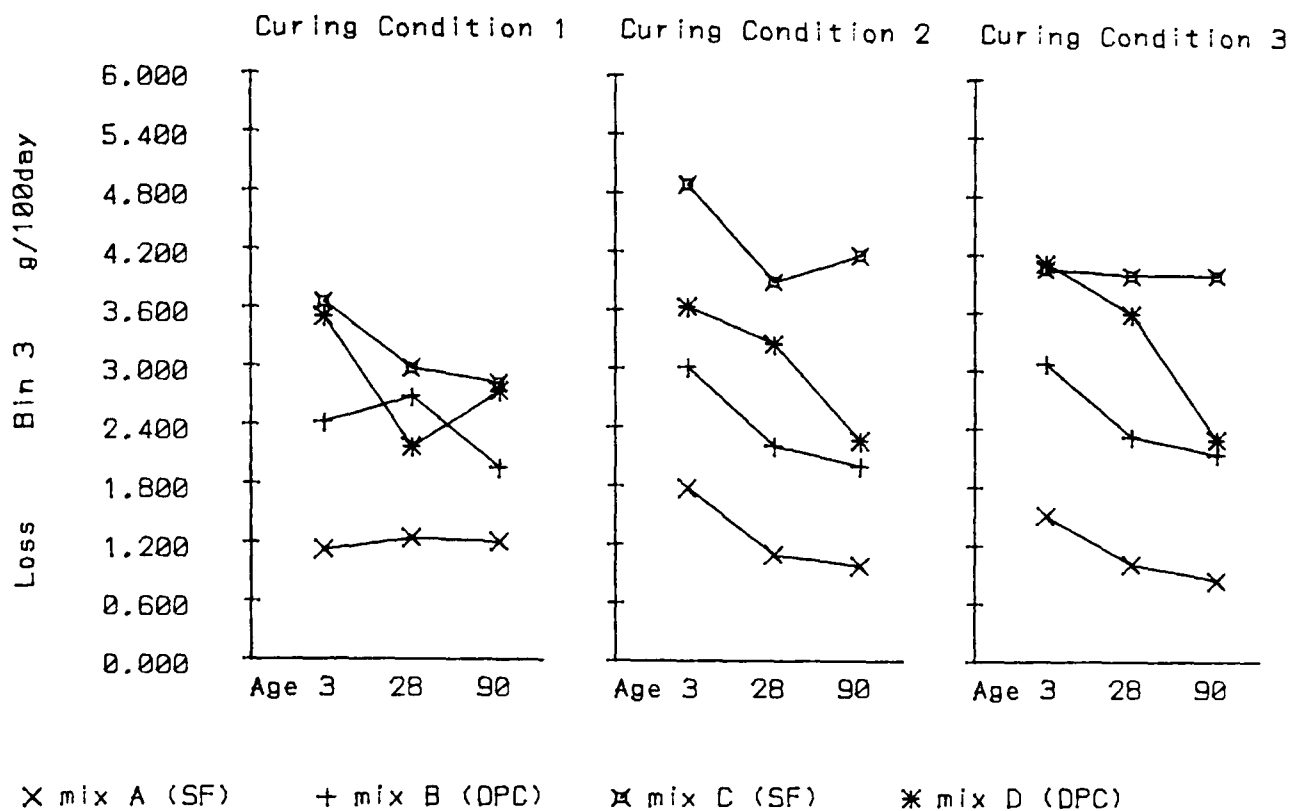
Fig. 6.5 Weight loss from the bottles in bin 3 (Sealed with a quantity of lithium chloride to give 12.4% RH)
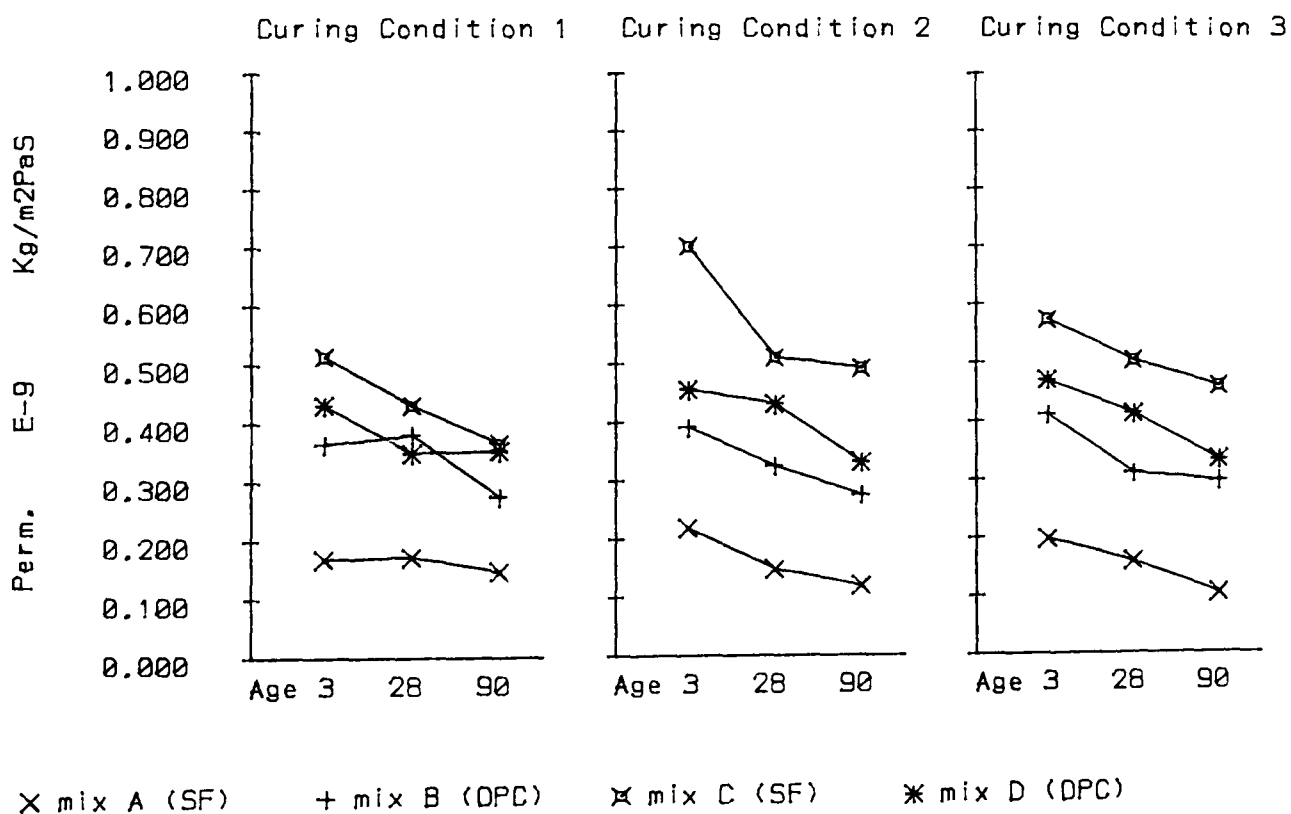
Fig. 6.6 Permeability calculated from a weighted average of the weight losses from the bottles in all three bins. As noted on fig.5.4 the ranking of mixes C and D is reversed by high energy mixing.

Curing Condition 1   Curing Condition 2   Curing Condition 3

X mix A (SF)   + mix B (OPC)   ⋈ mix C (SF)   ✳ mix D (OPC)
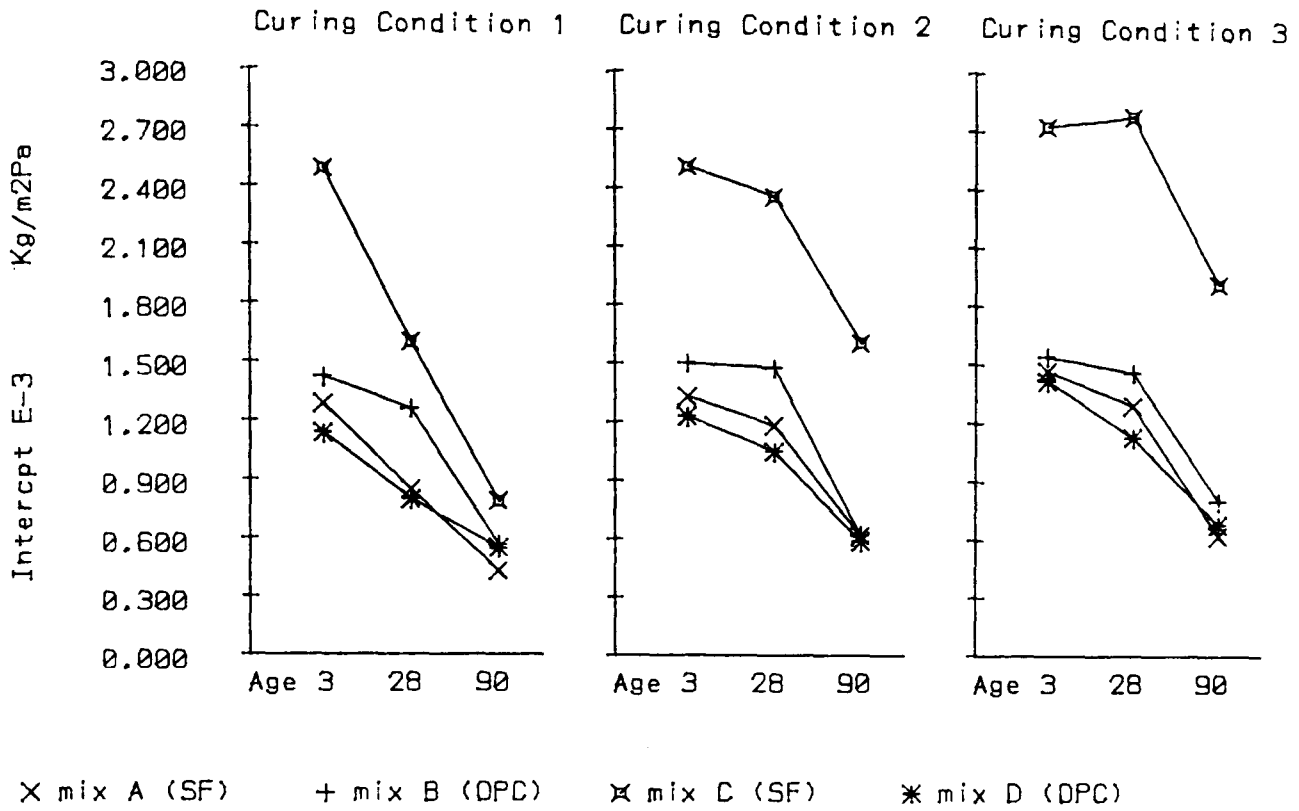
Fig. 6.7 The extrapolation of the linear weight loss back to
the time when exposure was started (see fig 5.2). This
measures the total effect of the initial processes of
completion of hydration and achievement of equilibrium
moisture content.

Curing Condition 1   Curing Condition 2   Curing Condition 3

X mix A (SF)   + mix B (OPC)   ⋈ mix C (SF)   ✳ mix D (OPC)
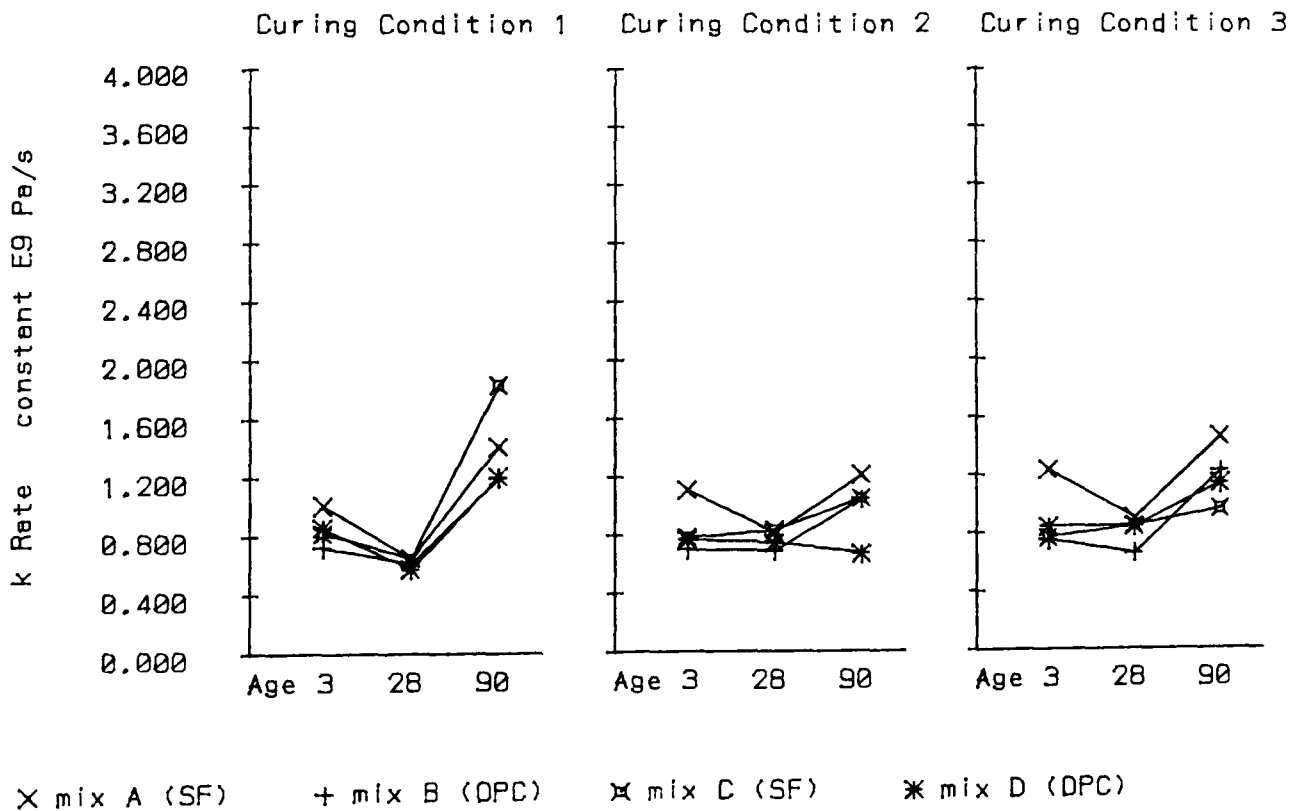
Fig. 6.8 The rate constant is a measure of the rate at which
the initial processes are completed and the mass loss
becomes constant.

7 Oxygen Transport.

7.1 Experimental method.

7.1.1 Introduction.

The rate of transmission of oxygen through mortar samples has been measured at applied pressures of 1 and 2 atmospheres. The apparatus used for testing was designed by Cabrera and Lynsdale (1988). The rate of flow was measured with a bubble flow meter. The apparatus is shown in fig.7.1. The seal is formed by first coating the sample with silicone rubber and then compressing it into a surround of synthetic rubber.

7.1.2 Preparation of samples.

Mortar samples were cast as 100mm cubes. When they were struck (after 1 day) 25mm cores were cut from them and 20mm long samples were cut from the central portion of the cores.

At the test age the samples were dried for 24 hours at 105°C and placed in a dessicator. When they had cooled a thin film of silicone rubber was applied to the curved surfaces and allowed 24 hours to set before testing.

Before testing the curing condition 2 samples any remaining curing agent on the end surfaces was removed using No 40 grit sandpaper. Penetration of this material into the pores could, however have reduced the flow rates.

7.1.3 Testing procedure.

The samples were tested at applied oxygen pressures of 1 and 2 atmospheres above ambient. Two samples were tested for each condition. Before testing, the samples were allowed a minimum of 30 minutes to equilibrate and to purge the air from the system, and for samples with very low flow rates this was increased to several hours. Two readings were made on each sample at each pressure and the average of these two readings was used. Different diameter bubble flow meters were used ranging from 1.7mm. for very low flows to 10mm. for high flows.

Leakage was checked for with some spare samples by spreading the silicone rubber over the flat surfaces as well as the curved surface and checking that there was no gas flow. No flow was observed. If there had been any substantial leakage the range of the data would have been reduced.

7.2 Calculation of a coefficient.

7.2.1 The basis of the method.

Lawrence (1981) discusses a number of different possible coefficients of permeability.

In later work (e.g. Lawrence 1986) he uses a method based on Darcy's law. This has also been used by Bamforth (1987), Nagataki and Ujike (1986) and Cabrera and Lynsdale (1988) and is easily derived as follows:

For one dimensional flow Darcy's law states that :

$$v = \frac{K}{e} \frac{dp}{dx} \qquad (1)$$

where :

v is the velocity of the fluid

K is the coefficient of permeability

e is the viscosity

x is the distance from the surface of the sample

p is the pressure at position x

If Q is the volume per second passing through the sample measured at the low pressure P_1 (assuming an ideal gas) :

$$Q = \frac{vAp}{P_1} \qquad (2)$$

where A is the cross sectional area of the sample
thus:

$$\frac{Q}{A} \frac{P_1}{p} = \frac{K}{e} \frac{dp}{dx} \qquad (3)$$

and:

$$\frac{dx}{dp} = \frac{AKp}{QeP_1} \qquad (4)$$

integrating across the sample:

$$t = \frac{AK(P_2^2 - P_1^2)}{2QeP_1} \qquad (5)$$

where:

P_2 is the high pressure

t is the sample thickness

thus:

$$K = \frac{2tQeP_1}{A(P_2^2 - P_1^2)} \quad m^2 \qquad (6)$$

The viscosity of oxygen gas $e = 2.02 * 10^{-5}$ Ns/m^2

$P_1 = 1$ atmosphere $= 0.101$ MPa

7.2.2 Relationship between readings at different pressures.

The relationship between the readings at the two pressures is shown in fig.7.2. which

is plotted logarithmically to spread the readings. It may be seen that the data lies very accurately on the line of equality indicating that the use of Darcy's equation was justified. The average of the two readings was used for all further analysis.

7.3 Results and discussion.

7.3.1 General.

The results are plotted in fig.7.3. Both Lawrence (1984) and Bamforth (1987) indicate that the expected range for concrete permeability is 10^{-15} to 10^{-18}. It may be seen that the present results for dense mortar are about half an order of magnitude below this range as would be expected. The reason for any variability in the data must lie in the samples or their installation and not in the readings because of the good relationship between the independent readings for the two pressures. The repeatability between the two samples tested was generally within 20% and checks were made to ensure that there was no systematic difference in the readings from each of the four cells.

7.3.2 Dependence on curing.

The OPC results decreased with age as expected but for some reason the SF samples from curing conditions 1 and 3 showed an increase in permeability with age. This observed increase would not have been caused by different surface conditions of the samples causing leakage past them because they were all cored at the same age immediately after casting. There must therefore have been a genuine effect which increased the permeability of these samples but did not affect the samples from curing condition 2. A possible explanation is that the oven drying caused microcracking but did not affect the curing condition 2 samples because the residual curing agent on them prevented them from drying out so fast. A method of testing this theory would be to use a different method of drying such as vacuum drying. A possible cause for a true increase in permeability associated with an observed increase of porosity in a particular pore size range is discussed in chapter 14.

7.3.3 Diffusion.

Lawrence (1984) has measured the coefficient of diffusion. This differs from the permeability in that an oxygen free gas (nitrogen) is introduced adjacent to the low pressure side of the sample and the oxygen is then detected in it. He suggests that the diffusivity is more relevant to real structures but presents data to indicate that it is linearly proportional to the permeability. Correlations to this permeability data should therefore be relevant to the diffusivity.

7.3.4 Liquid permeability.

Bamforth (1987) derived a relationship between gas and liquid permeability based on experimental observations and gas slippage theory. His relationship indicates that the water permeability corresponding to a gas permeability of $6*10^{-19}$ which was measured for one of the mix A samples would be below $1*10^{-21}$. The highest readings of $5*10^{-16}$ would give a water permeability greater than $5*10^{-17}$. This suggests that the large range of readings for gas permeability would correspond to an even larger range for water permeability.

7.4 Conclusions.

1. The oxygen permeability of small mortar samples has been measured.

2. The dependency of the results on pressure is accurately predicted by Darcy's law.

3. The permeability of the OPC results decreased with increasing age as expected. An unexpected increase with increasing age was observed for the SF samples. This is discussed in chapter 14.

POINT OF PRESSURE FROM CLAMP

PRESSURE GAUGE

S/S LID

GAS IN

S/S MOUNTING HOLDER

SAMPLE

SYNTHETIC RUBBER MOUNTING

PVC SLEEVE

GAS OUT

S/S CASING

D RING

S/S BOTTOM PLUG
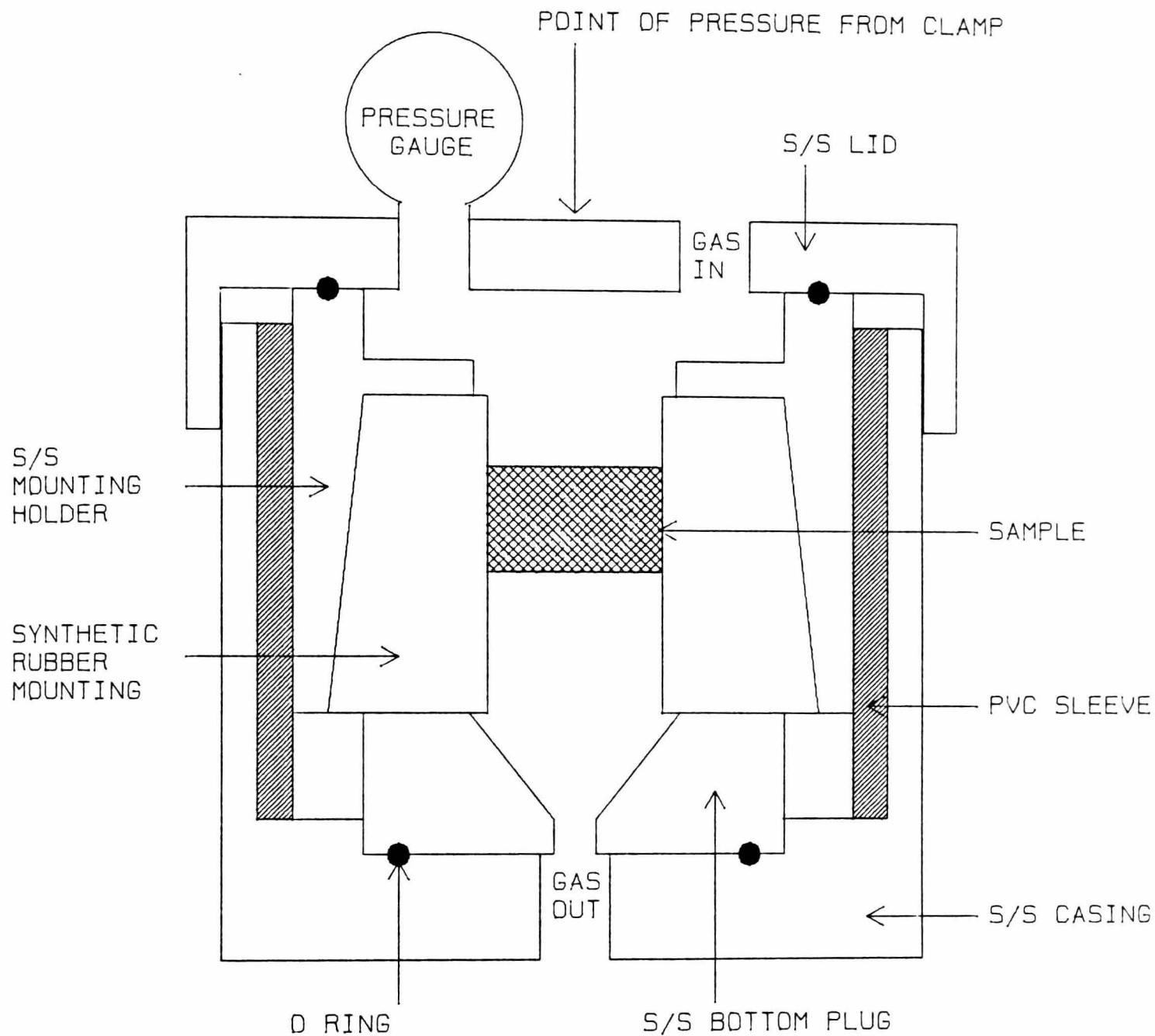
All machined parts drawn to scale
at full size, circular on plan.

VERTICAL SECTION THROUGH SAMPLE HOLDER FOR
OXYGEN PERMEABILITY MESUREMENTS.

Fig 7.1
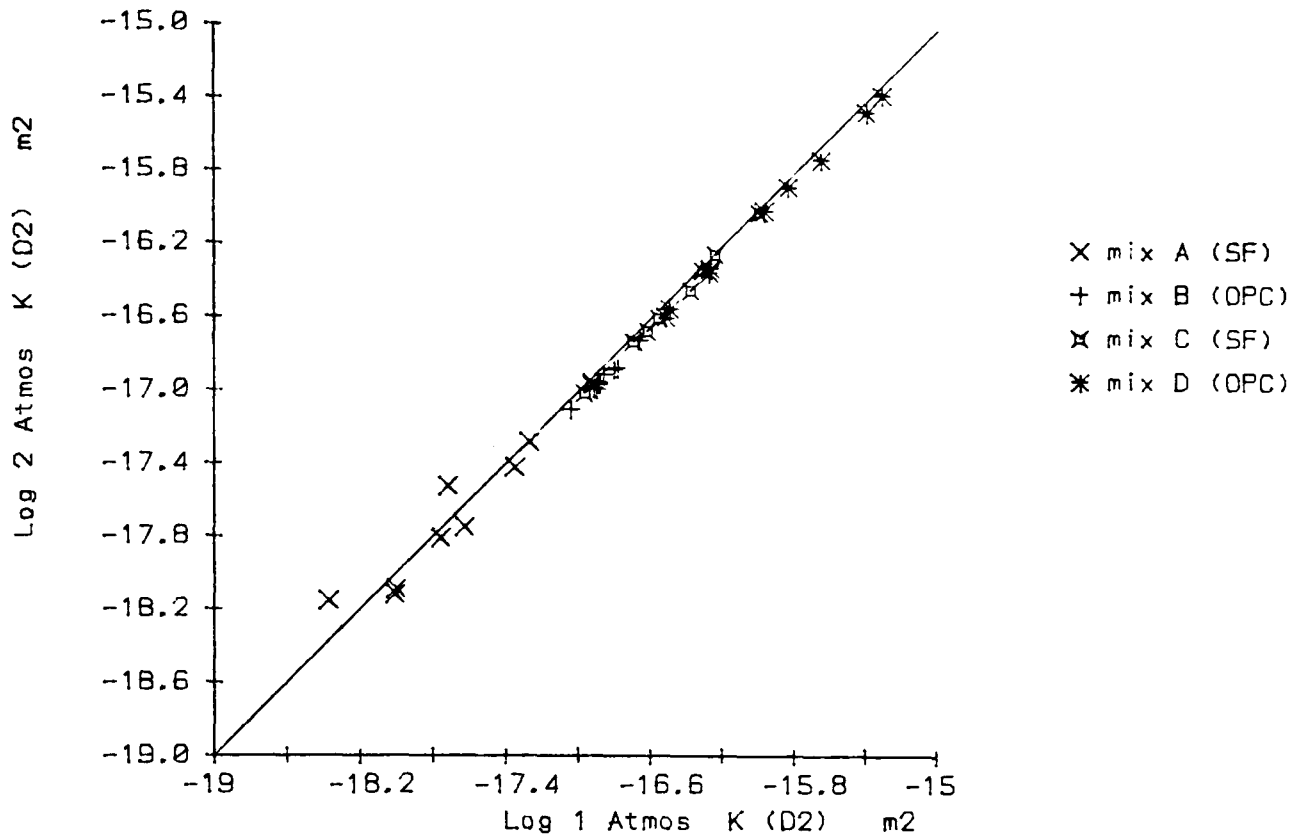
Fig. 7.2 Showing the good relationship between measurements of the oxygen permeability K made at 1 atmosphere pressure drop and those at 2 atmospheres. The line drawn is that of equality (Y=X)
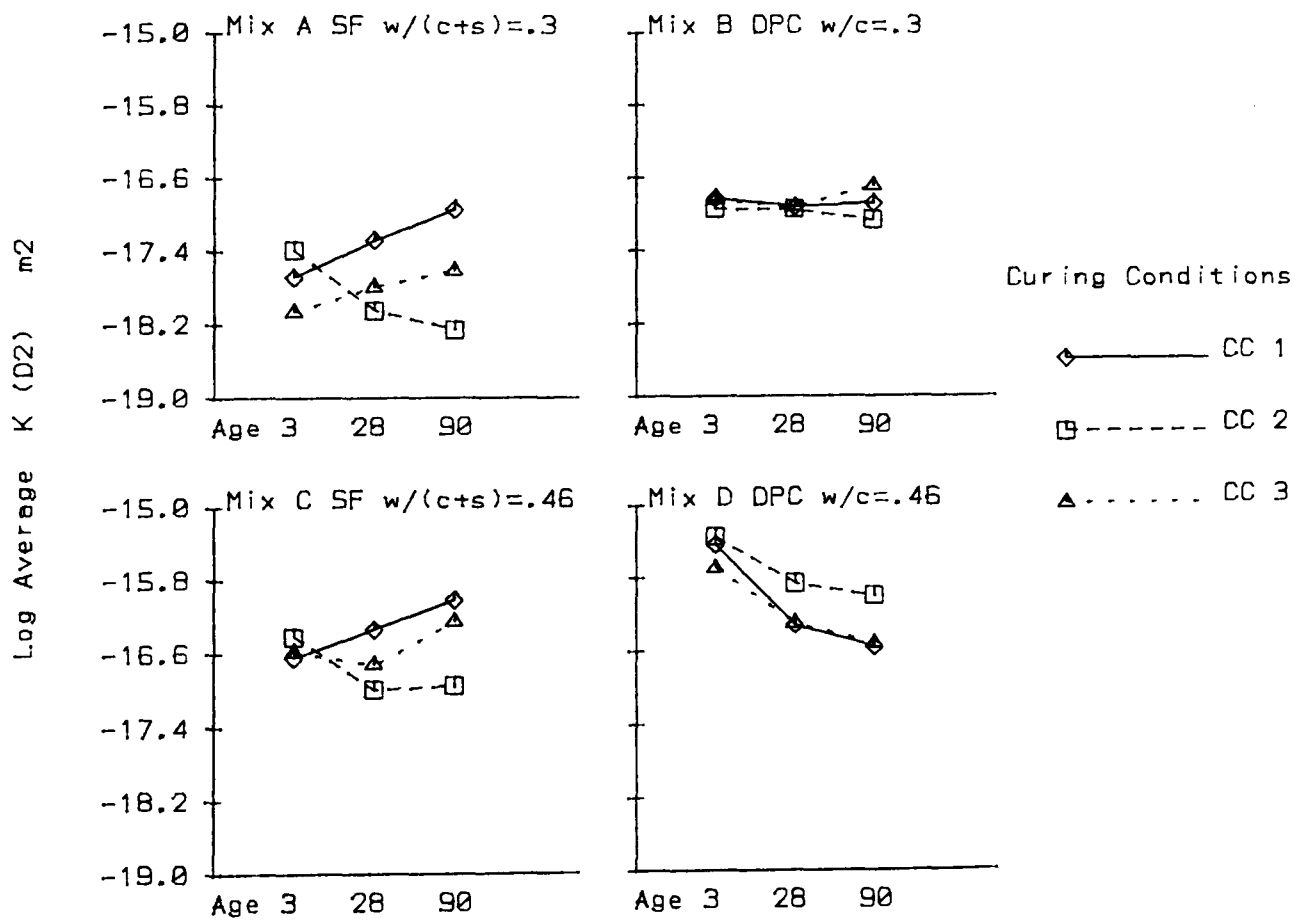
Fig. 7.3 The final results for the oxygen permeability K calculated from an average of the readings at 1 and 2 atmospheres.

8 Helium Intrusion.

8.1 Introduction.

In this chapter and the three that follow it experiments are described that measure fundamental properties of the mixes. These properties are not directly related to the aggressive processes that cause the deterioration of the concrete but are measured in order to understand and predict the processes.

8.2 Experimental apparatus.

8.2.1 General.

The helium pyconometer measures the volume of helium which a sample displaces. The sample is positioned in one of two chambers in the machine which initially have equal volumes. After evacuation an equal volume of helium is introduced into both chambers and the pressure in each one is measured. The machine then calculates a volume change to the empty chamber in order to make the volumes equal, i.e. to compensate for the presence of the sample. This volume change is effected by means of a piston and then helium is introduced again. The cycle repeats until equal pressures are found in both chambers at which time the volume of the sample is known from the position of the piston.

8.2.2 Error from sample size.

Initial tests were carried out on solid samples. It was found that if two identical samples were tested but one was cut in half before testing the results were different. This was interpreted as a failure of the gas to penetrate the closed pore structure which may be partially exposed by cutting the sample. For this reason all of the samples were ground before drying and tested as a powder.

8.2.3 Error from temperature.

The test is very temperature sensitive. In the machine the two chambers are formed in the same aluminium casting in order to keep them at the same temperature. The system is, however, badly disrupted if the sample is not at room temperature and testing samples within two hours of removing them from the oven was found to cause errors.

8.3 Experimental procedure.

8.3.1 Sample preparation.

The samples were cast in disposable plastic cups. The cups were full for concrete samples (approx 200cc) and half full for paste and mortar. Low energy mixing was used for the paste samples. All samples were dried for 24 hours at 105°C and then

stored in a dessicator in the same room as the testing machine for a further 24 hours before testing in order to reach equilibrium at the same temperature as the machine. All of the samples used were ground to pass a 1.18mm. sieve. It should be noted that grinding was continued until the entire sample would pass through the sieve. Thus the proportion of aggregate in the sample which was tested was representative of the whole mix.

8.3.2 Testing procedure.

The specific gravity of the samples was measured on a Micromeritics Helium Autopyconometer 1320. The samples were weighed before testing and the mass was manually entered onto a register on the machine which then calculated the specific gravity. Two samples were tested for each condition. The evacuation time was set to 3 minutes.

8.4 Results and discussion.

8.4.1 Results.

The specific gravity results for paste, mortar and concrete are presented in figures 8.1, 8.2 and 8.3. The maximum difference between pairs of readings was 0.03.

8.4.2 Materials tests.

The following values were obtained for the mix components after they had been prepared in the same way as the other samples (i.e. the aggregate was ground before drying).

Silica fume	2.214
Fine aggregate	2.670
Coarse aggregate	2.681

8.4.3 Calculations.

The specific gravity of concrete may be simply calculated from that for paste. If a sample of concrete of mass M and specific gravity SG contains a mass M_p of paste and M_a of aggregate with specific gravities SG_p and SG_a it may be seen that:

$$\frac{M}{SG} = \frac{M_p}{SG_p} + \frac{M_a}{SG_a} \qquad (1)$$

The results of calculating the specific gravity of concrete from that of paste and mortar is plotted against the measured values in figs.8.4 and 8.5. The graphs show the line of best fit to the data and the line of equality. It may be seen that in fig 8.4 the line of best fit is almost exactly coincidental with the line of equality. As was stated in section 8.3.1. the paste samples were made using low energy mixing and the good fit of the line for the paste samples is considered to be evidence that even when mixed in this way the paste has the same SG as the paste fraction of the concrete.

8.5 Conclusions.

1. The specific gravity of paste, mortar and concrete samples has been measured by helium intrusion.

2. In order to get repeatable readings it was necessary to grind the samples to powder and ensure that they reached thermal equilibrium.

3. There is evidence that paste mixed with low energy mixing has the same SG as the paste fraction of concrete.
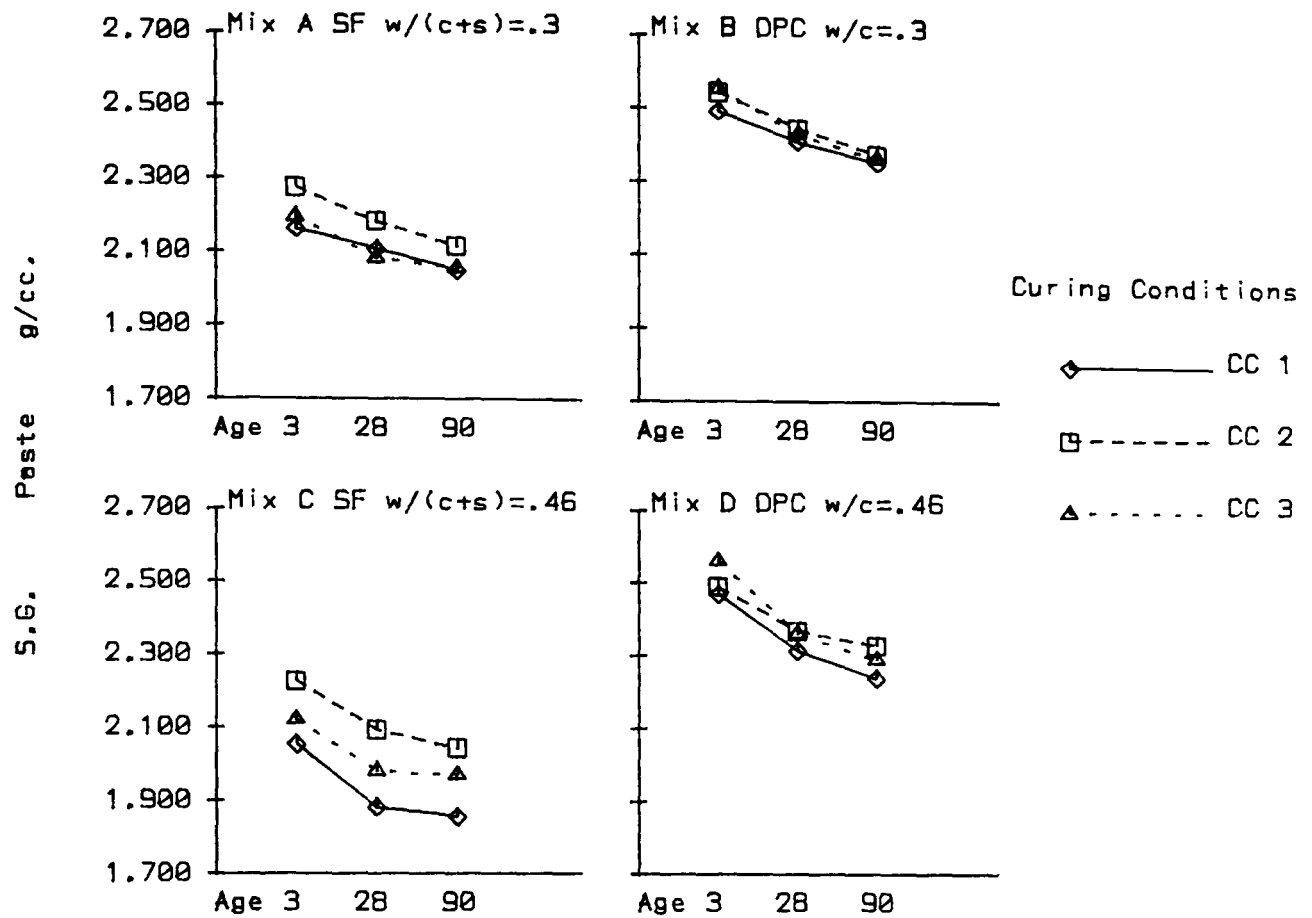
Fig. 8.1 The specific gravity of paste samples measured by helium intrusion.
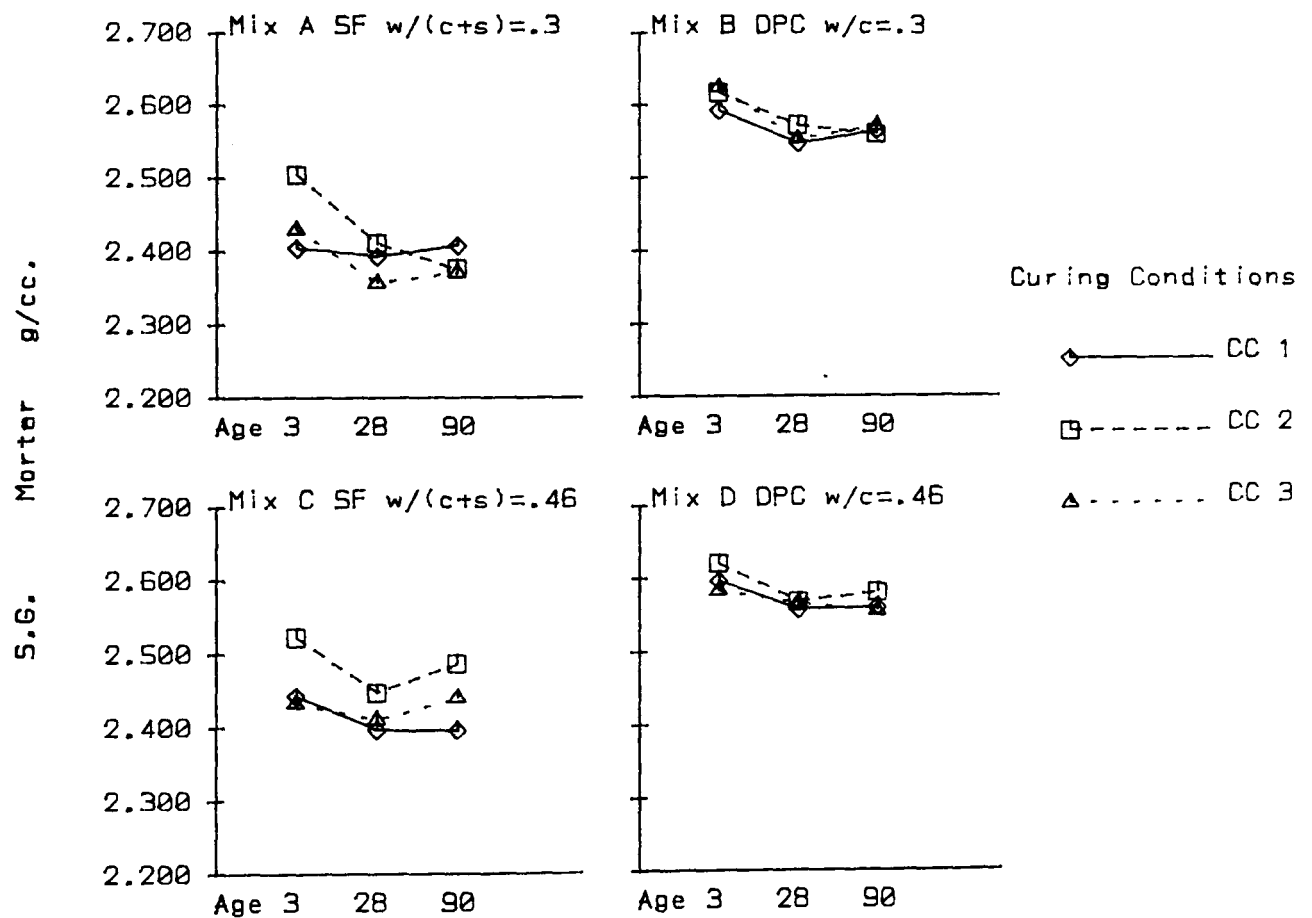
Fig. 8.2 The specific gravity of mortar samples measured by helium intrusion.
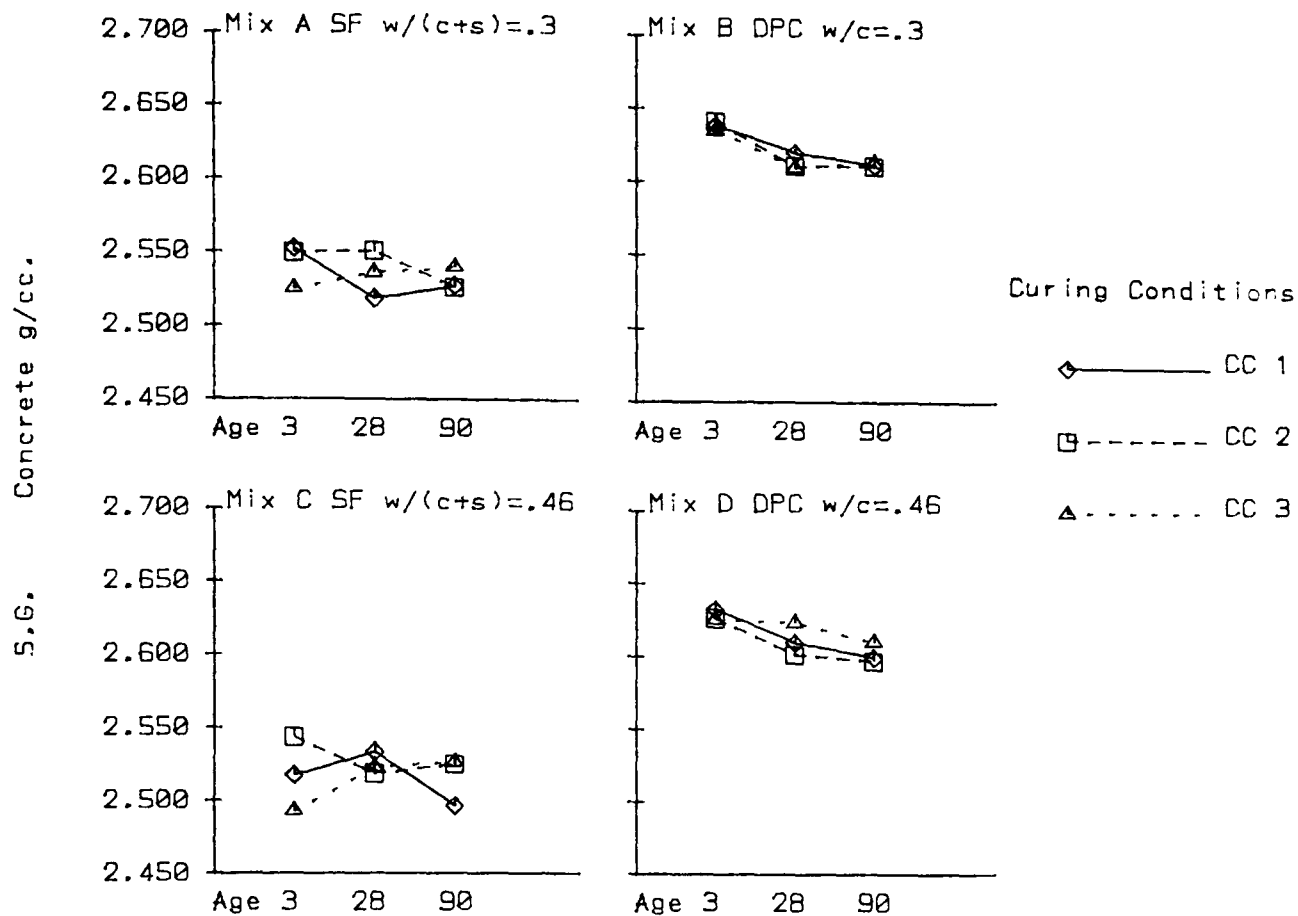
Fig. 8.3 The specific gravity of concrete samples measured by helium intrusion. Note that all of the samples were ground before testing.

Equation for line : Y=7.951988115E-3+X*0.9966389774
R squared=0.832
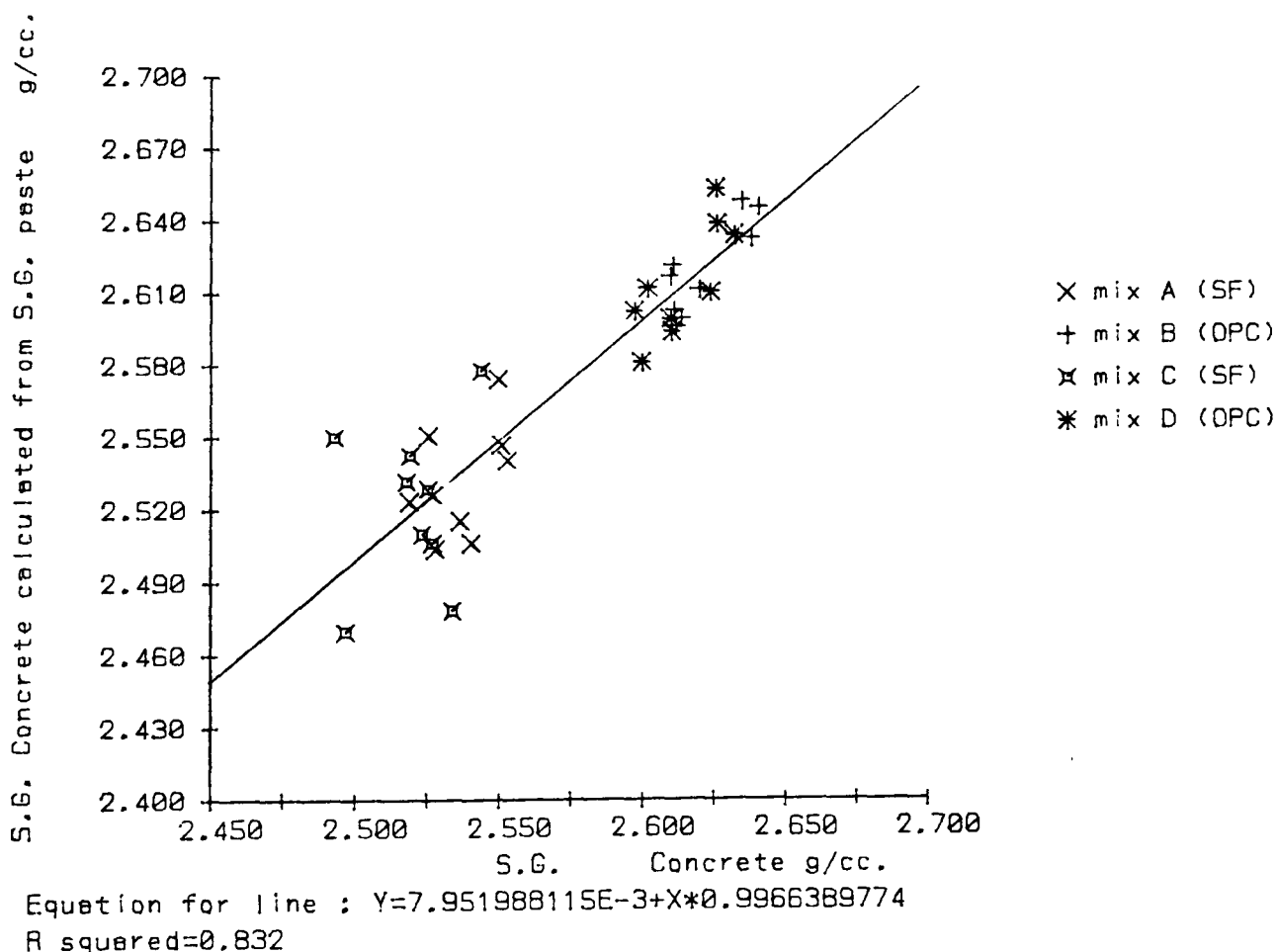
Fig. 8.4 The calculation of the specific gravity of concrete from that for paste. Note that the equation for the line of best fit is exceptionally close to Y=X.

Equation for line : Y=0.4274709084+X*0.8405044461
R squared=0.811
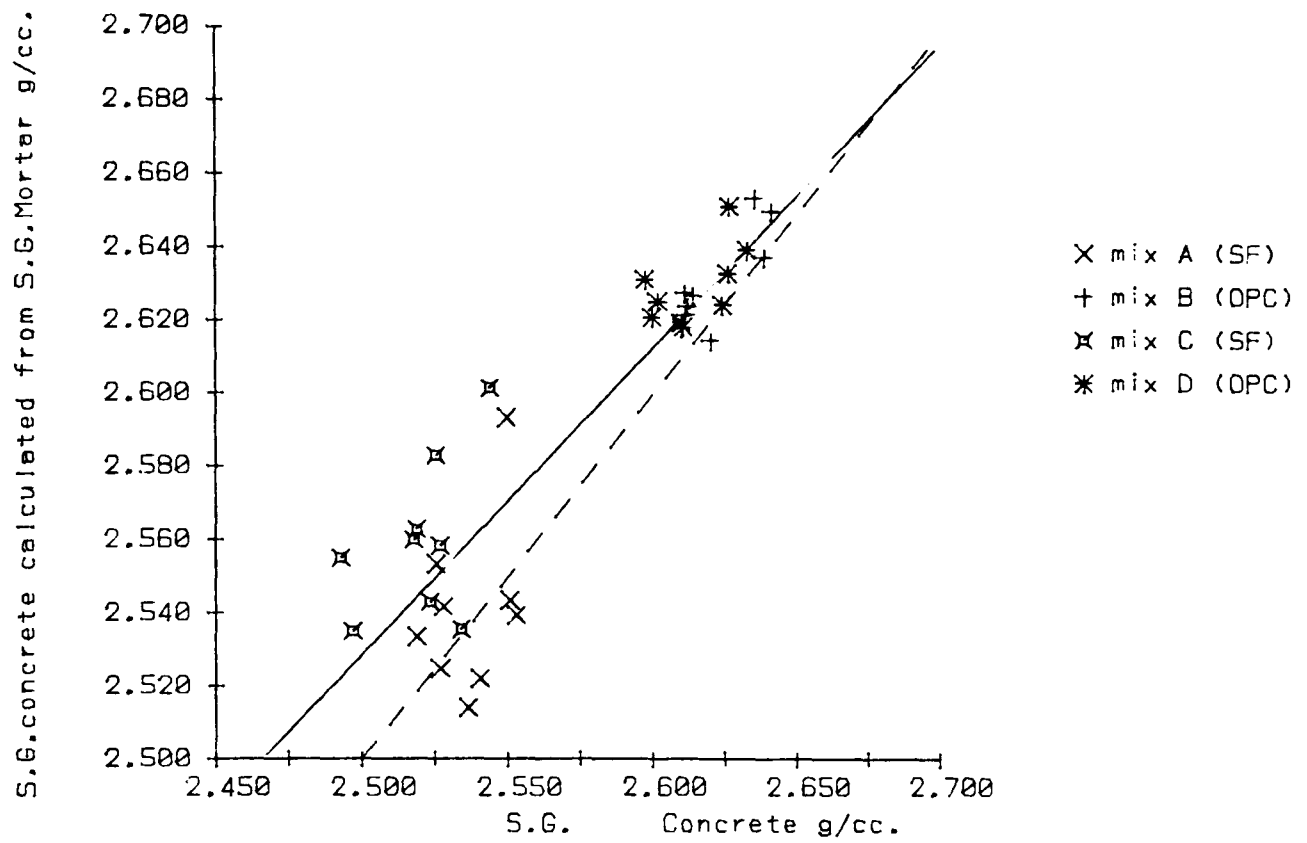
Fig. 8.5 Calculation of the S.G. of concrete from that for mortar. The dashed line is the line of equality and the solid line is the line of best fit described by the equation given.

9 Mercury Intrusion.

9.1 The method and limitations.

9.1.1 General.

Mercury intrusion is similar to helium intrusion in that it measures the volume of fluid displaced by a sample but it gives far more information. The mercury only penetrates the pores under pressure therefore at low pressure the bulk volume is measured. Subsequently the pore size distribution is obtained as the pressure increases. Solid samples are used because grinding would destroy the pore structure and thus the measured skeletal volumes include some closed pores and are greater than those obtained from helium intrusion.

9.1.2 Theory.

The theory of mercury intrusion (Sneck and Oinonen 1970) is based on the effect of surface tension limiting the entry of a fluid into small pores. The theoretical relationship for small pores which are assumed to be cylindrical is :

$$D = \frac{-4\gamma \cos\phi}{p} \qquad (1)$$

where:

D is the smallest diameter pore which the fluid can enter

γ is the surface tension of the fluid

ϕ is the contact angle of the fluid with the pore surfaces

p is the pressure

By measuring the volume of mercury that enters the sample at different pressures the total volume of pores at the corresponding diameter is calculated.

9.1.3 The contact angle.

It may be seen from equation (1) that an error in the value for the contact angle will cause an error in the calculated diameter. Provided the contact angle does not depend on the type of sample or the pressure this is not a major cause for concern in this project because it will have the same effect on all readings. Thus an observed increase in fine pore volumes will be genuine but the actual diameters may be incorrect. However, if comparisons are to be made with other methods of measuring actual diameters this could be important.

9.1.4 The effect of "ink bottle" pores.

Sneck and Oinonen (1970) discuss the effect of large pores with small necks. The measured diameter will clearly be that of the neck and not the maximum internal

diameter.

9.1.5 The effect of closed pores.

Closed pores will clearly not be measured. Feldman (1986b) claimed that in silica fume samples the divided structure of some of the closed pores is broken down at high pressures. He therefore attempted to dry all of the mercury out of the samples and carried out a second intrusion and used the readings from it. He assumed that the contact angle was the same for the second intrusions despite the effect of the wetting of the surfaces in the first intrusion.

9.2 Experimental method.

9.2.1 Apparatus.

The pore size distribution of paste samples was measured on a Micromeritics Auto-Pore 9200 mercury intrusion machine which has a maximum operating pressure of 414 Mpa. The values used for the contact angle and the surface tension were 130° and 484 dynes/cm so readings were obtained for pore diameters in the range 170 - .003 µm.

The principle of operation of this machine is that the sample is held in a glass container with a capillary tube extending from it (a penetrometer). The capillary tube is initially full of mercury but as the system is compressed under the action of hydraulic oil entering the open end of the tube the length of the mercury column in it is reduced. The outer surface of the tube is coated with a conducting material and electrical contacts are formed to this conductor and to the mercury. Because the oil and the glass are insulators the capillary tube forms a cylindrical capacitor acting between the two contacts. The value of the capacitance depends on the length of the column of mercury and by measuring the capacitance the volume of mercury intruded may be calculated. The machine evacuates the sample before introducing the mercury and after this the penetrometer is removed from the machine and weighed before being pressurised with hydraulic oil.

9.2.2 Procedure.

The mixes were prepared using high energy mixing and cast as 100mm cubes. After striking 25mm diameter cores were cut from the cubes. After curing the cores were dried for 24 hours at 105°C and permitted to cool in a dessicator. The tests were then carried out on two samples approximately 15mm long cut from the central portion of the cores.

Intrusion readings were taken at 40 different pressures while increasing the pressure and 10 while reducing it (recovery). The equilibration time was set to 30 seconds.

9.3 Analysis of results.

9.3.1 Choice of ranges.

The results were plotted in order to select ranges of pore size over which to calculate the intrusion volume in order to characterise the curves. Typical plots for two different sample conditions are shown in figs.9.1 and 9.2. These graphs show the cumulative and differential intrusion in units of cc/g which is the form in which the data is output by the machine. The following ranges were chosen:

$$170 \ - 10 \ \ \mu m$$
$$10 \ \ - 0.15 \ \mu m$$
$$0.15 \ - 0.01 \ \ \mu m$$
$$0.01 \ - 0.003 \ \mu m$$
$$0.003 - 10 \ \ \mu m \ (recovery)$$

These ranges are shown on the graphs and it may be seen that they permit a good measurement to be made of the salient features of the curves.

9.3.2 Other variables.

Each sample was weighed at the start of the experiment and the bulk volume was calculated from the volume of mercury displaced before pressurising. From the mass and bulk volume the dry density (DD) was calculated. The maximum intruded volume was subtracted from the bulk volume to give the skeletal volume and from this the specific gravity (SG) and the porosity were calculated. The results for the specific gravity, dry density and porosity are given in figs.9.3-9.5.

9.3.3 Calculations.

The intruded volumes were changed from the values of cc/g output by the machine to percentages of the bulk volume by multiplying by the dry density. This was carried out to make the total for the four ranges of intrusion add up to give the total porosity. The results for the four intrusion and one recovery ranges are given in figs.9.6-9.10.

9.4 Discussion.

9.4.1 Dependence on age and curing.

There is a great variation in scale for the different ranges. The maximum porosity in the .01-.15 μm range is 25% while the maximum in the 170-10 μm range is less than 1%. The absolute values of random errors will be the same for all ranges so the percentage errors of the readings for ranges with low porosities will be substantially greater. For this reason the effect of curing condition for the 170-10μm range indicated in fig.9.6 may not be significant. Overall there is very little effect of curing condition. With increasing age the SG decreases and the DD increases so the porosity decreases.

The main contribution to this decrease is the .01-.15 µm range, none of the other ranges show a systematic decrease with age.

9.4.2 Different ranges.

In table 9.1 the effect of choosing some other ranges is shown for the curing condition 1 samples for mixes A and D at 3 and 90 days. The first four ranges shown are those used in the analysis, the next group are some other possible ranges for the small pores and the last group are for the small pores.

Range Maximum µm	Range Minimum µm	Mix A Age 3 volume	Mix A Age 90 volume	Mix D Age 3 volume	Mix D Age 90 volume
170.000	10.000	0.314	0.516	0.411	0.270
10.000	0.150	0.863	0.829	0.352	0.195
0.150	0.010	6.255	6.122	27.026	21.223
0.010	0.003	8.461	4.970	1.700	1.524
170.000	100.000	0.125	0.100	0.131	0.109
170.000	30.000	0.201	0.266	0.297	0.236
170.000	3.000	0.596	0.799	0.485	0.310
170.000	1.000	0.884	1.113	0.544	0.338
170.000	0.300	1.027	1.275	0.654	0.397
0.030	0.003	12.620	10.552	6.619	5.545
0.100	0.003	14.659	11.042	28.205	22.635
0.150	0.003	14.716	11.091	28.890	22.747

Table 9.1 Intrusion volumes over different ranges for some CC1 samples. Volumes are given as percentages of the sample volume.

For the largest pore size range the mix A sample showed an increase with age and the mix D sample showed a decrease. The alternative ranges show the same trends except for the 170-100 µm range for mix A. This is, however, a very small range so the results are probably not significant. For the smallest range a decrease with age is evident for all of the ranges tested.

The multiple regression analysis which is presented in chapter 13 is only valid if the ranges are chosen using a pre-determined method (in this case using observed minima in the differential). Thus if the analysis was repeated with different ranges it would only be valid if a different but equally valid physical attribute was used to choose the

ranges.

9.4.3 *Recovery.*

The relationship between the total porosity and the percentage recovery is shown in fig.9.11. The lower percentage recovery for the SF samples could indicate a larger number of "ink bottle" pores. It would not be caused by breakdown of the divided structure because by the time the pressure was reduced such breakdown would be complete and would not prevent the escape of the mercury.

9.4.4 *Use of the results.*

In this project the results from this experiment are considered to be mainly of use for predictive applications. It may be that for some of the reasons given in section 9.1 the measurements are not precisely related to the diameters shown. The readings are, however very repeatable and if measurements of this type may be used to predict the durability of a mix they are of value for that reason alone. Multiple regression is used in chapter 13 to assess the relative influence of the different ranges on the principal physical properties.

9.5 Conclusions.

1. The pore size distribution of paste samples has been measured by mercury intrusion.

2. Some authors have cast doubt on the relationship between diameter and pressure used in this experiment but these considerations do not reduce its value as a predictive method for other properties such as durability.

Mix A CC 2 Age 3 Sample A (Solid lines)
Mix A CC 2 Age 3 Sample B (Dashed lines)
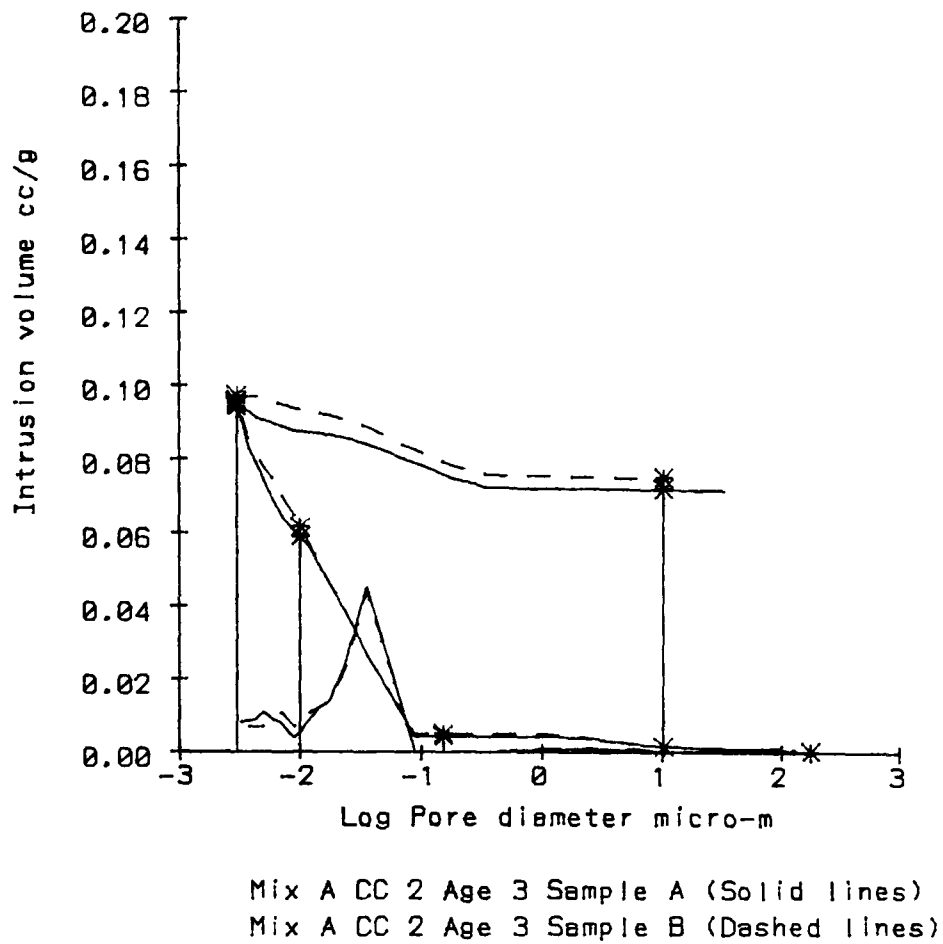
Fig 9.1   Figures 9.1 and 9.2 show typical cumulative and differential
mercury intrusion data. The vertical lines and marked points show the
ranges of pore sizes used in the analysis.

Mix D CC 2 Age 3 Sample A (Solid lines)
Mix D CC 2 Age 3 Sample B (Dashed lines)
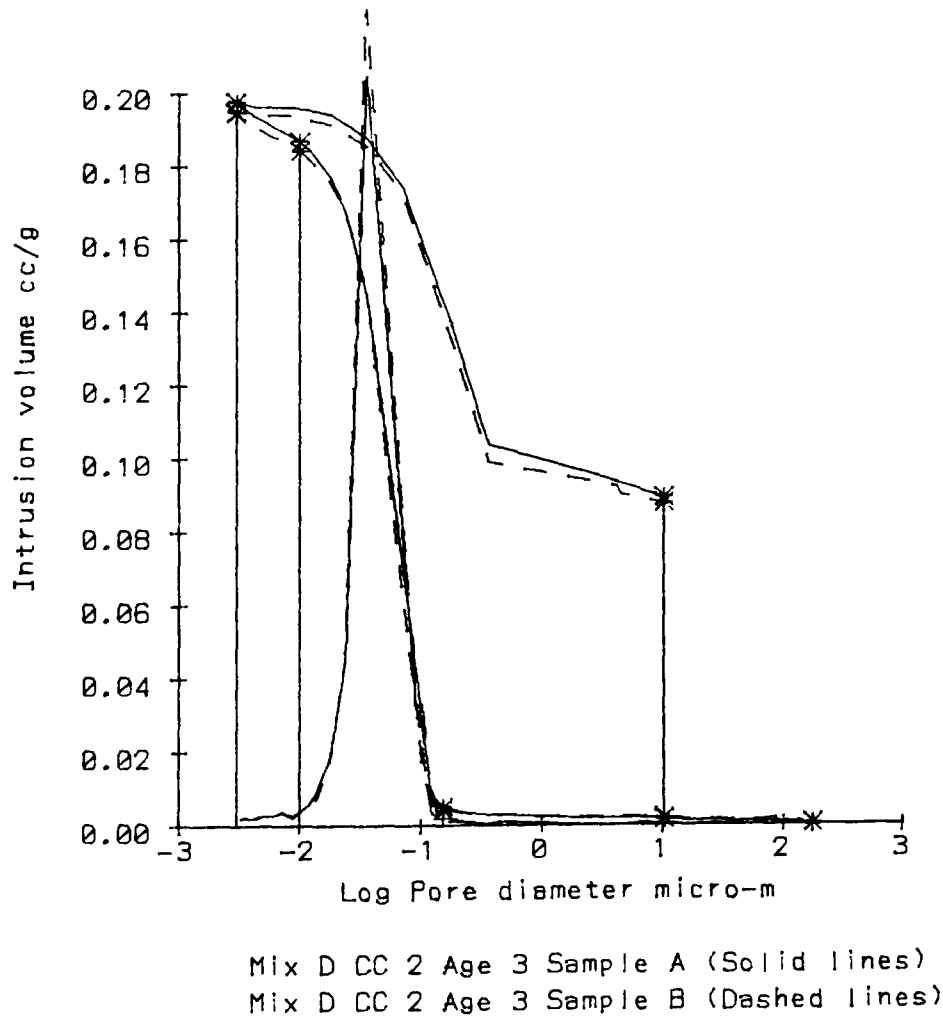
Fig.9.2 Graphs of this type were drawn for all 36 conditions and
the range boundaries occured at minima of the differential in
almost all cases.
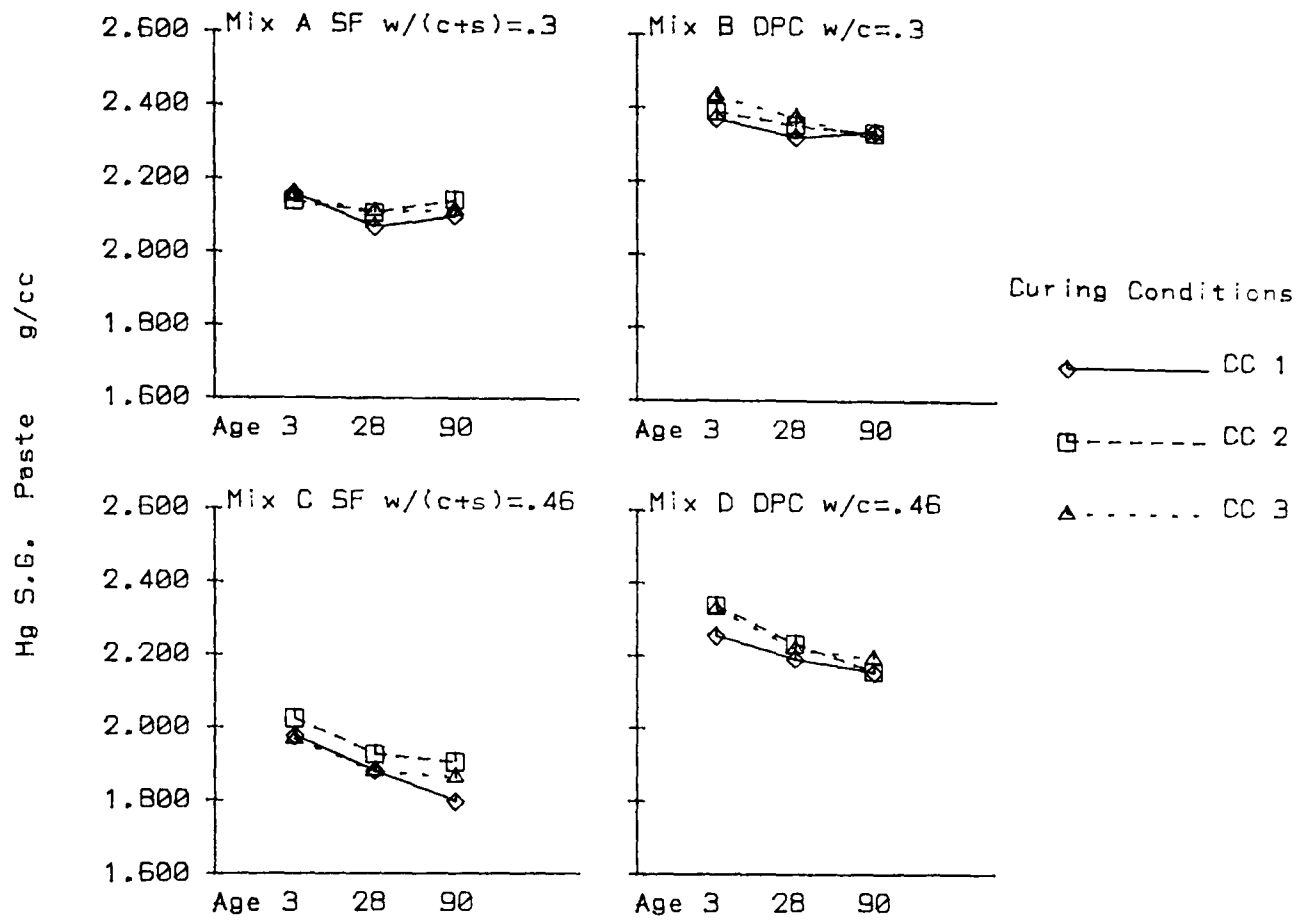
Fig. 9.3 The specific gravity of paste samples measured by mercury intrusion.
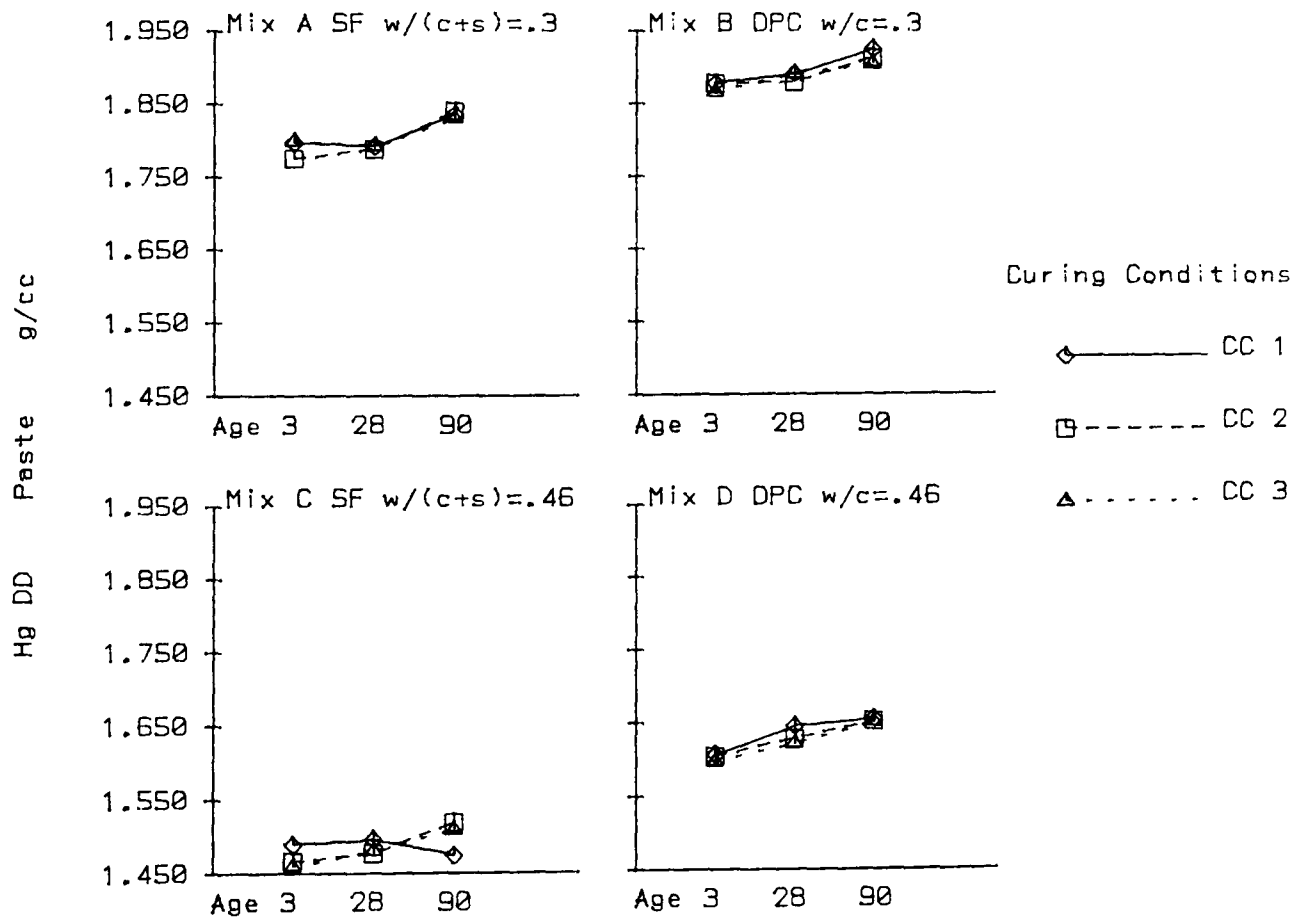
Fig. 9.4 The dry density of paste samples measured by mercury intrusion.
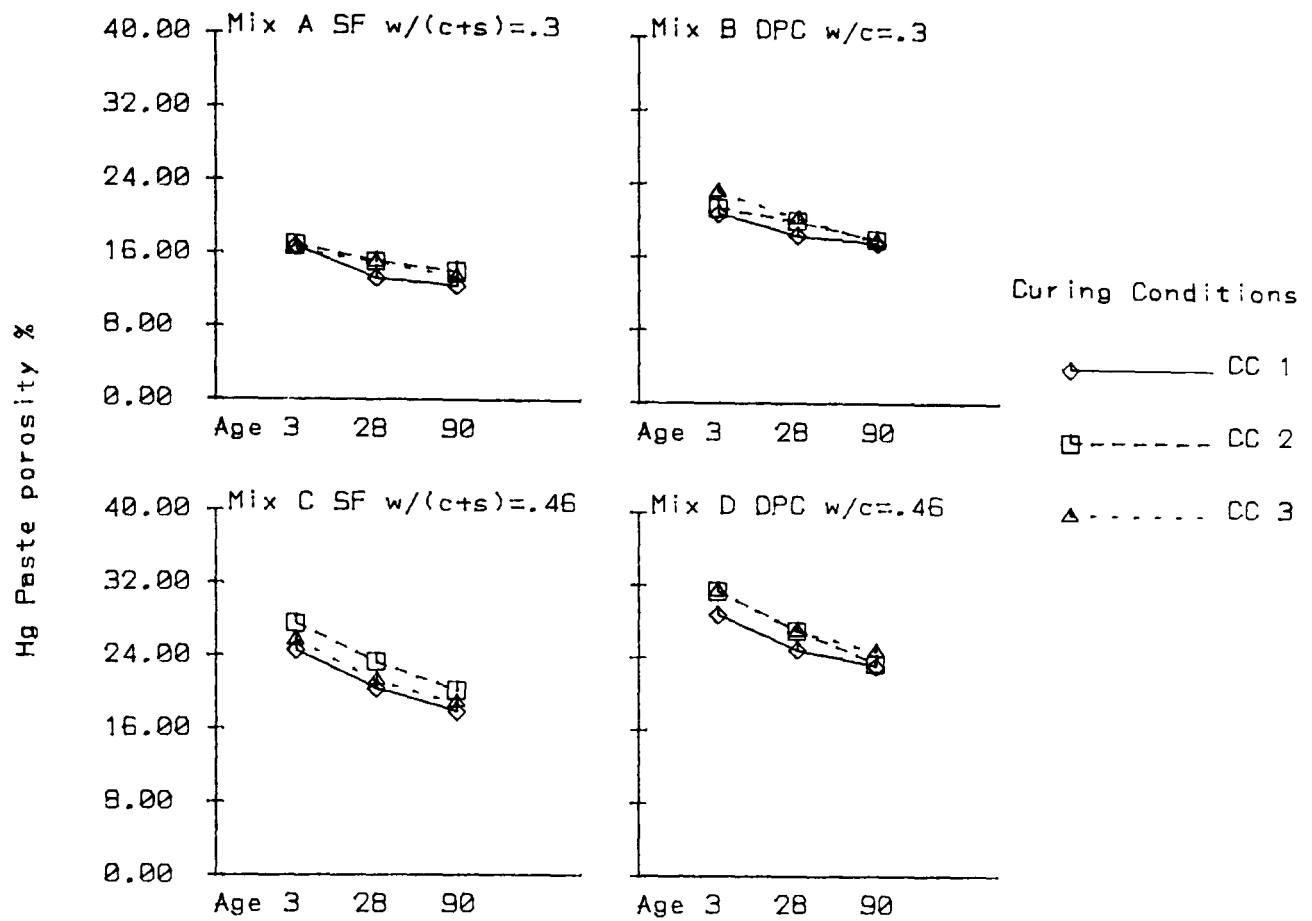
Fig. 9.5 The total porosity of paste samples measured by mercury intrusion.
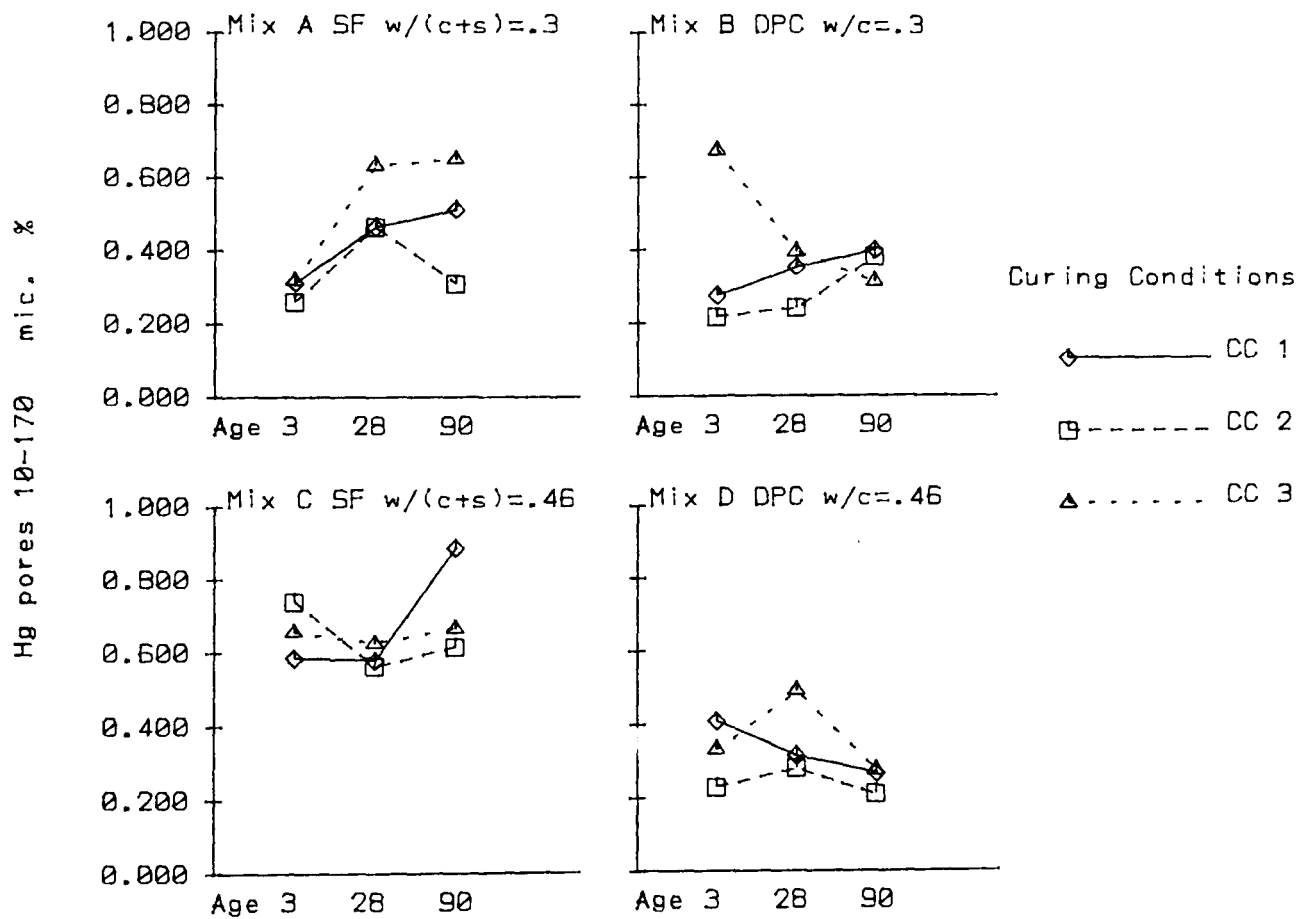
Fig. 9.6 Porosity in pores with diameters in the range 10-170 microns.
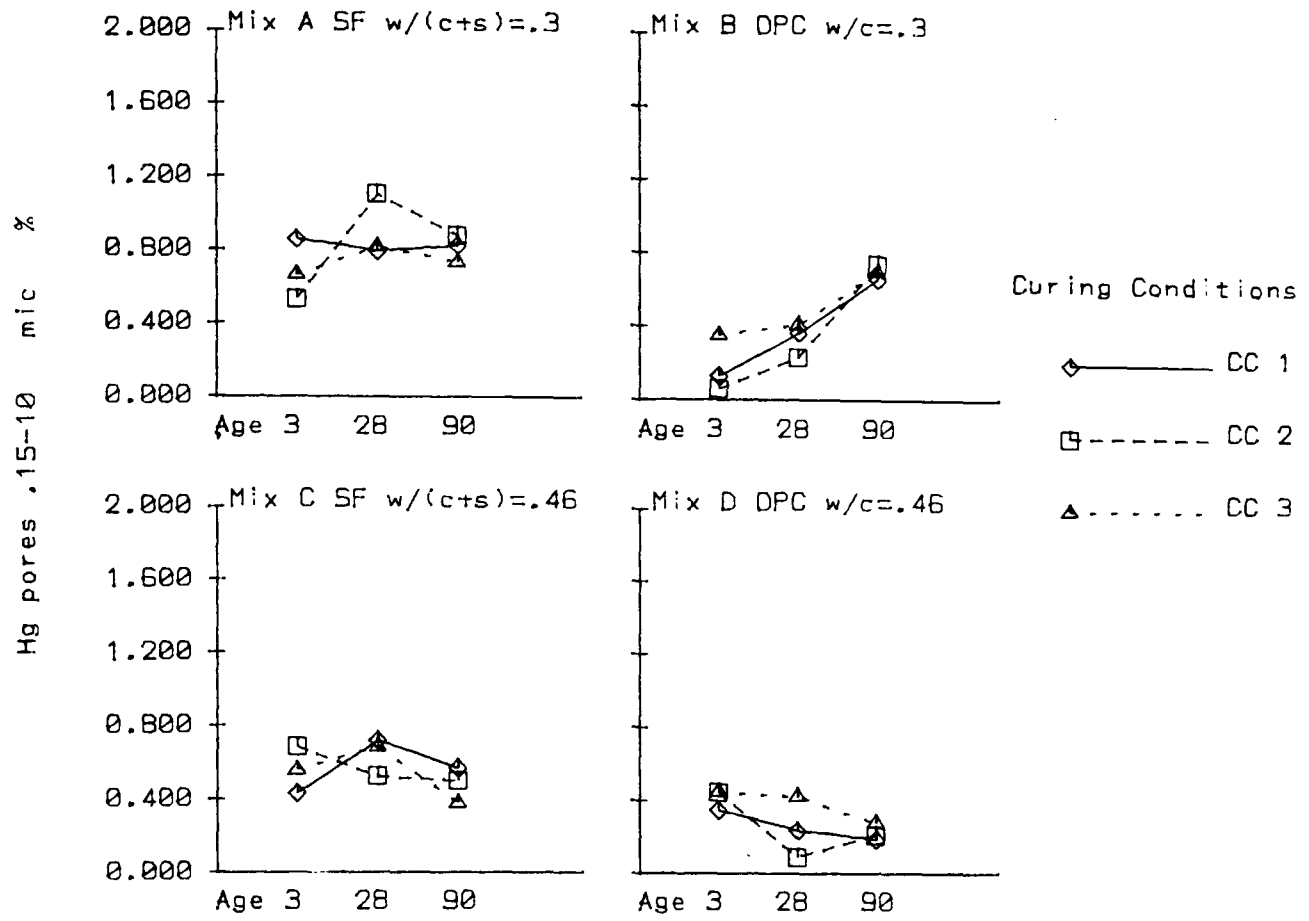
Fig. 9.7 Porosity in pores with diameters in the range .15-10 microns. Note the different scales of figures 9.5-9.10.
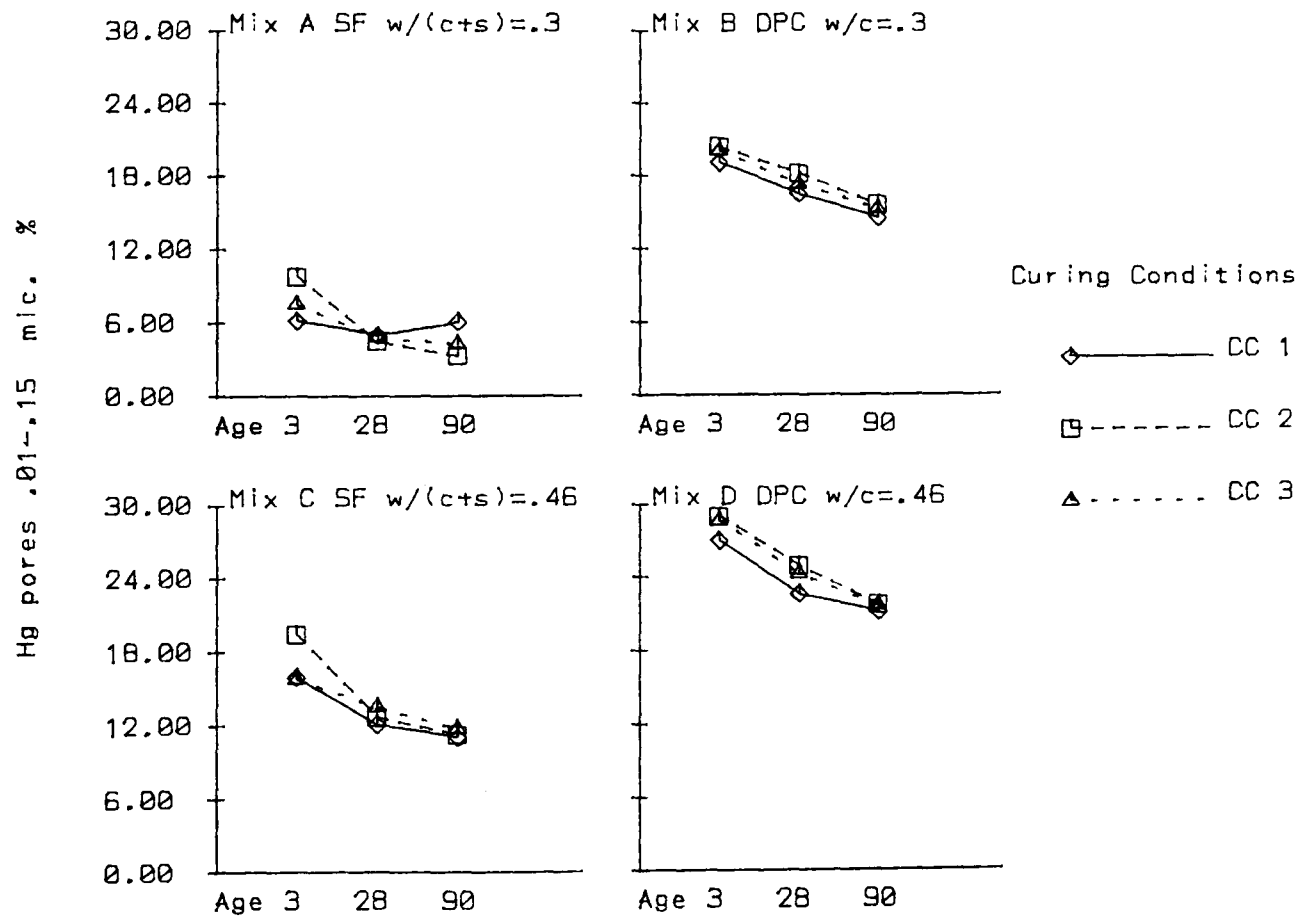
Fig. 9.8 Porosity in pores with diameters in the range .01-.15 microns. Note the difference between the SF and the DPC samples.
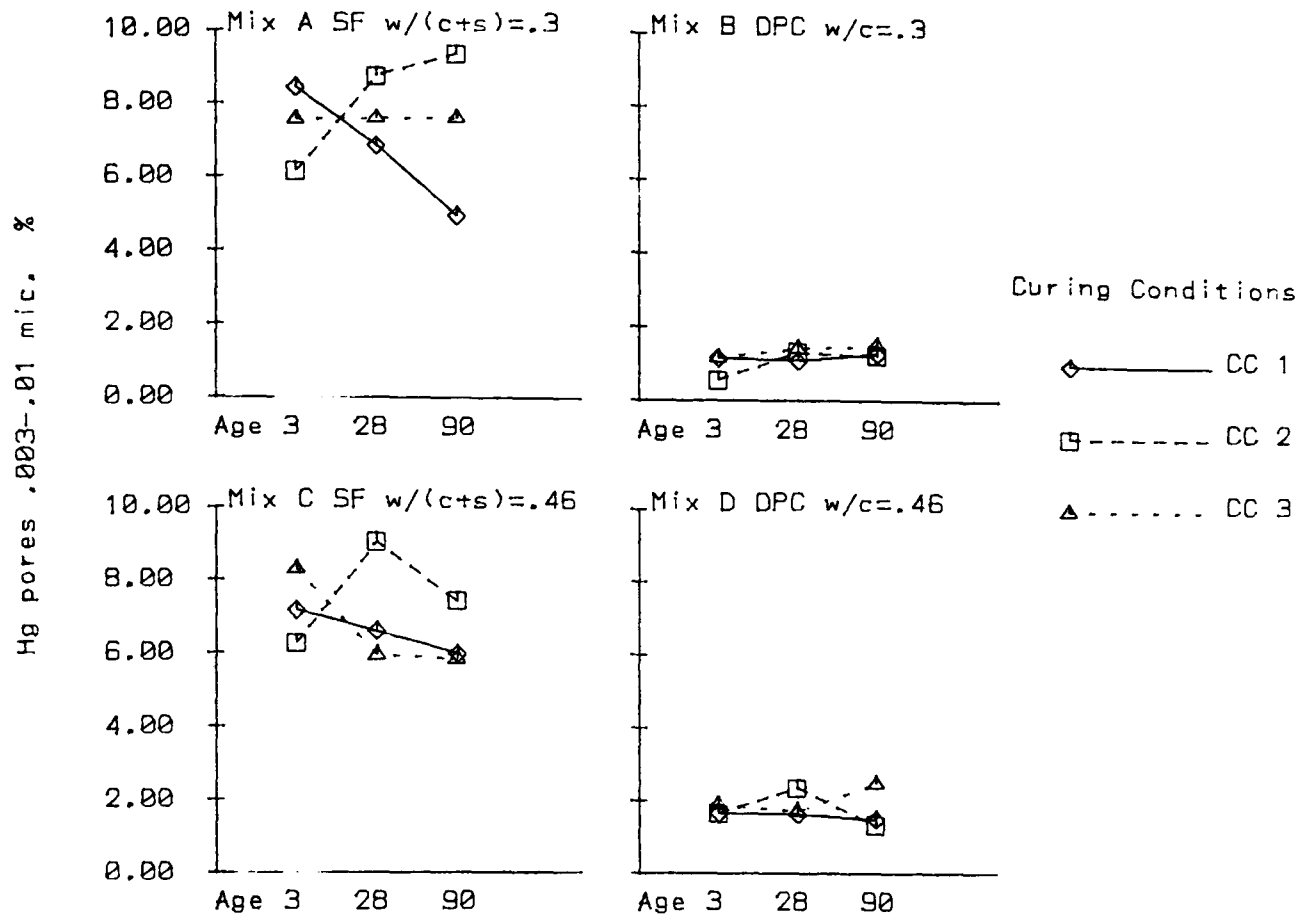
Fig. 9.9 Porosity in pores with diameters in the range .003-.01 microns.
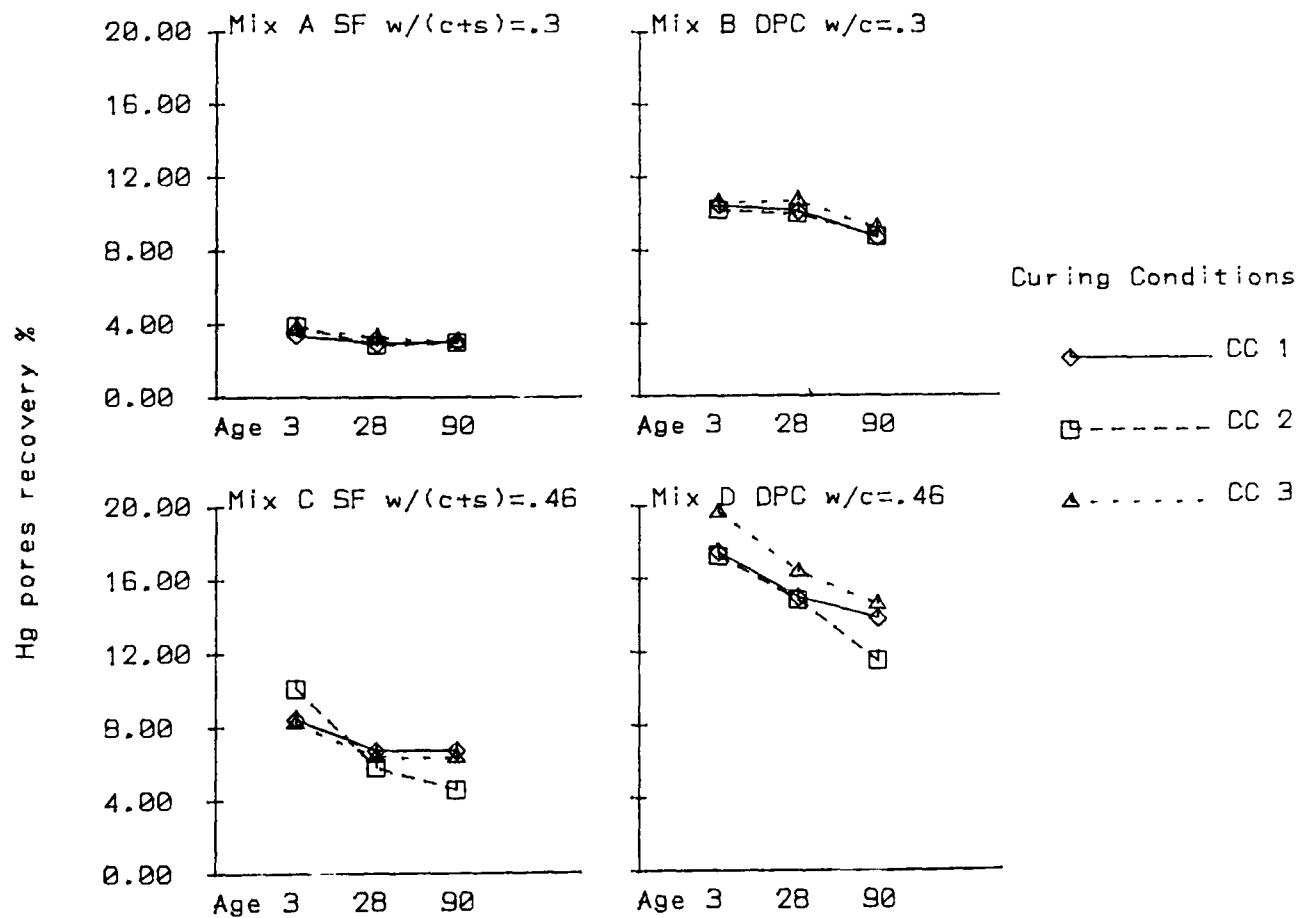
Fig. 9.10 Recovery porosity. i.e. the volume of mercury which came out of the sample when the pressure was reduced expressed as a fraction of the bulk volume of the sample.
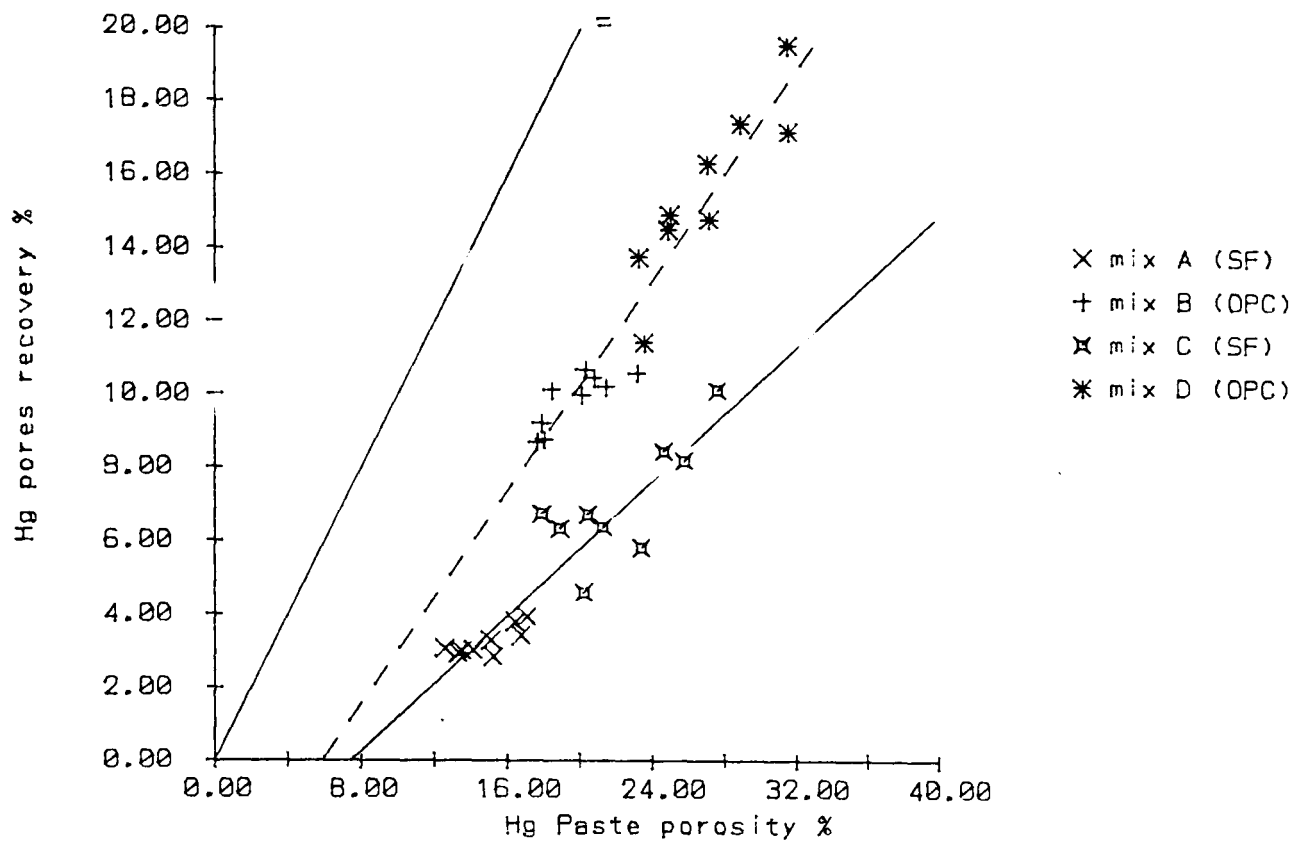
Fig. 9.11 Showing the relationship between the volume of mercury intruded into the paste (the porosity) and the volume which came out when the pressure was reduced (the % recovery). The dashed line is a best fit to the OPC results and the solid line through the SF results is a best fit to them.

10 Measurement of weight loss and density.

10.1 Introduction.

10.1.1 Calculation of specific gravity.

The purpose of measuring the weight loss on drying a sample is to calculate the amount of retained water. It is assumed that drying at 110°C removes the free water and therefore to a reasonable approximation the amount remaining is the amount which has been used in the hydration process. Thus:

$$M_w - (M_{wet} - M_{dry}) = M_{aw} \qquad (1)$$

where:

M_w = initial mass of water in mix

M_{wet} = mass of sample when mixed

M_{dry} = mass of sample when dried

M_{aw} = mass of absorbed water in sample

For OPC samples it is then possible to calculate the fraction of the cement which has hydrated by assuming that it combines with water in a fixed ratio. Neville (1981 p.27) gives the ratio of water to cement as .23 but the value of .25 (Cabrera 1985) is used here. Thus:

$$M_{hc} = 5M_{aw} \qquad (2)$$

Where:

M_{hc} = mass of hydrated cement

When the proportions of all of the constituents are known it is possible to calculate the specific gravity of the mix as follows (Cabrera 1985):

$$\frac{M}{SG} = \frac{M_a}{SG_a} + \frac{M_{c'}}{SG_c} + \frac{M_{hc}}{SG_{hc}} + \frac{M_{sp}}{SG_{sp}} \qquad (3)$$

where:

M, SG are the mass and specific gravity of the total sample

M_a, SG_a are the values for the aggregate

$M_{c'}$, SG_c are for the unhydrated cement

M_{sp}, SG_{sp} are for the small amount of superplasticiser.

The calculations are not possible for SF samples without a knowledge of the progress of the pozzolanic reaction. Calculations including data on the pozzolanic reaction from thermogravimetric analysis are carried out in chapter 13.

10.1.2 Dry Density.

In order to calculate the porosity from the specific gravity it is necessary to know the

dry density. This was obtained by measuring the density after curing and then correcting it for dry samples by using the data for the weight loss on drying. Measurements of density were made by weighing wet and surface dry samples.

10.2 Experimental procedure.

10.2.1 Measurements on specially cast samples.

For this purpose samples were cast in disposable plastic cups. This method was used because the cups were convenient and did not require mould oil which would have affected the weight. For each condition 2 samples of paste, mortar and concrete were tested. For paste and mortar the cups were approximately half filled (about 80cc.) but for concrete they were filled to the top. The following weights were recorded.

1. Wet weight when cast.
2. Weight of empty cup after sample struck (24 hours after casting).
3. For mortar and paste samples only, wet and surface dry weights after curing.
4. Dry weights after drying in a ventilated oven at 110°C until constant weight (up to 28 days).

The main set of paste samples described above were made using low energy mixing. In order to assess the effect of high energy mixing four additional paste samples for each mix were made. Two of these samples were made using high energy mixing and two using low energy mixing. The samples were cured in curing condition 1 and tested at 28 days.

10.2.2 Measurements on mechanical test samples.

Tests for concrete compressive strength were carried out after curing on three cubes for each sample condition (these are called set 1 samples). A further two cubes were stored in a room at 70%RH and 20°C for one year after curing and then tested. The results of the mechanical tests are in chapter 12. Before testing each cube was weighed wet and dry. After testing a fragment of the broken cube was weighed, dried at 110°C for 24 hours, and weighed again.

10.2.3 Superplasticiser.

The weight and volume of a sample of superplasticiser was measured. The sample was then dried and weighed again. The solids content was confirmed to be 40% as specified and the specific gravity of the solids was calculated to be 1.714 g/cc. This figure is needed in order to include the superplasticiser as a minor component when calculating the specific gravity.

10.3 Results and discussion.

10.3.1 Results for weight loss.

By assuming that any mixing water which was absorbed by the aggregate was lost during drying it is possible to work out theoretical values for the fractional weight loss from the concrete from the results for paste and mortar as follows:

$$WL*M = WL_a*M_a + WL_p*M_p$$

where:

WL, M are the fractional weight loss and mass of concrete

WL_a, M_a are for aggregate

WL_p, M_p are for paste

The results are shown plotted against the measured weight loss for the concrete samples in figs.10.1 and 10.2. It may be seen that the best fit line on fig.10.1 lies close to the line of equality and from the spread of the data it may be seen that the weight loss from the paste was not significantly different from that of the paste fraction of the concrete. The paste fraction of the concrete has undergone high energy mixing due to the action of the aggregate.

10.3.2 Results for dry density.

Using the same routines as were used in chapter 8 to calculate the SG of concrete the dry density has been calculated from the dry densities of paste and mortar and is shown in figs.10.3 and 10.4. The immediate observation is that the density of the mix C paste was much less than that of the paste fraction of the concrete.

10.3.3 Results for high energy mixing.

The results for the paste samples made using high energy mixing and the corresponding samples from the main set are in table 10.1.

It may be seen that high energy mixing decreases the density of mix B and D and increases the density of mix C. It would appear from fig.10.3 that this would make it more representative of the paste fraction of the concrete. The reduction in the density of the OPC mixes caused by high energy mixing was caused by a reduction in bleeding. The effect of this on the vapour transmission was noted in paragraph.6.4.3.

		High energy Mix	Low energy New samples	Low energy Main set
A	Weight loss	0.150	0.150	0.160
A	Density	1.772	1.745	1.721
B	Weight loss	0.120	0.126	0.148
B	Density	1.670	1.893	1.866
B	Calculated P	38.1	30.3	33.0
C	Weight loss	0.223	0.226	0.245
C	Density	1.468	1.412	1.342
D	Weight loss	0.193	0.201	0.219
D	Density	1.595	1.770	1.691
D	Calculated P	39.2	33.2	37.5

Table 10.1 Showing the effect of high energy mixing.

10.3.4 Calculation of porosity.

The basis of calculation of porosity for the different samples was slightly different and was as follows. For the paste and mortar samples the weight loss and dry density were measured. The wet volume was calculated as a total of the sum of the volumes of the ingredients as follows:

$$V_{wet} = \frac{M_{fa}}{SG_{fa}} + \frac{M_{ca}}{SG_{ca}} + \frac{M_c}{SG_c} + \frac{M_w}{SG_w} + \frac{M_{sp}}{SG_{sp}} \quad (4)$$

using the same notation as before with fa and ca being the fine and coarse aggregate. The shrinkage measured as the difference between the wet volume and the measured bulk volume was about 10% for the mix D paste samples but less than 5% for the mortar samples.

The porosity was calculated as:

$$P = 100\left[1 - \frac{DD}{SG}\right] \quad (5)$$

where

P = Porosity

SG = SG calculated from equation (3)

DD = measured dry density

In order to obtain the best value to use for the SG of hydrated cement different values

were tested to see how the calculated porosities compared with those obtain from the helium intrusion measurements. Fig.10.5 shows the effect of using a value of 2.51 taken from Neville (1981 p.29) for the SG of hydrated cement. Fig.10.6 shows the improvement with experimental values obtained by using a lower value of 2.15. 2.15 was used for all subsequent calculations.

For the concrete samples zero shrinkage was assumed so the calculated wet volume was used for porosity calculations and the bulk volume was not measured. The porosity was calculated as:

$$P = 100 \left[1 - \frac{M_{dry}}{V_{wet}SG} \right] \qquad (6)$$

For the samples from the cubes the calculated wet density was needed to calculate the weight loss from the dry density giving the following in place of equation (1):

$$M_{aw} = M_w - (M_{wet} - DD*V_{wet}) \qquad (7)$$

The results for the paste, mortar and concrete samples cast in cups are shown in figs.10.7-10.9. It may be seen that the paste samples which had greater weight losses and thus lower percentage errors appear to give the better results. The calculations cannot be used for the SF mixes so the mix C samples which were most affected by the low energy mixing are not included.

10.3.5 Comparison of porosities.

The comparison of porosities for paste, mortar and concrete is shown in figs.10.10 and 10.11. for the concrete samples which were cast in cups. The porosity of the aggregate was not included in the original calculation of porosity so it was not used to calculate this data. It was therefore possible to use the same routine which was used in section 10.3.1 for weight loss. The calculated porosity of the paste was well below that for the paste fraction of the concrete but for mortar the mixes lay each side of the line of equality. The low porosity of the paste is caused by the high density of these mixes which may be seen in fig.10.3. It may be seen from table 10.1 that high energy mixing caused an increase in the porosity of mix B and mix D of about 10-20%. This could account for the difference shown in fig.10.10. Because porosity is a marginal variable small differences in SG or density cause major differences in porosity.

10.3.6 Results from concrete cubes.

Fig.10.12. shows that the calculated porosity for the concrete samples cast in cups was less than that calculated from the cubes. These samples were cast from the same batch of concrete and cured together so the actual porosities would have been identical. Fig.10.13 indicates that the extra year of storage may have marginally decreased the porosity.

10.3.7 Progress of hydration.

Fig 10.14 shows the weight of hydrated cement as a fraction of the total weight of the paste samples. Mix D hydrated more than mix B because of the greater availability of water but the apparent maximum for CC2 must have been caused by experimental error.

10.4 Conclusions.

1. Low energy mixing does not have a major effect on the amount of combined water in paste mixes and it is therefore indicated that it does not greatly affect the rate of hydration.

2. Low energy mixing decreases the density of the mix C (SF) samples AND would therefore be expected to increase their porosity.

Equation for line : Y=8.603092127E-3+X*0.8123765241
R squared=0.719
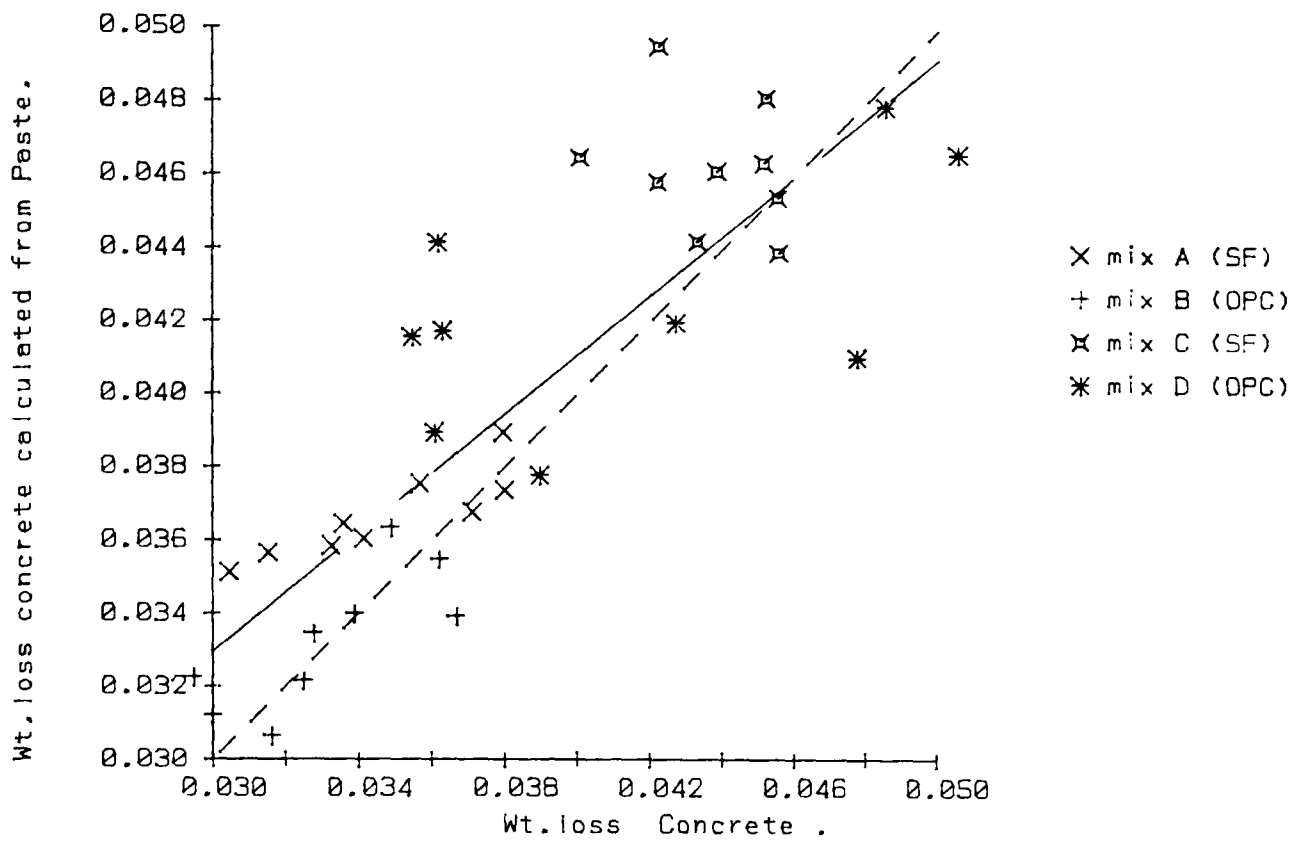
Fig. 10.1 Calculation of the weight loss of concrete during drying from that for paste. The solid line is the line of best fit and the dashed line is the line of equality.

Equation for line : Y=8.948896688E-3+X*0.717865987
R squared=0.629
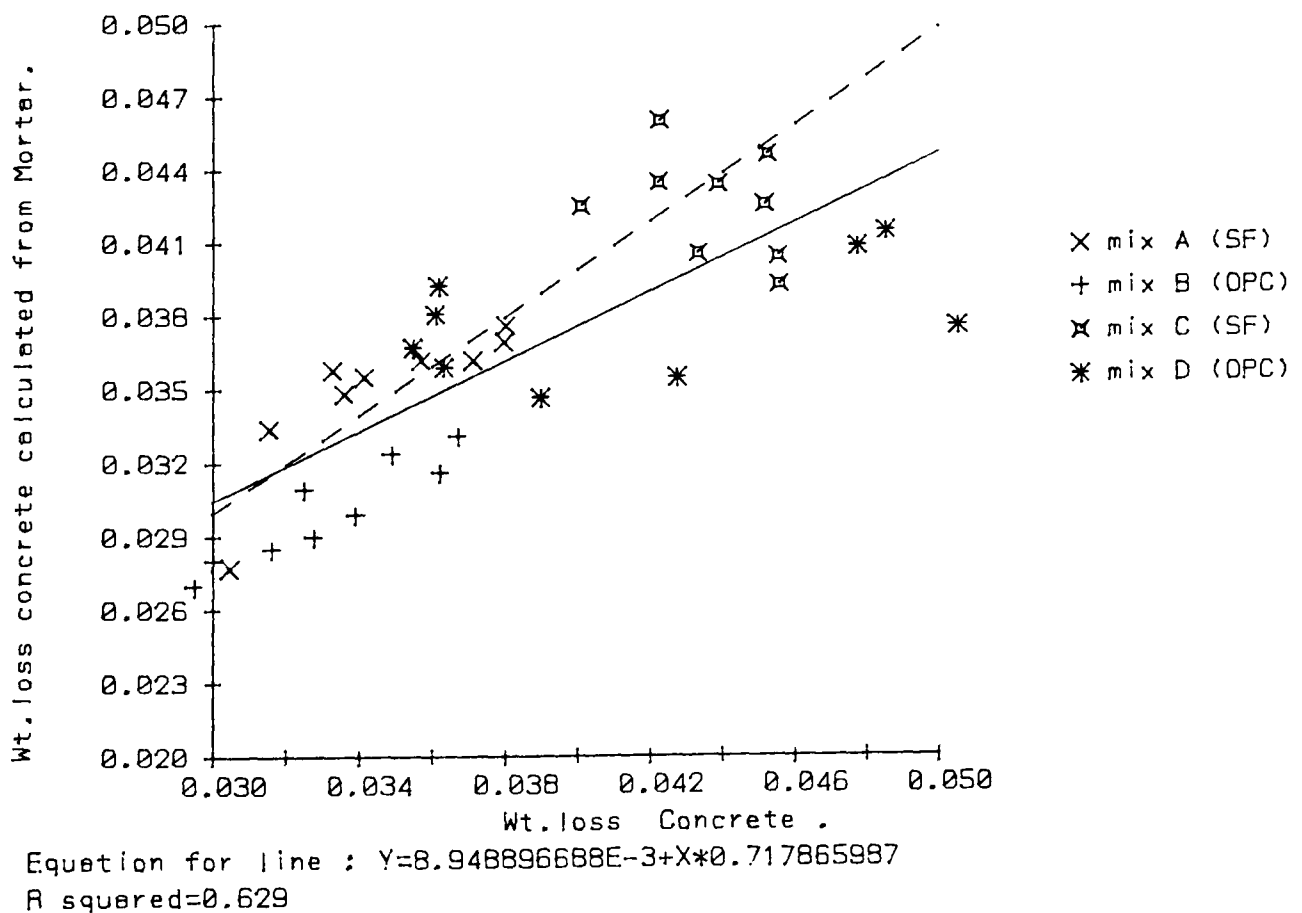
Fig. 10.2 Calculation of the weight loss of concrete during drying from that for mortar. The solid line is the line of best fit and the dashed line is the line of equality.
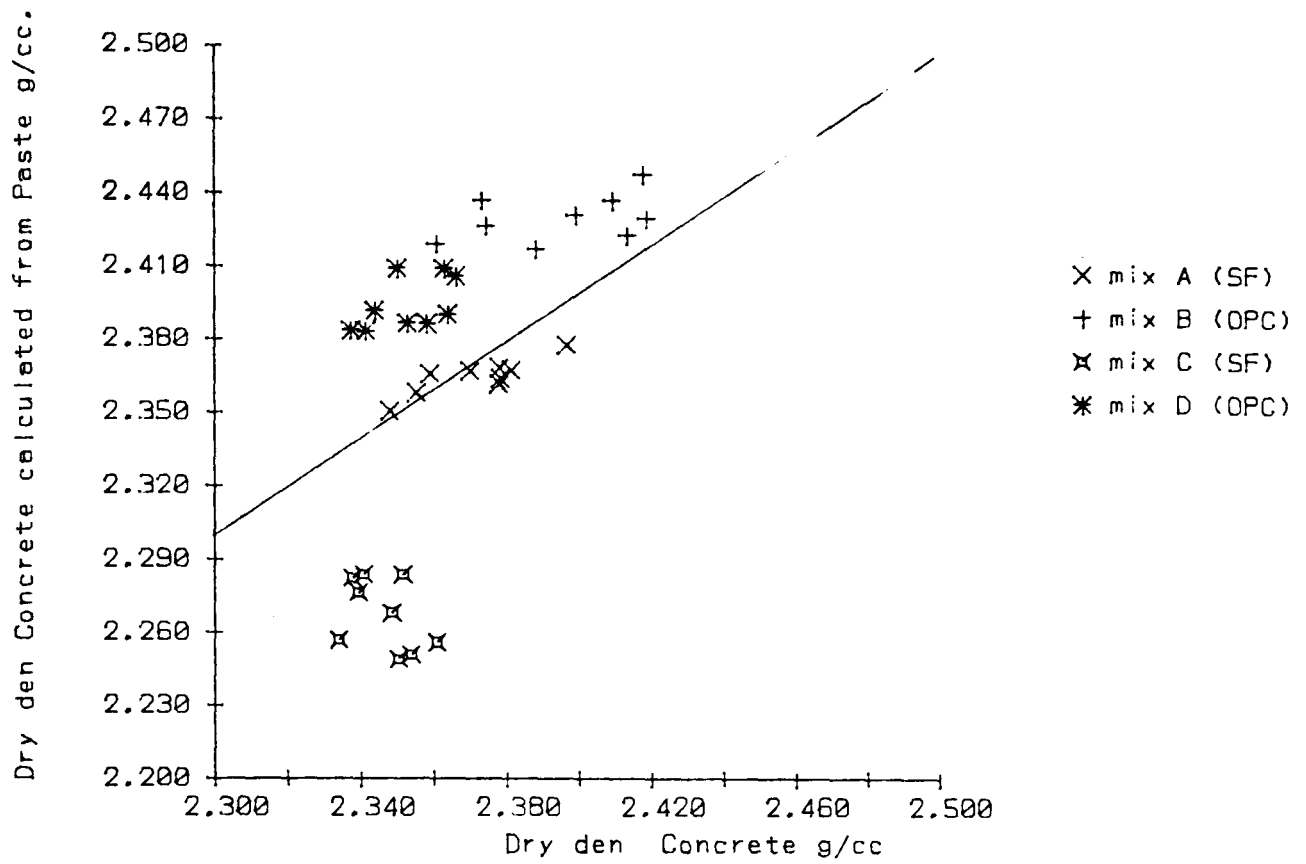
Fig. 10.3 Calculation of the dry density of concrete from that for paste. The line is the line of equality (Y=X)
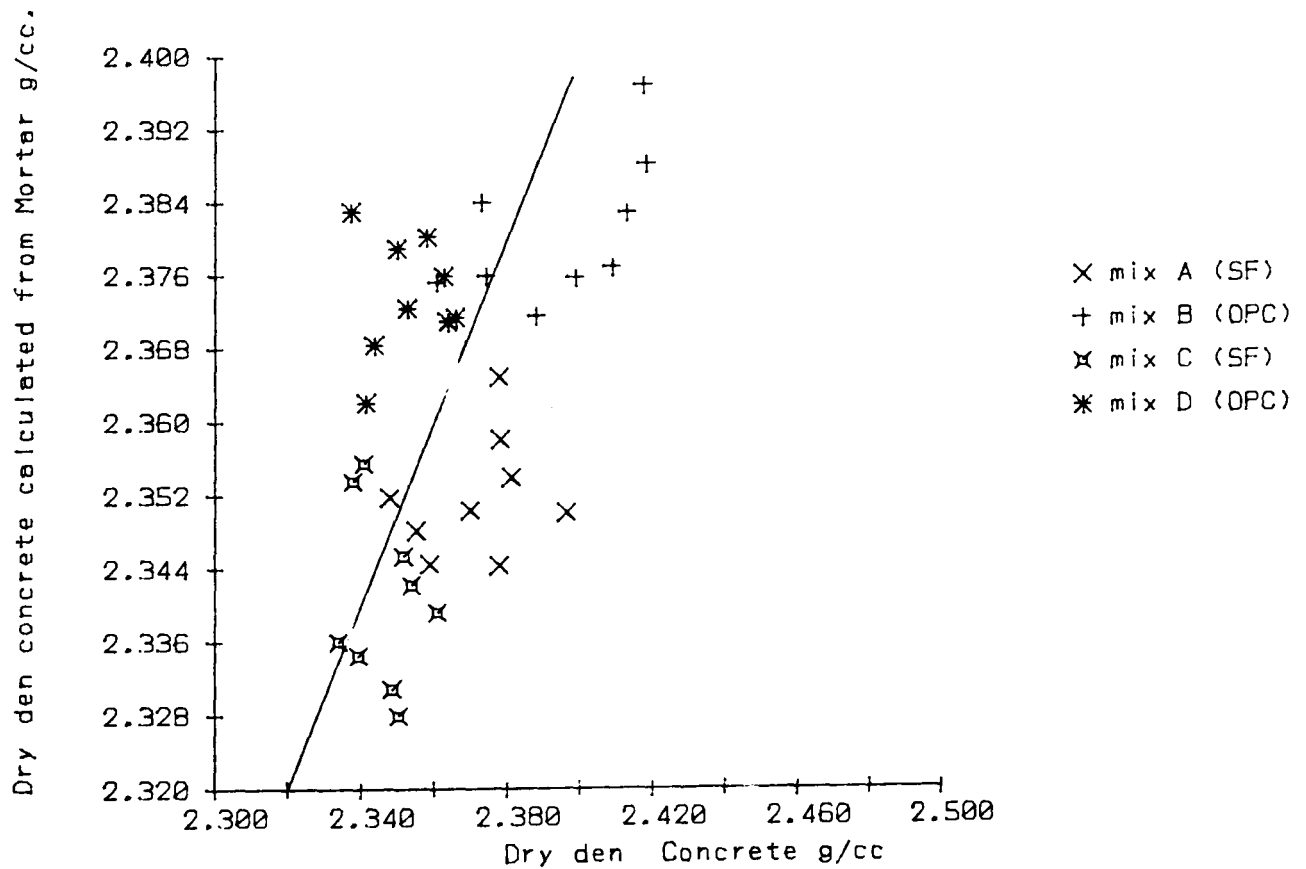
Fig. 10.4 Calculation ·of the dry density of concrete from that for mortar. The line is the line of equality (Y=X)
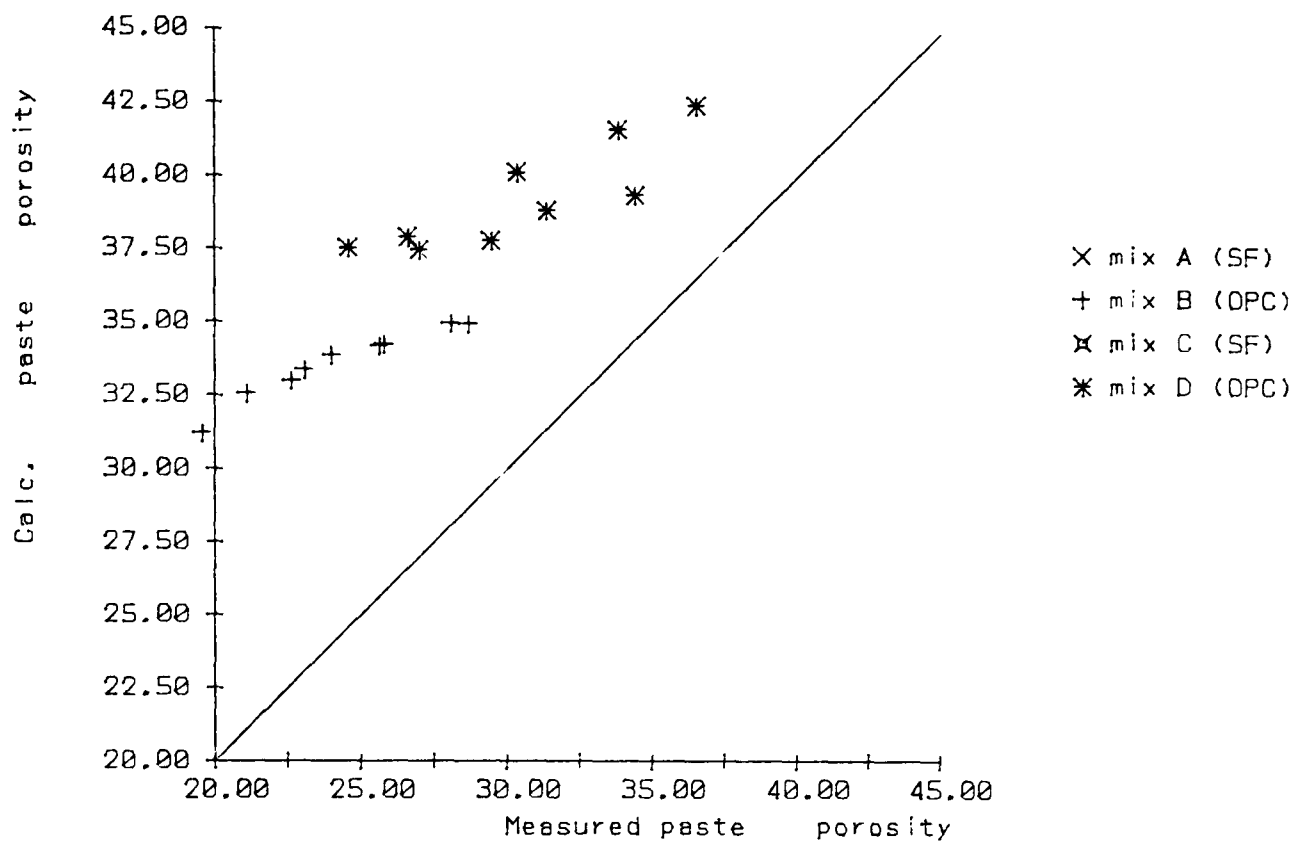
Fig.10.5 Showing the effectiveness of the model with the SG
of hydrated cement assumed to be 2.51. The results are
plotted against the porosity of paste measured from helium
intrusion
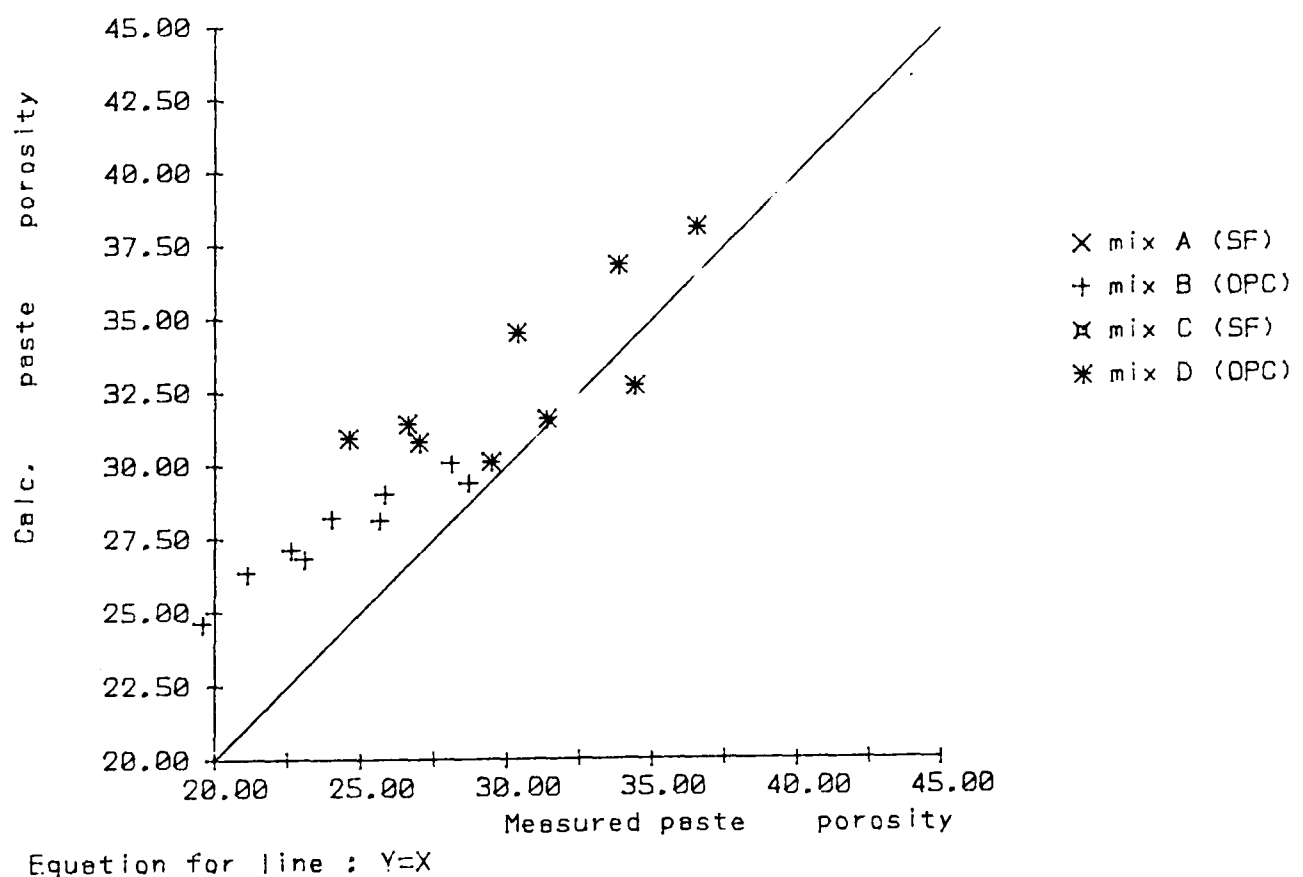
Fig.10.6 Showing the improvement to the model obtained by
assuming the SG of hydrated cement to be 2.15.
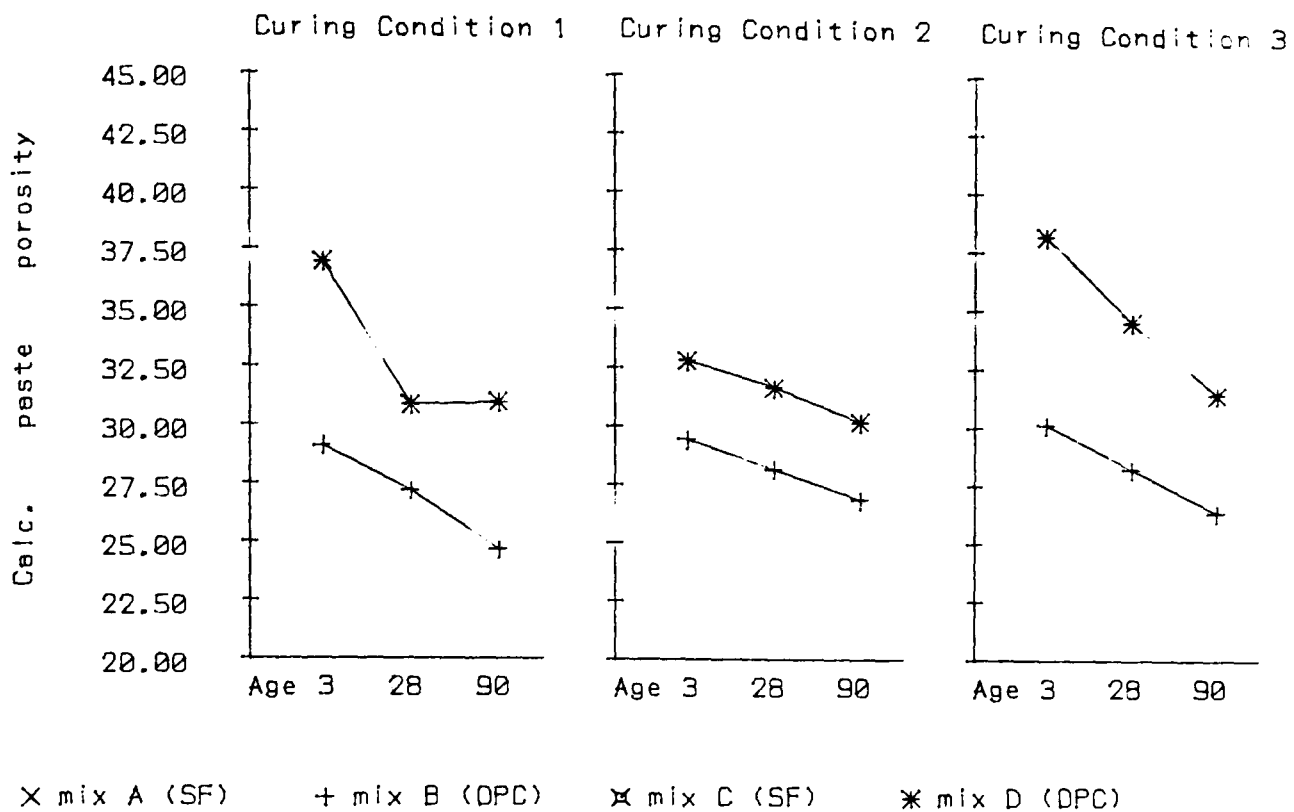
Fig.10.7 The porosity of the OPC paste mixes has been calculated from the weight loss on drying. In order to calculate the porosity of the SF mixes it is necessary to use data from the thermogravimetric analysis. These measurements and calculations are presented in subsequent chapters.
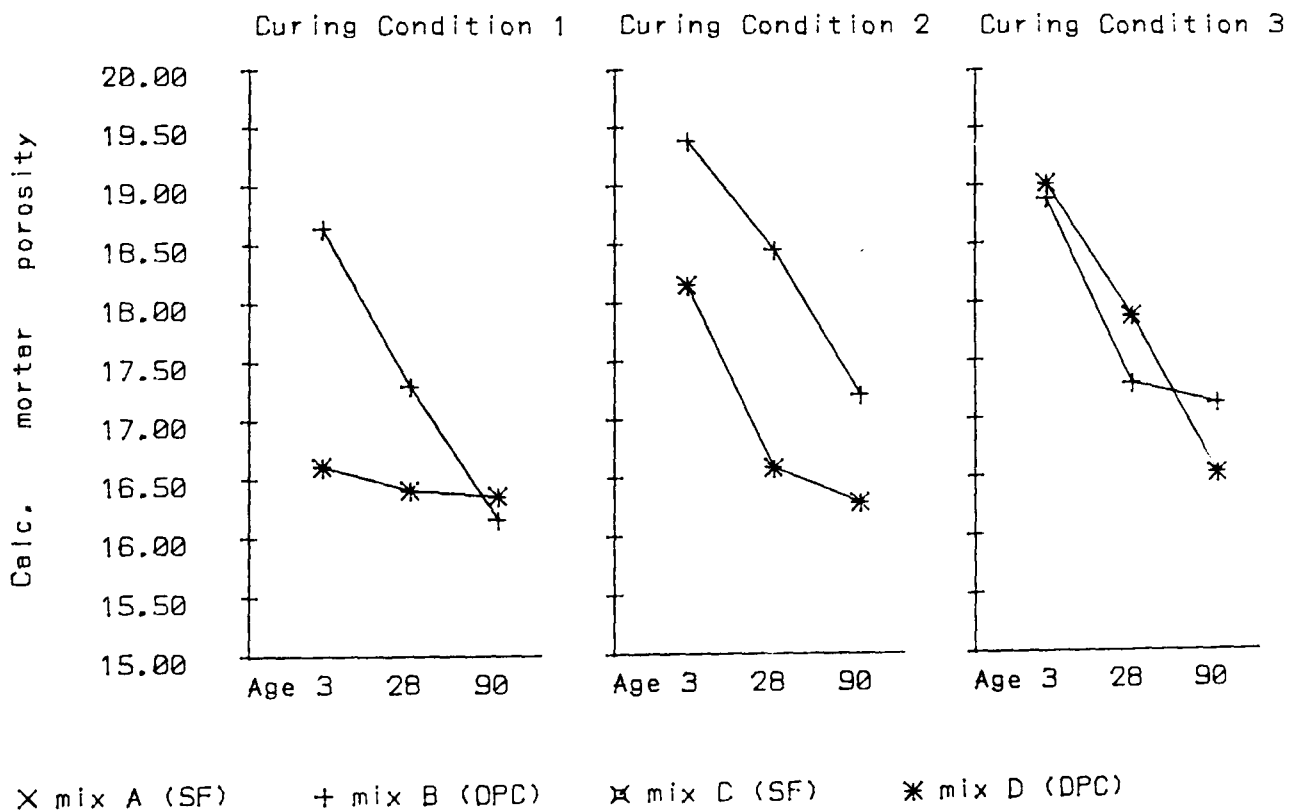
Fig.10.8 The mortar porosity has been calculated in the same way as the paste porosity shown above.

Curing Condition 1   Curing Condition 2   Curing Condition 3

X mix A (SF)   + mix B (OPC)   ⋈ mix C (SF)   ✳ mix D (OPC)
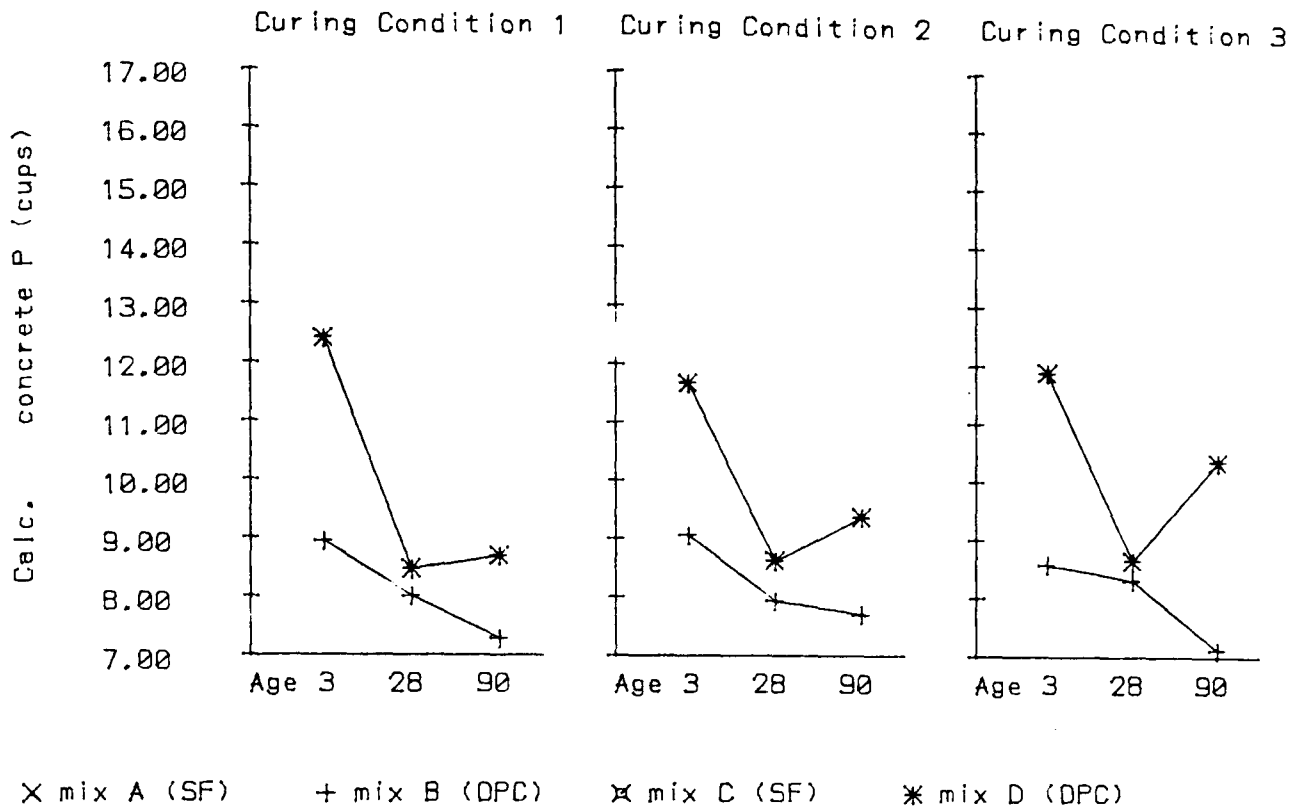
Fig.10.9 Porosity of OPC concrete mixes calculated from weight loss of samples cast for this purpose in cups.

X mix A (SF)
+ mix B (OPC)
⋈ mix C (SF)
✳ mix D (OPC)

Equation for line : Y=X
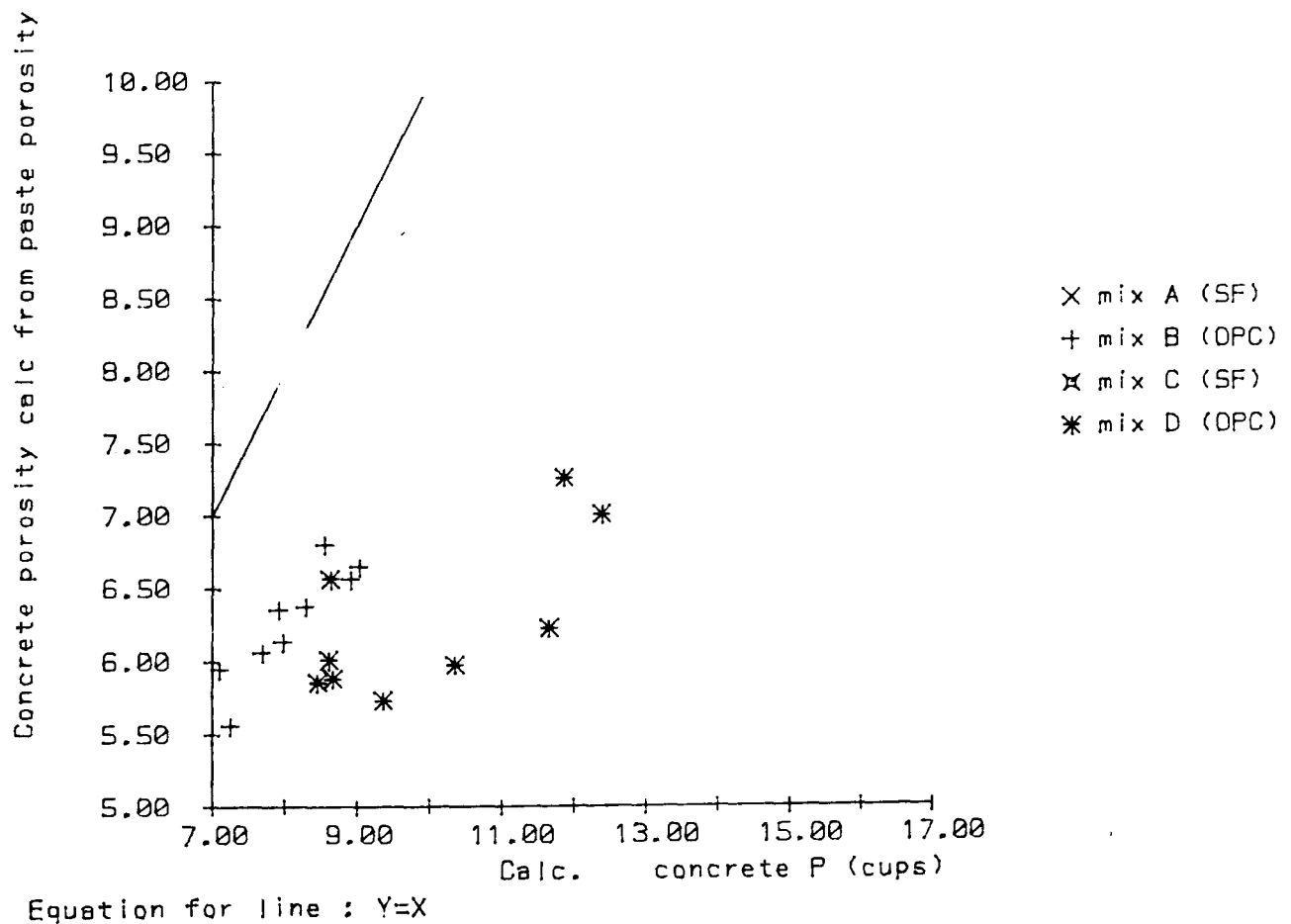
Fig.10.10 Comparison of concrete porosity derived from the paste porosity shown in fig.10.7 and that calculated directly and shown in fig.10.9.
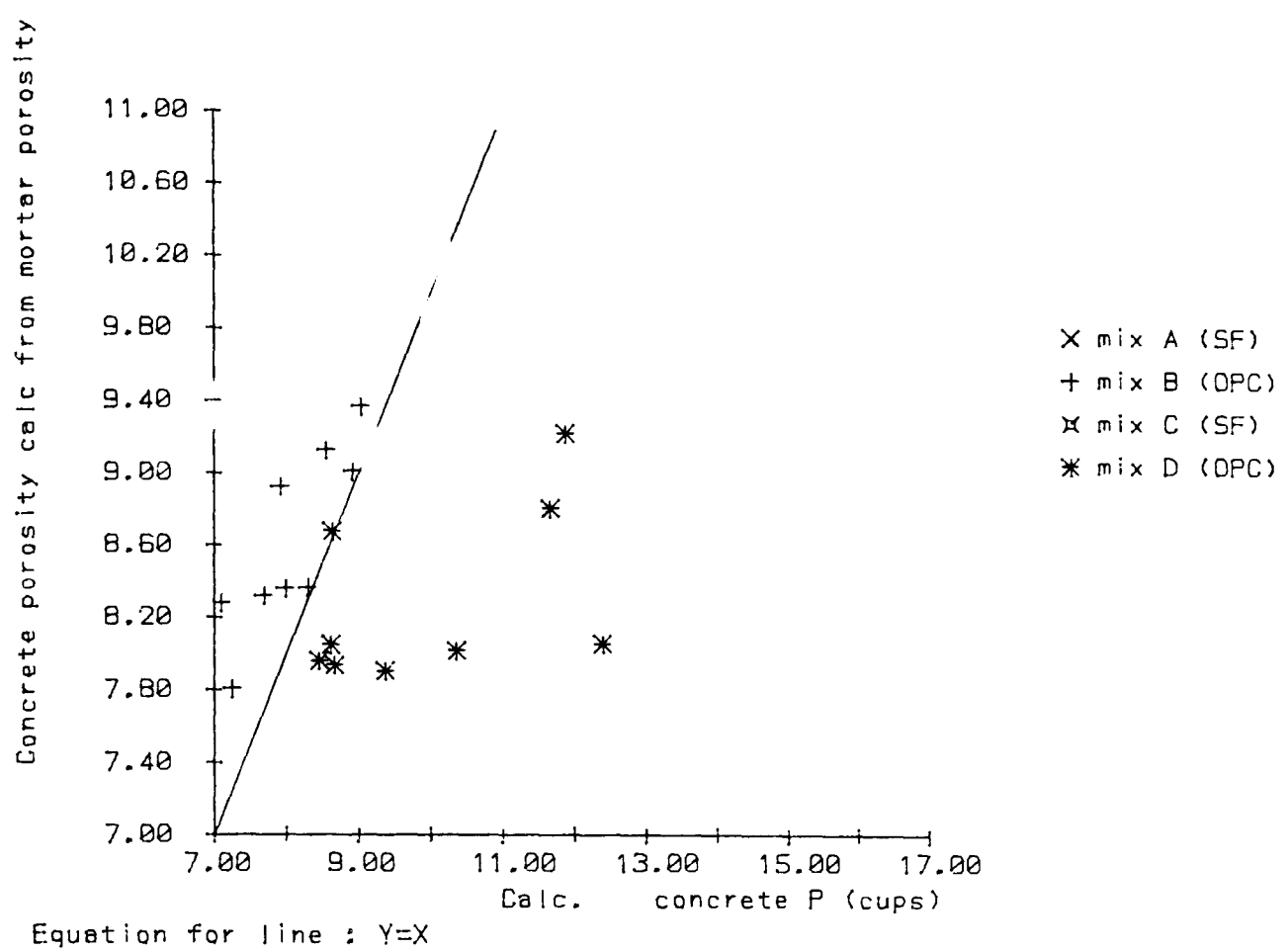
Fig. 10.11 Comparison of concrete porosity derived from the mortar porosity shown in fig.10.8 and that calculated directly and shown in fig 10.9
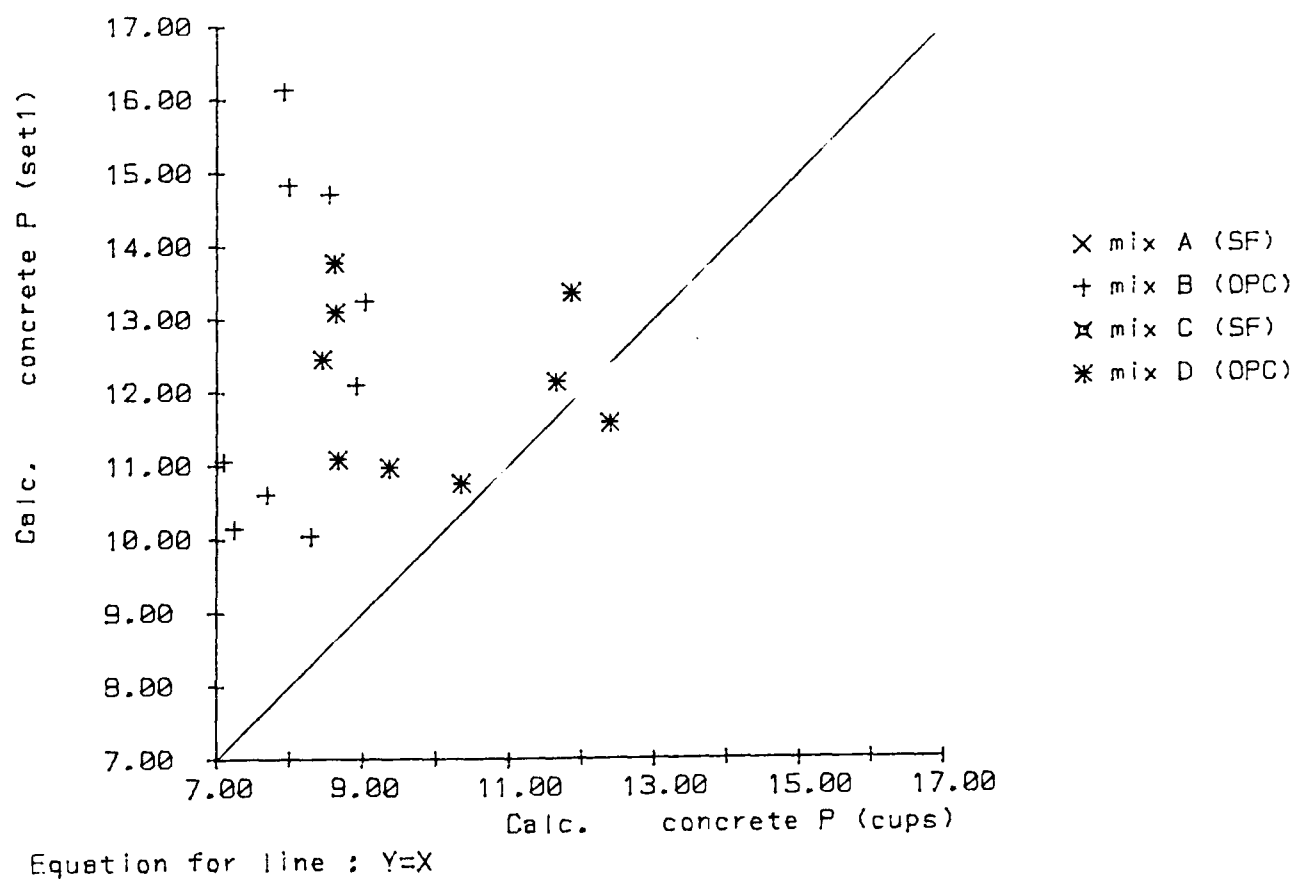
Fig.10.12 Comparison of porosity calculated from weight loss of samples cast in cups and that calculated from weight loss of fragments of cubes tested for compressive strength (set 1).
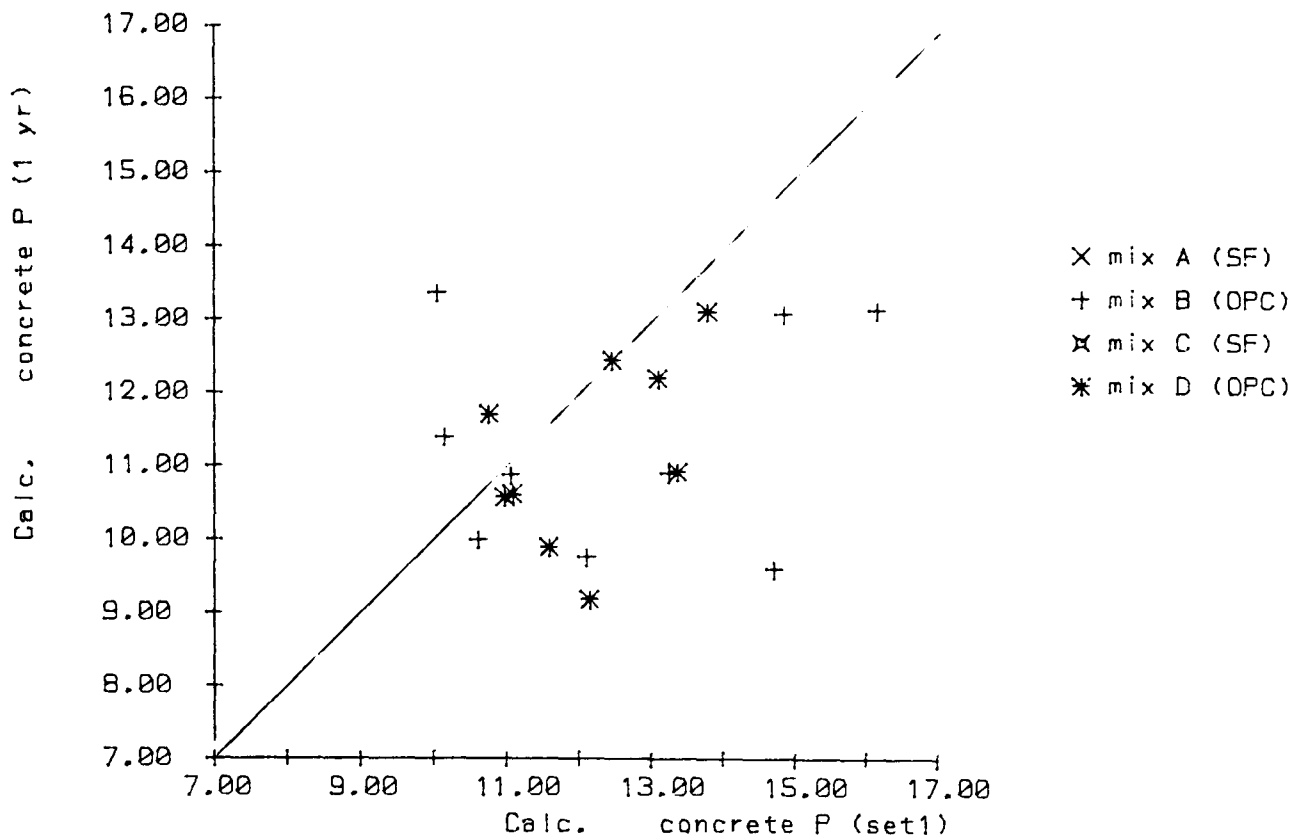
Fig. 10.13 Comparison of porosities calculated from weight loss of fragments remaining from concrete cubes. The set 1 samples were tested after curing and the 1 year samples were tested 1 year later after storage at 70% RH at 20 degrees centigrade. The line is that of equality.
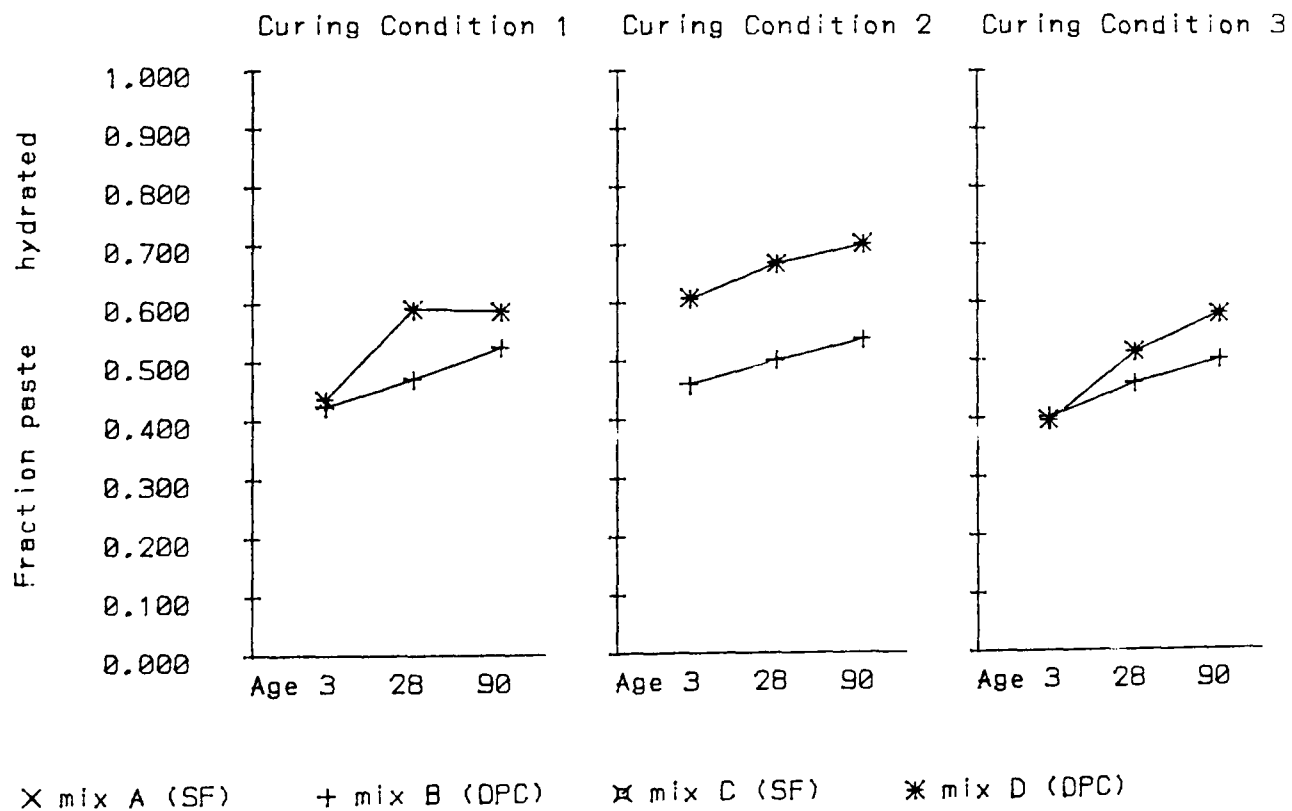
Fig. 10.14 Showing the calculated weight of hydrated cement as a fraction of the dry weight of the paste samples.

11 Thermogravimetric analysis.

11.1 Experimental apparatus.

11.1.1 The basis of the method.

When a sample is tested using thermogravimetric analysis it is heated and the loss of mass is measured. At different temperatures different physical and chemical changes take place depending on the constituents of the sample. Different components will cause loss of mass at different temperatures and the amount of loss will be proportional to the amount of the component that is present. It is not necessary to know the details of the changes that take place because the system can be calibrated by testing pure samples of the chemicals which are present in the test material.

11.1.2 The thermobalance.

A Stanton Redcroft TG750 Thermogravimetric (T.G.) Balance was used. This apparatus can heat samples up to 1000° C. The samples are suspended on one side of a balance which is kept level by a small electromagnet. If the weight changes and the balance goes out of level this is detected by a photoelectric sensor and the current through the electromagnet is changed to bring it back to level. In this way the balance is kept level by a feedback circuit. The weight is measured from a voltage output which is proportional to the current in the electromagnet.

The furnace which contains the sample also has two thermocouples in it. One is located directly below the sample and is used to make readings of temperature. The other is located at the side of the furnace and is used to control the furnace temperature. This temperature may be made to to increase a pre-set rate and is controlled by a circuit which turns the power to the furnace on and off.

11.1.3 Data retrieval system.

In order to facilitate the analysis of this, and subsequent data, the output from the balance control unit was fed directly into the analogue to digital converter of a BBC microcomputer. The BBC can only register positive voltages and has a theoretical resolution of 0.4 millivolts. The T.G. output can be either positive or negative and is accurate to 0.1 millivolts. It was therefore necessary to build an amplifier for the signal to bias it positive and amplify it by a factor of 4. The circuit for the system is shown in fig. 11.1 and is powered from the 5 V supply in the BBC.

The two stages are required because a single stage inverts the signal. The first stage is therefore used to bias the signal by about 0.5 volts using the output from the regulator and the second stage has the gain factor of 4. The output from the regulator has not been used to power the amplifiers because the minimum drop of 2 volts across it only leaves 3 volts which is not sufficient. The advantage to be gained if this was achieved

is considered to be minimal because by powering the amplifiers directly from the same source as the analogue to digital converter in the computer any increase in the supply to the converter is automatically compensated for by an increase in signal.

In order to ensure that the best possible readings were being obtained form the balance a separate converter with 3 microvolt resolution was temporarily connected to it. Both systems showed the same fluctuations of about 0.05%

11.2 Experimental procedure.

11.2.1 General.

All samples were tested at a heating rate of 30°C per minute. A stream of nitrogen gas was passed through the furnace during heating.

11.2.2 Procedure: paste samples.

Two paste samples were cast in plastic cups for each condition. High energy mixing was used. For this experiment only an extra test age of 7 days was included. After curing the samples were ground and then sieved through a 150 µm sieve. The free water was then removed by twice saturating them in acetone and drying them in nitrogen.

11.2.3 Procedure: Concrete samples.

After curing in the normal way 100mm concrete cubes were exposed in a room kept at 70%RH and 20°C for one year. Samples were taken by drilling with a hand held hammer drill with a 6mm masonary bit. One sample per condition was taken from the outer 1mm of the cube and one from a surface near the centre exposed by crushing it.

11.3 Results.

11.3.1 System of analysis.

Because this system has been used on a number of other projects a full description of the software has been written. This description is included in this document as appendix 1. A typical example of the raw data from one sample is shown in fig.11.2 (it was plotted using the program GPLOT2 described in appendix 1).

The results were analysed by fitting a sum of normal distributions to each differential mass curve. The mass loss was then calculated as the area under the curve which was obtained from the amplitude and standard deviation. The position of the final optimised curve is obtained by positioning the estimated curves.

For all samples the following positions were used for the 6 curves used:

Curves 1 and 2 to measure the water loss in the range 0-200°C .

Curve 3 to measure the calcium hydroxide.

Curve 4 to measure the carbonate.

Curve 5 to measure the narrow peak at about 250°C.

Curve 6 as a broad underlying peak to correct for uplift, machine drift and other losses which occured in the temperature range of the other curves but were not part of them. A plot of typical data and the curve fitting is shown in fig.11.3. For curve 5 there was a poor correlation between the 2 samples tested for each condition which was assumed to be caused by the rate of temperature gain being too rapid to map such a narrow peak. Some difficulty was experienced in separating the peaks and a small number of the results from the computer had to be corrected subsequent to inspection of the graphical output.

11.3.2 Results: Pure chemicals.

Tests on samples of calcium hydroxide and carbonate gave losses of 22% and 45%. The theoretical losses during calcination calculated from molecular weights would be $18/74 = .26$ and $44/100 = .44$.

11.3.3 Results: Paste samples.

The mass losses for water (peaks 1 and 2) , calcium hydroxide (peak 3) and calcium carbonate (peak 4) are shown in figs.11.4-11.6. The calcium hydroxide readings have been divided by .22 to give percentage concentrations in the samples. The temperature of the centre of the calcium hydroxide peak is included as fig.11.7. This shows that although there was apparently some variation in the calibration of the machine during the 3 months of readings the three curing conditions which were tested on the same day gave peaks at very similar temperatures.

11.3.4 Results: Concrete samples.

The results for the calcium hydroxide for the concrete samples are shown in figs.11.8 and 11.9. and the results for the carbonation are in figs.11.10 and 11.11. Note the different scales on these graphs. Because of the generally small mass losses and the unknown amounts of fine aggregate in the samples this data is not considered accurate enough for use in correlations with other readings but the show clear trends for qualitative analysis.

11.4 Discussion.

11.4.1 Mechanisms of gain and loss.

The only mechanism of gain of calcium hydroxide in the samples is the hydration of the cement. The amount in the sample has been measured as a percentage of the weight after removal of all of the free water and would thus be expected to be the same for any fully hydrated paste sample made with the same cement at any w/c ratio sufficient for full hydration. The total hydroxide produced in the SF samples if they hydrated fully would be 20% less than the OPC samples because they were made with 20% less

cement. Hydroxide could have been lost by three different mechanisms, pozzolanic activity to form CSH gel, carbonation to form calcium carbonate and there may have been some loss by dissolution in the curing water. The ratio of the weights of the molecules carbonate/hydroxide is 100/74 so each 1% of hydroxide lost will have formed 1.3% of carbonate. This will show as an additional 1.3*.45=0.6% mass loss in the carbonate peak.

The calcium carbonate was all formed from the carbonation of hydroxide. The evidence from fig.11.6 which shows that some of the samples had very low carbonate contents indicates that almost all of the carbonation in the paste samples took place while they were being prepared and tested. There was no mechanism for loss of carbonate, any that formed remained and was measured.

11.4.2 The paste samples.

The maximum loss in the carbonate peaks was only about 4.5% which has been shown above to account for 7.5% loss in the hydroxide percentage. The OPC samples showed the expected increase in hydroxide content for the initial readings but at 90 days the CC1 and CC3 results were lower. This loss of about 3% cannot have been caused by carbonation because the carbonate content decreased for CC1 and only marginally increased for CC3, so it must either have been experimental error or caused by dissolution of hydroxide in the curing water. It may be seen from fig.11.5 that virtually no pozzolanic activity took place in the SF samples during cold curing (CC3) but at 20°C (CC1) all of the available calcium hydroxide was used up after 90 days.

The paste samples should theoretically not have carbonated. As has been noted above the very low readings for some samples indicate that little carbonation took place during curing and the apparatus for testing used nitrogen to prevent carbonation during heating. The data must therefore indicate that the older samples tended to carbonate less during preparation for testing.

11.4.3 Concrete samples.

The results from the OPC concrete samples show the expected trends (allowing for the random effect of the aggregate). For these samples the hydroxide has been plotted as a mass loss and 1% mass loss corresponds to 4.5% hydroxide content and would cause 2.6% mass loss in the carbonate peak if carbonated. The hydroxide contents increase with age for the inner samples but decrease with age for the outer samples because of the high carbonate contents. At the outside of the one year SF concrete cubes carbonation has clearly depleted the reserve of calcium hydroxide (figs.11.9 and 11.11) but at the centre (figs.11.8 and 11.10) the pozzolanic reaction has progressed to completion for all types of initial curing. This implies that the effect of cold curing is only temporary provided the temperature is eventually raised. The consequences of this conclusion for concrete durability are that the benefits from the action of the SF will eventually appear even if a structure is poorly cured. This is discussed further in

chapter 14.

11.5 Conclusions.

1. A system for the retrieval an analysis of data from a thermogravimetric balance has been built. Clear data on the progress of the pozzolanic reaction has been obtained.

2. For future work on this system a connection is being made between a relay in the microcomputer and the system which increases the temperature in the thermobalance furnace. This will enable an active system to be used which will stop the increase in temperature when a major loss of mass is detected. This will permit analysis of fine peaks but will mean that it will be necessary to sort the data into order of increasing temperature before analysis.
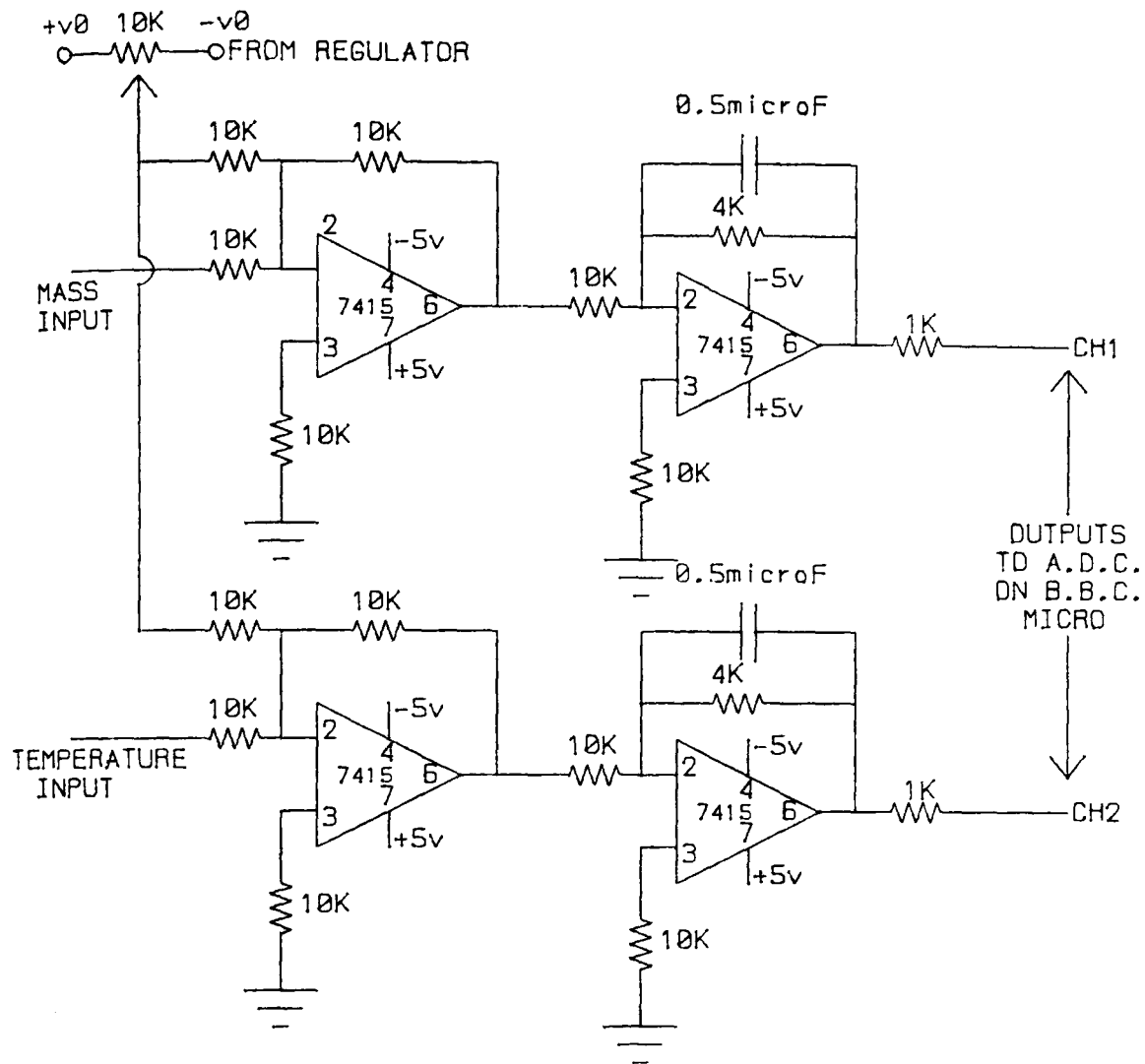
CIRCUIT FOR INTERFACE BETWEEN TG BALANCE AND BBC MICRO

Fig 11.1a
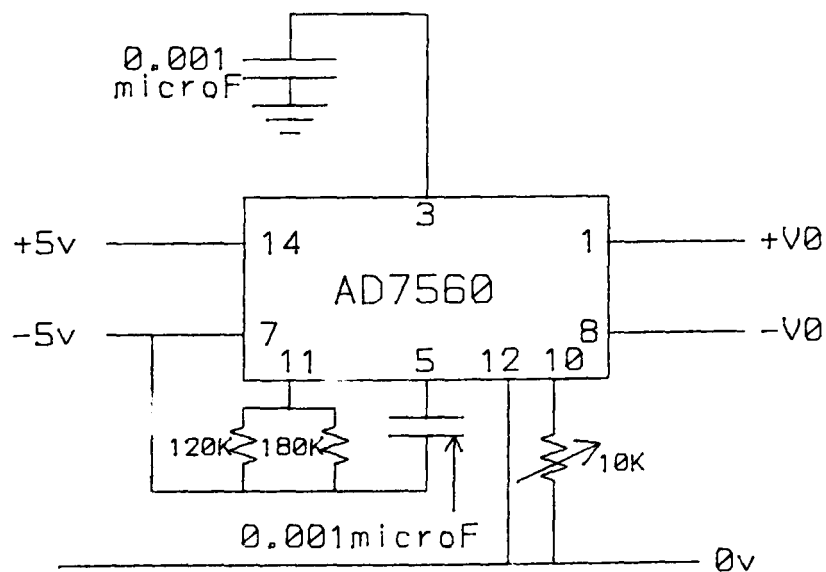
VOLTAGE REGULATOR FOR CIRCUIT SHOWN IN FIG 10.1a

Fig 11.1b

Differential ranges: Mass=2 Temperature=2
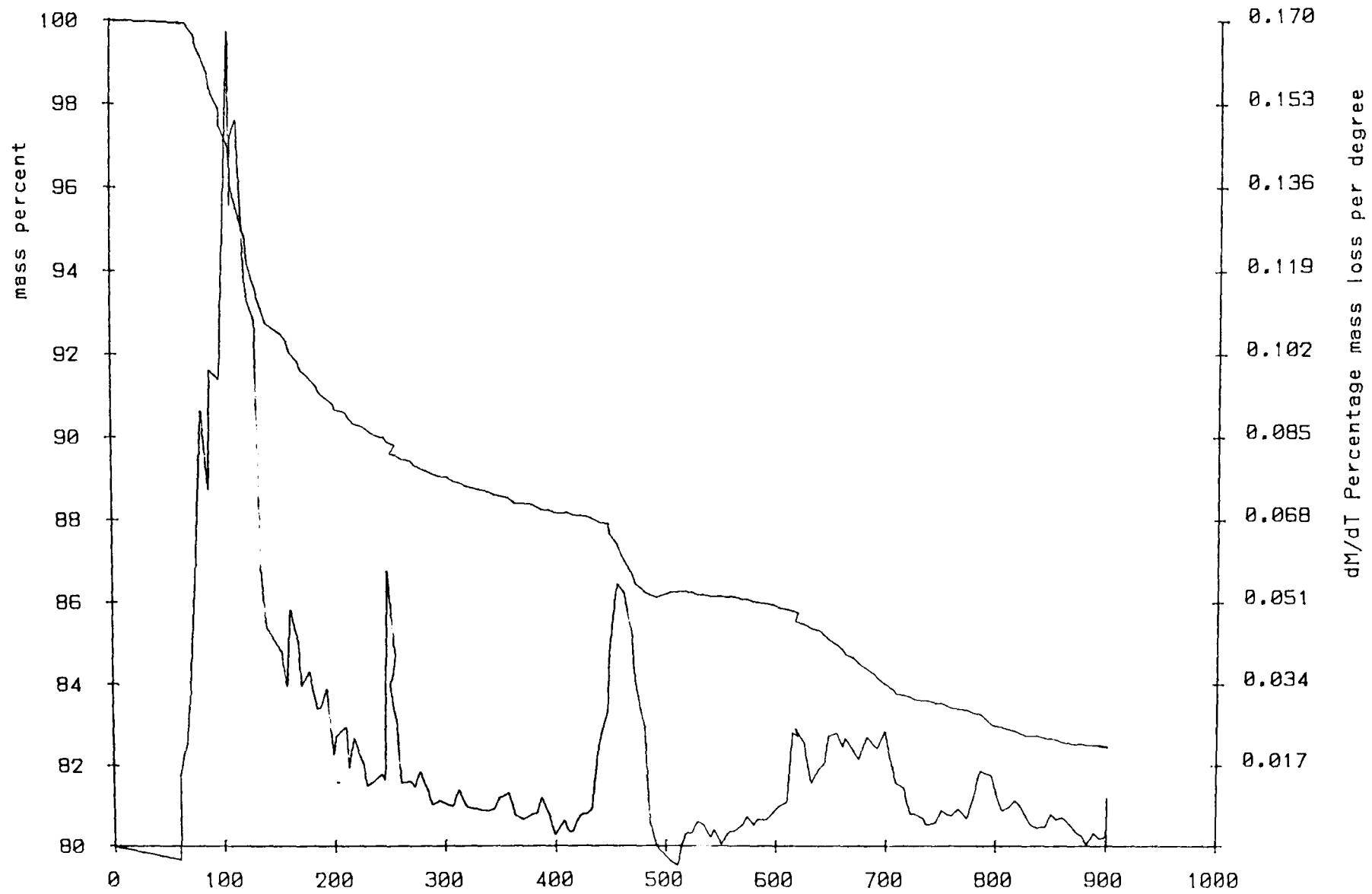
File B27B   TYPICAL PASTE SAMPLE   temperature degrees C.

Fig.11.2 Cumulative and differential output from TG balance for mix B, age 7, CC 2, sample B.

Detail of the components of the optimised curve
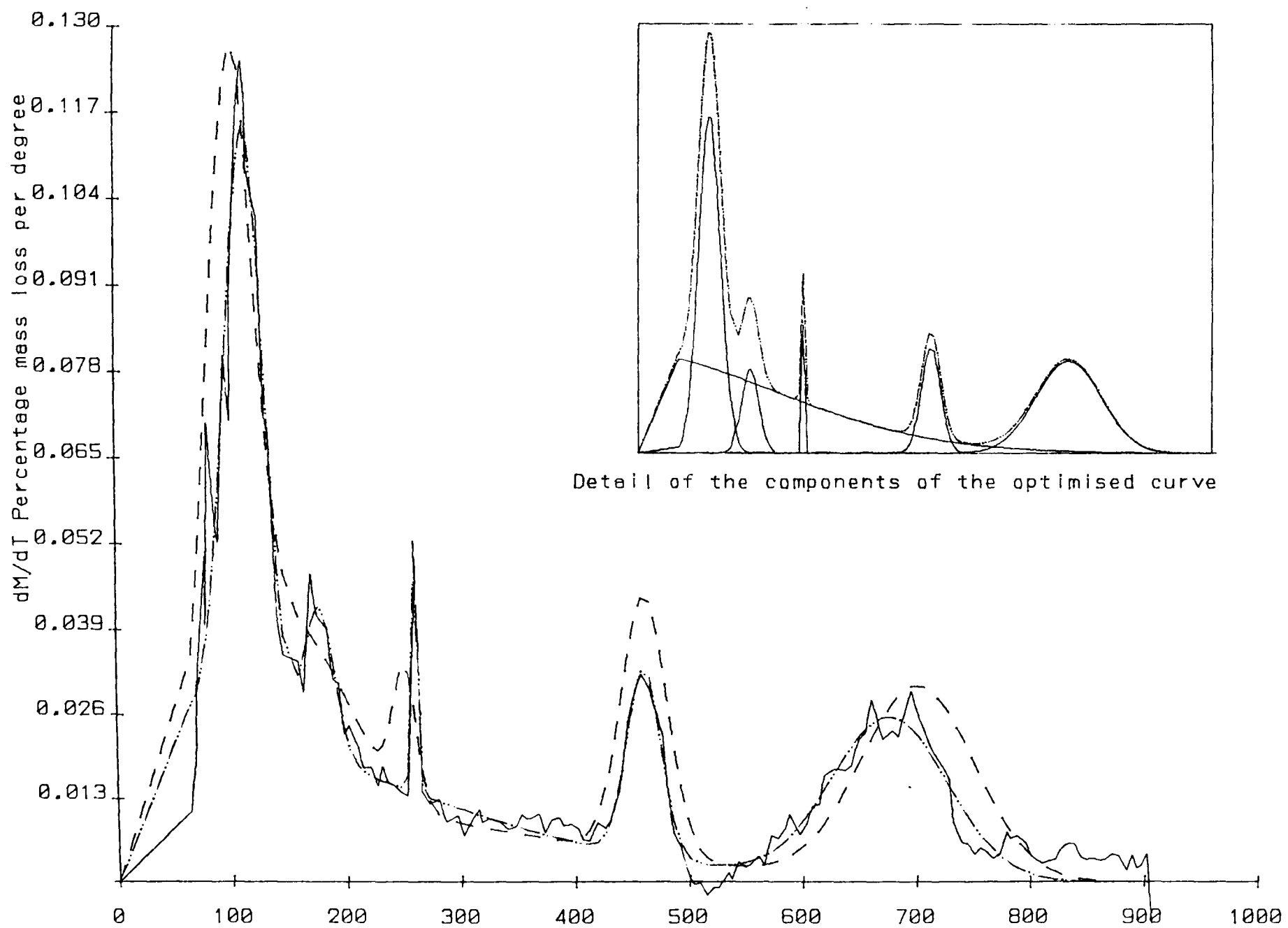
File A13B (Mix A CC. 1 Age 3 Sample B)   Temperature degrees C.

Fig.11.3 showing the estimated (_ _ _ _) and optimised (_.._.._..) curves fitted to typical differential TG data
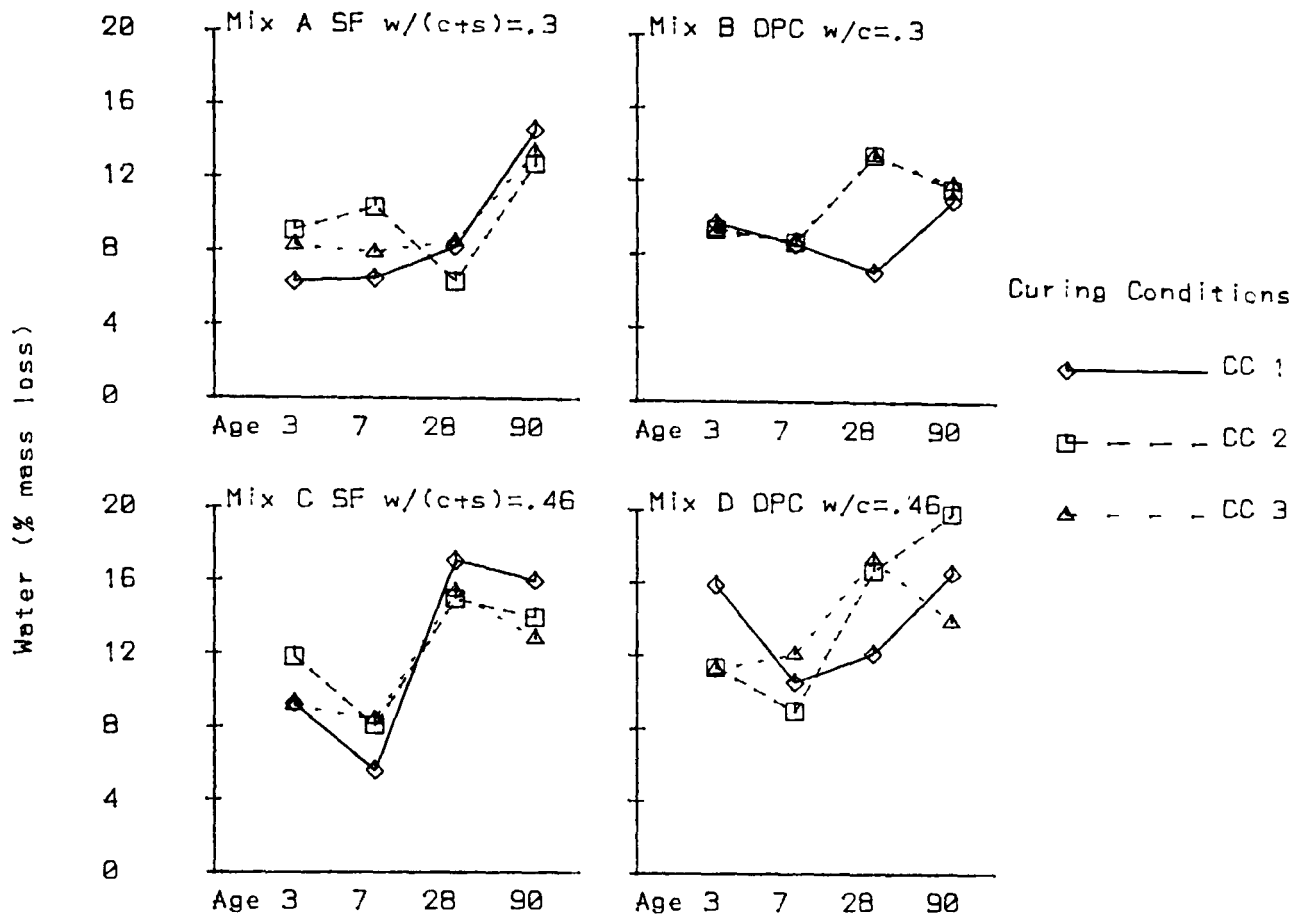
Fig. 11.4 Water loss in the low temperature region (up to 300 degrees) during thermogravimetric analysis.
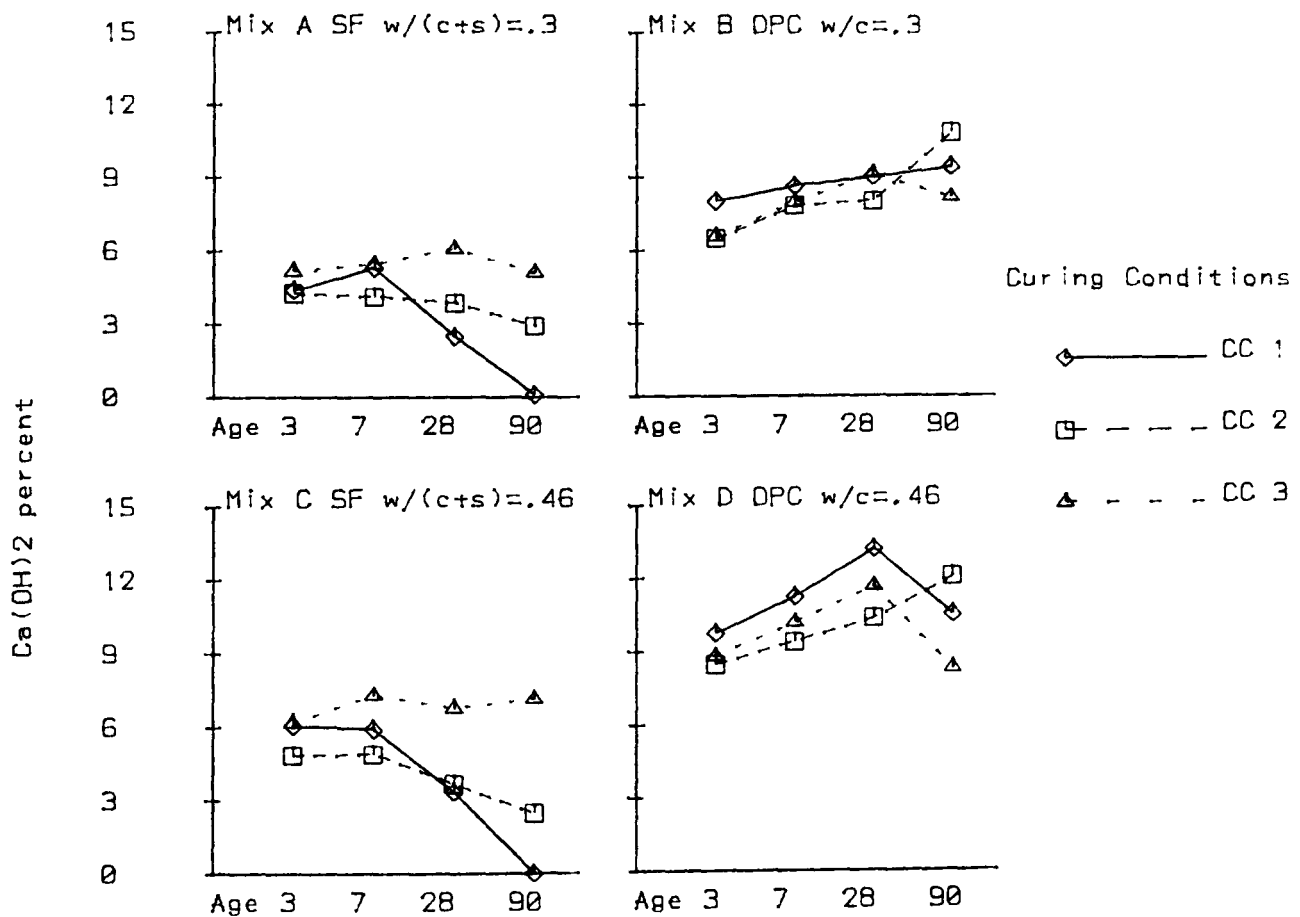
Fig. 11.5 Calcium hydroxide percentages from thermogravimetric analysis of paste samples.
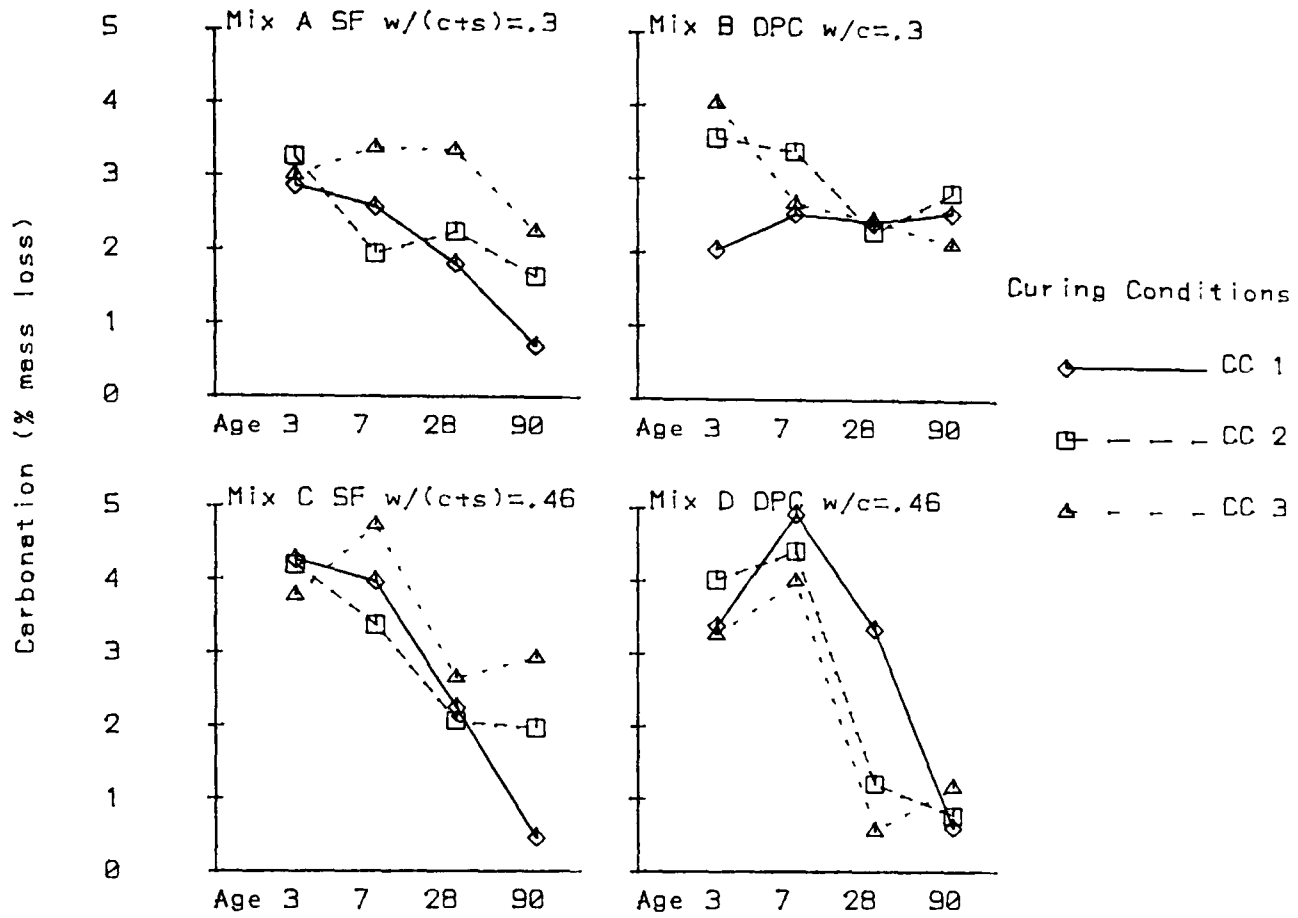
Fig. 11.6 Percentage mass loss of paste samples in the carbonate peak in thermogravimetric analysis.
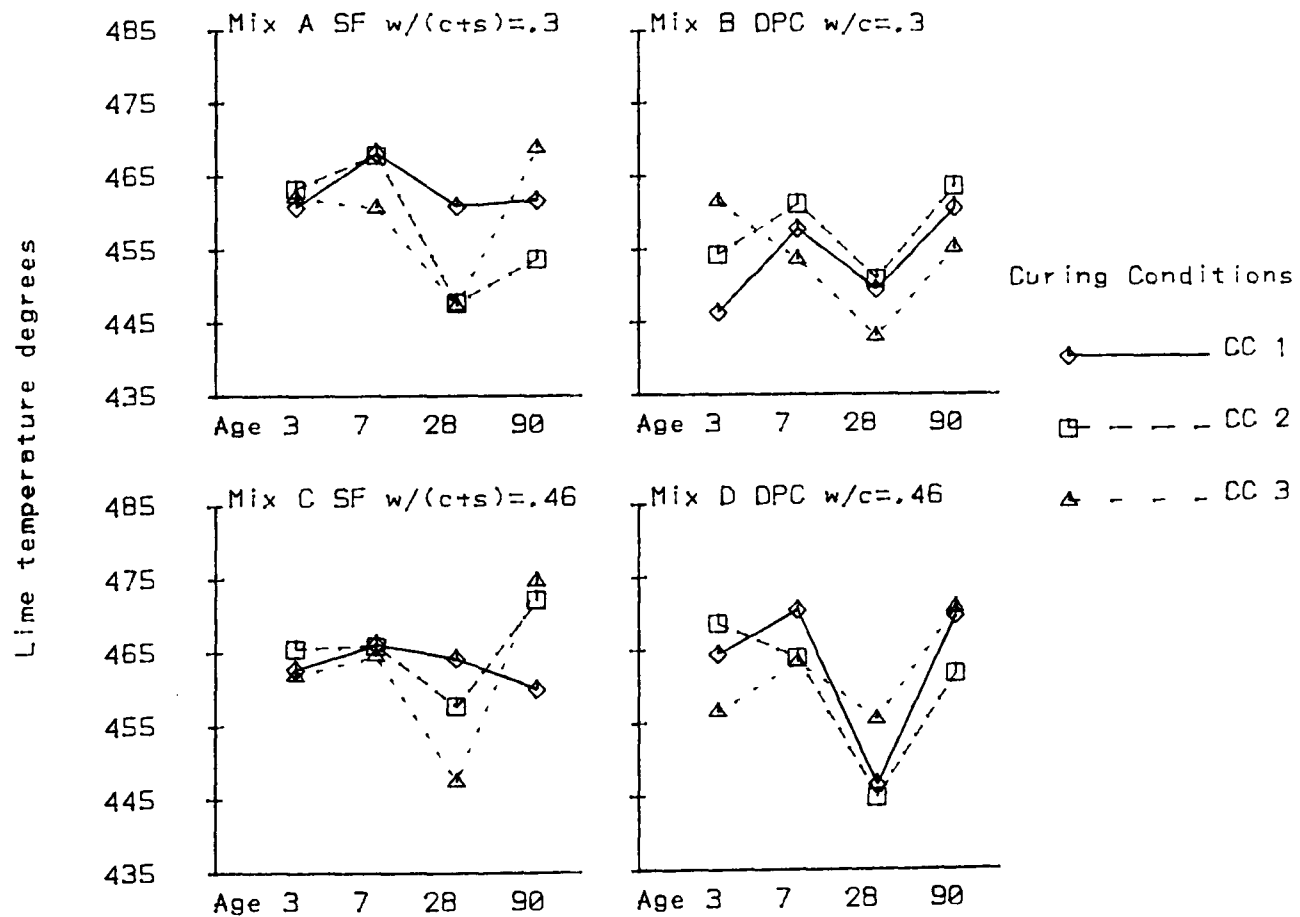
Fig. 11.7 Mean temperature of lime peak in thermogravimetric analysis
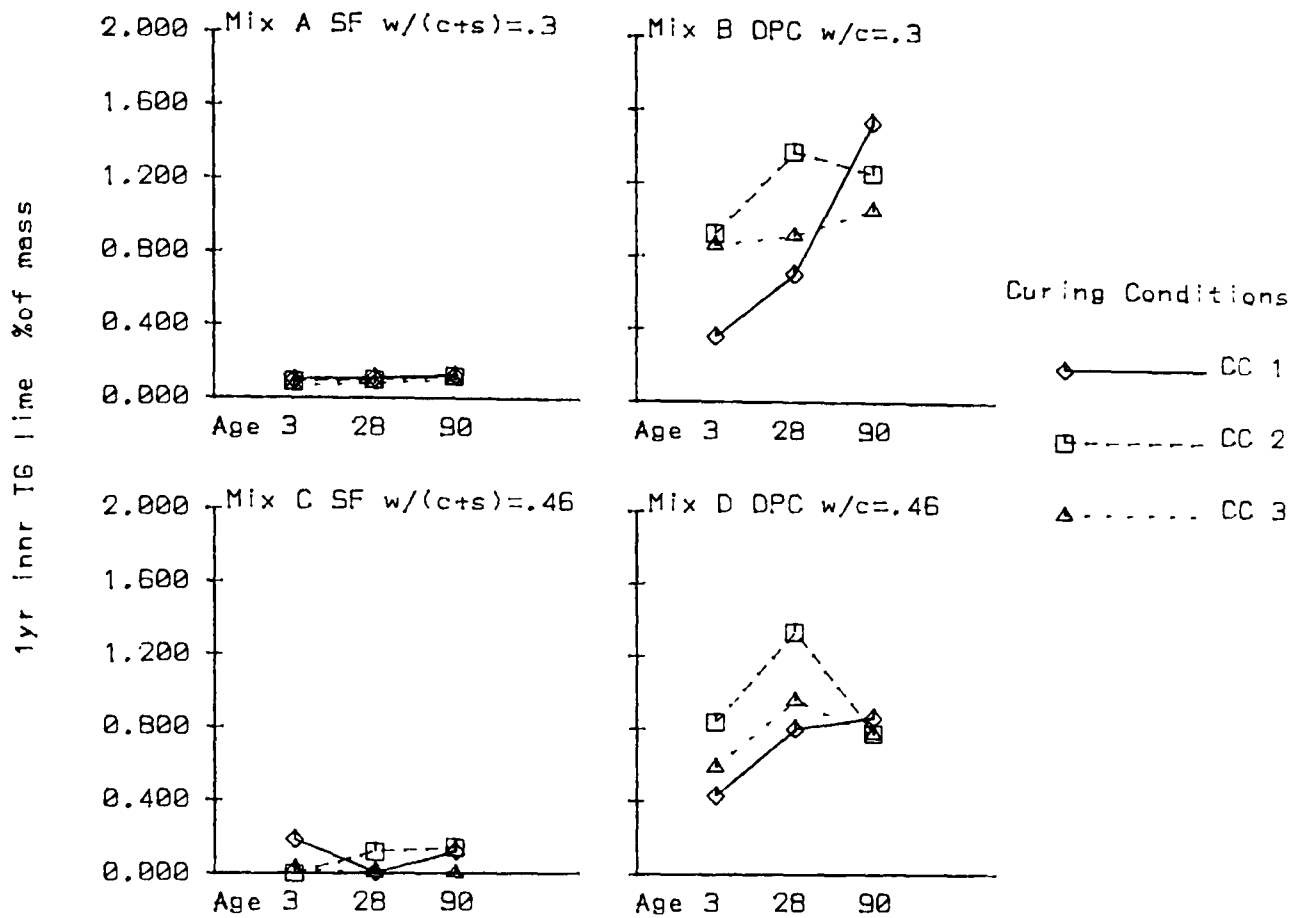
Fig. 11.8 The two graphs on this page show the mass loss in the calcium hydroxide peak detected by TG analysis in samples drilled from concrete cubes kept in a room at 20 degrees for one year after curing. Samples from a freshly broken inner face are shown above and those from an outer face below.
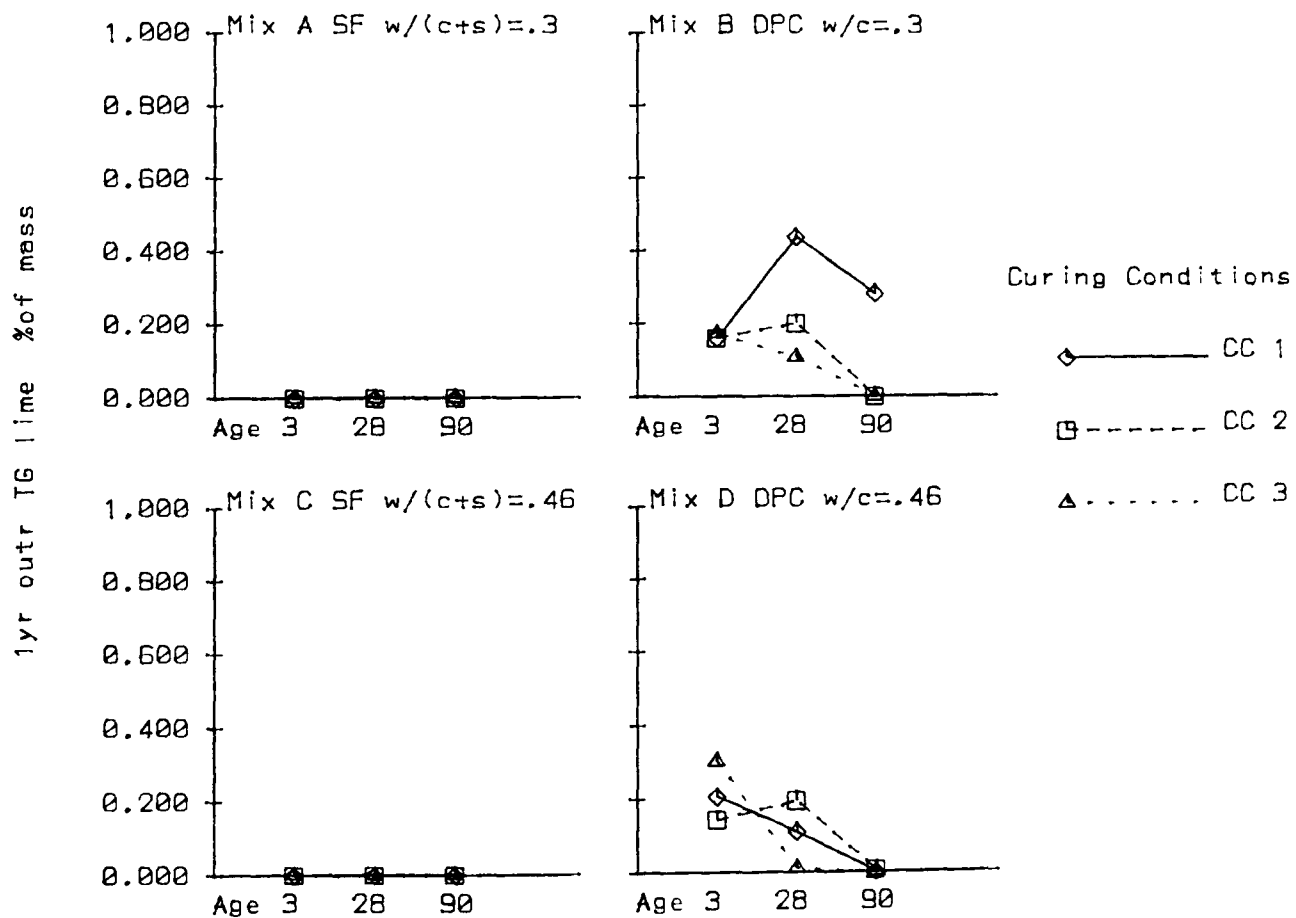
Fig. 11.9 In this graph it may be seen that all of the hydroxide in the SF samples has gone. Note the different scales on figs.11.8 and 11.9.
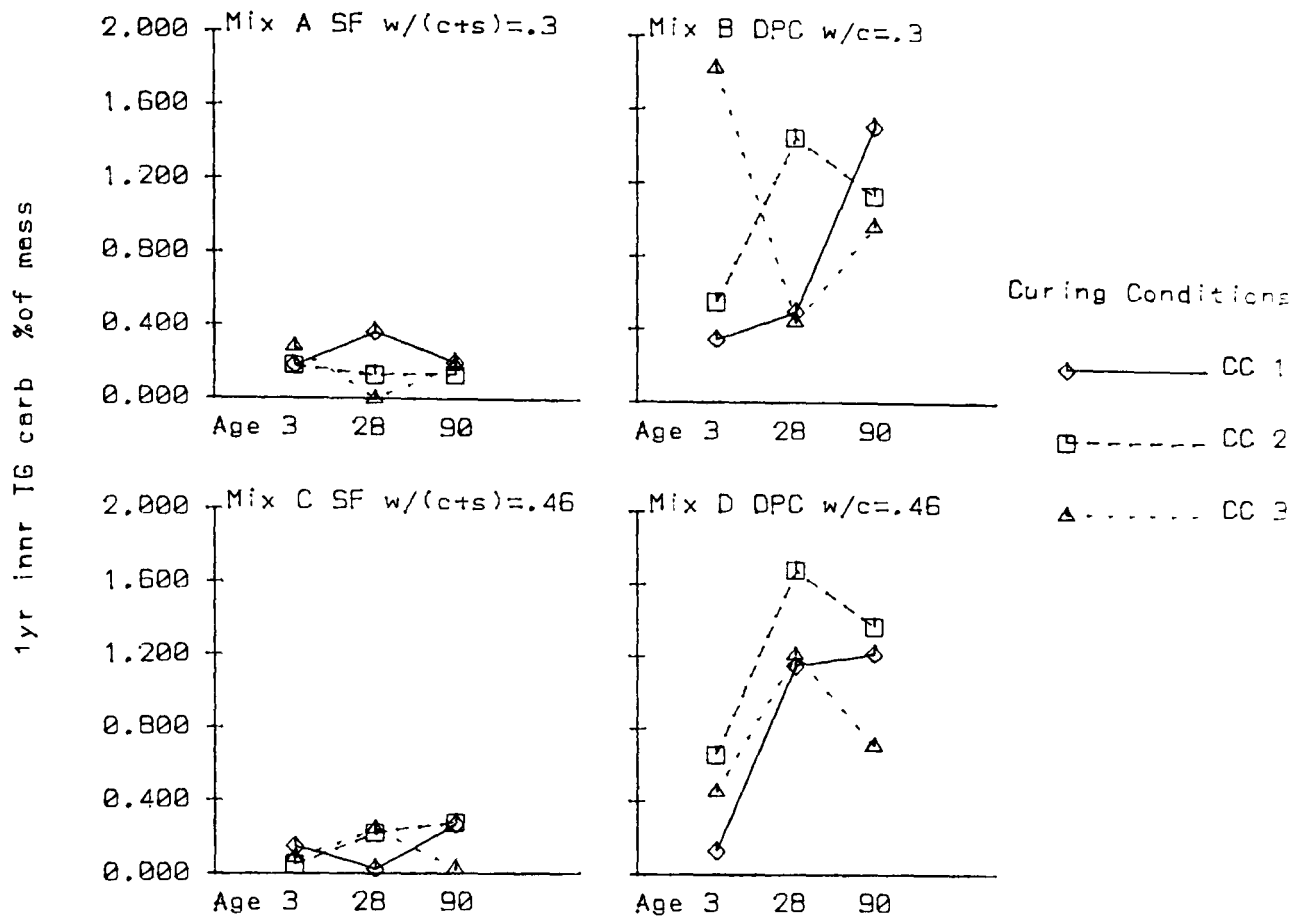
Fig. 11.10 Carbonate peak for the same samples as fig 11.8
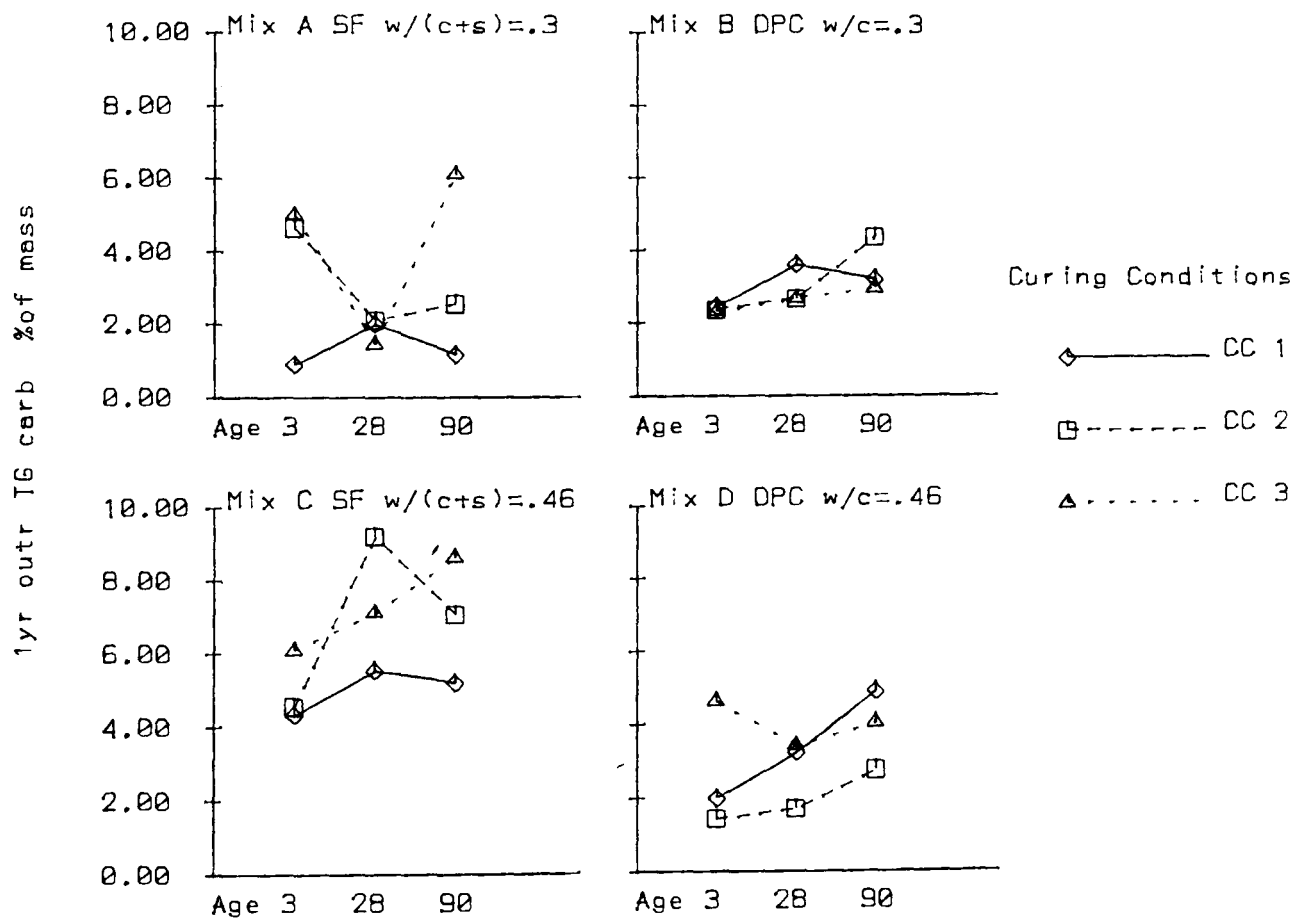
Fig. 11.11 Carbonate peak for the same samples as fig 11.9.
Note the different scales

12. Mechanical Tests.

12.1 Experimental procedure.

12.1.1 Sample preparation.

Mechanical tests were carried out on concrete samples of each of the 4 mixes for each of the 9 sample conditions (i.e 3 test ages and 3 curing conditions). No mechanical tests were carried out on paste or mortar samples.

12.1.2 Compressive strength.

Three 100mm. cubes were tested for each condition using the method in BS 1881 (1983) part 116. A further two were tested after one year of exposure in a room kept at 70% RH and 20°C.

12.1.3 Flexural strength.

The flexural strength was measured using two 500*100*100mm. prisms for each condition using the method in BS 1881 (1970) part 4.

12.1.4 Tensile strength.

Two 150mm. diameter cylinders were split for each condition using the method in BS 1881 (1983) part 117.

12.1.5 Static modulus.

The static modulus was measured on two 500*100*100mm. prisms for each condition. Measurements were made over a length of approximately 200mm. between points fixed with adhesive. Strains were measured for between 4 and 6 different stresses up to approximately 33% of the measured cube strength and the result was obtained by calculating the best line fit for all of the readings.

12.1.6 Dynamic modulus.

The acoustic resonance of two 500*100*100mm. prisms for each condition was measured and the modulus calculated as described in B.S.1881 (1970) part 5. The density was calculated from wet and dry weights of cubes recorded before the compression tests.

12.1.7 Poisson's Ratio.

An estimate of the Poisson's ratio was obtained from measurements of the ultrasonic pulse velocity in the prisms used for the measurement of dynamic modulus. The results were calculated using the formula in B.S.4408 (1971) part 5.

12.2 Results and discussion.

12.2.1 Effect of curing.

Each of the seven sets of results are plotted to show the effect of curing in figs.12.1-12.7. In figure 12.1 it may be seen that the compressive strength ot the SF mixes is more sensitive to curing than the strength of the OPC mixes. Failure of the aggregate was observed in the strongest mixes and with a stronger aggregate in the SF mixes the increase from 28 to 90 days would probably have exceeded the incease from 3 to 28 days giving the plots the same shape as for mix B. Fig.12.2 showing the "one year" strengths indicates that the substantial effect of curing noted in fig 12.1 is only temporary and the highest strength recorded was 148.9 MPa for mix A with 90 days curing in CC3. The effect of age for mix C was probably caused by drying out early in the hydration process. Failure of aggregate was also observed in the flexural strength tests (fig.12.3) and had similar consequences to those for the compressive strength. For some of the mix A samples inspection of the broken surface showed that every visible piece of aggregate had broken. For the tensile strengths (fig 12.4) the effect of curing is not so great (this is quantified in chapter 13), the shape of the graphs indicates that aggregate failure may still have reduced the 90 day SF results. Comparison of the static and dynamic moduli (figs 12.5 and 12.6) indicates that using the dynamic modulus to predict the static modulus may underestimate the static modulus for SF mixes because the SF caused a greater increase in it than for the dynamic modulus. This greater effect is associated with a greater dependence on curing.

12.2.2 Relationship with compressive strength after curing.

It is normal practice to estimate all other properties from the compressive strength measured after curing therefore any change in the relationship is cause for concern. The results are plotted in figs.12.8-12.13. In fig.12.8 showing the increase in strength for the "one year" cubes the points of greatest interest are the 90 day results which form a set of three points of highest "original" strength for each mix. These points are all about the same distance above the line of equality indicating that the gain in strength was approximately the same for all mixes. This situation could have been different if the samples had remained in water. The relationships of the flexural and tensile strength with compressive strength are in figs.12.9 and 12.10. With the exception of some mix A samples where the tensile strength may have been affected by aggregate failiure the same linear relationships apply all mixes. Curves have been fitted to the relationships with static and dynamic modulus (figs 12.11 and 12.12) because the relationships were not linear. For the static modulus the mixes are generally distributed about the line but for the dynamic modulus the SF mixes are all below it. This is because the SF had a major effect on the strength but virtually no effect on the

dynamic modulus.

12.3 Loss of mechanical strength on heating.

12.3.1 Introduction.

Hertz (1984) carried out some tests on the mechanical properties of SF concretes after heating and found that some of the samples exploded during heating. Because of the serious implications that a tendency to explode would have on the use of SF concrete in applications such as tall structures and nuclear containment a limited experiment was added to this program to try to replicate the effect. A heating rate of 1°C per minute was used by Hertz and was therefore chosen for this experiment.

12.3.2 Mix design for heated samples.

The samples which Hertz caused to explode had very low w/c ratios and in order to try to observe the same effect two additional mixes X and Y were made with w/c=0.22. Mixes A,B,C, and D were the same as those used in the rest of this project. The proportions of the mixes are shown in table 12.1.

Mix	X	Y	A	B	C	D
Cement (Kg/m^3)	480	600	344	430	252	315
Silica (Kg/m^3)	120	0	86	0	63	0
w/(c+s)	.22	.22	.3	.3	.46	.46
SP2 (% of c+s)	1.0	1.7	1.4	1.	1.9	1.9
5-20 mm. agg./(c+s)	2	2	3	3	4	4
Fine agg./(c+s)	1	1	1.5	1.5	2.3	2.3

Table 12.1. Mix design for heated samples.

SP2 is the superplasticiser, the percentages given are for the quantities of solids. The amount of superplasticiser added was in all cases sufficient to produce a workable mix. It is interesting to note the at w/c=.22 less is required for the SF concrete than for the OPC concrete.

For this experiment only the SF samples were made using an SF/water premixed slurry. This slurry was supplied from the same source as the powder used in the other experiments (Elkem Chemicals Ltd.) and consisted of equal weights of SF and water.

12.3.3 Experimental procedure for heated samples.

100mm. concrete cubes were cast and after 28 days curing in curing condition 1 (the fog room) they were heated to 600°C and then permitted to cool and tested for compressive strength. Control samples were tested directly after curing. For mixes

A,B,C and D two samples were tested after heating and one control sample was tested. For mixes X and Y two heated and two control samples were tested.

12.3.4 Results.

None of the samples exploded.
The results are shown in table 12.2

Mix	X	Y	A	B	C	D
Compressive strengths						
Heated samples	110.8	83.7	103.8	79.5	73.5	47.3
Control	125.1	98.6	113.7	82.9	83.6	47.5
Main set	-	-	113.2	80.4	88.4	55.4
% loss	11.4	15.1	8.7	4.1	12.1	0.4
Dry density						
Heated samples	2.362	2.418	2.411	2.406	2.383	2.340
Control	2.395	2.392	2.375	2.412	2.337	2.324
Main set	-	-	2.396	2.373	2.354	2.350

Table 12.2 Results for heated samples.

Readings from the main sets of samples (see paragraph 12.1.2) are included for comparison. The percentage loss of strength due to heating was calculated from the results for the heated and control samples. Densities were obtained by weighing wet and dry. For the control samples which were not dried in the kiln small samples of the broken cubes were dried at 110°C for 24 hours to obtain the moisture content as a correction factor for the dry density.

12.3.5 Discussion - heated samples.

The effect of the use of SF slurry in place of powder may be seen by comparing the control and main set values for the SF mixes in table 12.2. No significant effect is evident. The effect of heating on the compressive strength is shown as the percentage loss. At w/c=.46 the performance of the SF mix would appear to be substantially worse than the OPC but there is a relatively large differenc between the control and main set strengths for mix D. The reasons why the explosive effects observed by Hertz were not repeated are believed to be as follows:

1. Hertz used an even lower w/c ratio (w/c=.16)

2. The maximum strength obtained by Hertz (207.5 MPa) indicates that he was using a stronger aggregate.

For the purpose of nuclear waste containment the experimental conditions used were

severe enough to simulate the worst case and the mix design is therefore safe. For structures with relatively thin structural sections which might be exposed to intense heat from fire both the rate of heating and the maximum temperature could be exceeded. Hertz, however, suggests that the explosions that he observed were caused by a build up of steam in an impermeable matrix and in many applications the concrete would dry so this could not occur. For saturated conditions further experimental work could establish whether the SF mixes are more susceptible to explosion than the OPC mixes by progressively increasing the rate of heating or maximum temperature to see which mix failed first.

12.4 Conclusions.

1. The remarkable mechanical properties of SF concrete are well reported in the literature (e.g. Loland and Hustad 1981b) and the present measurements have only been obtained for the purpose of correlation with other properties and measuring the effect of different curing conditions.

2. Poor curing would appear to have a major short term effect on SF concrete. This conclusion is quantified by analysis of variance in chapter 13 and the long term effects are discussed in chapter 14.

3. Limited data has been obtained on the heat induced explosion effect which has been reported by Hertz (1984) and it does not appear to affect the mixes used in this project.
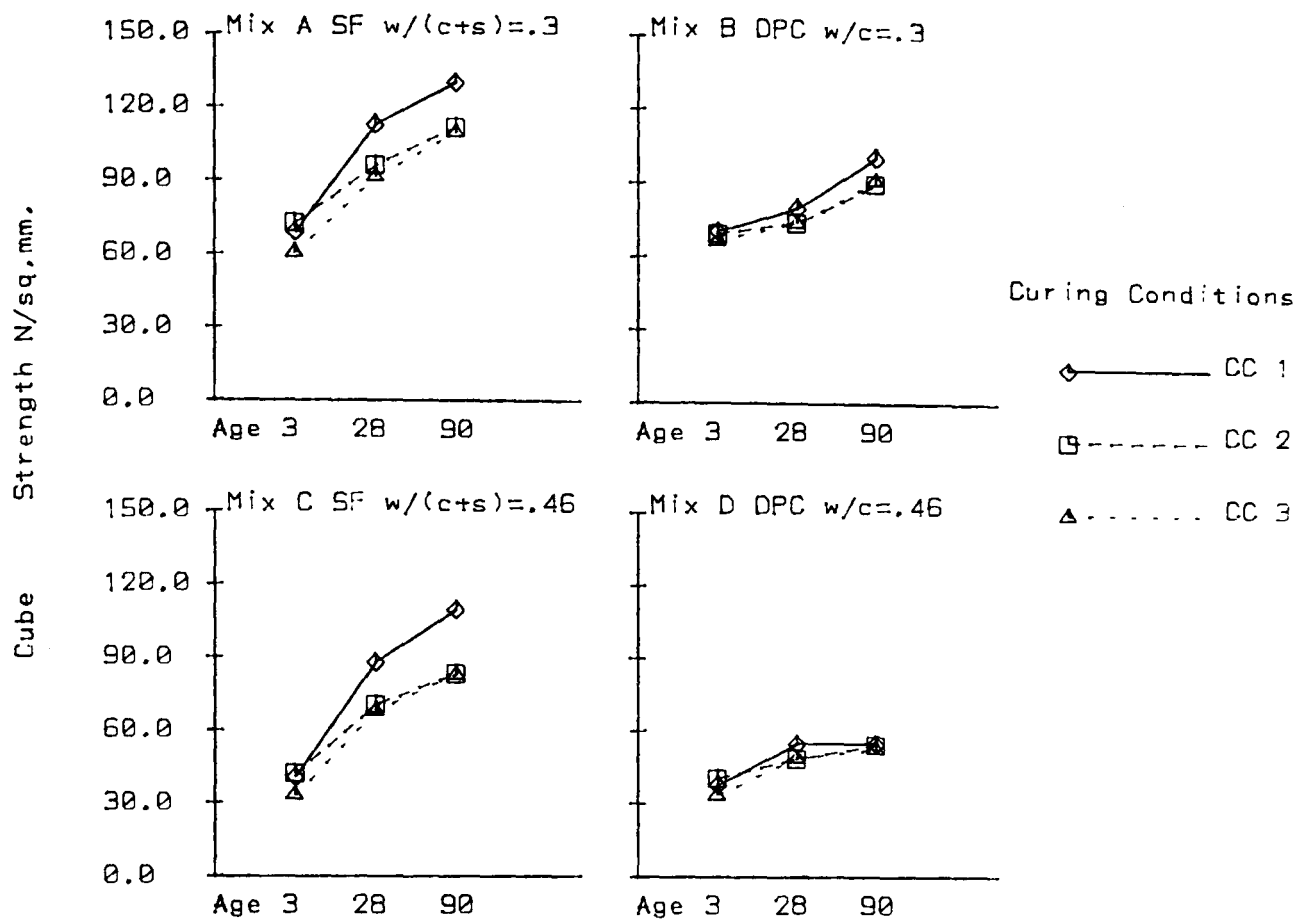
Fig. 12.1 compressive strengths of 100mm cubes immediately after curing.
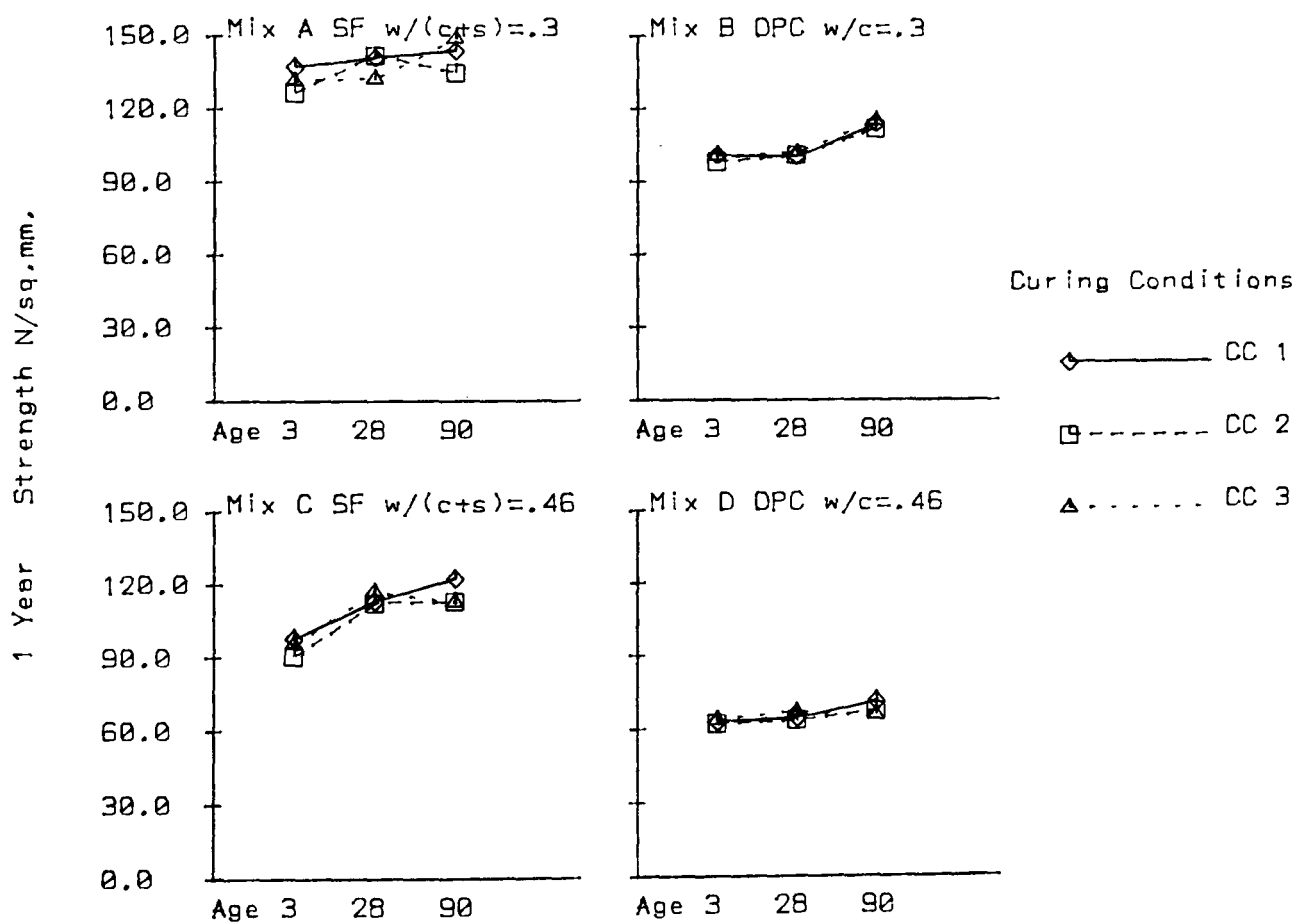
Fig. 12.2 compressive strengths of 100mm cubes after being stored for 1 year in a room at 20 degrees after curing.
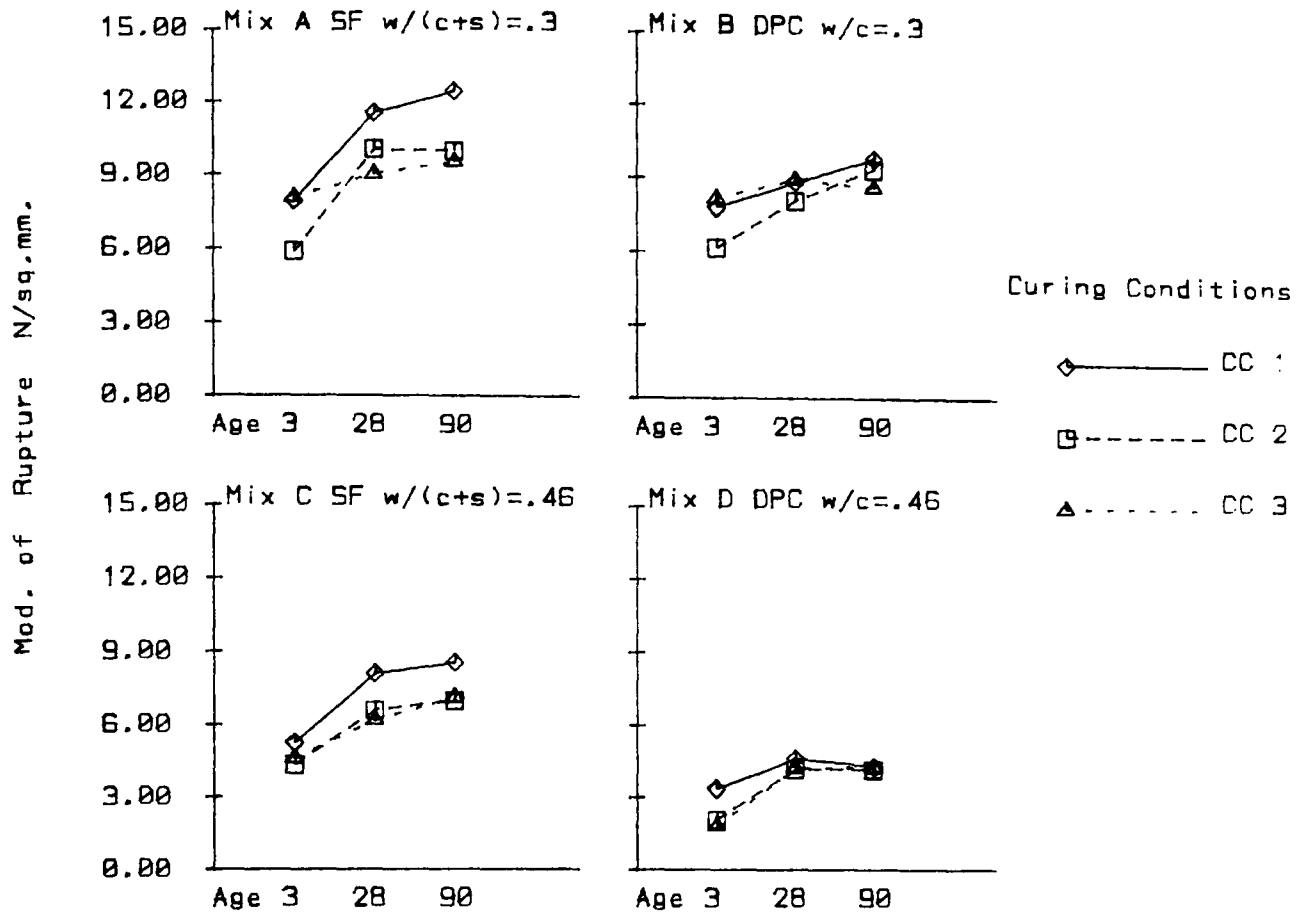
Fig. 12.3 Modulus of rupture of 100mm*100mm*500mm concrete samples.
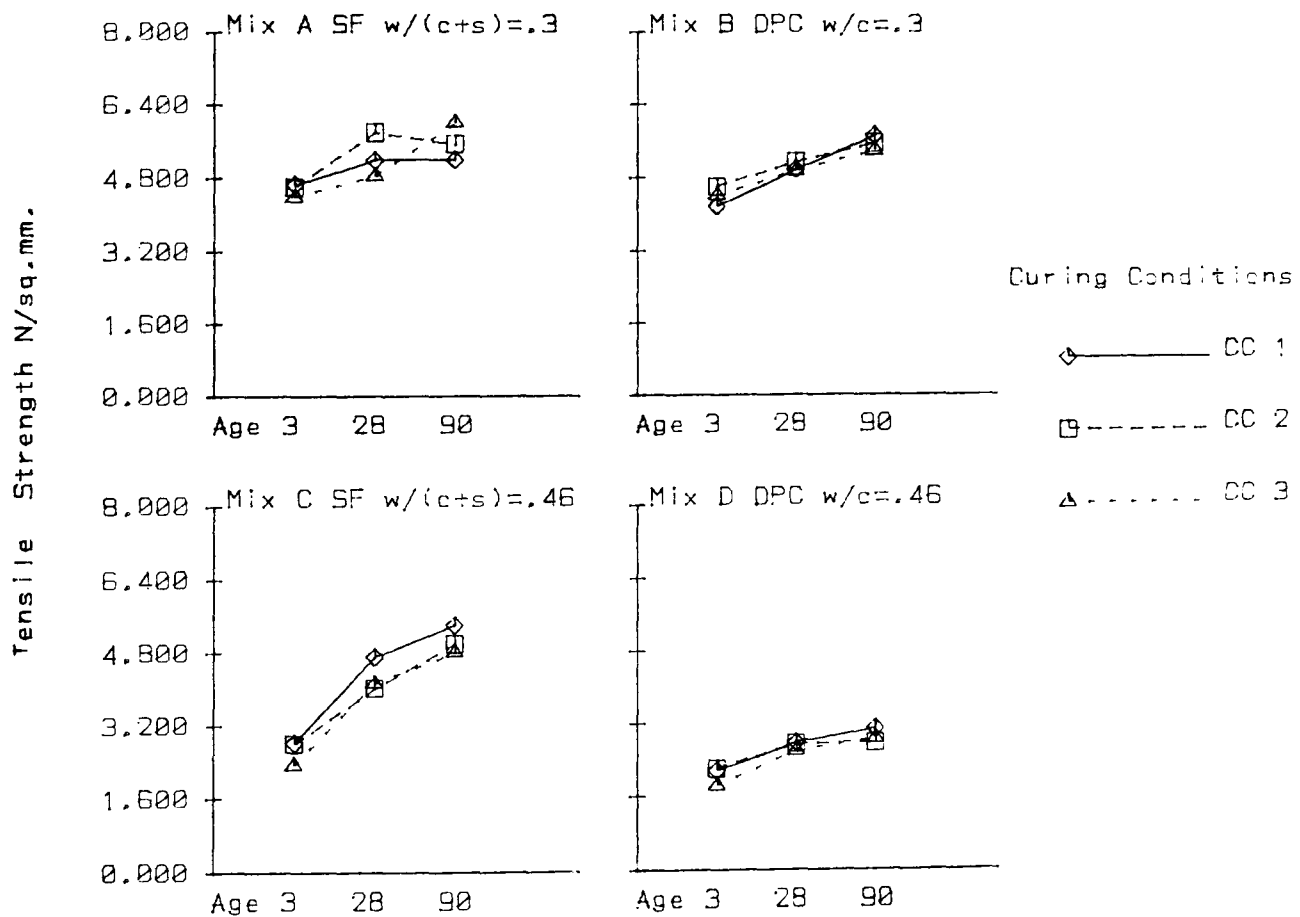
Fig. 12.4 Tensile strength obtained by splitting 150mm diameter concrete cylinders.
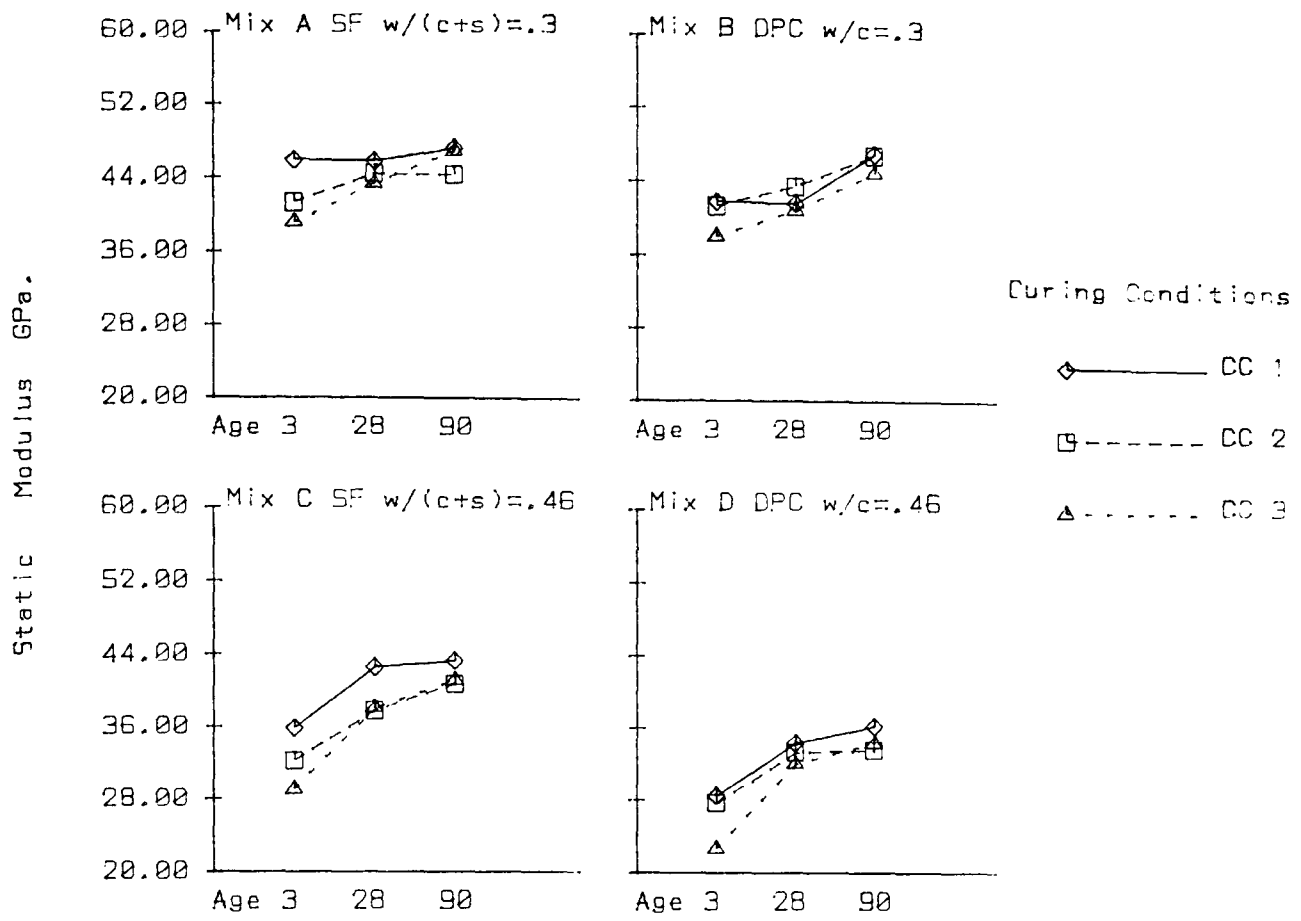
Fig. 12.5 Static modulus of 100mm*100mm*500mm concrete beams.
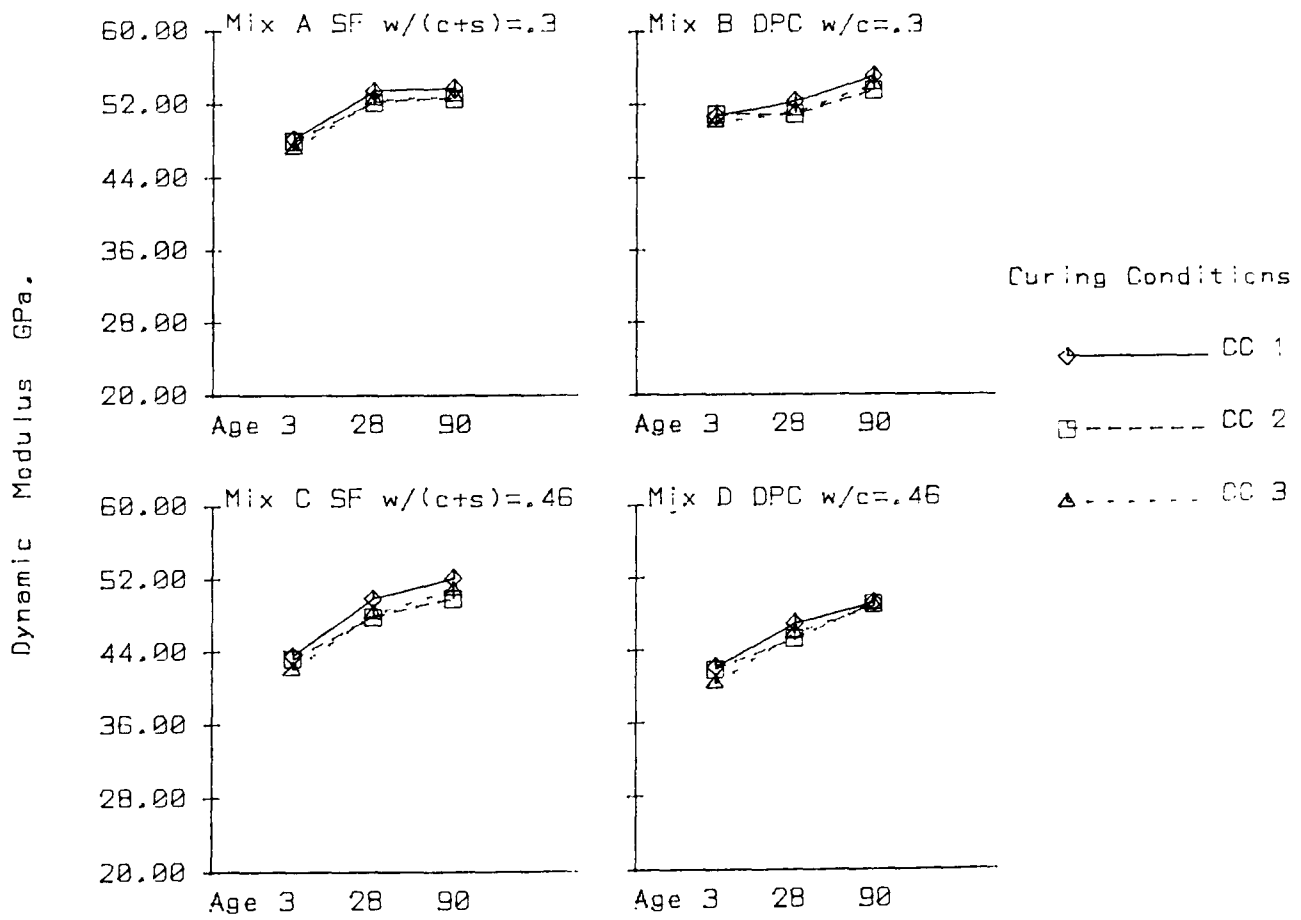
Fig. 12.6 Dynamic modulus obtained by measuring the acoustic resonance of 100mm*100mm*500mm concrete beams.
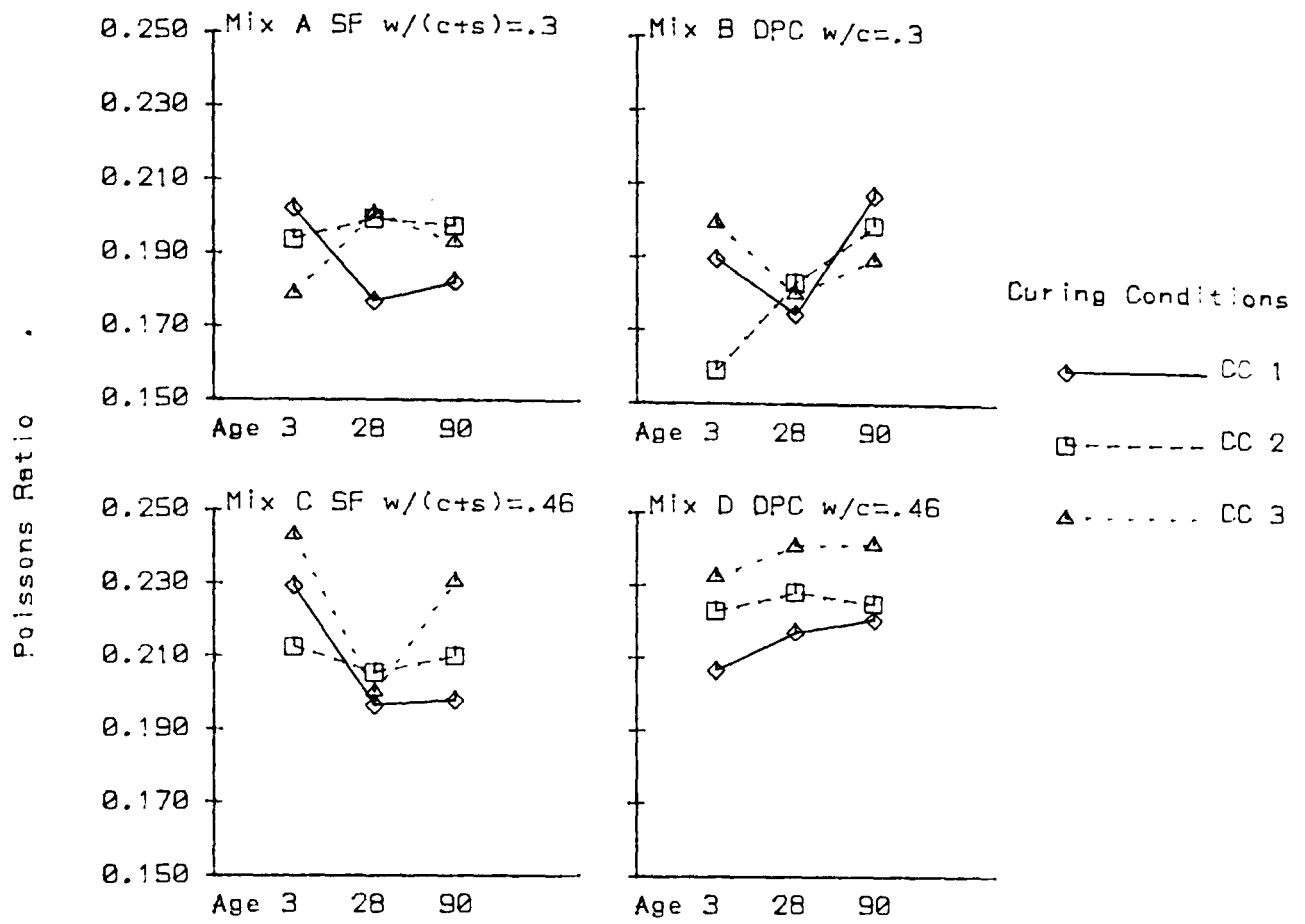
Fig. 12.7 Values for Poisson's ratio calculated from the ultrasonic pulse velocity.
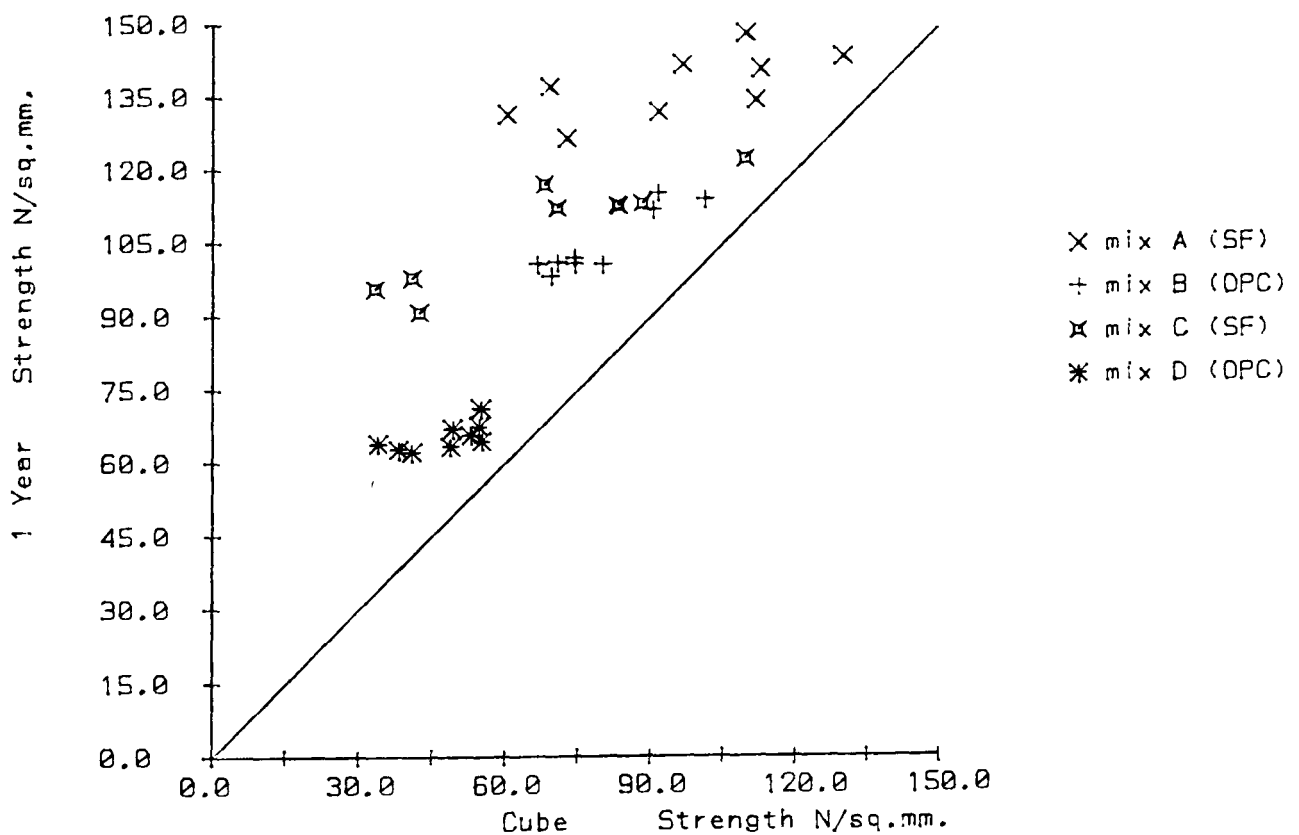
Fig. 12.8 Comparison of the compressive strength after curing and after one year of subsequent dry storage. The line of equality is drawn.
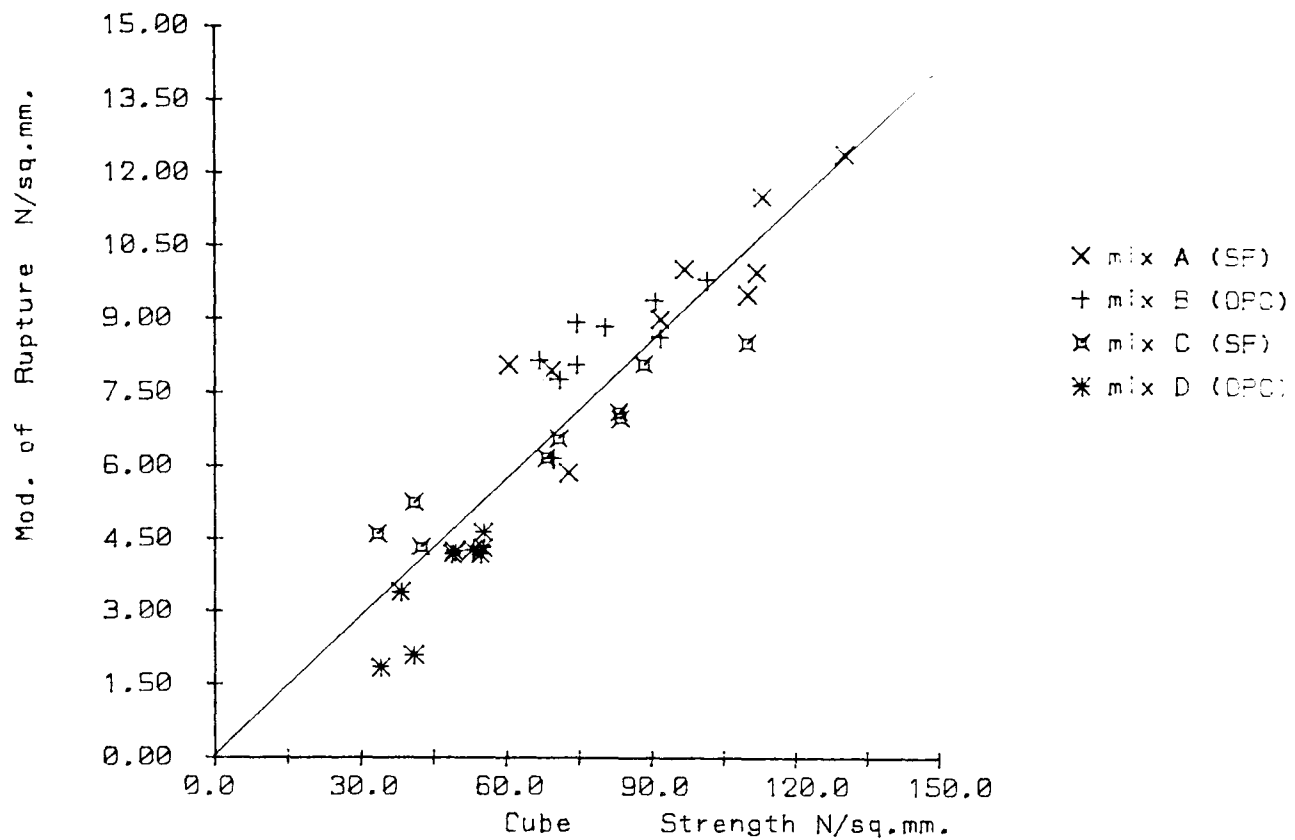
Equation for line : Y=6.890274087E-2+X*9.504872817E-2
R squared=0.832

Fig. 12.9 Relationship between compressive strength and modulus of rupture. The line is a best fit to all of the data.
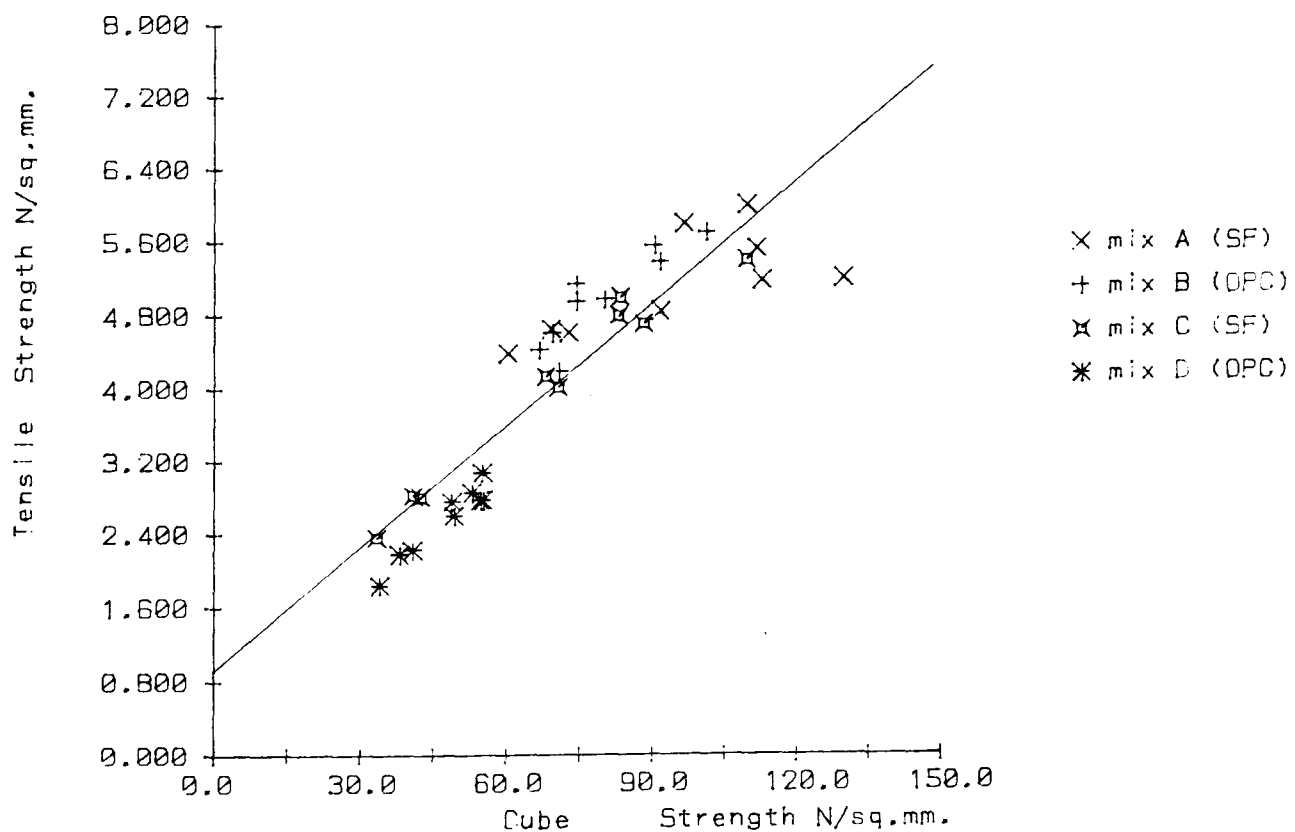
Equation for line : Y=0.9344460012+X*4.459274391E-2
R squared=0.814

Fig. 12.10 Relationship between compressive strength and tensile strength. The line is a best fit to all of the data.
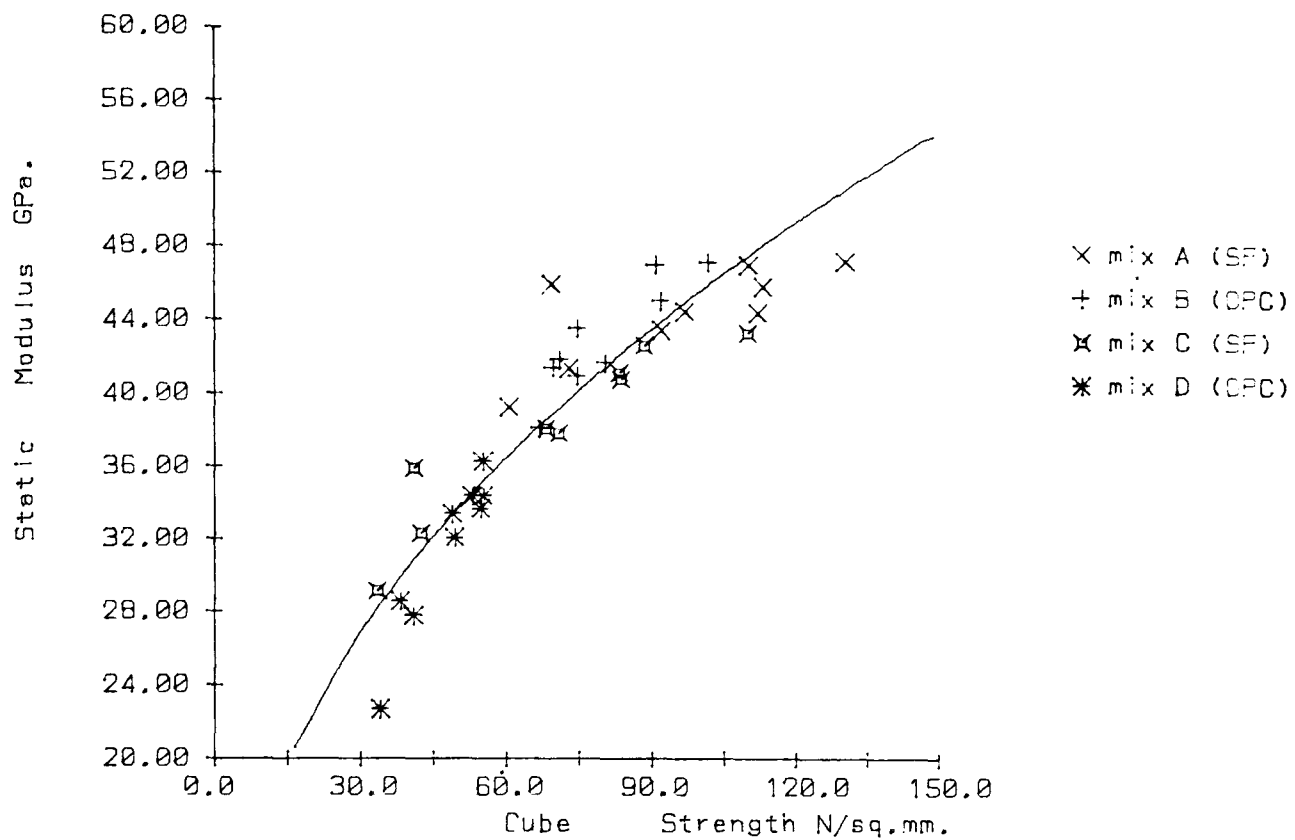
Equation for line : Y=5.992949719*X^0.440887364
R squared=0.829

Fig. 12.11 Compressive strength vs. static modulus. The curve is an exponential best fit to all of the data.
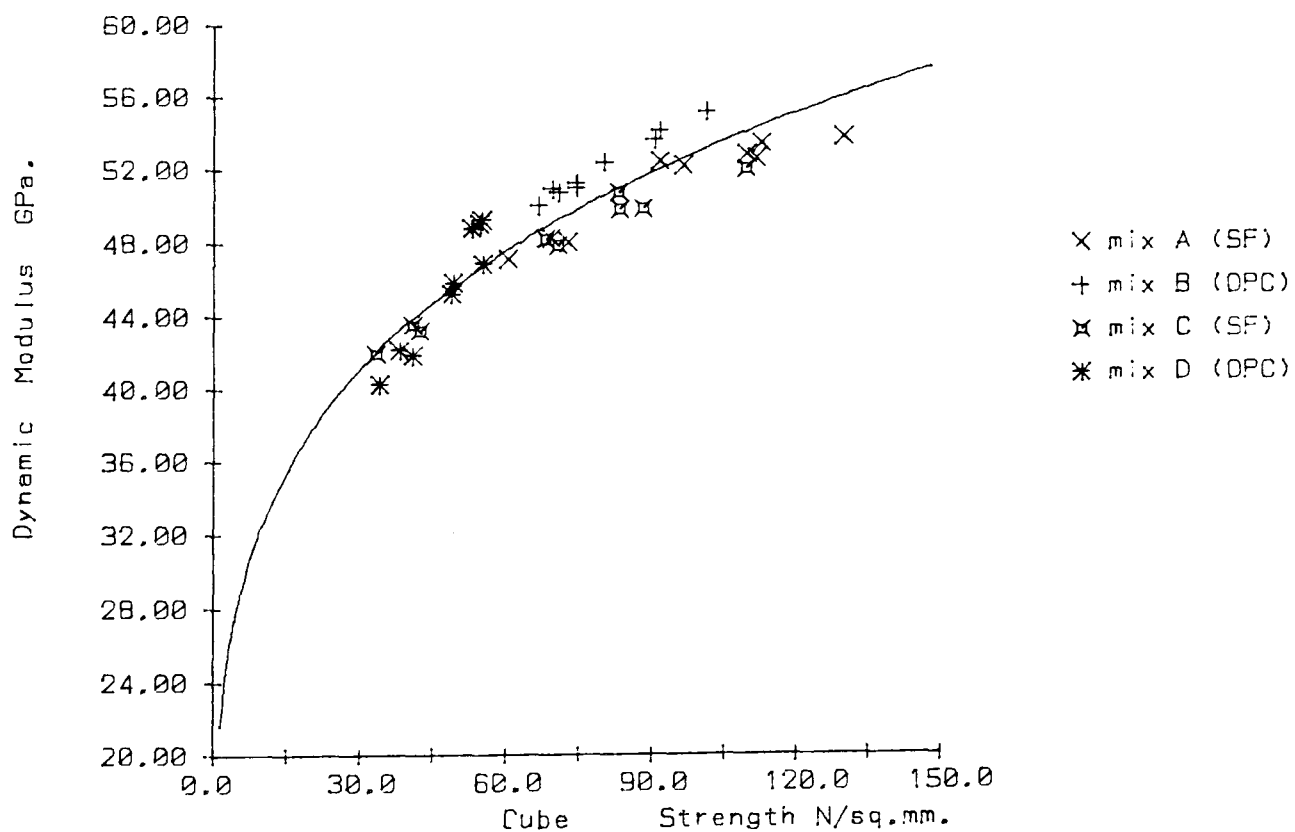
Equation for line : Y=19.88639781*X^0.2132340356
R squared=0.856

Fig. 12.12 Compressive strength vs. dynamic modulus. The curve is an exponential best fit to all of the data.
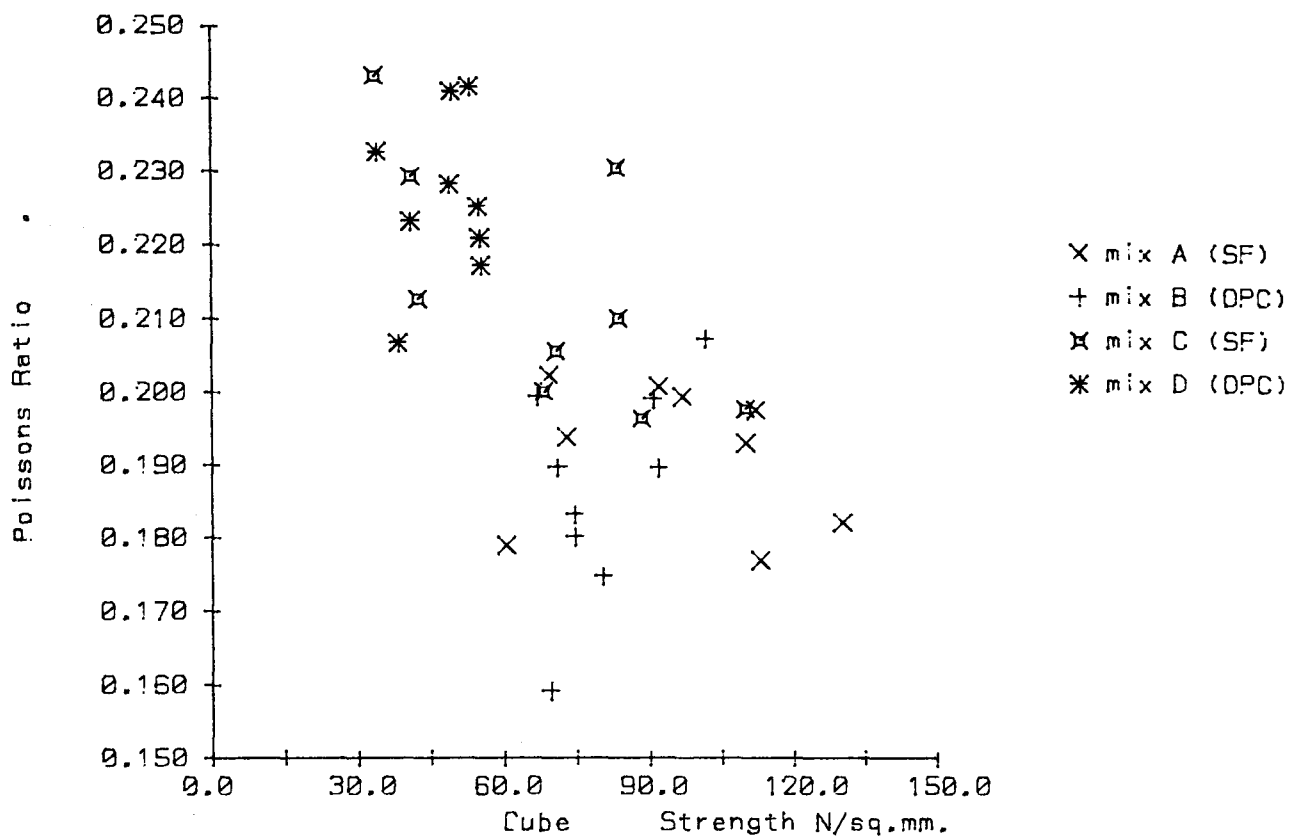
Fig. 12.13 Compressive strength vs. Poisson's ratio

13 Data Analysis.

13.1 Introduction.

In this chapter some statistical analysis on the experimental results is presented. In section 13.2 individual properties are analysed for the effects of the SF and its effect on the sensitivity of the properties to w/c ratio, test age and curing conditions. In section 13.3 the effect of basic properties on those properties which are dependent on several factors is analysed using multiple regression. In section 13.4 the method of calculating porosity used in chapter 10 is applied to the SF mixes and in section 13.5 the total porosity and concrete resistivity are both correlated with other properties.

13.2 Analysis of variance.

13.2.1 Introduction.

The purpose of this analysis is to assess the effect of the silica fume on the principal properties of the mixes. In addition to the overall effect of the SF the effect on the sensitivity of the mixes to changes in other factors (w/c ratio, test age and curing conditions) has been analysed. For this purpose it is necessary to compare the average effect of the factors affecting the mixes both with and without SF. These averages are shown graphically and the statistical significance of the differences between them has been calculated using the F statistic. The sensitivity of the other factors to the SF is given by the interaction terms.

13.2.2 Analysis of two typical properties.

In order to indicate the method used to calculate the F statistic tables 13.1 and 13.2 show the analysis for two typical properties. The type of analysis is ANOVA with four variables and the results are from computer programs written using methods from Kennedy and Neville (1986). Table 13.1 shows the analysis for compressive strength where each result was based on an average of three observations and table 13.2 shows flexural strength where each result was an average of two observations. The experimental results for all properties are in the tables in Appendix 3, these two examples are from chapter 11 (table A3.11). All of the values for sum of squares (SoS) except for the total and the error have been obtained from the data given in appendix 3. The total was obtained from the original readings and the error and the values of F were calculated from it.

Source	SoS	DF	Mean Sq	F	Fcrit
SF in mix	8871	1	8871	2540	7.04
w/c ratio	23097	1	23097	6600	7.04
Test Age	24178	2	12089	3455	4.93
Curing	2445	2	1223	349	4.93
SF in mix-w/c ratio	253	1	253	72	7.04
SF in mix-Test Age	4705	2	2353	673	4.93
SF in mix-Curing	688	2	344	98	4.93
Other interactions	1861	24	78	22	
Error	252	72	3		
TOTAL	66350	107	620		

Table 13.1 Analysis of variance for compressive strength

Source	SoS	DF	Mean Sq	F	Fcrit
SF in mix	62	1	62	201	7.36
w/c ratio	270	1	270	918	7.36
Test Age	85	2	43	145	5.10
Curing	21	2	10	35	5.10
SF in mix-w/c ratio	14	1	14	47	7.36
SF in mix-Test Age	5	2	3	8	5.10
SF in mix-Curing	4	2	2	7	5.10
Other interactions	17	24	1	2	
Error	11	36	0		
TOTAL	489	71	7		

Table 13.2 Analysis of variance for flexural strength.

The critical values of F (Fcrit) are for 1% significance. The tables indicate that all of the interactions are statistically significant.

The other interactions are as follows:

w/c ratio-age (2)

w/c ratio-curing (2)

age-curing (4)

SF in mix-w/c ratio-age (2)

SF in mix-w/c ratio-curing (2)

SF in mix-age-curing (4)

w/c ratio-age-curing (4)

SF in mix-w/c ratio-age-curing (4)

The figures in brackets are the numbers of degrees of freedom for the interactions. None of these other interactions are considered to have any particular physical significance to the present analysis.

13.2.3 Graphical representation.

The F statistic only indicates whether an interaction is statistically significant. Because it measures the relative sizes of the interaction and the experimental error a large interaction combined with a large error will give the same result as small values of both. It also does not measure the direction of the interaction (i.e. whether SF increases or decreases the effect of age) and is, for example, unchanged by interchanging the results for two different ages. The size and nature of the interactions for the two properties shown in tables 13.1 and 13.2 is shown in figures 13.1 and 13.2. In fig.13.1 the bars on the left entitled "Total" indicate average values for all SF and all OPC samples. The difference is very much greater than the experimental error so the F statistic listed below them is large. The left hand bar in the group entitled "w/c ratio" gives the average for SF samples with w/c=0.3 (i.e. all of the mix A samples) and the other three bars in this group give the averages for the other three mixes. From this group it may be seen that the compressive strength of the SF mixes is less dependent on w/c ratio than the strength of the OPC mixes. Reference to the F statistic and its critical value below it shows that this is again significant.

In this way the results from these two graphs may be summarised as follows:

	compressive	rupture
total effect of SF	increase	increase
dependence on w/c ratio	decrease	decrease
dependence on age	increase	increase
dependence on curing	increase	increase

13.2.4 ANOVA - Results and discussion.

The results for the analysis of variance are presented in figs.13.1-13.14. Some measurements (e.g. chloride transmission) were not calculated as a simple average of more than one observation and could thus not be analysed in this way. The properties which are shown have thus been selected on the basis of physical relevance and suitability of the data.

The principal mechanical properties are in figs.13.1-13.4. Neither the tensile strength nor the static modulus show the increased sensitivity to curing which was noted for the

compressive and flexural strength. The static modulus also shows no significant increased sensitivity to age. All of the mechanical properties, however, show a major total effect of the SF and a decreased sensitivity to w/c ratio.

The corrosion rates for the concrete samples measured by linear polarisation immediately after immersion in the salt solution are shown in fig.13.5 and the rates after 28 days application of an anodic voltage are shown in fig 13.6. It should be noted that these graphs are linear (not logarithmic) and that the scales are different by a factor of 10. Fig 13.5 shows the expected total effect of the SF and its increase in the sensitivity to curing. Fig. 13.6 is dominated by the mix D (OPC, w/c=.46) results. The chloride has caused a massive increase in the mix D corrosion rate. The SF has greatly reduced the sensitivity to an increase in w/c ratio. Figures 13.7 and 13.8 show the a.c. resistivities of the samples for which the corrosion rates were shown in figs.13.5 and 13.6. The results for the OPC samples are very different from the SF samples although it is interesting to note that the fractional difference between, for example, the results for the w/c ratios is similar with and without SF. The absolute differences cause the large value of F. Most of the results from the small mortar corrosion samples did not show statistical significance due to considerable variations between samples but an exception was the resistivities immediately after the samples were placed in the salt solution. Figure 13.9 shows the results for the samples which had been in the carbonation tank and fig.13.10 is for the control samples which had been kept in the room. The great increase in the resistivity of the mix D (OPC w/c=.46) samples caused by carbonation in the tank is of note.

Figure 13.11 shows the vapour permeability and fig.13.12 the oxygen permeability. As was noted in chapter 5 the sensitivity of the vapour permeability of the SF mixes to w/c ratio could be reduced by high energy mixing.

Fig.13.13 shows the percentage mass loss in the calcium hydroxide peak of the paste samples tested in the thermogravimetric balance. Fig.13.14 gives similar data for the carbonate peak. From these two graphs it may be concluded that the pozzolanic effect of the SF is highly statistically significant and that in the absence of deliberate carbonation the carbonate content is not noticeably affected by the SF.

Using the notation D for decrease and I for increase the results are summarised in table 13.3.

Property	Total	Sensitivity to		
	SF	w/c	age	cure
Mechanical properties				
Comp. strength	I	D	I	I
Rupture	I	D	I	I
Tensile strength	I	D	I	-
Static modulus	I	D	-	-
Electrical properties (concrete)				
Initial corrosion	D	-	-	I
28 day corrosion	D	D	D	D
Initial resistivity	I	I	I	I
28 day resistivity	I	I	I	I
Electrical resistances (mortar)				
Carbonated samples	I	D	-	-
Control samples	I	I	I	-
Permeability				
Vapour	D	I	-	-
Oxygen	D	D	D	D

Table 13.3. Summary of results from ANOVA (I=increase, D=decrease).

13.3 Multiple Regression.

13.3.1 Introduction.

The purpose of this analysis is to form a model of the effect of a number of basic properties on a more complex property. The model assumes that the value of the complex property (the dependent variable) may be predicted as a linear combination of the values of the basic properties in addition to a constant term. This analysis has been applied at two levels.

First the properties which affect the corrosion rate and were measured in chapters 3-7 are analysed using the results from mercury intrusion for the porosity over different ranges of pore sizes as predictors.

Secondly the corrosion rates which were measured in chapter 3 were analysed, using the properties which were analysed in detail at the first level as predictors.

13.3.2 Analysis of a typical property.

The example chosen as a typical analysis is the vapour permeability using the porosity

over different ranges of pore sizes as predictors. The analysis was carried out using the "Microtab" statistics package (Higginbotham 1985). A further computer program has been written to produce a graphical output and an example of this is shown in fig.13.15. At the top of the page the dependent variable and the predictors are listed and the remainder of the page is divided into three analyses, one for all mixes, one for the SF mixes and one for the OPC mixes. Each analysis is presented as a pie chart, a table and a graph.

In the top row (all samples) the centre column of the table shows the coefficients for each of the predictors. These coefficients are for the following equation:

Predicted value = Coefficient for constant term

+ (Coefficient no.2 * value for predictor no.2)

+ (Coefficient no.3 * value for predictor no.3)

+ ....

The value of these coefficients has little physical significance because a range of pores such as .01-.15 μm(where up to 30% porosity has been observed) will tend to have a lower coefficient then the .15-10 μm range (where the maximum observed porosity was less than 1%) irrespective of their relative effects on the dependent variable. In order to assess the relative importance of each range the coefficient for the range has therefore been multiplied by the standard deviation (i.e.standard deviation for porosity) for the range and the relative sizes of the absolute values of these products is shown in the pie chart. Thus the pie chart indicates that the pores in the range .01-.15 μm have the greatest effect on vapour permeability. The value of Student's t for this predictor is 6.75. The critical value for 1% significance (31 degrees of freedom) is 2.75 and there is thus statistical evidence that the permeability is dependent on the porosity in this range. The coefficient for the .15-10 μm range is negative indicating that porosity in this range decreases permeability but the value of t is too low for this to be a statistically valid conclusion.

The graph to the right of the table is included to give an indication of the accuracy of the model. The line of equality has been drawn on it to make it easier to see how well the points fit to it.

13.3.3 Multiple regression - results and discussion.

The results of analysis using the porosity in the different ranges of pore sizes as predictors are in figs.13.15-13.21. The properties shown are vapour permeability (13.15), oxygen permeability (13.16), initial and 28 day a.c. resistivity for concrete (13.17 and 13.18), compressive strength (13.19), carbonation depth of mortar samples (13.20) and average chloride concentration from the ponded concrete samples (13.21). For the resistivity and the oxygen permeability logarithms have been used because the range is substantially greater than the range of porosities.

The remarkable aspect of these graphs is the similarity of the pie charts for all of the properties. The .01-.15 μm range is dominant for all of the charts of all mixes and for

the OPC samples it is so large that it is the only significant range. Even for the SF samples where the porosity in this range was much smaller (see fig.9.8) it is the only significant range. The fine pores are not statistically significant.

The analysis of the initial and 28 day corrosion rates is shown in figs.13.21 and 13.22. The predictors are vapour and oxygen permeability, resistivity, carbonation depth and chloride concentration. In a trial analysis compressive strength was included but it was not significant. The corrosion current, oxygen permeability and resistivity were included as logarithms. In general the most significant property appears to be the resistivity. These results should, however, be treated with caution, for example in fig.13.22 the vapour permeability shows t=4.00 for the sample of all mixes which would be significant, however the coefficient is negative and it would be expected to be positive.

13.4 Calculation of porosity.

13.4.1 Calculation for pozzolanic materials.

In chapter 10 a method for calculating the porosity of OPC samples was presented. This method depended on the assumption that in the hydration reaction water and cement combine at a ratio of 1:4 to form hydration products. If there is a pozzolan present it will react with calcium hydroxide released in the cement hydration process and with water to form more hydration products (Neville 1981). This means that several more assumptions must be made in order to analyse the hydration process. The following method is suggested as a possible basis for the calculation but only very limited data has been obtained for the estimates of the constants.

In the review on the literature on pozzolanic activity (section 1.2.7.) the minimum percentage of SF addition for total calcium hydroxide depletion was discussed. The conclusion was that about 20% addition was required. The mixes used in this project had 20% replacement which gives the same ratio as 25% addition and total depletion was certainly observed.

In order to calculate the total amount of calcium hydroxide released by one of the OPC mixes it is necessary to include the fraction that has carbonated. In the thermogravimetric results (Chapter 9) the percentages of the mass of the mix B CC1 90 day samples lost in the hydroxide and carbonate peaks were 2.3% and 2.6% respectively. This sample has been chosen because the corresponding SF sample (mix A) was one where total calcium hydroxide depletion occured. Tests with pure calcium hydroxide and carbonate gave losses of 22% and 45% thus the total original hydroxide content of the mix B sample was :

$$2.3/.22 + 2.6/.45 = 16.2\%$$

If 20% of the cement had been replaced with SF this would have been reduced to 13%. In a sample with 20% SF replacement and w/c=.3 the SF forms 15% of the

original weight so for the purpose of calculation it is estimated that the SF and hydroxide combine in equal weights.

In order to calculate the amount of hydroxide available to react in each sample it has been assumed that the SF does not affect the progress of the cement reaction. This is probably not accurate but it is necessary in order to proceed with the calculation. Thus:

$$L_{use} = 0.8\, L_{opc} - L_{sf}$$

where:

L_{use} = the hydroxide used in the reaction

L_{sf} = the hydroxide (+carbonate) measured in the SF sample

L_{opc} = the hydroxide (+carbonate) measured in the corresponding OPC sample

For the calculation of porosity for the OPC samples the value of 2.15 was used for the specific gravity of the hydrated cement. This is an average value for all of the products including the calcium hydroxide. Thus when it was used for the pozzolanic samples it was necessary to subtract the volume of the hydroxide which had been removed from it (the specific gravity of calcium hydroxide was measured at 2.35 g/cc).

The only remaining question is what happened to the water. The total amount used in the reactions was known but the relative amounts for the SF and OPC were not. Because the SF is a minor constituent in the mix the porosity was not found to be very dependent on the ratio chosen. Calculations using ratios of hydroxide : SF : water of 1:1:0.5 and 1:1:1 were carried out and the difference was found to be only 1% of porosity. Because it corresponds to the same ratio used for the OPC 1:1:0.5 was used.

13.4.2 Results for porosity.

Measured porosities were obtained from mercury intrusion and by using helium intrusion readings for specific gravity (SG) in combination with dry densities (DD) from chapter 9 in the equation:

$$\text{Porosity} = 100 \left[1 - \frac{DD}{SG} \right]$$

The relationship between the two measurements of paste porosity is shown in fig.13.24 and may be seen to be good especially considering that the samples for helium intrusion were made with low energy mixing but high energy mixing was used for the mercury intrusion. The relationship between calculated porosity and helium intrusion porosity for paste, mortar and concrete is shown in figs. 13.25, 13.26 and 13.27 from which it may be seen that the OPC values form a reasonable line but the calculated SF values are very high.

13.5 Correlation with porosity and resistivity.

The correlation coefficient R^2 for the measured porosity (from helium intrusion) with some other properties is given in table 13.4. An alternative predictor which is considered here is the concrete resistance R_c. Because of its wide range of values and

the fact that it is higher for "better" samples the inverse of the logarithm is used. Because it is also higher for better concrete the inverse of the compressive strength is used. The 1% statistical significance level of R^2 is .174.

	Porosity	$1/Log(R_c)$
Concrete properties		
Initial corrosion current	0.22	0.54
28 day corrosion current	0.13	0.04
Chloride content (gravity test)	0.59	0.57
1/compressive strength	0.45	0.80
Mortar properties		
Log(Oxygen permeability)	0.38	0.23
Log(charge passing) in electrical		
Chloride diffusion test	0.40	0.90
Carbonation depth	0.20	0.34
Paste property		
Vapour diffusion	0.81	0.29

Table 13.4. R^2 for relationships between properties.

Log-Log relationships were calculated for raw data. i.e. 0.90 is the value for the relationship between $1/R_c$ and charge passing not their logarithms.

Porosity would appear to be a good predictor of vapour diffusion and resistivity appears good for compressive strength. The values for charge passing have been included to show that this is actually just another measure of resistivity (see chapter 5).

13.6 Conclusions.

1. Four way analysis of variance has been used to quantify the effect of the SF on some of the principal measured properties of the mixes. This has made it possible to draw conclusions which are statistically justified.

2. Multiple regression analysis has been used to obtain information on the contribution of different pore size ranges to the variations in the measured properties and the contribution of those properties to the corrosion rates.

3. By using TG data the method of calculating porosity developed in chapter 10

has been extended to cover the SF mixes.

4. The total porosity and the resistivity have been found to be good predictors for some of the other properties.

AVERAGE VALUES OF THE EFFECT OF W/C RATIO, AGE AND CURING

Mixes containing Silice Fume :

Mixes without Silice Fume :

F Statistic	2539.69	72.52	673.53	98.42
Fcritical	7.04	7.04	4.93	4.93
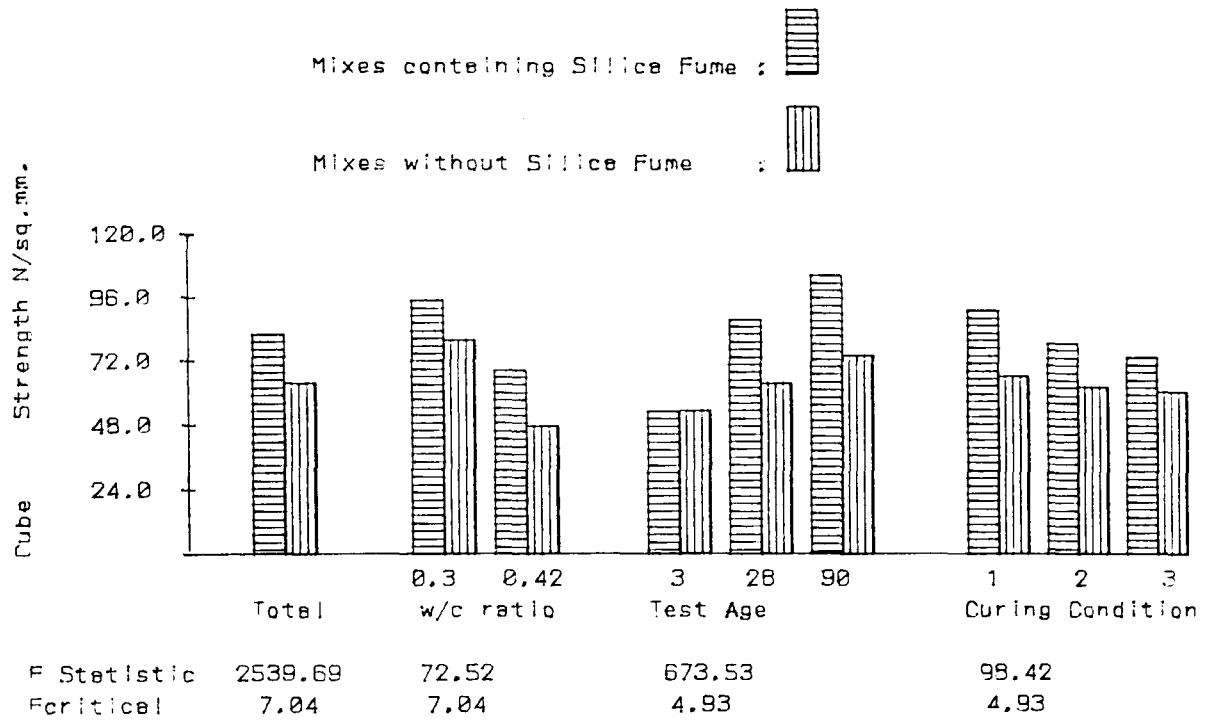
SST=642875.00 Number of observations=3.00

Fig. 13.1 Analysis of variance for compressive strength.

AVERAGE VALUES OF THE EFFECT OF W/C RATIO, AGE AND CURING

Mixes containing Silice Fume :

Mixes without Silice Fume :

F Statistic	200.97	46.58	8.29	6.73
Fcritical	7.36	7.36	5.10	5.10
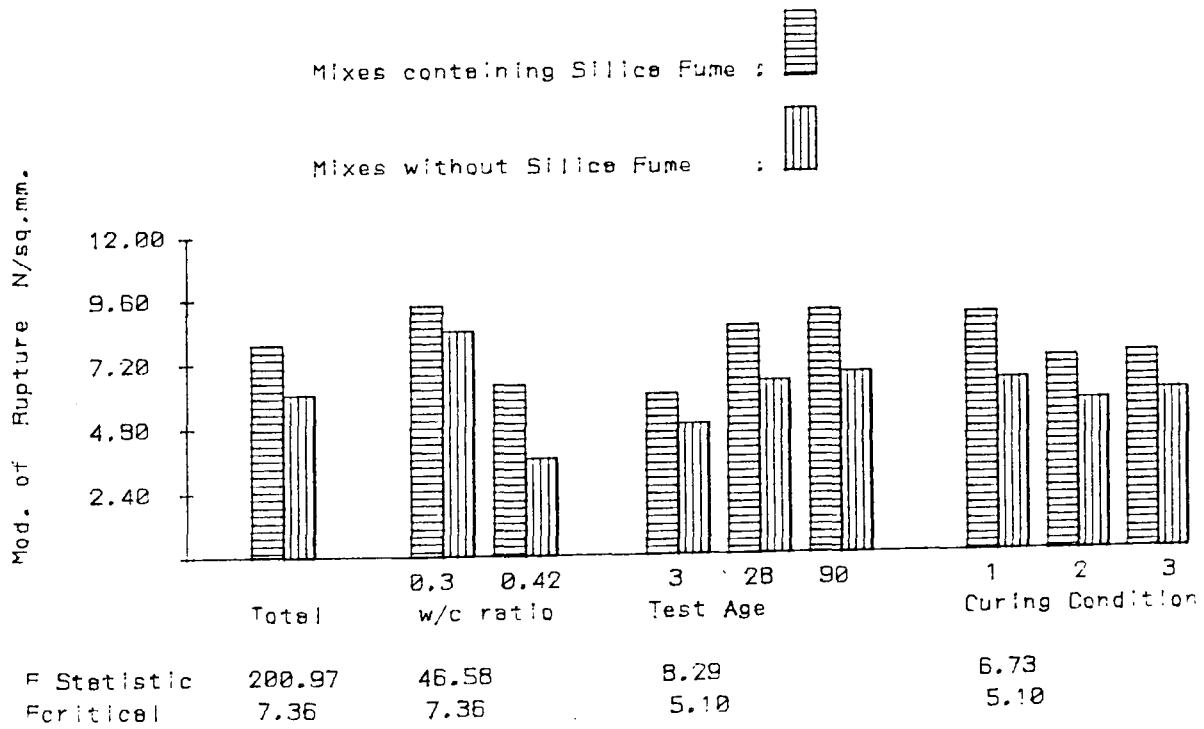
SST=4031.00 Number of observations=2.00

Fig. 13.2 Analysis of variance for flexural strength.

AVERAGE VALUES OF THE EFFECT OF W/C RATIO, AGE AND CURING

Mixes containing Silica Fume :

Mixes without Silica Fume :

F Statistic	230.10	154.10	17.81	0.33
Fcritical	7.36	7.36	5.10	5.10
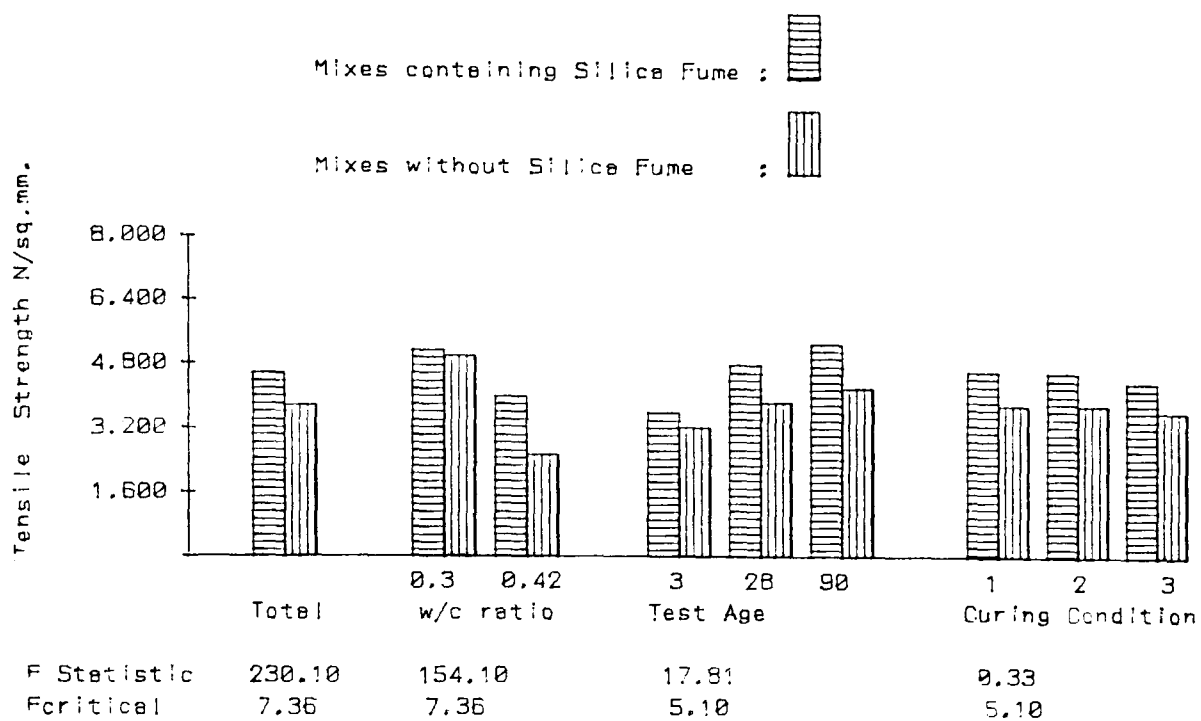
SST=1375.00 Number of observations=2.00

Fig. 13.3 Analysis of variance for tensile strength.

AVERAGE VALUES OF THE EFFECT OF W/C RATIO, AGE AND CURING

Mixes containing Silica Fume :

Mixes without Silica Fume :

F Statistic	120.24	51.07	0.62	5.03
Fcritical	7.36	7.36	5.10	5.10
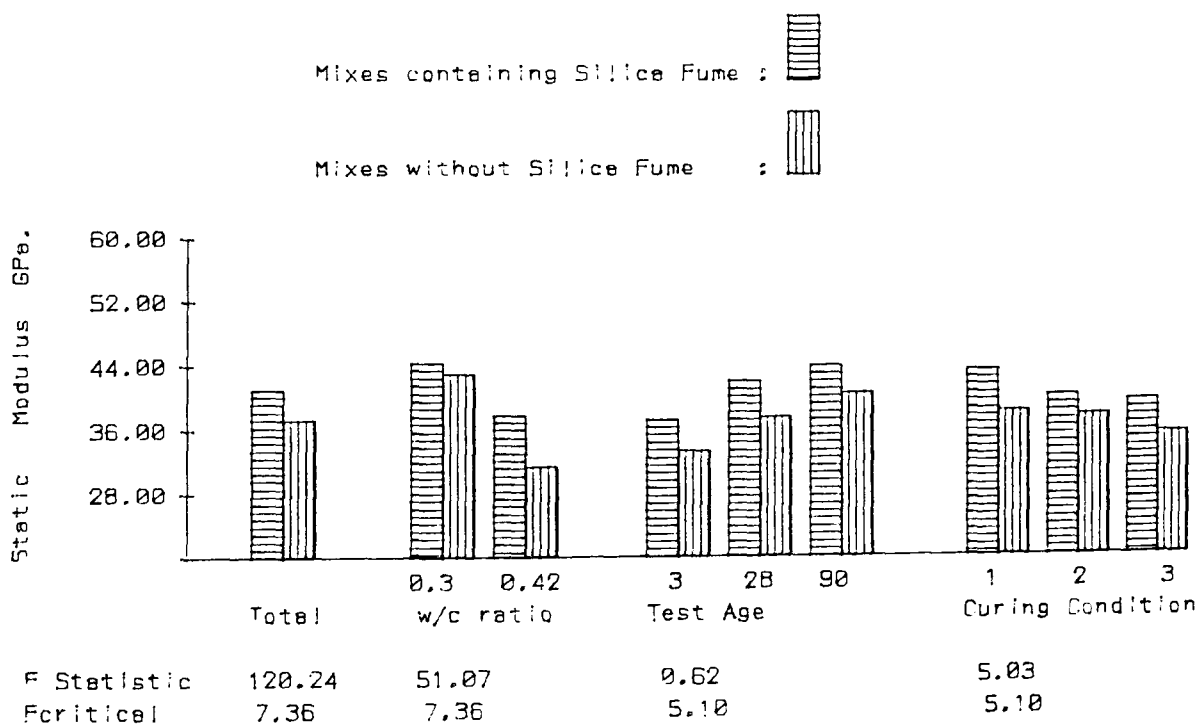
SST=113709.50 Number of observations=2.00

Fig. 13.4 Analysis of variance for static modulus.

AVERAGE VALUES OF THE EFFECT OF W/C RATIO, AGE AND CURING

Mixes containing Silica Fume :

Mixes without Silica Fume :

	Total	w/c ratio	Test Age	Curing Condition
F Statistic	52.59	0.20	2.61	6.52
Fcritical	7.36	7.36	5.10	5.10
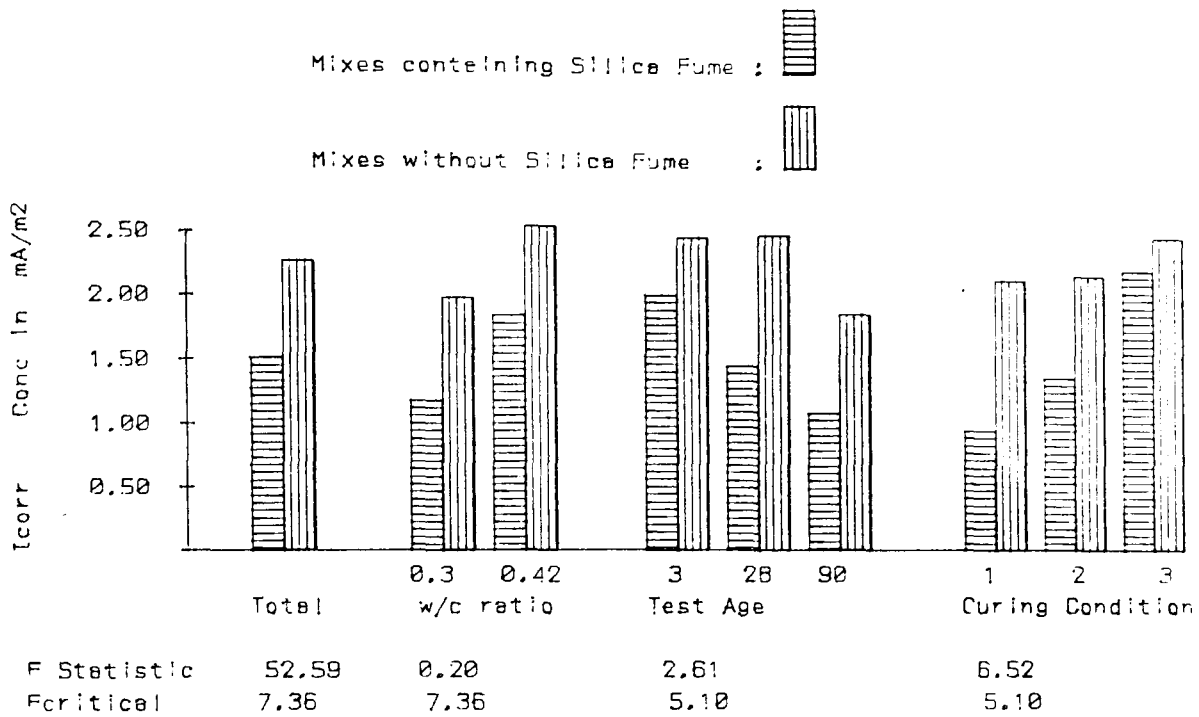
SST=326.35 Number of observations=2.00

Fig. 13.5 Analysis of variance for corrosion current of set 2 concrete samples when first exposed to salt solution.

AVERAGE VALUES OF THE EFFECT OF W/C RATIO, AGE AND CURING

Mixes containing Silica Fume :

Mixes without Silica Fume :

	Total	w/c ratio	Test Age	Curing Condition
F Statistic	29.62	25.78	5.95	11.27
Fcritical	7.36	7.36	5.10	5.10
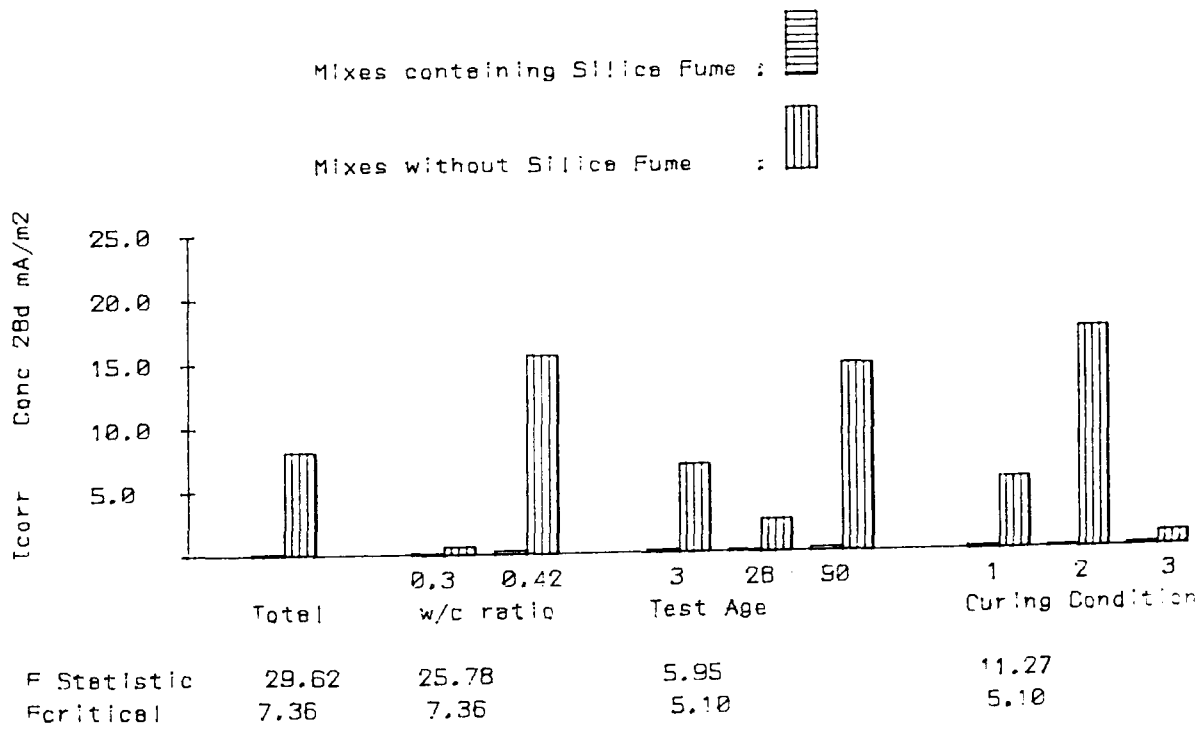
SST=14556.00 Number of observations=2.00

Fig. 13.6 Analysis of variance for corrosion current of set 2 concrete samples after 28 days of exposure.

AVERAGE VALUES OF THE EFFECT OF W/C RATIO, AGE AND CURING

Mixes containing Silice Fume :

Mixes without Silice Fume :

	Total	w/c ratio		Test Age			Curing Condition		
		0.3	0.42	3	28	90	1	2	3
F Statistic	9533.64	1894.82		3683.87			2976.34		
Fcritical	7.36	7.36		5.10			5.10		
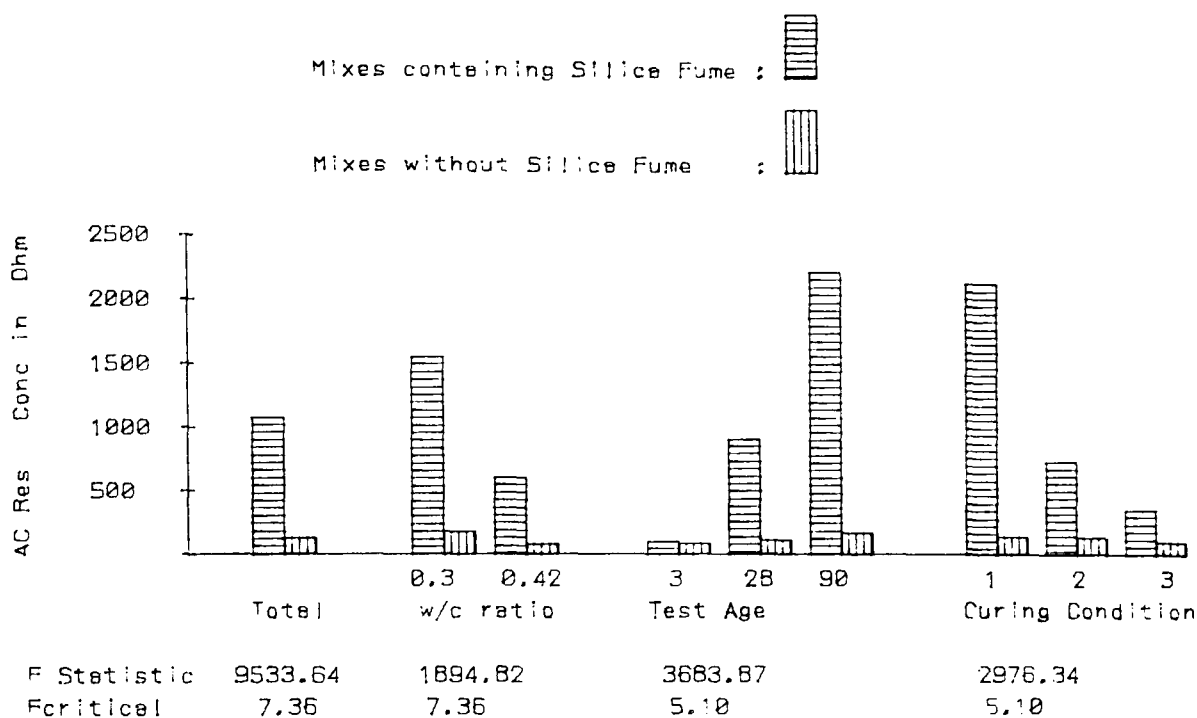
SST=129240000 Number of observations=2.00

Fig. 13.7 Analysis of variance for resistance of set 2 concrete samples when first exposed to salt solution.

AVERAGE VALUES OF THE EFFECT OF W/C RATIO, AGE AND CURING

Mixes containing Silice Fume :

Mixes without Silice Fume :

	Total	w/c ratio		Test Age			Curing Condition		
		0.3	0.42	3	28	90	1	2	3
F Statistic	21629.84	4362.44		156.12			231.34		
Fcritical	7.36	7.36		5.10			5.10		
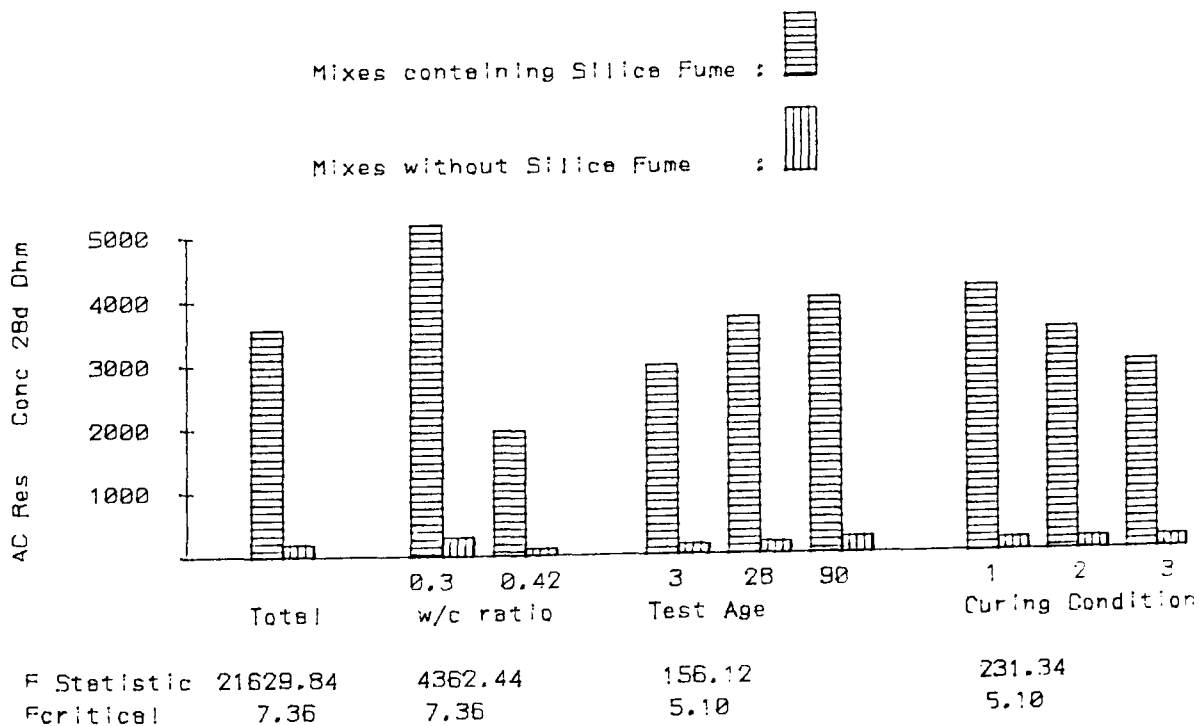
SST=585130000 Number of observations=2.00

Fig. 13.8 Analysis of variance for resistance of set 2 concrete samples after 28 days of exposure.

AVERAGE VALUES OF THE EFFECT OF W/C RATIO, AGE AND CURING

Mixes containing Silice Fume ;

Mixes without Silice Fume ;

	Total	0.3	0.42	3	28	90	1	2	3
		w/c ratio		Test Age			Curing Condition		
F Statistic	50.02	30.73		0.22			1.48		
Fcritical	7.36	7.36		5.10			5.10		
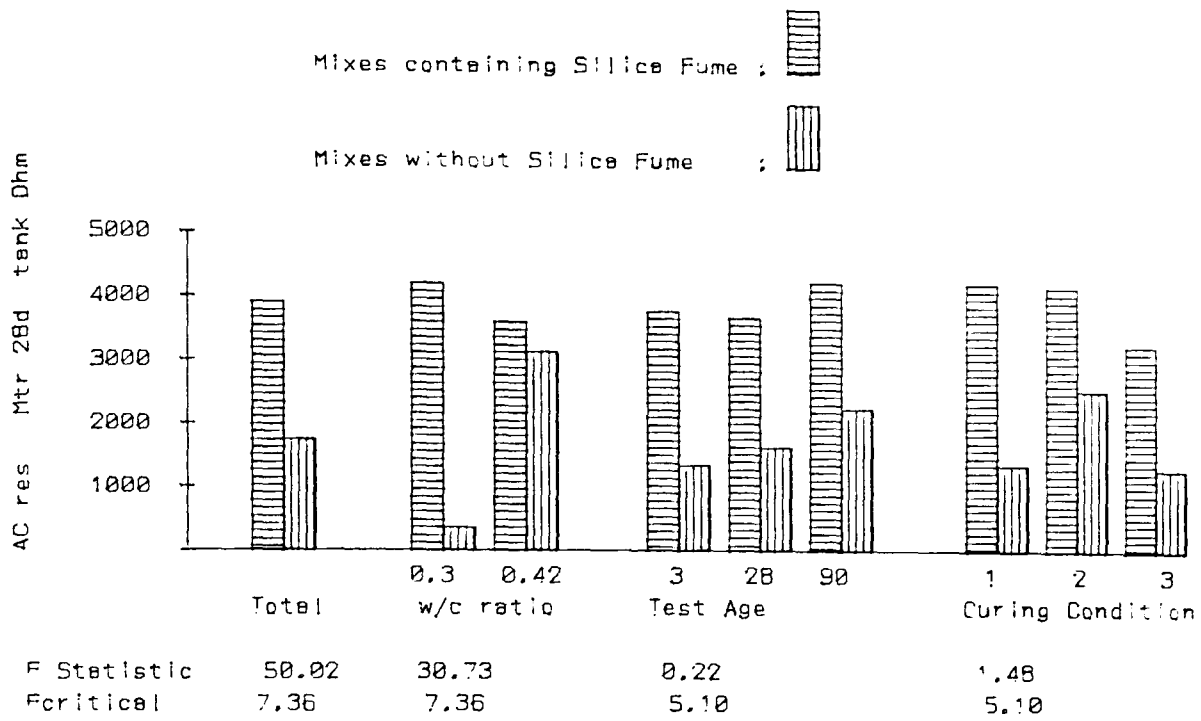
SST=865650000 Number of observations=2.00

Fig. 13.9 Analysis of variance for resistance of carbonated mortar samples when first exposed to salt solution.

AVERAGE VALUES OF THE EFFECT OF W/C RATIO, AGE AND CURING

Mixes containing Silice Fume ;

Mixes without Silice Fume ;

	Total	0.3	0.42	3	28	90	1	2	3
		w/c ratio		Test Age			Curing Condition		
F Statistic	50.72	3.28		5.81			2.92		
Fcritical	7.36	7.36		5.10			5.10		
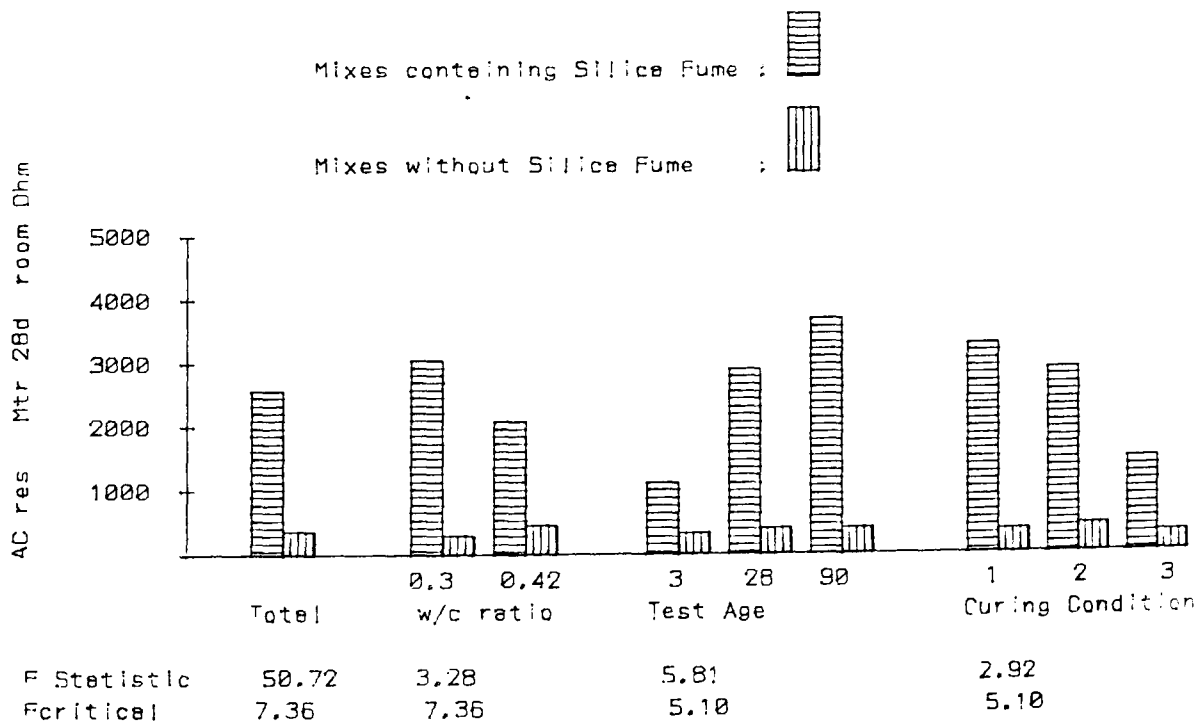
SST=398010000 Number of observations=2.00

Fig. 13.10 Analysis of variance for mortar control samples when first exposed to salt solution.

AVERAGE VALUES OF THE EFFECT OF W/C RATIO, AGE AND CURING

Mixes containing Silice Fume :

Mixes without Silice Fume :

	Total	w/c ratio	Test Age	Curing Condition
F Statistic	15.49	274.95	0.63	3.54
Fcritical	7.04	7.04	4.93	4.93
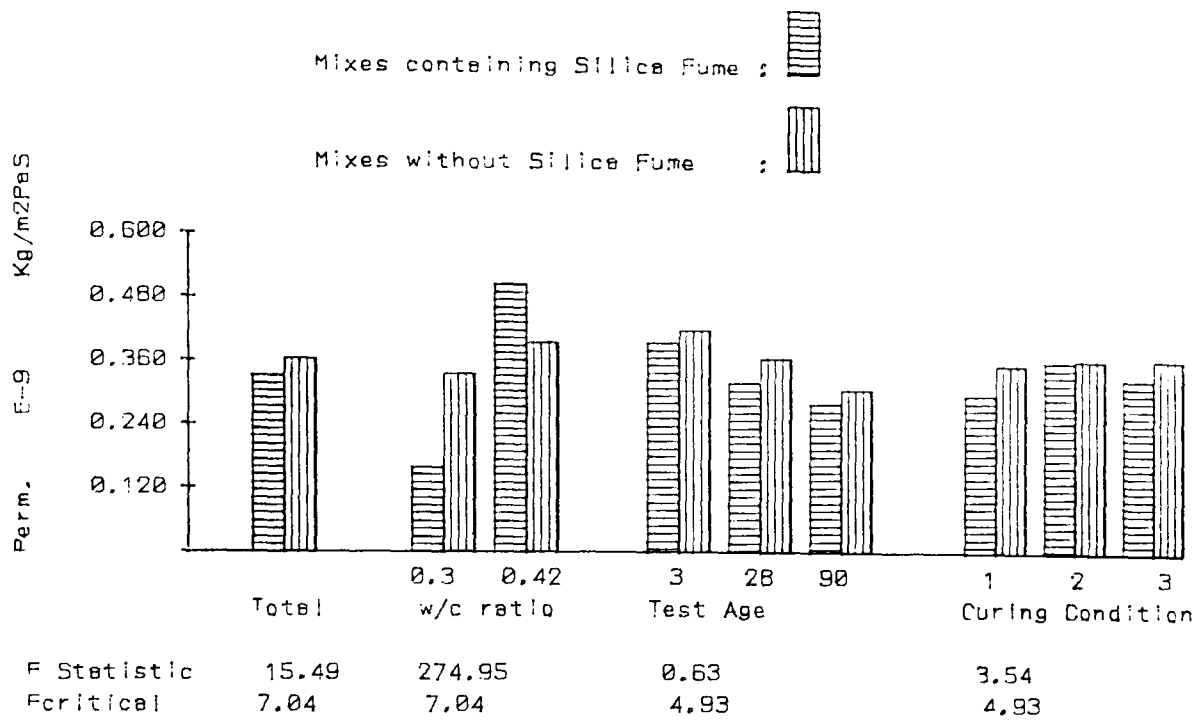
SST=15.34 Number of observations=3.00

Fig. 13.11 Analysis of variance for vapour permeability.

AVERAGE VALUES OF THE EFFECT OF W/C RATIO, AGE AND CURING

Mixes containing Silice Fume :

Mixes without Silice Fume :

	Total	w/c ratio	Test Age	Curing Condition
F Statistic	64.78	46.77	35.81	7.55
Fcritical	7.36	7.36	5.10	5.10
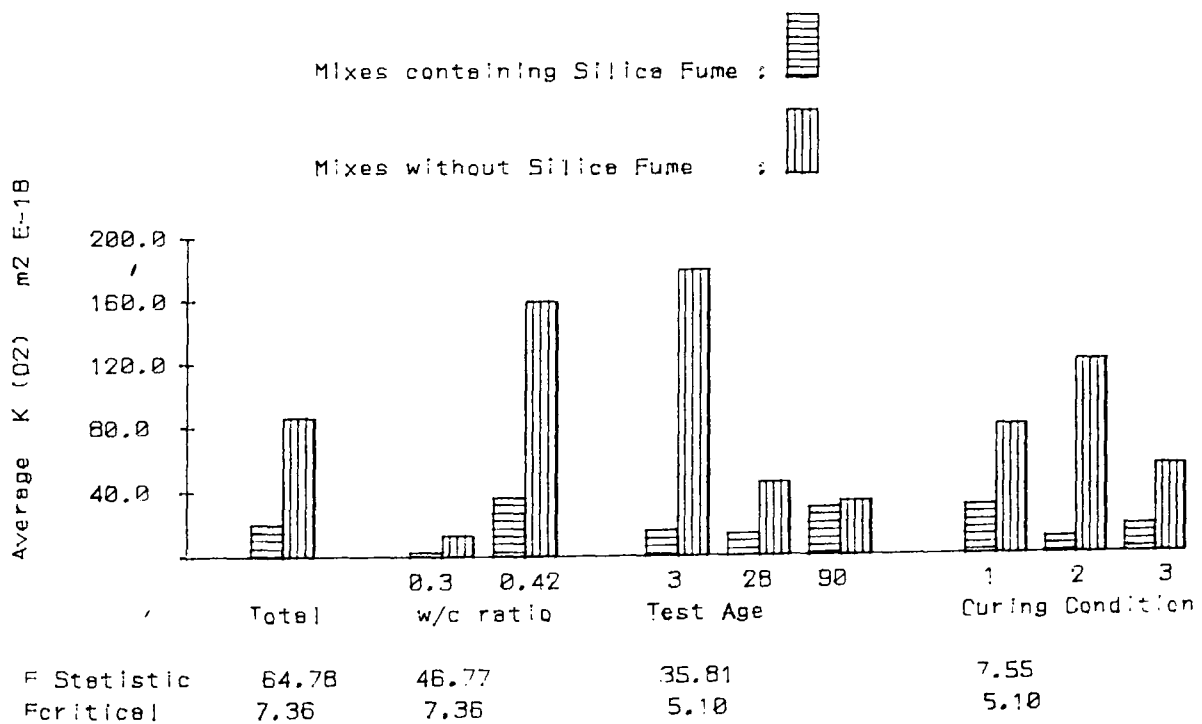
SST=947370.00 Number of observations=2.00

Fig. 13.12 Analysis of variance for oxygen permeability.

AVERAGE VALUES OF THE EFFECT OF W/C RATIO, AGE AND CURING

Mixes containing Silica Fume :

Mixes without Silica Fume :

Lime loss(TG) %of mass

	Total	w/c ratio	Test Age	Curing Condition
F Statistic	751.37	10.34	40.68	49.32
Fcritical	7.36	7.36	5.10	5.10
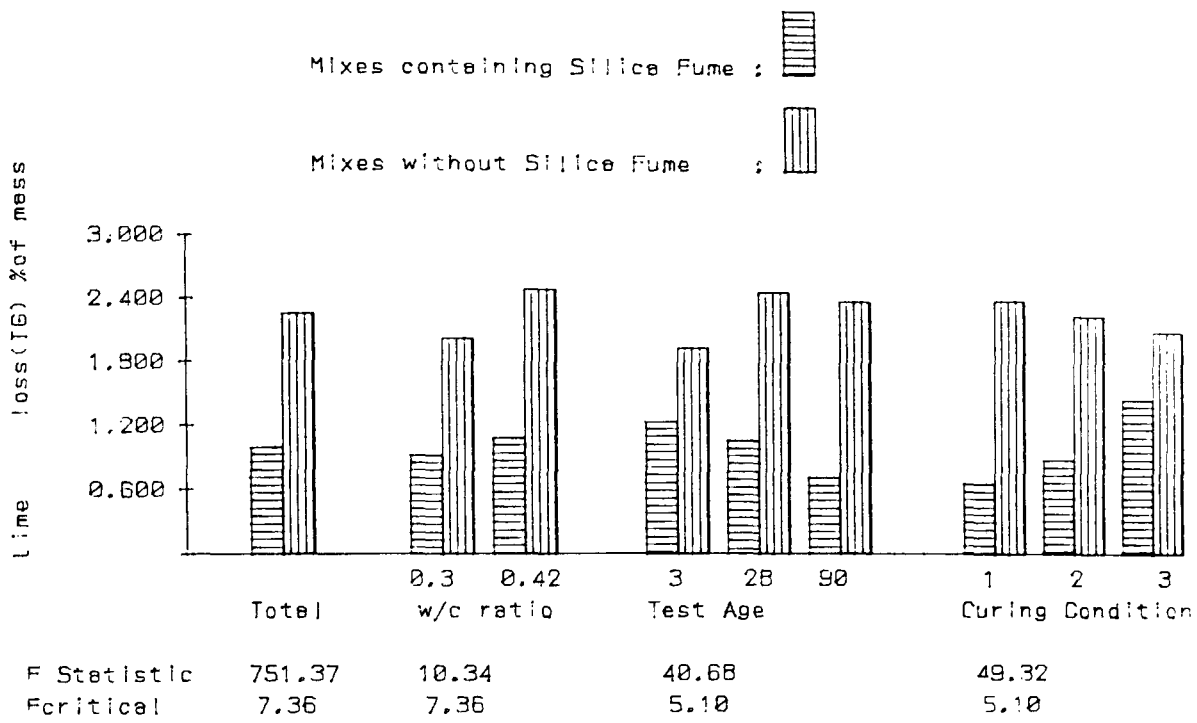
SST=236.68 Number of observations=2.00

Fig. 13.13 Analysis of variance for mass loss in hydroxide peak in TG analysis of paste samples.

AVERAGE VALUES OF THE EFFECT OF W/C RATIO, AGE AND CURING

Mixes containing Silica Fume :

Mixes without Silica Fume :

Carbonat loss(TG) %of mass

	Total	w/c ratio	Test Age	Curing Condition
F Statistic	0.53	5.75	0.23	1.96
Fcritical	7.36	7.36	5.10	5.10
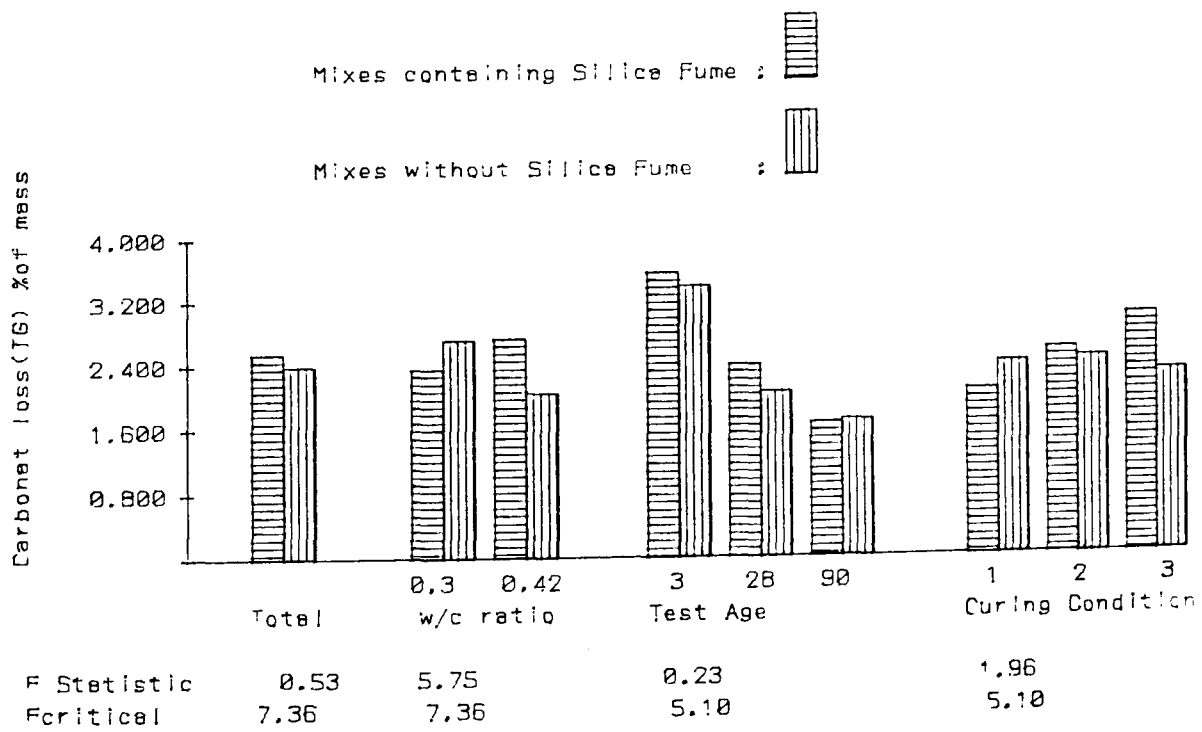
SST=553.42 Number of observations=2.00

Fig. 13.14 Analysis of variance for mass loss in carbonate peak in TG analysis of paste samples

PREDICTION OF DEPENDENT VARIABLE BY MULTIPLE REGRESSION

Dependent Variable
Perm.   E-9   Kg/m2PaS

Predictors

1 Constant term

2 Hg pores 10-170   mic.   %

3 Hg pores .15-10   mic   %

4 Hg pores .01-.15 mic. %

5 Hg pores .003-.01 mic. %

$\times$ mix A (SF)

$+$ mix B (OPC)

⋈ mix C (SF)

✳ mix D (OPC)
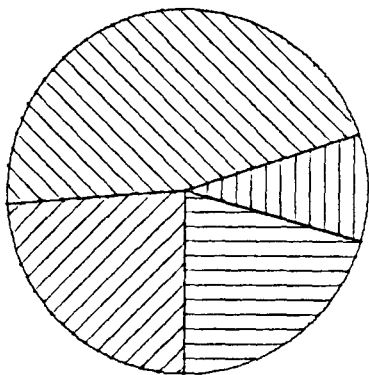
Relative proportions

t critical=2.75

Predictor	Coeff.	t
1	-1.6E-1	-1.93
2	3.6E-1	4.61
3	-1.2E-1	-1.58
4	2.0E-2	6.75
5	2.4E-2	3.62

ALL MIXES
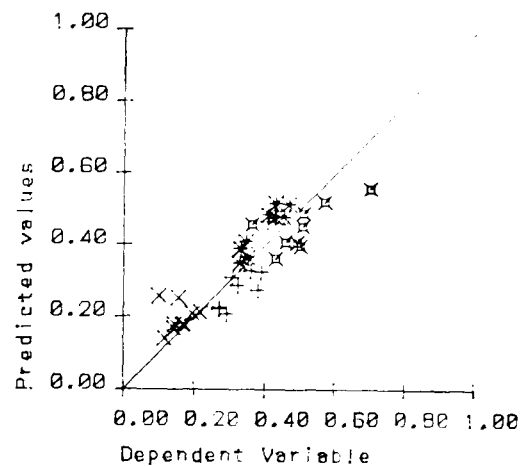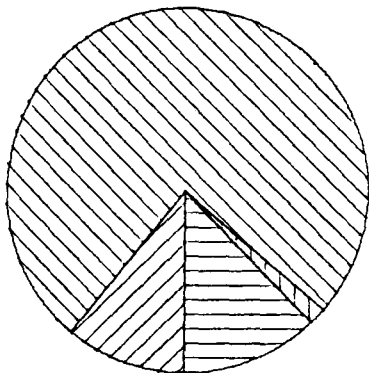
Relative proportions

t critical=3.01

Predictor	Coeff.	t
1	-2.5E-1	-2.29
2	1.7E-1	2.16
3	-2.0E-2	-0.24
4	3.7E-2	11.04
5	2.0E-2	2.07

MIXES CONTAINING SILICA FUME
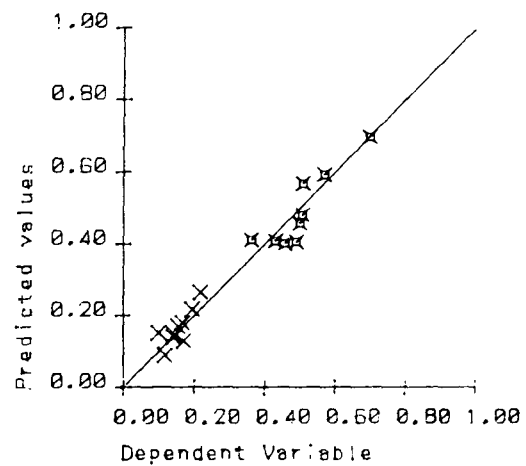
Relative proportions
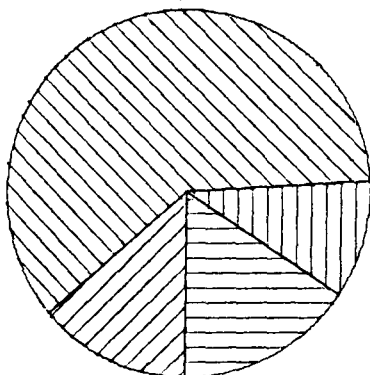
t critical=3.01

Predictor	Coeff.	t
1	1.1E-1	2.60
2	1.3E-1	2.00
3	-4.8E-2	-1.21
4	1.3E-2	6.67
5	-2.8E-2	-1.57

MIXES WITHOUT SILICA FUME
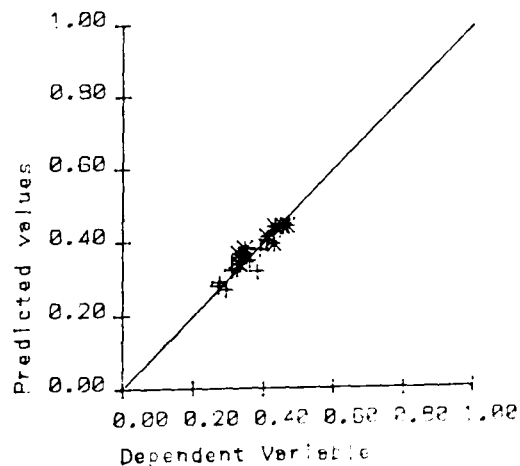
Fig 13.15 Analysis of vapour permeability

PREDICTION OF DEPENDENT VARIABLE BY MULTIPLE REGRESSION

Dependent Variable
Log Average K (D2)   m2 E-18

Predictors

1 Constant term
2 Hg pores 10-170   mic.   %
3 Hg pores .15-10   mic   %
4 Hg pores .01-.15   mic. %
5 Hg pores .003-.01 mic. %

X mix A (SF)
+ mix B (OPC)
⋈ mix C (SF)
✻ mix D (OPC)
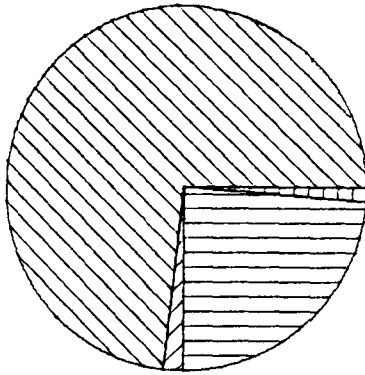
Relative proportions

t critical=2.75

Predictor	Coeff.	t
1	-7.9E-1	-1.86
2	1.2E0	3.09
3	4.4E-2	0.12
4	9.2E-2	6.25
5	5.2E-3	0.15

ALL MIXES
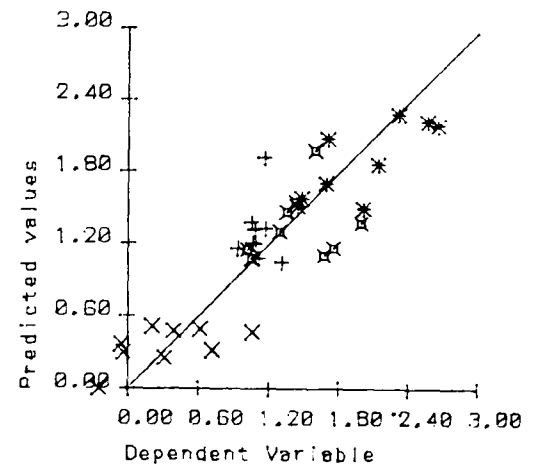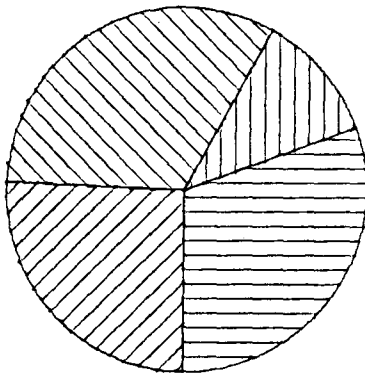
Relative proportions

t critical=3.01

Predictor	Coeff.	t
1	1.1E0	1.56
2	1.5E0	3.07
3	-5.2E-1	-1.00
4	5.7E-2	2.68
5	-1.7E-1	-2.80

MIXES CONTAINING SILICA FUME
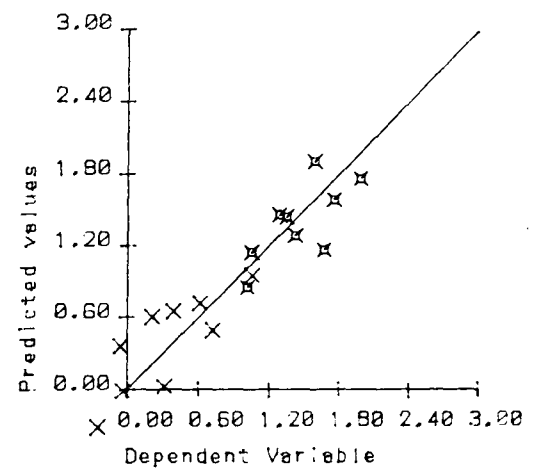
Relative proportions
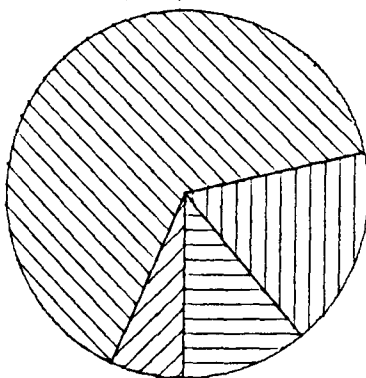
t critical=3.01

Predictor	Coeff.	t
1	-1.0E0	-2.90
2	-7.7E-1	-1.49
3	7.0E-1	2.19
4	1.2E-1	7.57
5	1.1E-1	0.79

MIXES WITHOUT SILICA FUME
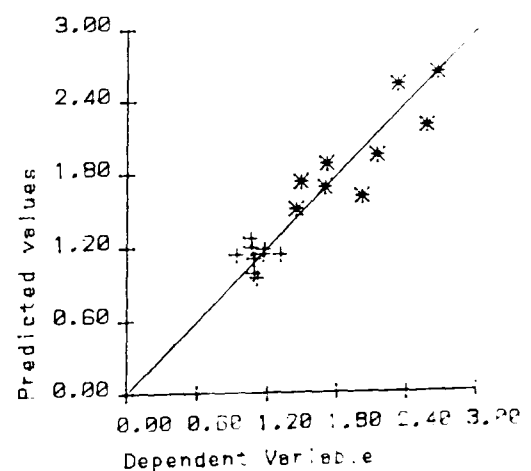
Fig 13.16 Analysis of oxygen permeability

PREDICTION OF DEPENDENT VARIABLE BY MULTIPLE REGRESSION

Dependent Variable
Log AC Res   Conc in Ohm

Predictors

1 Constant term
2 Hg pores 10-170   mic.   %
3 Hg pores .15-10   mic   %
4 Hg pores .01-.15   mic.   %
5 Hg pores .003-.01 mic.   %

X mix A (SF)
+ mix B (OPC)
¤ mix C (SF)
* mix D (OPC)
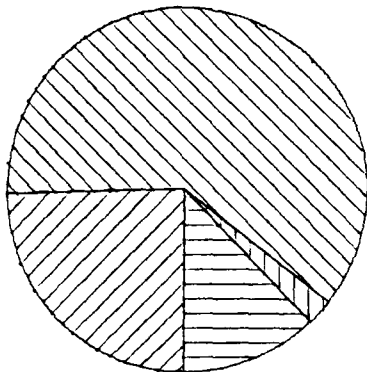
Relative proportions   t critical=2.75

Predictor	Coeff.	t
1	3.5E0	8.07
2	5.9E-1	1.47
3	8.2E-2	0.22
4	-7.2E-2	-4.81
5	-6.9E-2	-2.01

ALL MIXES
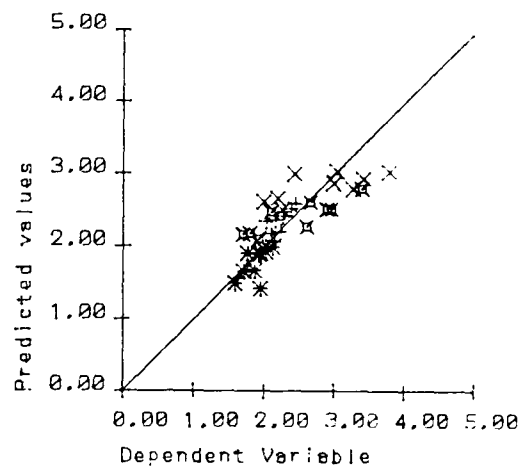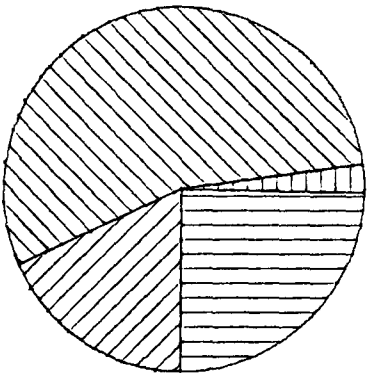
Relative proportions   t critical=3.01

Predictor	Coeff.	t
1	3.9E0	3.39
2	1.4E0	1.75
3	1.3E-1	0.16
4	-1.1E-1	-3.22
5	-1.4E-1	-1.39

MIXES CONTAINING SILICA FUME
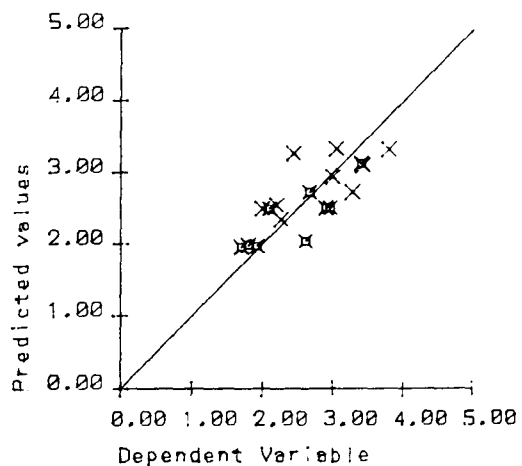
Relative proportions   t critical=3.01
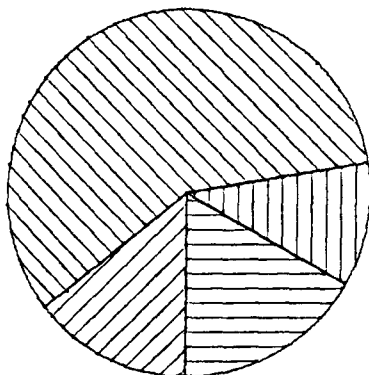
Predictor	Coeff.	t
1	3.2E0	23.99
2	-4.7E-1	-2.45
3	1.7E-1	1.46
4	-4.2E-2	-7.32
5	-1.0E-1	-1.88

MIXES WITHOUT SILICA FUME
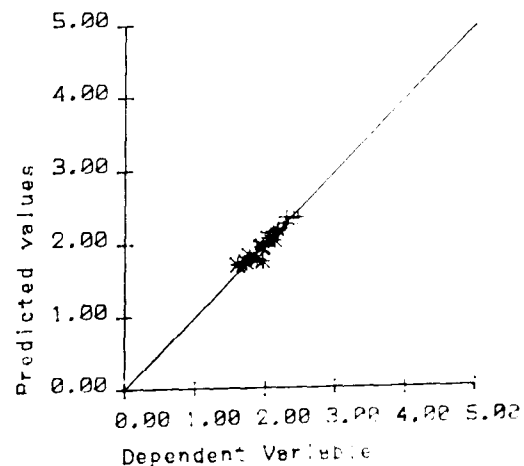
Fig 13.17 Analysis of initial AC resistivity

PREDICTION OF DEPENDENT VARIABLE BY MULTIPLE REGRESSION

Dependent Variable
Log AC Res   Conc 28d Ohm

Predictors

1 Constant term
2 Hg pores 10-170   mic. %
3 Hg pores .15-10   mic   %
4 Hg pores .01-.15 mic. %
5 Hg pores .003-.01 mic. %

X mix A (SF)
+ mix B (OPC)
⋈ mix C (SF)
✳ mix D (OPC)
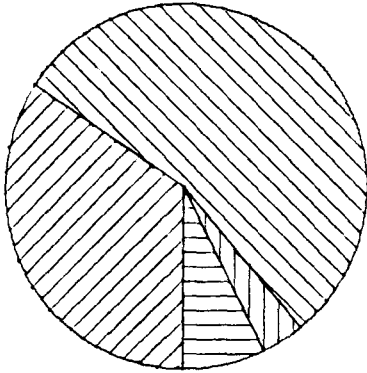
Relative proportions   t critical=2.75

Predictor	Coeff.	t
1	3.2E0	15.99
2	3.0E-1	1.60
3	1.1E-1	0.61
4	-5.3E-2	-7.77
5	8.1E-2	5.08

ALL MIXES
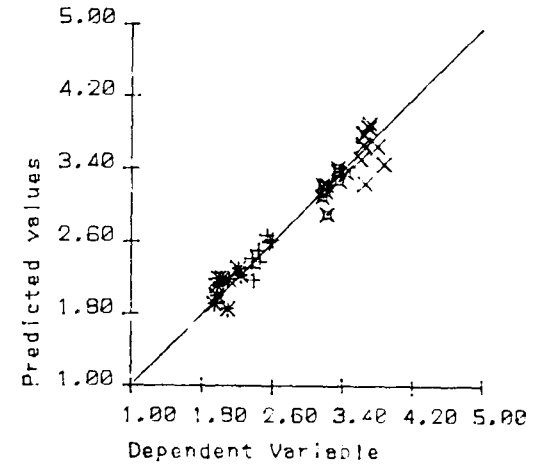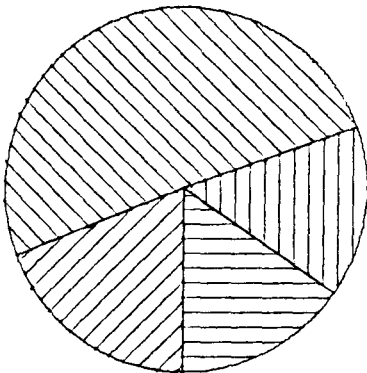
Relative proportions   t critical=3.6.

Predictor	Coeff.	t
1	4.2E0	18.89
2	-3.1E-1	-1.94
3	2.8E-1	1.70
4	-3.5E-2	-5.30
5	-5.1E-2	-2.61

MIXES CONTAINING SILICA FUME
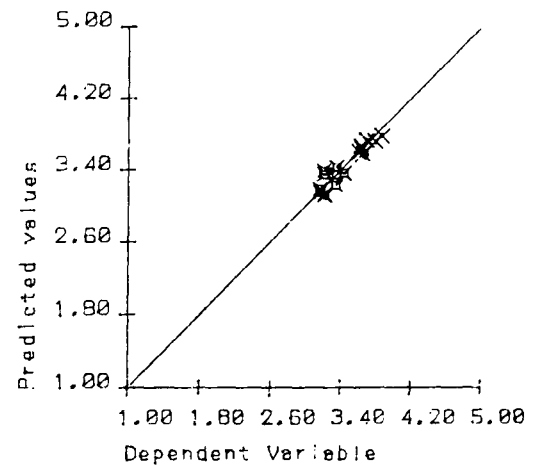
Relative proportions   t critical=3.01
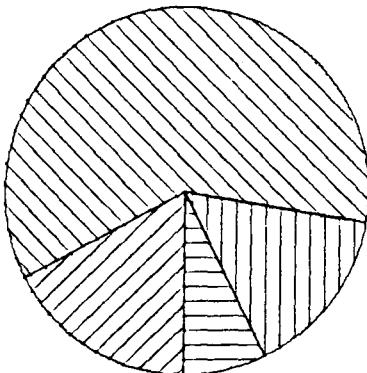
Predictor	Coeff.	t
1	3.2E0	23.46
2	-1.8E-1	-0.91
3	2.2E-1	1.75
4	-3.9E-2	-6.56
5	-1.1E-1	-1.94

MIXES WITHOUT SILICA FUME
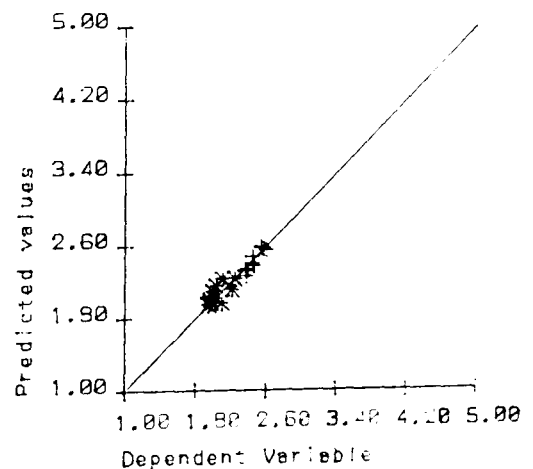
Fig 13.18 Analysis of 28 day AC resistivity

PREDICTION OF DEPENDENT VARIABLE BY MULTIPLE REGRESSION

Dependent Variable
Cube   Strength N/sq.mm.

Predictors

1 Constant term
2 Hg pores 10-170   mic.   %
3 Hg pores .15-10   mic   %
4 Hg pores .01-.15   mic.   %
5 Hg pores .003-.01 mic.   %

X mix A (SF)
+ mix B (OPC)
⋈ mix C (SF)
✳ mix D (OPC)
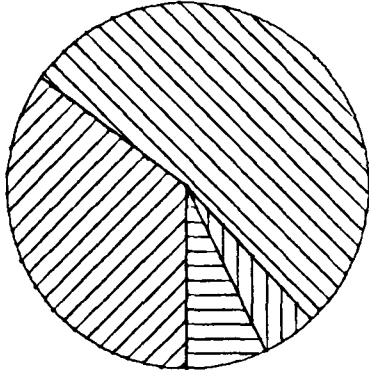
Relative proportions

t critical=2.75

Predictor	Coeff.	t
1	1.5E2	11.63
2	2.4E1	1.96
3	1.2E1	0.99
4	-4.3E0	-9.45
5	-6.9E0	-6.52

ALL MIXES
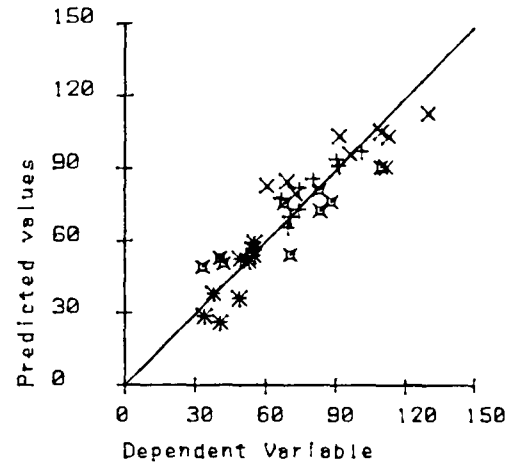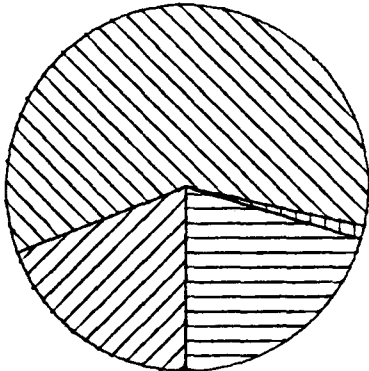
Relative proportions

t critical=3.01

Predictor	Coeff.	t
1	1.6E2	4.64
2	5.7E1	2.36
3	3.1E0	0.12
4	-5.8E0	-5.68
5	-7.2E0	-2.42

MIXES CONTAINING SILICA FUME
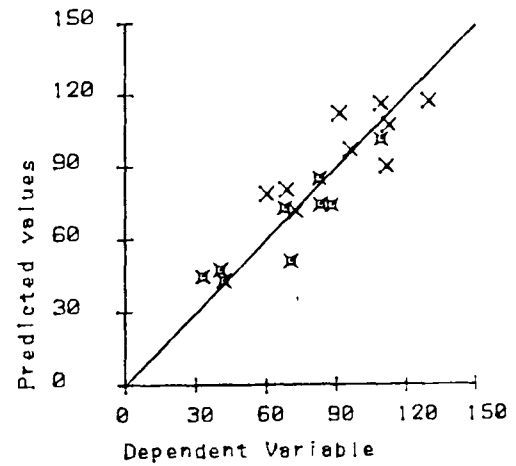
Relative proportions
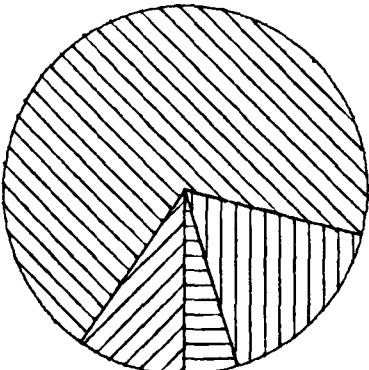
t critical=3.01

Predictor	Coeff.	t
1	1.5E2	20.27
2	-9.9E0	-0.95
3	1.9E1	3.00
4	-3.7E0	-11.91
5	-5.0E0	-1.74

MIXES WITHOUT SILICA FUME
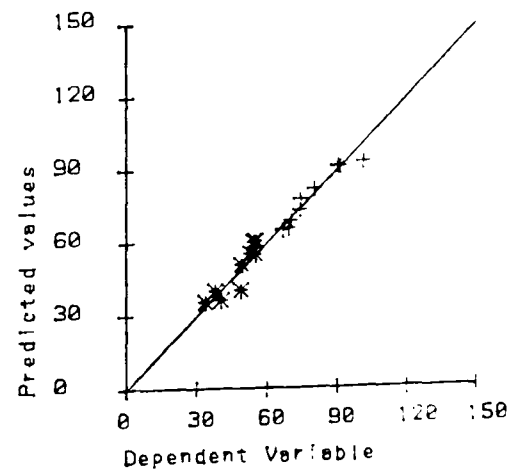
Fig 13.19 Analysis of compressive strength

PREDICTION OF DEPENDENT VARIABLE BY MULTIPLE REGRESSION

Dependent Variable
Mtr cups carb.   depth mm

Predictors

1 Constant term
2 Hg pores 10-170   mic. %
3 Hg pores .15-10   mic   %
4 Hg pores .01-.15 mic. %
5 Hg pores .003-.01 mic. %

X mix A (SF)
+ mix B (OPC)
¤ mix C (SF)
＊ mix D (OPC)
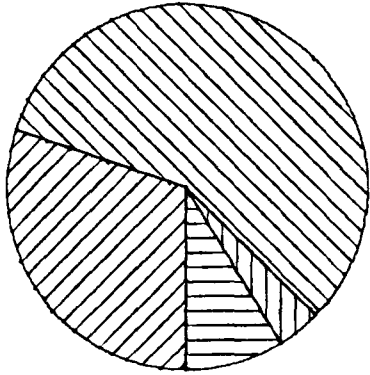
Relative proportions   t critical=2.75

Predictor	Coeff.	t
1	-1.8E1	-3.35
2	-7.5E0	-1.49
3	2.4E0	0.50
4	1.2E0	6.35
5	1.5E0	3.49

ALL MIXES
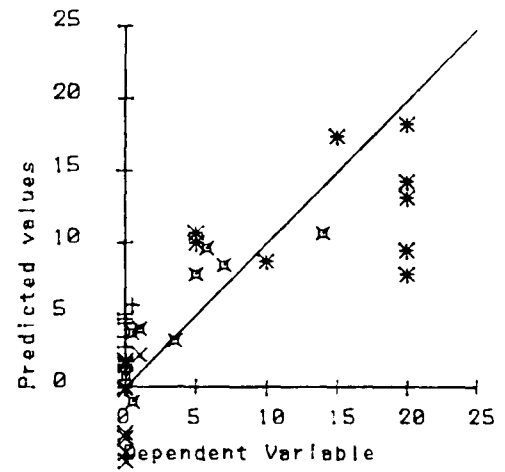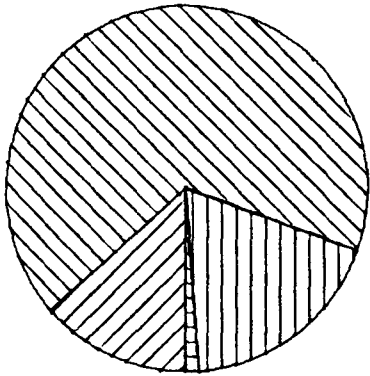
Relative proportions   t critical=3.01

Predictor	Coeff.	t
1	-1.5E1	-2.70
2	4.3E-1	0.11
3	5.8E0	1.46
4	8.1E-1	5.02
5	6.2E-1	1.32

MIXES CONTAINING SILICA FUME
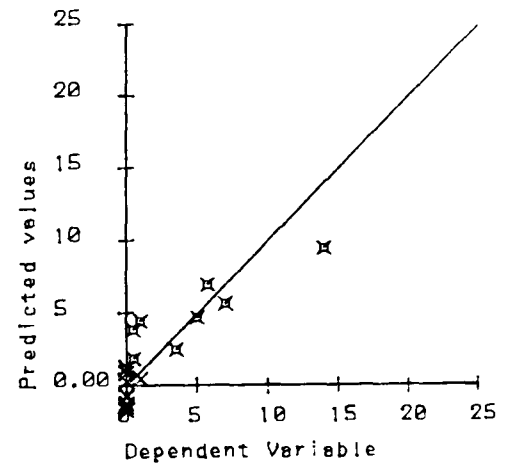
Relative proportions   t critical=3.01
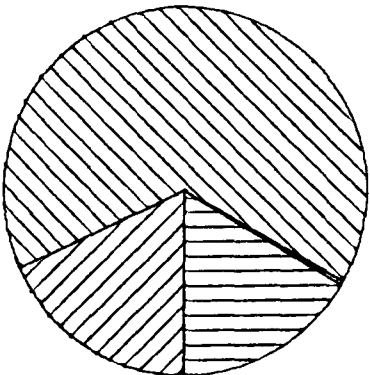
Predictor	Coeff.	t
1	-2.2E1	-2.41
2	-1.3E1	-1.01
3	-1.7E-1	-0.02
4	1.4E0	3.45
5	3.7E0	1.01

MIXES WITHOUT SILICA FUME
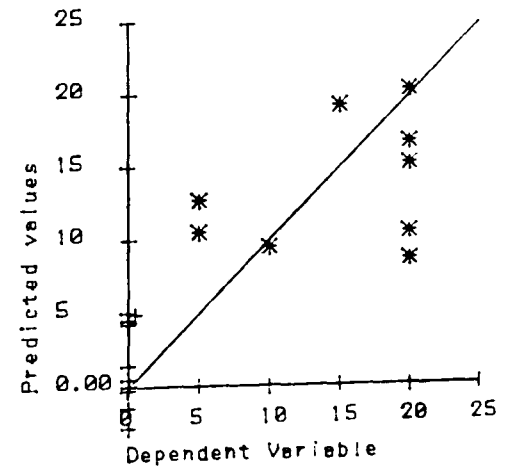
Fig 13.20 Analysis of measured carbonation depth

PREDICTION OF DEPENDENT VARIABLE BY MULTIPLE REGRESSION

Dependent Variable
Cl conc average %

Predictors

1 Constant term
2 Hg pores 10-170   mic. %
3 Hg pores .15-10   mic   %
4 Hg pores .01-.15 mic. %
5 Hg pores .003-.01 mic. %

X mix A (SF)
+ mix B (OPC)
¤ mix C (SF)
⁕ mix D (OPC)
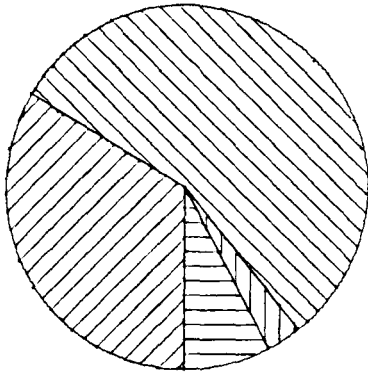
Relative proportions   t critical=2.75

Predictor	Coeff.	t
1	-1.4E0	-3.08
2	-8.6E-1	-2.02
3	-2.4E-1	-0.60
4	1.5E-1	9.55
5	2.2E-1	6.00

ALL MIXES
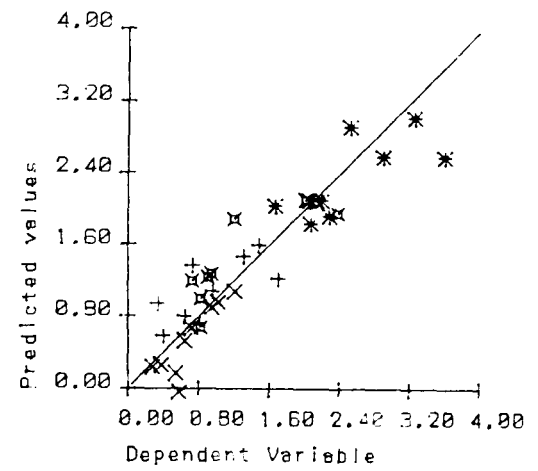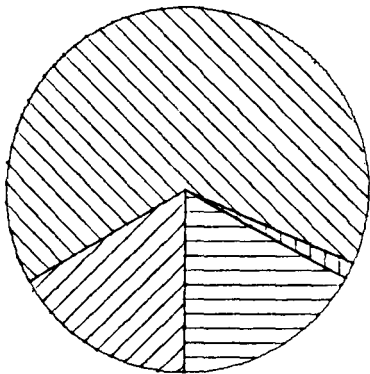
Relative proportions   t critical=3.01

Predictor	Coeff.	t
1	-5.0E-1	-0.65
2	-9.2E-1	-1.68
3	-7.7E-2	-0.14
4	1.2E-1	5.31
5	1.2E-1	1.78

MIXES CONTAINING SILICA FUME
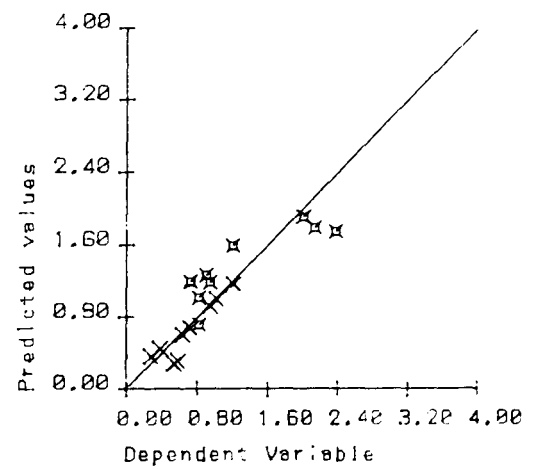
Relative proportions   t critical=3.01
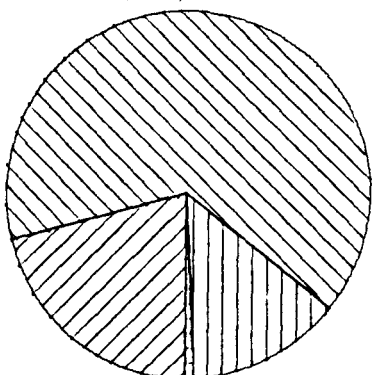
Predictor	Coeff.	t
1	-2.2E0	-3.51
2	8.9E-2	0.10
3	-7.5E-1	-1.33
4	1.6E-1	5.96
5	5.1E-1	2.01

MIXES WITHOUT SILICA FUME
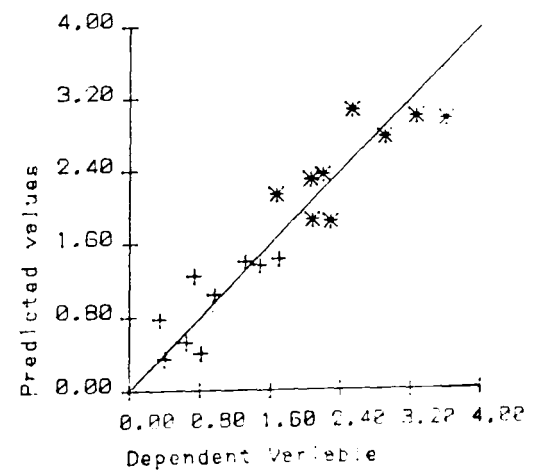
Fig 13.21 Analysis of chloride transmission rate

PREDICTION OF DEPENDENT VARIABLE BY MULTIPLE REGRESSION

Dependent Variable
Log Icorr   Conc 28d mA/m2

Predictors

1 Constant term
2 Vapour Perm. E-9 Kg/m2PaS
3 Log Average K (O2)   m2 E-18
4 Log AC Res   Conc 28d Ohm
5 Mtr cups carb.   depth mm
6 Cl conc average %

X mix A (SF)
+ mix B (OPC)
⋈ mix C (SF)
✳ mix D (OPC)
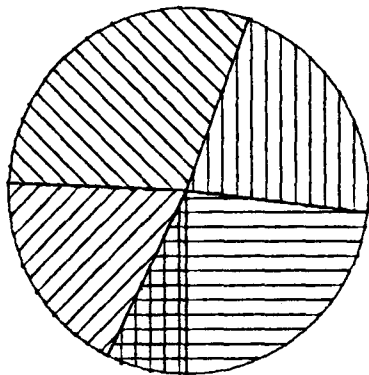
Relative proportions

t critical=2.75

Predictor	Coeff.	t
1	1.3E0	3.26
2	-1.8E0	-4.00
3	3.4E-1	2.76
4	-5.1E-1	-4.98
5	2.9E-2	2.40
6	9.1E-2	0.85

ALL MIXES
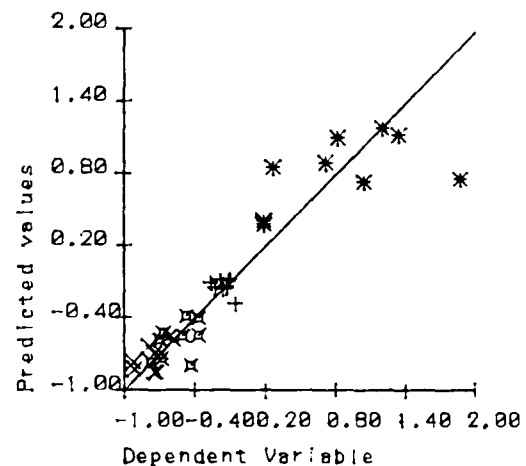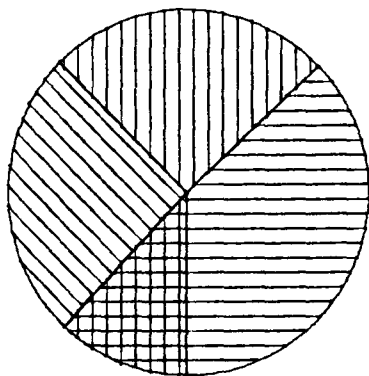
Relative proportions

t critical=3.01

Predictor	Coeff.	t
1	1.5E0	0.82
2	-1.1E0	-1.32
3	2.0E-1	2.52
4	-6.0E-1	-1.31
5	3.0E-5	0.00
6	1.1E-1	1.05

MIXES CONTAINING SILICA FUME
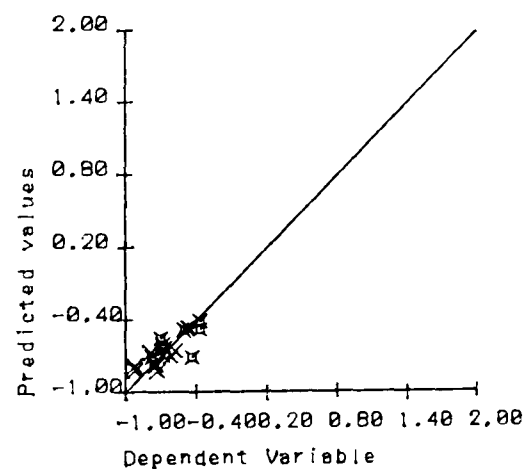
Relative proportions
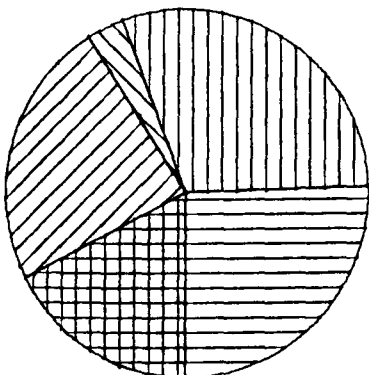
t critical=3.01

Predictor	Coeff.	t
1	8.9E-1	0.31
2	-4.3E0	-1.73
3	5.5E-1	1.39
4	-1.4E-1	-0.15
5	2.7E-2	1.27
6	1.8E-1	0.77

MIXES WITHOUT SILICA FUME
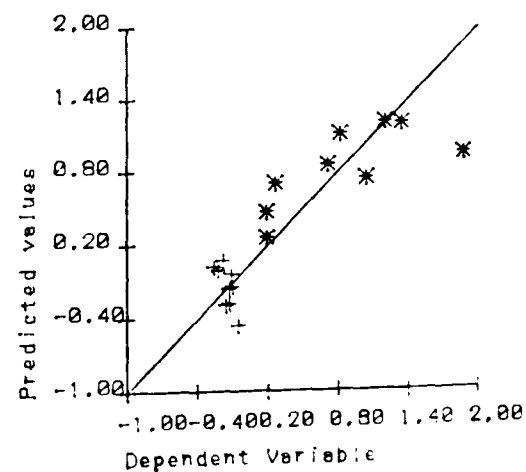
Fig 13.22 Analysis of 28 day corrosion current

PREDICTION OF DEPENDENT VARIABLE BY MULTIPLE REGRESSION

Dependent Variable
Log Icorr   Conc in mA/m2

Predictors

1 Constant term
2 Vapour Perm. E-9 Kg/m2PaS
3 Log Average K (O2)   m2 E-18
4 Log AC Res   Conc in Ohm
5 Mtr cups carb.   depth mm
6 Cl conc average %

X mix A (SF)
+ mix B (OPC)
⋈ mix C (SF)
* mix D (OPC)
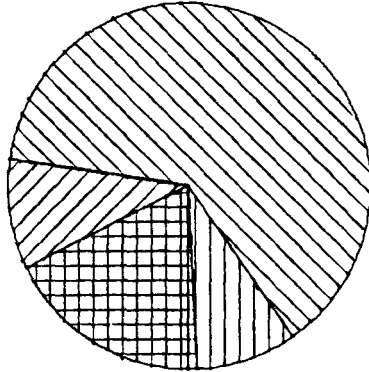
Relative proportions

t critical=2.75

Predictor	Coeff.	t
1	9.7E-1	4.00
2	1.7E-2	0.06
3	-3.7E-2	-0.55
4	-3.3E-1	-4.57
5	-3.9E-3	-0.55
6	5.9E-2	0.84

ALL MIXES
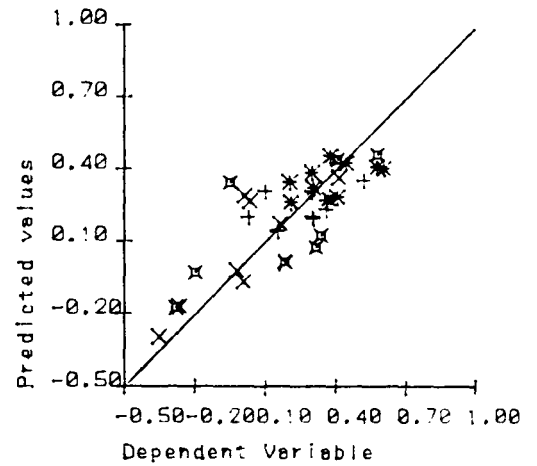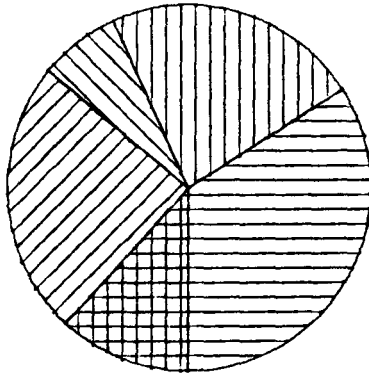
Relative proportions

t critical=3.01

Predictor	Coeff.	t
1	5.4E-2	0.15
2	2.0E0	3.82
3	-3.6E-1	-3.59
4	-1.3E-1	-1.35
5	-7.1E-2	-3.64
6	2.2E-1	1.74

MIXES CONTAINING SILICA FUME
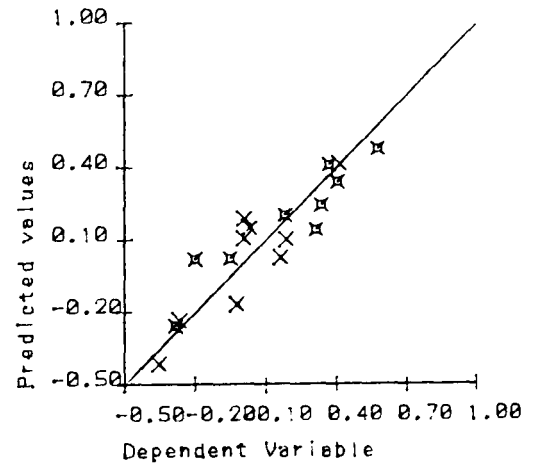
Relative proportions
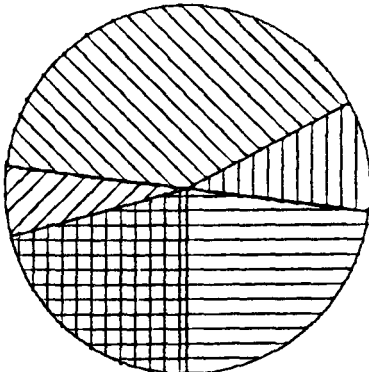
t critical=3.01

Predictor	Coeff.	t
1	2.0E0	2.26
2	-1.3E0	-1.36
3	-5.8E-2	-0.41
4	-5.8E-1	-2.03
5	-2.3E-3	-0.32
6	7.2E-2	0.89

MIXES WITHOUT SILICA FUME
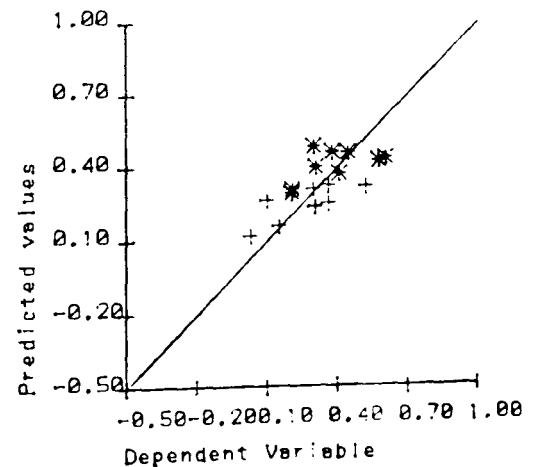
Fig 13.23 Analysis of initial corrosion current
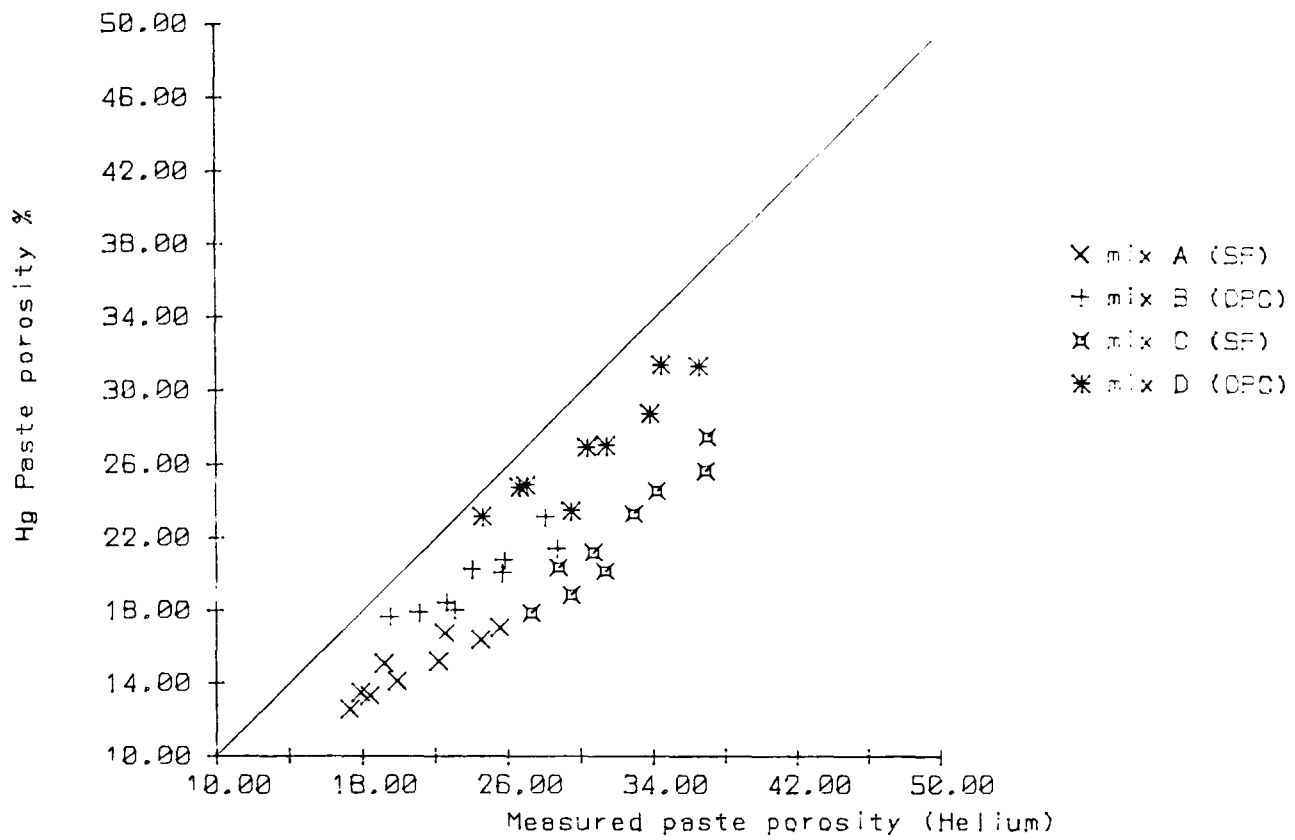
Fig. 13.24 Comparison of measured paste pososity from helium intrusion with the porosity obtained from mercury intrusion.
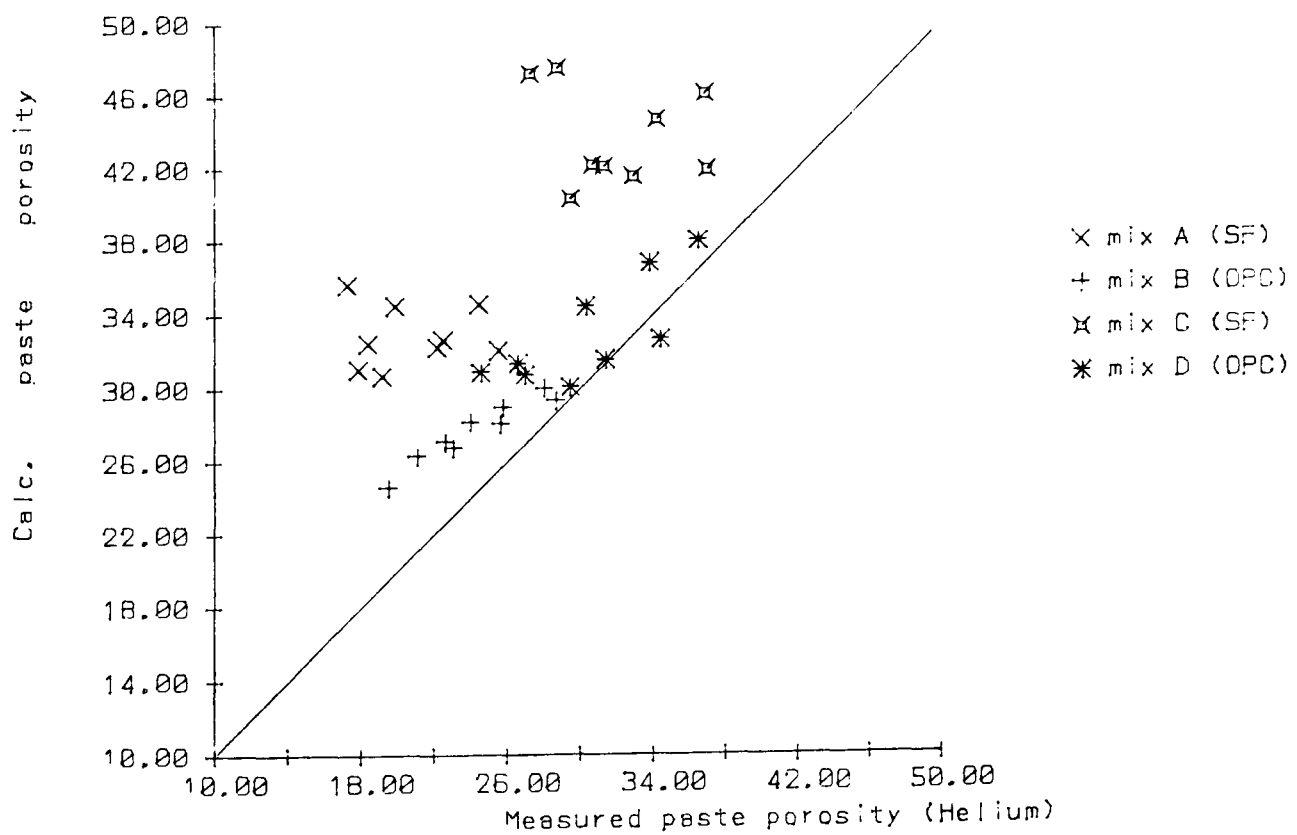
Fig. 13.25 Comparison of measured paste porosity with porosity calculated from weight loss.
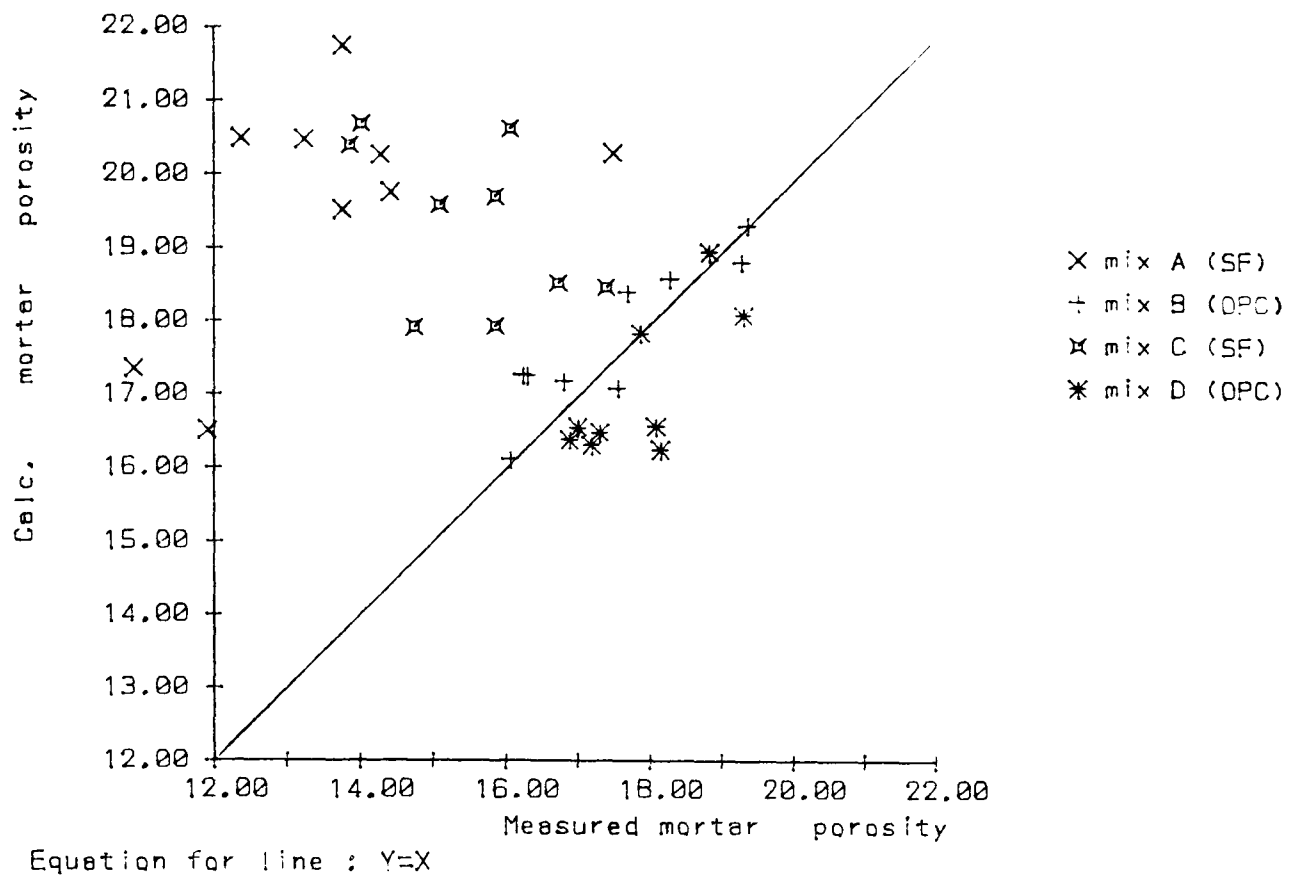
Fig. 13.26. Comparison of mortar porosity measured by helium intrusion with porosity calculated from weight loss.
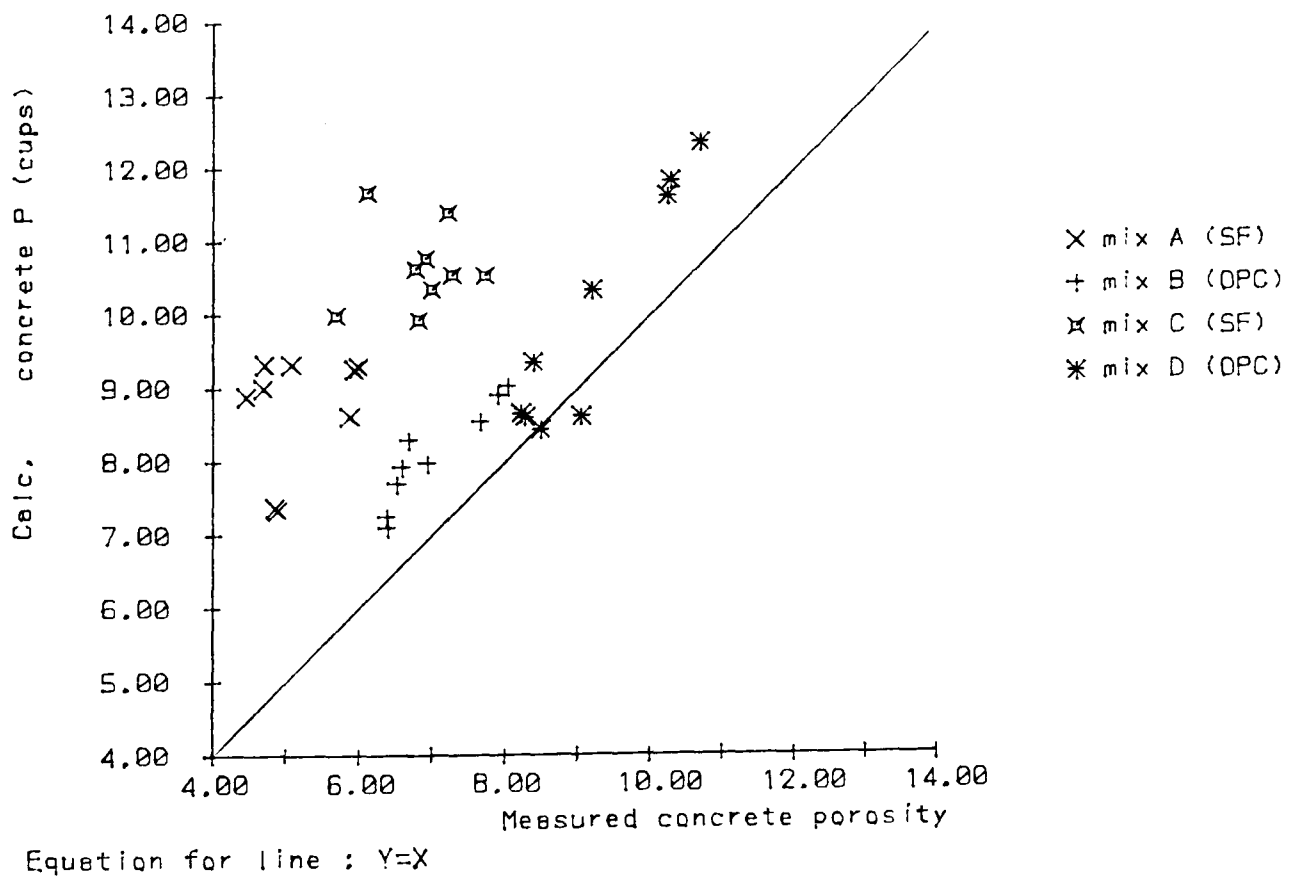
Fig. 13.27. Comparison of concrete porosity measured by helium intrusion with porosity calculated from weight loss.

14 Conclusions.

14.1 The purpose of using silica fume in high strength concrete.

SF changes many of the properties of concrete and when conclusions are drawn about whether or not it is beneficial it is necessary to define the purpose for which it is intended to be used. For example, for an office building in London, it has been calculated that reducing the column size by increasing the strength of the concrete will produce one million pounds of extra rent over a 20 year period (Anon 1988) and the use of SF concrete might be justified on strength grounds alone.

This work is intended to provide data for the use of the mixes in applications where durability, and in particular the protection of reinforcement from corrosion, is the primary concern. Typical applications could be bridges or external elements of buildings. In these applications the strength of the control mixes would probably be adequate and the only purpose of the SF would be to increase the durability.

14.2. The effect of silica fume on the rate of corrosion and the properties that determine it.

14.2.1 The effect of the silica fume on the corrosion rate.

The silica fume clearly reduces the corrosion rate. The clear reduction of corrosion current measured by linear polarisation from both sets of samples and the good correlation with the measured current under an applied anodic voltage give considerable confidence to this conclusion. The detailed analysis of the set 2 samples (figs. 13.5 and 13.6) indicates that the reduction is far more significant after exposure to chloride. The data for the corrosion rate after exposure is dominated by the mix D samples where the chloride penetration reached the steel. Of the five properties which have been measured as contributing to the corrosion rate (resistivity, carbonation and permeability to chloride, oxygen and water vapour) the resistivity showed the greatest effect from the silica fume replacement (fig 13.8). The analysis of variance also showed a major decrease in the oxygen permeability and a smaller but significant decrease in the vapour permeability. The measurements of carbonation and chloride permeability did not yield suitable data for analysis of variance but it is evident from figs.4.8 and 5.3 that there was some improvement. The multiple regression analysis shown in fig. 13.23 confirms that resistivity was a major factor in the initial corrosion rate. It can therefore be concluded that the SF concrete will provide better protection for reinforcement in almost any environment but the effect will be greatest where there is a macro-cell such as might be found in the tidal range of a marine structure where the circuit will have a greater path length in concrete.

14.2.2 The effect of silica fume on the sensitivity of the corrosion rate of the mixes to type of curing and age at testing.

An increase in sensitivity to curing would be important because concrete is often cured in poor conditions. If this has a more serious effect on the SF concrete than on the control the use of SF concretes would have to be restricted to applications where good curing could be assured. For the purpose of corrosion protection an increased sensitivity to age, however, indicates a probable advantage. This is because the amount of corrosion which takes place before the concrete offers maximum protection will not be significant and the increased sensitivity indicates a higher ultimate value.

The analysis of variance indicates that the SF made the concrete more sensitive to curing conditions for the initial corrosion rate but less sensitive for the rate after exposure. The initial corrosion rates indicate a small but statistically significant increase in sensitivity to curing condition but no significant increase in sensitivity to age.

There was a small increase in oxygen permeability with age for the SF samples and no significant trends occur with the vapour permeability data. No significant effect is evident for carbonation or chloride permeability (figs 4.8 and 5.3) so the situation is again dominated by the resistivity where a massive effect of both age and curing may be seen (figs.13.7 and 13.8). The data for resistivity (table A3.3 in appendix 3) shows that the major effect of curing decreases after 28 days of exposure and for the set 1 samples after 10 months of exposure the remaining effect is only about 10% which should be compared with the order of magnitude difference between the SF and OPC samples. The sensitivity of the corrosion rate of the SF mixes to cold curing would therefore be expected to become minimal as the concrete matures.

14.2.3 The effect of silica fume on the sensitivity of the corrosion rate to w/c ratio.

An increase in sensitivity of corrosion rate to w/c ratio would be a cause for concern because the SF causes a decrease in the sensitivity of the strength to w/c ratio. Thus a mix with a higher water content would not necessarily fail in routine testing procedures but would provide much reduced protection to the reinforcement.

Fortunately there is no significant change in sensitivity of the corrosion rate. The apparent increase for vapour permeability has been noted as being due to the use of low energy mixing. No significant effects are evident for the other properties except resistivity which again shows a significant increase in sensitivity.

14.3 The effect of silica fume on the porosity of concrete.

14.3.1 Pore size distribution.

The major trend in all of the multiple regression analysis indicated that the pores in the range .01 to .15 μm have by far the most significant effect on the all of the properties analysed. The intrusion data (figs.9.8 and 9.9) indicates that SF redistributes the

porosity to the finer pore range and it will thus make a reduced contribution to the parameters that limit the durability. Fig.9.11 shows evidence of a more tortuous pore structure in the SF samples by comparing the intruded and recovery volumes, this should also improve the durability.

14.3.2 Effect on oxygen permeability.

It was noted in section 7.3.2 that the O_2 permeability of the SF samples apparently increased with age for CC1 and CC3 (fig.7.3). From fig.9.6 it appears that the volume of pores in these samples in the range 10 - 170μm also increased with age and fig.13.16 shows that the large pore size range forms the major contributing factor to the O_2 permeability of the SF samples. Both of these data columns contain substantial experimental variations but if this is a genuine effect a possible explanation would be that a connected pore system is created when the calcium hydroxide is used up in the pozzolanic reaction.

14.4 Conclusions from the thermogravimetric analyses.

In chapter 11 it was concluded that provided the material is maintained at 20°C for some months at some stage after casting then the pozzolanic activity in the SF mixes will proceed until all of the calcium hydroxide is used up. This would apply to all concrete placed in a climate like that in the UK. Fig. 14.1 shows the relationship between the calcium hydroxide content and the resistivity and shows that the SF samples which had been fully depleted of calcium hydroxide had maximum resistivities. This observation is in agreement with the conclusion from chapter 5 that the hydroxide ions are the main mechanism for the conduction of electricity in the SF samples. (It is interesting to note from fig 14.1 that the resistivity of the OPC samples does not increase with decreasing calcium hydroxide content, it actually appears to increase slightly, showing the more mature samples to have higher resistivities.) A conclusion from the thermogravimetric analysis is therefore that it provides an explanation for the slow increase in resistivity of the SF samples. This confirms that the early sensitivity to curing is not of major concern for durability.

A cause for concern is the possible effect which the calcium hydroxide depletion may have on the pH of the pore solution and the consequences of this on the corrosion rate. However with the major exception of cementitious nuclear waste repositories which are designed to maintain pH for thousands of years no evidence has been located to show that the pozzolanic reaction will increase corrosion rates.

14.5 The effects of low energy mixing.

14.5.1 General.

It was noted in chapter 2 that high energy mixing was only used for some of the paste

samples. Due to the action of the aggregate during the mixing of mortar and concrete samples the paste fraction in them is subject to high energy mixing. High energy mixing was used for the mercury intrusion and TG analysis but for the vapour permeability, helium intrusion and measurement of weight loss low energy mixing was used for the main sets of samples, so additional small sets were tested using high energy mixing to assess the consequences. The effects were discussed in the individual chapters and are collated here.

14.5.2 Vapour permeability.

It may be seen from table 6.1 that high energy mixing caused a significant increase in the permeability of the mix D (OPC) samples and a decrease in the mix C (SF) samples.

14.5.3 Helium intrusion.

In chapter 7 evidence was observed that the specific gravity of the paste samples of all mixes had the same specific gravity as the paste fraction of the concrete samples.

14.5.4 Weight loss.

Fig. 10.1 indicates that the weight loss on drying of low energy mixed paste is the same as that of the paste fraction of concrete which has undergone high energy mixing. This indicates that the hydration rates are the same. Table 10.1 shows an increase in the density of the SF samples caused by high energy mixing but a larger decrease in the density of the OPC samples. Figure 10.3 indicates that high energy mixing would make the density of the paste samples more representative of the paste fraction of concrete.

14.5.5 Porosity.

If high energy mixing decreased the density of the OPC samples but did not change their specific gravity it will have increased their porosity. The method of calculating porosity from weight loss for OPC samples was found to be effective (fig.10.6) and the results of applying it to the high energy mixed samples are shown in table 10.1 and confirm the increase in porosity. A corresponding decrease for the SF mix C samples and possibly a small effect for mix A would be expected. This effect may be seen in fig.13.24 which compares porosities measured from mercury and helium intrusion. The mercury samples had high energy mixing and the helium low energy mixing so the SF samples lie on a separate line with lower mercury intrusion porosities. This separation may also have been contributed to by the fineness of the pore structure of the SF samples which inhibited the penetration of the mercury.

14.5.6 Conclusion.

There is insufficient data to draw firm conclusions on the mechanism for these effects.

The lack of a change in the specific gravity and weight loss indicates that the high energy mixing did not affect the rate of hydration, it just caused the OPC mixes to form a more open structure and the SF ones a denser structure. For the OPC samples the more open structure had a much higher vapour permeability and the reverse effect applied to the SF. For mix D it was seen that the extra mixing caused the matrix to take up more water but the greater change in density was for mix B where no bleeding was observed for low energy mixing. Incorporation of more water could, however, be the mechanism for the OPC mixes. For the SF mixes it is suggested that the high energy mixes may have improved the dispersion of the dry SF powder in the water and superplasticiser.

14.6 The effect of drying.

It was noted in the literature review on mechanical properties (section 1.2.9) that SF concretes had been found to be more sensitive to drying than OPC concretes. In section 3.6.5 the effect of drying on the corrosion rate was discussed and it was concluded that the benefits of the SF were substantially lost. In section 4.5.1 it was concluded that drying shrinkage in SF mixes is greater and less reversible than for OPC mixes. The conclusion from these limited observations is to give cause for concern on the effects of drying SF concretes especially since the effect may be permanent unlike the effect of cold curing. This could be a major problem because the concrete in the region of the cover to the reinforcement which provides the corrosion protection is most vulnerable to early drying.

14.7 Recommendations for further study.

Recommendations for development of the apparatus and experimental techniques used have been included in the conclusions at the end of the chapters. The most promising of these concerns the use of the measurement of concrete resistivity. There are, at present, a number of programs in progress which involve measuring the rest potential of the steel reinforcement in structures, especially bridges. The main difficulty of this work is often the provision of access to the structure and measuring the resistivity would therefore not add greatly to the cost and would yield data on carbonation, depth of cover and even concrete strength (a good correlation between strength and resistance was noted in section 13.5). Comparison with other structures would also yield data on mix design. Measuring the complex impedance gives a measure of the polarisation resistance and from it the corrosion rate.

The following areas of work on SF mixes have not been covered by this project or other work located in the literature search:

1. The effect of dry curing was discussed briefly in section 14.6. A particular area of interest would be to establish whether the effect of drying is reversed by subsequent wetting.

2. When this project was started no reported uses of SF concrete in this country were located. Since then "normal strength" SF mixes have been marketed by a readymix supplier. These mixes in which possibly 30% of the cement is replaced by a 10% SF addition and mixed with a high w/c ratio are not of the type that has generally been the subject of international research but the limited data available indicates that they may, for example, carbonate rapidly. Unless their limitations are rapidly identified and, most importantly, publicised there will be some failures with SF concretes and the material may even be prohibited from use. This situation has already occured for calcium chloride accelerators and high alumina cements which are both good materials if applications are chosen to accommodate their limitations.

3. There is an apparent lack of applications for very high strength concretes in this country. They appear to be a "solution without a problem". Research is called for to identify suitable areas of use, these might include building some types of small bridges and other structures without reinforcement and thus totally avoiding the problem of corrosion.

4. This work has been concerned with the properties and performance of the mixes and only briefly touched on some aspects of the chemistry. A substantial amount of work has been carried out on the chemistry of SF mixes but it remains a major area for further research.
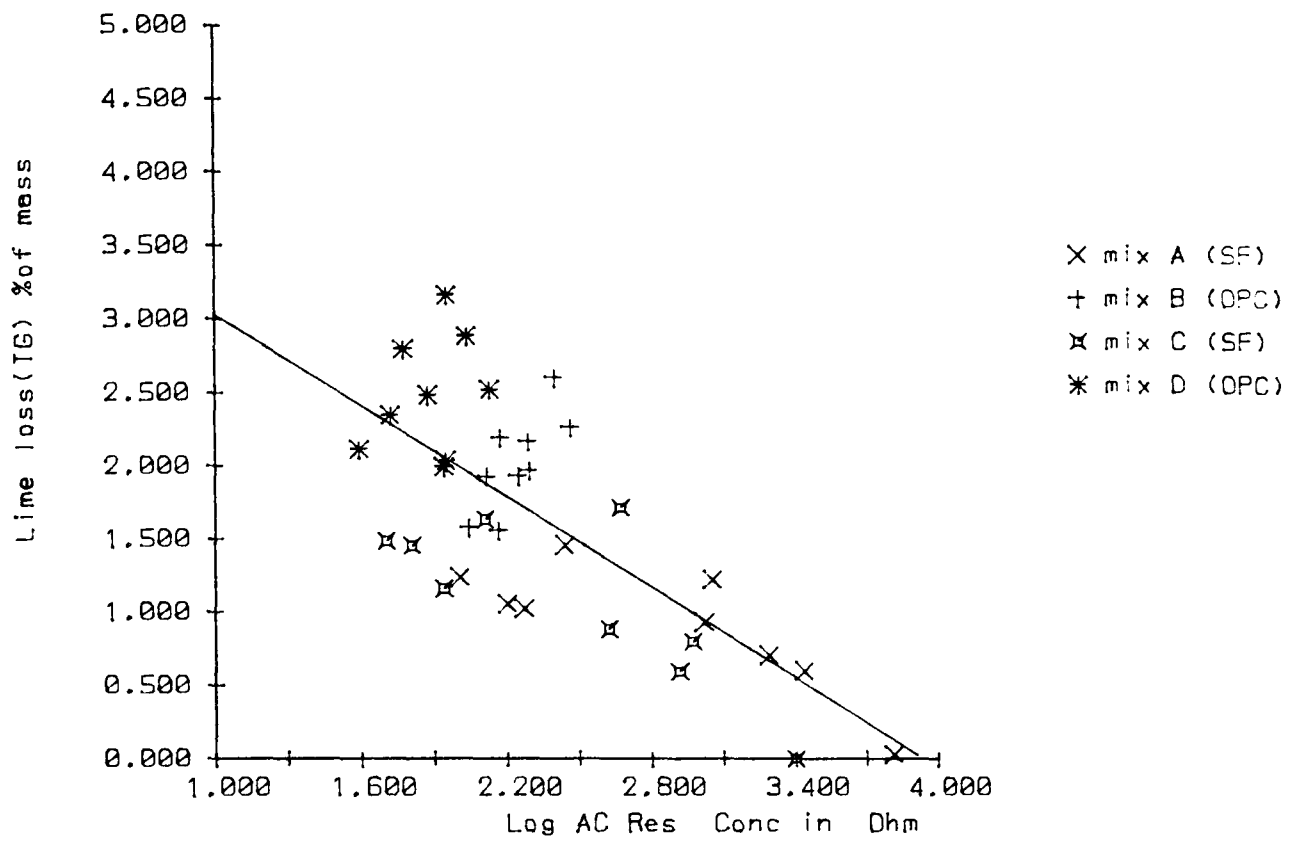
Equation for line : Y=4.06799583+X*-1.032579589
R squared=0.528

Fig. 14.1 Relationship between resistance and calcium hydroxide content.

Appendix 1

The data retrieval system for the Thermogravimetric balance.

General Description.

The circuit contains operational amplifiers for the mass and temperature signals. These amplifiers use an offset voltage from a voltage regulator to ensure that the voltage output is always positive. This is necessary because the BBC cannot measure negative voltages. The amplification factor is 4 which gives the system a theoretical resolution of 0.1 millivolt on a single reading. This corresponds to 10°C or 0.1% of mass. The program always uses an average of 500 readings. The unit is powered from the power supply in the BBC.

The output program has been kept as simple as possible to avoid the possibility of errors which could result in loss of readings. The temperature is calculated as a linear function of the thermocouple voltage. Corrections for this and analysis of the results are carried out with other programs.

Procedure for running the apparatus.

The controls for the balance should be set to Range=3, Ratio=1, Damping=3, Rate=30

The output program is on the disc with the name "RECORD".

When the program is run its first screen message is a request for an output file name. Ensure that there is a disc in the drive to receive the data before entering this. The use of a name which has already been used on the disc will result in the loss of the previous file.

The next screen message is "When empty crucible is in position and thermocouple is in ice hit return". When return is hit it will record the furnace temperature and assume that it is 20°C and record the mass and assign the value to 0%.

The next screen message is "When sample is in position hit return" When return is hit the mass will be recorded and assigned the value 100% and the run will start. The furnace controls should therefore be turned on.

While the system is running it will record results at intervals of approximately 12 seconds until the sample has heated and then cooled to below 50°C.

When a run has been completed the program will ask for the next file name. At this

point the disk may be changed or the program may be stopped with the escape key.

NOTE : It is essential that the system is warmed up for two hours before use. The program "WARM" is similar to "RECORD" but does not create any output files and is intended for this.

Procedures for analysing the results.
Three procedures are available:

Procedure 1. A plot of mass and differential mass against temperature may be obtained using the program GPLOT2. Selecting a differential range of 2 will cause the program to calculate the differential at a given point from the values two readings before it and two readings after it.

Procedure 2. Screen graphics may be used to measure the mass loss on any part of the curves. Running the program MEAS2 will display a the mass and differential mass curves on the screen together with two cursors and the value of the following variables: mass and temperature at the cursors, mass loss between the cursors and dM/dT. Typing 2,3,4 or 5 (return characters are not required) will move the cursors and the displayed variables will be continually updated. Typing 1 will print out the results and prepare for the next file. Note that the program LINES2 must be available on the disc when this procedure is used.

Procedure 3. The procedure involves the use of a NAG library routine on the Amdahl and is as follows:

*** NOTE : TWO OF THESE PROGRAMMES REQUIRE THE PRINTER AND ONE REQUIRES THE PLOTTER. THESE PERIPHERALS MUST BE TURNED OFF BEFORE THEY ARE CONNECTED TO THE BBC. ***

1. The files to be analysed must be on a disk with room for at least 4 more files on the same side of the disk with them, i.e. not more than 26 files in the catalogue.
2. A text file of the names of the files to be processed must be made with file name FLIST (e.g. in Wordwise). If the data file names are A1 and A2 the contents of this will be:
A1
A2
END
The word END must be included and must have a return character after it.

3. Run program TGP1. This processes the data using the table for the thermocouple and differentiates it using a differential range of 2. It takes a long time to run.

4. Run program TGP2. THE PRINTER MUST BE CONNECTED FOR THIS PROGRAM. This is an interactive program which is used to set estimates for the line of best fit which will subsequently be optimised. It is the only program which requires keyboard input.

When the program is run it will display the first data set on the screen with a curve of a fit to a typical paste sample. The question "Change ?" will then be displayed. If N is typed the parameters of this curve will be used. If Y is typed the changing routine is entered. This requires an initial input of 0,1,2,3,4,5 or 9 as follows :

   0 is used to change the number of normal curves in use. After typing 0 enter the number required (maximum 7) and then enter further initial input.

   9 will return to the main program and produce a new plot.

   1-5 are used to change the parameters of the curves numbered 1 to 5 from low to high temperature. After typing one of these numbers the existing values of the Amplitude, mean temperature, and standard deviation will be printed. Enter the new values and then enter further initial input.

5. Log on to the Amdahl and return control to the BBC.

6. Run program TGP3. This will load the data onto the Amdahl and will chain program TGP4 which will load the initial estimates onto it. If TGP4 is not on the disk in the drive the program will stop and TGP4 must be loaded separately.

7. With a disk with the files TGPROG, TGEXEC and TGSUB on it in the disk drive run program TGP8. This will load the program and exec files onto the Amdahl.

8. Return control to the Amdahl and type TGPROG. This will EXEC the FORTRAN program TGPROG.

Alternatively typing TGSUB will submit the job to the batch queue. The queue can be checked with the command QBATCH B * * . The command Q RDR will check if the output file is in the reader and it may then be obtained by typing RECEIVE. Typing RECEIVE again will clear the reader.

9. Return control to the BBC and run program TGP6. THE PRINTER MUST BE CONNECTED FOR THIS PROGRAM. This will get the results from the Amdahl, store them on disk and print them out. Check the value of IFAIL which is printed with each set. If it is not 0 the results may not be correct.

10. Log off the Amdahl.

11.If plots are required run program TGP7. THE PLOTTER MUST BE CONNECTED FOR THIS PROGRAM. This will plot each file in turn showing curves for the estimated parameters and those output by the Amdahl.

12. If it is required to make another attempt at fitting suitable curves the results file on the Amdahl (TGPROG RESULTS) ma be edited and used for input. (renamed TGEST DATA)

Contents of files on completion of a run.

BBC Files:

FLIST (ASCII text)

names of original data files i.e. number of runs

END

TGDATA (tokenised data)

number of runs

number of readings in run 1

data for run 1 :temperature, differential mass

.

.

number of readings in run 2

.

.

TGDATA2 (tokenised data)

number of runs

number of curves for run 1

NULL

initial estimates for run 1 : amplitude, mean temperature, standard deviation

.

.

number of curves for run 2

.

.

TGDATA3 (tokenised data)

number of runs

number of curves for run 1

IFAIL for run 1

final values for run 1 : amplitude, mean temperature, standard deviation

.

.

number of curves for run 2

.

.

AMDAHL files (ASCII data)

TGPROG DATA
as in BBC file TGDATA

TGEST DATA
as in BBC file TGDATA2

TGPROG RESULTS
as in BBC file TGDATA3

Appendix 2

Procedure for High Voltage Chloride Diffusion Apparatus

1 Samples should be vacuum saturated if they are not saturated from curing.

2 Check each half of each cell for electrical continuity from the terminal to the gauze.

3 Install samples in cells (note numbers on cells). Seal with silicon rubber and rubber membranes.

4 Set timer to run for about 8 hours. (see instructions).

5 Wait about 10 minutes for initial set of silicone rubber and fill cells with solutions: (carry out steps 6,7 and 8 while waiting)

NaCl (30g/l) on the - side

NaOH (12g/l) on the + side

When mixing solutions use the beaker and funnel marked for each in order to avoid cross contamination.

6 Check that lead from computer is plugged into MFI and not TAC line.

7 Turn on MFI and run program MFP3. This will load the program which is in the file CYRPROG into the MFI

8 Type:

  *VDU

   LIST

This should list the program.

use the control f9 key to return control to the BBC.

9 If required measure the ac resistivity and rest potential of the cells.

10 Connect the cells to the power supply unit and run the program BPROG.

11 When readings commence turn the power supply on.

12 Check that sensible reading are being printed every 5 minutes.

13 When the run is complete take a second set of ac resistivity and rest potential readings if required.

APPENDIX 3   TABLES OF THE MAIN DATA

The results from all of the experiments are tabulated in this appendix

The data is arranged in chapter order, table A3.3 contains the results from chapter 3, table A3.4 the results from chapter 4 etc.

The accuracy of the results as listed does not indicate the accuracy used for analysis. All results were held as real numbers on the computer and loaded directly into the plotting and analysis routines.

Data column			1	2	3	4	5
Mix	Test Age	Curing Condn.	Initial Resist ohms	Initial Rest pot mV	28 day Resist ohms	28 day Rest pot mV	AC Res Set 1 Ohm
A	3	1	112	-400.0	4513	-40.0	11098
A	3	2	113	-205.0	2902	-8.0	10982
A	3	3	71	-532.0	2993	-5.0	10673
A	28	1	2185	-340.0	5156	37.0	10152
A	28	2	576	-385.0	3918	20.0	9398
A	28	3	204	-532.0	3471	32.0	10364
A	90	1	4904	-314.0	6085	41.0	9516
A	90	2	1150	-465.0	4630	16.0	7866
A	90	3	645	-428.0	4077	18.0	8590
B	3	1	104	-166.0	213	-92.0	457
B	3	2	177	-180.0	213	-92.0	440
B	3	3	96	-442.0	231	-94.0	447
B	28	1	205	-231.0	258	-63.0	453
B	28	2	154	-232.0	298	-71.0	455
B	28	3	116	-495.0	258	-47.0	410
B	90	1	249	-347.0	281	-45.0	429
B	90	2	258	-468.0	223	-111.0	392
B	90	3	147	-418.0	465	-39.0	422
C	3	1	39	-343.0	934	-72.0	3401
C	3	2	56	-184.0	1122	-75.0	4730
C	3	3	28	-486.0	842	-95.0	2945
C	28	1	706	-512.0	1421	-45.0	2349
C	28	2	242	-443.0	1379	-66.0	3756
C	28	3	71	-515.0	918	-107.0	2730
C	90	1	1770	-292.0	2240	-171.0	2916
C	90	2	682	-352.0	2165	-78.0	3265
C	90	3	297	-443.0	1094	-167.0	2794
D	3	1	68	-225.0	138	-349.0	180
D	3	2	106	-208.0	157	-184.0	409
D	3	3	55	-328.0	111	-139.0	188
D	28	1	115	-267.0	126	-483.0	115
D	28	2	128	-284.0	142	-107.0	340
D	28	3	151	-424.0	158	-126.0	222
D	90	1	209	-228.0	177	-78.9	213
D	90	2	127	-435.0	154	-91.1	278
D	90	3	104	-435.0	132	-133.3	277

Column 1: Resistance of set 1(concrete) samples when first exposed
Column 2: Rest potential of set 1 samples when first exposed
Column 3: Resistance of set 1 samples after 28 days exposure
Column 4: Rest potential of set 1 samples after 28 days exposure
Column 5: Resistance of set 1 samples after 10 months exposure

TABLE A3.3a   (data from chapter 3)

Data column			1	2	3	4	5
Mix	Test Age	Curing Condn.	Rest Pot Set 1 mV	I_{corr} Set 1 mA/m²	AC Res Conc in Ohm	Rest Pot Conc in mV	I_{corr} Conc in mA/m²
A	3	1	37.7	0.3	158	-162.5	1.03
A	3	2	51.2	0.3	186	-262.5	1.08
A	3	3	50.0	0.2	101	-465.0	2.61
A	28	1	4.4	0.2	2725	-262.5	0.55
A	28	2	-160.1	0.4	1045	-366.5	1.54
A	28	3	-25.4	0.2	276	-448.5	1.47
A	90	1	50.7	0.2	6496	-294.0	0.44
A	90	2	-239.4	0.7	1935	-240.0	1.02
A	90	3	-118.4	0.3	1132	-359.2	0.95
B	3	1	57.2	0.7	131	-373.0	2.00
B	3	2	41.6	0.6	146	-257.5	1.27
B	3	3	-52.6	0.7	110	-536.0	3.36
B	28	1	-76.1	0.7	194	-338.0	1.08
B	28	2	-9.1	0.6	175	-360.5	2.32
B	28	3	-319.5	1.6	149	-411.0	2.31
B	90	1	41.4	0.4	291	-276.5	1.43
B	90	2	-30.0	0.8	248	-288.0	2.04
B	90	3	-38.6	0.5	195	-321.0	2.02
C	3	1	24.9	0.1	64	-350.5	2.58
C	3	2	22.4	0.2	87	-186.0	0.89
C	3	3	-63.7	0.2	50	-456.5	3.85
C	28	1	-380.7	1.3	938	-257.0	0.63
C	28	2	-208.2	0.4	419	-320.5	2.18
C	28	3	-258.2	0.4	129	-510.0	2.37
C	90	1	-213.5	0.3	2513	-196.0	0.52
C	90	2	-342.1	0.6	821	-261.0	1.53
C	90	3	-199.4	0.3	469	-446.5	2.08
D	3	1	-530.9	55.7	52	-236.0	4.07
D	3	2	-343.1	4.6	89	-207.0	1.61
D	3	3	-539.4	70.9	39	-416.2	2.41
D	28	1	-597.9	131.6	89	-181.0	2.58
D	28	2	-139.1	0.6	75	-288.5	3.78
D	28	3	-535.7	4.8	59	-431.5	2.81
D	90	1	-585.5	8.9	135	-336.5	1.63
D	90	2	-375.5	1.7	107	-316.0	2.04
D	90	3	-498.0	4.0	87	-437.0	2.01

Column 1: Rest potential of set 1 samples after 10 months of exposure
Column 2: Corrosion current of set 1 samples after 10 months of exposure
Column 3: Resistance of set 2 (concrete) samples when first exposed
Column 4: Rest potential of set 2 samples when first exposed
Column 5: Corrosion current of set 2 samples when first exposed

TABLE A3.3b   (data from chapter 3)

Data column			1	2	3	4	5
Mix	Test Age	Curing Condn.	I at .1V Conc in μA	AC Res Conc 28d Ohm	Rest Pot Conc 28d mV	I_{corr} Conc 28d mA/m^2	I at .1V Conc 28d μA
A	3	1	0	4378	7.5	0.2	0
A	3	2	1	4677	19.2	0.2	0
A	3	3	1	4193	-10.7	0.2	0
A	28	1	1	6385	6.0	0.2	0
A	28	2	0	5123	52.0	0.1	0
A	28	3	1	4563	34.5	0.1	0
A	90	1	1	7812	-20.5	0.2	0
A	90	2	1	5201	38.5	0.2	0
A	90	3	2	4439	4.5	0.3	0
B	3	1	3	232	-86.5	0.8	0
B	3	2	1	248	-89.0	0.7	0
B	3	3	1	237	-79.0	0.7	0
B	28	1	0	284	-86.5	0.9	0
B	28	2	0	291	-82.0	0.7	0
B	28	3	1	284	-76.5	0.8	0
B	90	1	3	351	-5.0	0.6	0
B	90	2	3	378	-39.0	0.6	0
B	90	3	5	398	-29.5	0.7	0
C	3	1	3	1504	-26.0	0.4	0
C	3	2	1	1705	-7.5	0.2	0
C	3	3	4	1502	-9.0	0.3	0
C	28	1	1	2365	12.0	0.2	1
C	28	2	1	2275	8.5	0.2	0
C	28	3	5	1669	-28.5	0.2	1
C	90	1	2	2842	9.5	0.3	0
C	90	2	3	2269	12.5	0.4	0
C	90	3	5	1699	-35.5	0.4	0
D	3	1	421	94	-584.0	16.1	1007
D	3	2	345	127	-515.5	21.9	764
D	3	3	11	88	-200.0	1.9	0
D	28	1	11	108	-303.0	5.2	89
D	28	2	9	94	-513.0	6.6	298
D	28	3	13	99	-99.0	1.6	2
D	90	1	2	176	-515.0	11.2	704
D	90	2	2	127	-653.5	75.1	2650
D	90	3	3	165	-223.0	1.5	23

Column 1 : Initial external current with applied voltage through set 2 samples
Column 2 : Resistance of set 2 samples after 28 days exposure
Column 3 : Rest potential of set 2 samples after 28 days exposure
Column 4 : Corrosion current of set 2 samples after 28 days exposure
Column 5 : External current through set 2 samples after 28 days exposure

TABLE A3.3c   (data from chapter 3)

Data column			1	2	3	4	5
Mix	Test Age	Curing Condn.	AC res Mtr 28d tank Ohm	Rest Pot Mtr 28d tank mV	I_{corr} Mtr 28d ta mA/m²	AC res Mtr 28d rm Ohm	Rest Pot Mtr 28d room mV
A	3	1	2421	-221.5	56.5	1886	-356.0
A	3	2	3408	-195.5	-48.8	1592	-367.5
A	3	3	3408	-137.0	13.1	1660	-357.0
A	28	1	5372	-232.0	8.8	3708	-351.0
A	28	2	4262	-398.5	31.4	5101	-343.0
A	28	3	2857	-424.5	26.0	1869	-397.0
A	90	1	6793	-332.5	13.1	5310	-318.5
A	90	2	4761	-374.0	11.5	4156	-378.0
A	90	3	4556	-408.0	-19.0	2296	-366.5
B	3	1	254	71.0	1.2	291	-68.5
B	3	2	462	51.0	15.6	381	-70.0
B	3	3	329	-211.0	40.9	298	-124.0
B	28	1	290	-479.0	10.7	296	-84.0
B	28	2	526	-188.0	3.9	333	-123.0
B	28	3	270	-531.5	19.6	264	-148.5
B	90	1	420	-251.5	1.3	361	-113.0
B	90	2	479	-298.0	5.5	336	-91.0
B	90	3	287	-198.5	5.8	246	-159.5
C	3	1	4218	2.0	5.4	683	-425.5
C	3	2	4856	11.5	8.4	493	-413.5
C	3	3	4417	72.5	6.2	459	-413.0
C	28	1	3086	-232.5	6.9	2786	-314.0
C	28	2	4065	-309.0	9.2	2857	-362.5
C	28	3	2463	-339.5	7.3	1142	-372.5
C	90	1	3532	-377.7	10.0	5532	-114.5
C	90	2	3791	-298.0	14.5	3350	-363.5
C	90	3	1979	-403.5	12.4	1560	-393.0
D	3	1	1680	-46.0	9.5	266	-203.0
D	3	2	3744	36.5	5.3	454	-53.5
D	3	3	1652	5.5	10.3	396	-52.5
D	28	1	1930	-9.0	7.8	495	-37.5
D	28	2	4714	2.5	5.0	663	6.5
D	28	3	2144	-53.5	6.8	372	-79.5
D	90	1	3672	-44.0	3.6	573	-10.5
D	90	2	5470	-39.5	4.0	574	-19.5
D	90	3	3217	-65.2	4.7	344	-91.7

Column 1 : Resistance of mortar samples when removed from carbonation tank.
Column 2 : Rest potential of mortar samples when removed from carbonation tank
Column 3 : Corrosion current of mortar samples when removed from carbonation tank
Column 4 : Resistance of mortar samples when removed from room (control)
Column 5 : Rest potential of mortar samples when removed from room (control)

TABLE A3.3d   (data from chapter 3)

Data column			1	2	3	4	5
Mix	Test Age	Curing Condn.	I_{corr} Mtr 28d rm mA/m^2	ACres Mtr 49d tank Ohm	RestPot Mtr 49d tank mV	I_{corr} Mtr 49d ta mA/m^2	ACres Mtr 49d room Ohm
A	3	1	7.7	2047	-511.5	24.0	5870
A	3	2	8.8	4534	-361.5	9.4	6834
A	3	3	6.9	4181	-241.0	6.6	4782
A	28	1	5.7	6285	-280.5	6.1	4518
A	28	2	4.9	4889	-393.0	7.5	3252
A	28	3	7.4	2771	-538.5	13.5	2661
A	90	1	7.6	8883	-258.0	6.6	5519
A	90	2	6.4	5860	-400.5	6.0	5740
A	90	3	9.0	4743	-318.0	4.5	2901
B	3	1	0.7	287	-85.5	0.3	330
B	3	2	0.5	436	-114.0	0.8	363
B	3	3	2.2	315	-628.0	63.4	346
B	28	1	0.3	296	-18.0	0.6	309
B	28	2	0.4	324	-300.5	2.5	331
B	28	3	0.4	243	-110.0	0.8	309
B	90	1	0.4	413	-163.0	0.8	368
B	90	2	0.3	350	-116.0	0.3	489
B	90	3	0.4	310	-127.5	0.6	317
C	3	1	6.0	890	-561.5	40.5	2135
C	3	2	7.2	146	-626.5	53.8	2180
C	3	3	10.5	673	-568.5	48.8	1927
C	28	1	4.2	2514	-223.5	5.0	2911
C	28	2	10.0	2757	-536.0	20.4	3025
C	28	3	8.5	1925	-386.0	10.6	769
C	90	1	1.4	5519	-294.0	-7.9	3565
C	90	2	8.8	3073	-522.5	16.3	3413
C	90	3	7.8	2325	-374.5	4.9	2007
D	3	1	1.2	726	-575.0	45.7	161
D	3	2	0.2	2726	-313.0	6.1	221
D	3	3	0.2	932	-422.2	13.1	210
D	28	1	0.1	1356	-258.0	8.9	308
D	28	2	0.1	3052	-220.5	7.8	325
D	28	3	0.1	1356	-244.5	6.3	164
D	90	1	0.2	2282	-165.5	3.0	356
D	90	2	0.2	3143	-281.0	7.4	323
D	90	3	0.2	1742	-306.0	6.0	216

Column 1 : Corrosion current of mortar samples when removed from room (control)
Column 2 : Resistance of carbonated mortar samples after exposure in salt
Column 3 : Rest potential of carbonated mortar samples after exposure in salt
Column 4 : Corrosion current of carbonated mortar samples after exposure in salt
Column 5 : Resistance of control mortar samples after exposure in salt

TABLE A3.3e   (data from chapter 3)

Data column			1	2

Mix	Test Age	Curing Condn.	Rest Pot Mtr 49d rm mV	I_{corr} Mtr 49d rm mA/m^2
A	3	1	-370.0	3.9
A	3	2	-322.5	3.2
A	3	3	-412.0	5.2
A	28	1	-408.5	16.7
A	28	2	-348.0	2.3
A	28	3	-431.0	8.9
A	90	1	-494.0	6.6
A	90	2	-392.5	3.1
A	90	3	-327.0	4.1
B	3	1	-149.5	0.8
B	3	2	-106.5	0.3
B	3	3	-99.5	0.2
B	28	1	-166.0	2.3
B	28	2	-96.5	0.2
B	28	3	-218.5	1.4
B	90	1	-77.5	0.3
B	90	2	-92.5	0.3
B	90	3	-332.0	4.1
C	3	1	-393.0	4.4
C	3	2	-416.0	7.3
C	3	3	-404.5	4.0
C	28	1	-333.5	3.3
C	28	2	-385.5	4.5
C	28	3	-542.5	18.7
C	90	1	-278.0	1.9
C	90	2	-389.5	3.9
C	90	3	-356.0	4.3
D	3	1	-580.5	12.6
D	3	2	-425.5	8.7
D	3	3	-533.0	11.0
D	28	1	-259.5	4.8
D	28	2	-277.5	6.0
D	28	3	-496.0	7.5
D	90	1	-82.0	0.2
D	90	2	-110.2	0.1
D	90	3	-415.2	10.6

Column 1 : Rest potential of control mortar samples after exposure in salt.
Column 2 : Corrosion current of control mortar samples after exposure in salt.

TABLE A3.3f   (data from chapter 3)

Data column			1	2	3	4
Mix	Test Age	Curing Condn.	strain curing μ str	strain drying μ str	strain 4 day μ str	strain 18 day μ str
A	3	1	-262.5	-368.7	-118.7	-337.5
A	3	2	-581.2	-100.0	-25.0	-187.5
A	3	3	-175.0	-300.0	-181.2	-400.0
A	28	1	31.2	-75.0	-93.7	-262.5
A	28	2	-468.7	-387.5	-100.0	-231.2
A	28	3	-25.0	-168.7	-206.2	-412.5
A	90	1	31.2	-25.0	-75.0	-237.5
A	90	2	-443.7	-18.7	-100.0	-287.5
A	90	3	112.5	6.2	-162.5	-437.5
B	3	1	-187.5	-300.0	-56.2	-268.7
B	3	2	-468.7	-75.0	100.0	-81.2
B	3	3	-193.7	-318.7	-62.5	-262.5
B	28	1	112.5	-100.0	-137.5	-312.5
B	28	2	-268.7	-81.2	-106.2	-225.0
B	28	3	112.5	-100.0	-193.7	-368.7
B	90	1	237.5	12.5	-75.0	-375.0
B	90	2	-243.7	-18.7	-137.5	-331.2
B	90	3	293.7	31.2	-93.7	-456.2
C	3	1	-118.7	-318.7	87.5	-31.2
C	3	2	-687.5	-200.0	193.7	175.0
C	3	3	-93.7	-287.5	62.5	-37.5
C	28	1	81.2	-100.0	25.0	-43.7
C	28	2	-593.7	-62.5	18.7	-37.5
C	28	3	125.0	-50.0	-43.7	-168.7
C	90	1	100.0	-81.2	18.7	-56.2
C	90	2	-637.5	-56.2	12.5	-93.7
C	90	3	0.6	-93.7	37.5	-125.0
D	3	1	-137.5	-193.7	93.7	31.2
D	3	2	-443.7	-143.7	462.5	481.2
D	3	3	-206.2	-231.2	137.5	106.2
D	28	1	93.7	-25.0	-6.2	-75.0
D	28	2	-125.0	-143.7	-0.6	-31.2
D	28	3	-362.5	-12.5	-43.7	-112.5
D	90	1	18.7	-12.5	-18.7	-87.5
D	90	2	-187.5	18.7	-18.7	-81.2
D	90	3	31.2	25.0	-25.0	-137.5

Column 1 : Strain during curing and drying
Column 2 : Strain during drying
Column 3 : Strain during the first 4 days of exposure
Column 4 : Strain during 18 days of exposure

TABLE A3.4a   (data from chapter 4)

Data column			1	2	3	4	5
Mix	Test Age	Curing Condn.	Mtr cups carb. depth mm	Carbon. depth mm mortar	Carbon. depth mm concrete	AC res ratio	AC res Mtr 28d room Ohm
A	3	1	0.00	0.000	0.00	1.28	1886
A	3	2	1.00	1.000	0.00	2.14	1592
A	3	3	0.00	0.000	0.00	2.05	1660
A	28	1	0.00	0.000	0.00	1.45	3708
A	28	2	0.00	0.000	0.00	0.84	5101
A	28	3	0.00	0.000	0.00	1.53	1869
A	90	1	0.00	0.000	0.00	1.28	5310
A	90	2	0.00	0.000	0.00	1.15	4156
A	90	3	0.00	0.000	0.00	1.98	2296
B	3	1	0.00	0.000	0.00	0.87	291
B	3	2	0.50	0.000	1.00	1.21	381
B	3	3	0.00	0.000	0.00	1.10	298
B	28	1	0.00	0.000	0.00	0.98	296
B	28	2	0.00	0.000	0.00	1.58	333
B	28	3	0.00	0.000	0.00	1.02	264
B	90	1	0.00	0.000	0.00	1.16	361
B	90	2	0.00	0.000	0.00	1.43	336
B	90	3	0.00	0.000	0.00	1.16	246
C	3	1	7.00	1.500	4.50	6.17	683
C	3	2	14.00	5.000	5.00	9.84	493
C	3	3	5.75	2.000	5.00	9.61	459
C	28	1	0.50	0.000	0.00	1.11	2786
C	28	2	5.00	0.500	0.00	1.42	2857
C	28	3	1.00	0.000	0.00	2.16	1142
C	90	1	0.50	0.000	0.00	0.64	5532
C	90	2	3.50	0.500	1.00	1.13	3350
C	90	3	0.00	0.000	0.50	1.27	1560
D	3	1	20.00	0.000	8.00	6.30	266
D	3	2	20.00	4.000	10.00	8.24	454
D	3	3	15.00	1.000	3.50	4.17	396
D	28	1	20.00	0.000	3.50	3.90	495
D	28	2	20.00	0.500	1.50	7.10	663
D	28	3	5.00	0.000	2.00	5.75	372
D	90	1	20.00	0.000	0.75	6.41	573
D	90	2	10.00	0.500	0.50	9.53	574
D	90	3	5.00	0.000	0.50	9.35	344

Column 1 : Carbonation depth measured on mortar samples cast in cups
Column 2 : Carbonation depth measured on mortar prisms
Column 3 : Carbonation depth measured on concrete cubes
Column 4 : Ratio of resistances carbonated/uncarbonated for cylinders
Column 5 : Resistance of control cylinders

TABLE A3.4b   (data from chapter 4)

| Data column | | | 1 | 2 |

Mix	Test Age	Curing Condn.	1yr innr TG carb %of mass	1yr outr TG carb %of mass
A	3	1	0.185	0.93
A	3	2	0.186	4.66
A	3	3	0.285	5.03
A	28	1	0.370	2.04
A	28	2	0.133	2.13
A	28	3	0.000	1.48
A	90	1	0.208	1.19
A	90	2	0.139	2.57
A	90	3	0.185	6.13
B	3	1	0.348	2.46
B	3	2	0.553	2.39
B	3	3	1.830	2.34
B	28	1	0.508	3.63
B	28	2	1.459	2.68
B	28	3	0.449	2.69
B	90	1	1.522	3.22
B	90	2	1.141	4.39
B	90	3	0.973	2.97
C	3	1	0.152	4.35
C	3	2	0.055	4.58
C	3	3	0.090	6.10
C	28	1	0.029	5.55
C	28	2	0.227	9.23
C	28	3	0.246	7.13
C	90	1	0.273	5.20
C	90	2	0.281	7.09
C	90	3	0.031	8.66
D	3	1	0.133	2.01
D	3	2	0.663	1.45
D	3	3	0.456	4.66
D	28	1	1.156	3.25
D	28	2	1.687	1.73
D	28	3	1.217	3.43
D	90	1	1.227	4.90
D	90	2	1.373	2.77
D	90	3	0.714	4.05

Column 1 : % mass loss for carbonate in TG analysis (inner sample)
Column 2 : % mass loss for carbonate in TG analysis (outer surface sample)

TABLE A3.4c   (data from chapter 4)

Data column			1	2	3	4
Mix	Test Age	Curing Condn.	Cl conc average %	Total charge Coulomb	Initial Current Amps	Final Current Amps
A	3	1	0.958	2065	0.099	0.080
A	3	2	1.219	1382	0.068	0.058
A	3	3	1.026	3981	0.201	0.104
A	28	1	0.390	95	0.006	0.004
A	28	2	0.655	208	0.010	0.009
A	28	3	0.296	1559	0.069	0.067
A	90	1	0.590	6	0.001	0.000
A	90	2	0.733	132	0.006	0.006
A	90	3	0.544	334	0.016	0.015
B	3	1	1.315	3740	0.146	0.183
B	3	2	1.484	3732	0.146	0.179
B	3	3	1.711	5188	0.197	0.246
B	28	1	0.349	2493	0.096	0.122
B	28	2	0.740	2537	0.095	0.127
B	28	3	0.973	3485	0.134	0.175
B	90	1	0.400	1656	0.065	0.082
B	90	2	0.818	1907	0.070	0.095
B	90	3	0.652	2923	0.110	0.146
C	3	1	2.390	6592	0.389	0.112
C	3	2	2.022	5370	0.260	0.114
C	3	3	2.147	7045	0.640	0.068
C	28	1	0.730	458	0.020	0.020
C	28	2	1.212	777	0.033	0.036
C	28	3	0.905	4055	0.167	0.155
C	90	1	0.824	182	0.009	0.009
C	90	2	0.946	417	0.017	0.020
C	90	3	0.829	971	0.040	0.047
D	3	1	2.907	6830	0.250	0.334
D	3	2	3.269	5139	0.201	0.242
D	3	3	2.534	9376	0.501	0.311
D	28	1	1.668	3399	0.135	0.168
D	28	2	3.615	2928	0.108	0.152
D	28	3	2.057	5461	0.201	0.277
D	90	1	2.076	2354	0.095	0.115
D	90	2	2.291	2502	0.092	0.128
D	90	3	2.194	4533	0.174	0.225

Column 1 : Average chloride content from drilled samples
Column 2 : Total charge passed
Column 3 : Initial current
Column 4 : Final current

TABLE A3.5   (data from chapter 5)

Data column			1	2	3	4	5
Mix	Test Age	Curing Condn.	Loss Bin 1 g/100day	M_0 Bin 1 g.	B1 Rate constant 1/day	Loss Bin 2 g/100day	M_0 Bin 2 g.
A	3	1	0.623	0.646	0.099	0.893	0.726
A	3	2	0.856	0.707	0.108	0.912	0.728
A	3	3	0.761	0.755	0.116	0.889	0.832
A	28	1	0.917	0.397	0.070	0.592	0.432
A	28	2	0.455	0.513	0.075	0.789	0.710
A	28	3	0.812	0.671	0.096	0.631	0.684
A	90	1	0.569	0.156	0.109	0.599	0.289
A	90	2	0.463	0.291	0.131	0.483	0.369
A	90	3	0.366	0.310	0.141	0.457	0.344
B	3	1	1.710	0.741	0.071	1.578	0.892
B	3	2	1.604	0.819	0.078	1.671	0.856
B	3	3	1.717	0.828	0.073	1.761	0.923
B	28	1	1.963	0.624	0.060	1.402	0.742
B	28	2	1.433	0.625	0.073	1.471	0.947
B	28	3	1.391	0.717	0.071	1.238	0.944
B	90	1	1.209	0.284	0.178	1.164	0.340
B	90	2	1.265	0.285	0.121	1.104	0.390
B	90	3	1.303	0.346	0.109	1.263	0.483
C	3	1	2.456	1.213	0.056	2.042	1.525
C	3	2	3.461	1.324	0.049	2.736	1.575
C	3	3	2.756	1.399	0.054	2.261	1.697
C	28	1	1.914	0.736	0.064	1.904	0.906
C	28	2	2.119	1.245	0.070	2.160	1.496
C	28	3	2.149	1.525	0.077	1.984	1.697
C	90	1	1.539	0.546	0.143	1.500	0.364
C	90	2	1.907	1.008	0.093	1.950	0.837
C	90	3	1.828	1.217	0.087	1.726	0.940
D	3	1	1.779	0.533	0.075	1.721	0.793
D	3	2	1.977	0.624	0.061	1.760	0.827
D	3	3	1.894	0.600	0.088	1.721	0.878
D	28	1	1.589	0.384	0.051	1.637	0.512
D	28	2	1.744	0.484	0.064	1.885	0.622
D	28	3	1.829	0.565	0.061	1.355	0.593
D	90	1	1.590	0.367	0.123	1.353	0.199
D	90	2	1.456	0.409	0.080	1.473	0.256
D	90	3	1.303	0.443	0.071	1.640	0.261

Column 1 : Steady state loss for bin 1
Column 2 : Initial mass loss for bin 1
Column 3 : Rate constant K for bin 1
Column 4 : Steady state loss for bin 2
Column 5 : Initial mass loss for bin 2

TABLE A3.6a   (data from chapter 6)

Data column			1	2	3	4
Mix	Test Age	Curing Condn.	B2 Rate constant 1/day	Loss Bin 3 g/100day	M_0 Bin 3 g.	B3 Rate constant 1/day
A	3	1	0.097	1.121	0.935	0.088
A	3	2	0.103	1.778	0.935	0.098
A	3	3	0.109	1.505	1.027	0.115
A	28	1	0.049	1.238	0.742	0.061
A	28	2	0.068	1.091	0.910	0.079
A	28	3	0.068	1.012	0.983	0.084
A	90	1	0.124	1.200	0.328	0.149
A	90	2	0.120	0.978	0.449	0.093
A	90	3	0.121	0.842	0.479	0.139
B	3	1	0.065	2.419	0.846	0.065
B	3	2	0.061	3.009	0.975	0.058
B	3	3	0.053	3.073	0.951	0.076
B	28	1	0.055	2.681	0.883	0.055
B	28	2	0.055	2.201	1.066	0.062
B	28	3	0.056	2.323	0.894	0.057
B	90	1	0.069	1.964	0.380	0.092
B	90	2	0.087	2.003	0.432	0.086
B	90	3	0.076	2.140	0.620	0.138
C	3	1	0.065	3.653	1.682	0.095
C	3	2	0.066	4.883	1.461	0.091
C	3	3	0.068	4.056	1.681	0.082
C	28	1	0.041	2.972	1.268	0.070
C	28	2	0.067	3.900	1.348	0.087
C	28	3	0.060	3.996	1.624	0.090
C	90	1	0.177	2.825	0.481	0.183
C	90	2	0.087	4.177	0.968	0.104
C	90	3	0.079	4.002	1.238	0.095
D	3	1	0.065	3.503	0.637	0.090
D	3	2	0.062	3.631	0.650	0.082
D	3	3	0.070	4.111	1.081	0.076
D	28	1	0.036	2.172	0.502	0.065
D	28	2	0.052	3.255	0.776	0.082
D	28	3	0.058	3.587	0.903	0.100
D	90	1	0.109	2.738	0.434	0.106
D	90	2	0.071	2.262	0.371	0.044
D	90	3	0.140	2.288	0.543	0.106

Column 1 : Rate constant K for bin 2
Column 2 : Steady state loss for bin 3
Column 3 : Initial mass loss for bin 3
Column 4 : Rate constant K for bin 3

TABLE A3.6b   (data from chapter 6)

Data column			1	2	3
Mix	Test Age	Curing Condn.	Perm. $*10^{-9}$ Kg/m^2PaS	Intercpt $*10^{-3}$ Kg/m^2Pa	k Rate constant $*10^9Pa/s$
A	3	1	0.169	1.284	1.010
A	3	2	0.218	1.324	1.103
A	3	3	0.197	1.463	1.227
A	28	1	0.172	0.847	0.649
A	28	2	0.147	1.178	0.805
A	28	3	0.157	1.291	0.895
A	90	1	0.145	0.428	1.411
A	90	2	0.118	0.618	1.203
A	90	3	0.102	0.625	1.457
B	3	1	0.364	1.420	0.723
B	3	2	0.391	1.499	0.693
B	3	3	0.409	1.540	0.741
B	28	1	0.381	1.259	0.606
B	28	2	0.325	1.472	0.680
B	28	3	0.309	1.459	0.655
B	90	1	0.273	0.565	1.192
B	90	2	0.274	0.621	1.037
B	90	3	0.296	0.800	1.217
C	3	1	0.514	2.490	0.816
C	3	2	0.700	2.505	0.779
C	3	3	0.572	2.724	0.762
C	28	1	0.431	1.598	0.650
C	28	2	0.509	2.355	0.827
C	28	3	0.502	2.782	0.844
C	90	1	0.364	0.791	1.832
C	90	2	0.490	1.604	1.044
C	90	3	0.459	1.916	0.956
D	3	1	0.431	1.136	0.850
D	3	2	0.455	1.223	0.764
D	3	3	0.468	1.416	0.837
D	28	1	0.348	0.795	0.571
D	28	2	0.430	1.046	0.740
D	28	3	0.410	1.129	0.839
D	90	1	0.352	0.546	1.205
D	90	2	0.329	0.586	0.663
D	90	3	0.332	0.681	1.133

Column 1 : Permeability
Column 2 : Intercept of steady state loss gradient
Column 3 : Rate constant k

TABLE A3.6c   (data from chapter 6)

Data column			1	2	3
Mix	Test Age	Curing Condn.	1 Atmos $K(O_2)$ m^2*10^{-18}	2 Atmos $K(O_2)$ m^2*10^{-18}	Average $K(O_2)$ m^2*10^{-18}
A	3	1	2.4	1.8	2.1
A	3	2	4.5	3.9	4.2
A	3	3	1.0	0.8	0.9
A	28	1	5.4	5.3	5.4
A	28	2	1.0	0.8	0.9
A	28	3	1.8	1.6	1.7
A	90	1	12.1	11.2	11.6
A	90	2	0.4	0.7	0.6
A	90	3	1.9	3.0	2.5
B	3	1	16.7	13.7	15.2
B	3	2	12.3	10.5	11.4
B	3	3	15.9	13.4	14.7
B	28	1	13.0	11.5	12.2
B	28	2	12.8	10.4	11.6
B	28	3	13.2	11.0	12.1
B	90	1	14.0	12.5	13.2
B	90	2	9.2	8.1	8.7
B	90	3	22.3	19.3	20.8
C	3	1	24.3	21.5	22.9
C	3	2	42.4	36.2	39.3
C	3	3	28.2	25.5	26.9
C	28	1	49.3	46.3	47.8
C	28	2	10.9	9.9	10.4
C	28	3	20.4	19.0	19.7
C	90	1	100.9	96.4	98.6
C	90	2	12.0	11.1	11.5
C	90	3	58.0	56.6	57.3
D	3	1	398.8	346.8	372.8
D	3	2	487.6	433.5	460.6
D	3	3	223.5	190.1	206.8
D	28	1	53.9	45.1	49.5
D	28	2	146.3	134.0	140.2
D	28	3	54.1	47.8	51.0
D	90	1	30.7	25.7	28.2
D	90	2	107.6	98.4	103.0
D	90	3	32.3	28.7	30.5

Column 1 : Permeability at 1 atmosphere
Column 2 : Permeability at 2 atmospheres
Column 3 : Average permeability

TABLE A3.7   (data from chapter 7)

Data column			1	2	3
Mix	Test Age	Curing Condn.	S.G. Paste g/cc.	S.G. Mortar g/cc.	S.G. Concrete g/cc.
A	3	1	2.164	2.405	2.553
A	3	2	2.276	2.507	2.550
A	3	3	2.197	2.430	2.526
A	28	1	2.109	2.394	2.519
A	28	2	2.185	2.413	2.551
A	28	3	2.085	2.358	2.537
A	90	1	2.051	2.409	2.528
A	90	2	2.119	2.378	2.527
A	90	3	2.059	2.372	2.541
B	3	1	2.495	2.593	2.639
B	3	2	2.548	2.619	2.641
B	3	3	2.558	2.625	2.635
B	28	1	2.413	2.548	2.620
B	28	2	2.450	2.573	2.611
B	28	3	2.432	2.554	2.610
B	90	1	2.355	2.566	2.612
B	90	2	2.380	2.561	2.611
B	90	3	2.367	2.572	2.614
C	3	1	2.058	2.444	2.518
C	3	2	2.228	2.523	2.544
C	3	3	2.122	2.435	2.493
C	28	1	1.885	2.399	2.534
C	28	2	2.096	2.449	2.519
C	28	3	1.985	2.412	2.524
C	90	1	1.859	2.397	2.497
C	90	2	2.048	2.487	2.526
C	90	3	1.973	2.441	2.527
D	3	1	2.470	2.598	2.632
D	3	2	2.492	2.621	2.627
D	3	3	2.562	2.584	2.626
D	28	1	2.316	2.558	2.610
D	28	2	2.371	2.569	2.602
D	28	3	2.365	2.567	2.624
D	90	1	2.243	2.561	2.600
D	90	2	2.330	2.581	2.598
D	90	3	2.293	2.555	2.610

Column 1 : Specific gravity of paste
Column 2 : Specific gravity of mortar
Column 3 : Specific gravity of concrete

TABLE A3.8. (data from chapter 8)

Data column			1	2	3
Mix	Test Age	Curing Condn.	Hg S.G. Paste g/cc	Hg DD Paste g/cc	Hg Paste porosity %
A	3	1	2.162	1.799	16.81
A	3	2	2.143	1.776	17.11
A	3	3	2.156	1.801	16.45
A	28	1	2.071	1.794	13.39
A	28	2	2.112	1.790	15.24
A	28	3	2.113	1.793	15.13
A	90	1	2.102	1.837	12.60
A	90	2	2.146	1.841	14.18
A	90	3	2.117	1.831	13.52
B	3	1	2.373	1.879	20.80
B	3	2	2.392	1.878	21.48
B	3	3	2.432	1.867	23.23
B	28	1	2.322	1.893	18.50
B	28	2	2.356	1.881	20.15
B	28	3	2.376	1.893	20.35
B	90	1	2.341	1.927	17.70
B	90	2	2.337	1.914	18.11
B	90	3	2.322	1.905	17.95
C	3	1	1.979	1.491	24.67
C	3	2	2.028	1.468	27.63
C	3	3	1.969	1.460	25.80
C	28	1	1.883	1.498	20.45
C	28	2	1.930	1.478	23.40
C	28	3	1.882	1.481	21.29
C	90	1	1.798	1.475	17.95
C	90	2	1.907	1.521	20.25
C	90	3	1.865	1.511	18.96
D	3	1	2.260	1.607	28.85
D	3	2	2.344	1.606	31.50
D	3	3	2.333	1.599	31.47
D	28	1	2.195	1.647	24.98
D	28	2	2.236	1.629	27.13
D	28	3	2.224	1.623	27.04
D	90	1	2.159	1.657	23.25
D	90	2	2.162	1.652	23.57
D	90	3	2.197	1.651	24.86

Column 1 : Specific gravity of paste from mercury intrusion
Column 2 : Dry Density from mercury intrusion
Column 3 : Porosity from mercury intrusion

TABLE A3.9a (data from chapter 9)

Data column			1	2	3	4	5
Mix	Test Age	Curing Condn.	Hg pores 10-170 μm %	Hg pores .15-10 μm %	Hg pores .01-.15 μm %	Hg pores .003-.01 μm %	Hg pores recovery %
A	3	1	0.314	0.863	6.26	8.46	3.48
A	3	2	0.261	0.537	9.89	6.16	3.99
A	3	3	0.321	0.667	7.58	7.60	3.82
A	28	1	0.468	0.800	5.04	6.89	2.97
A	28	2	0.468	1.112	4.58	8.80	2.88
A	28	3	0.637	0.822	4.87	7.63	3.33
A	90	1	0.516	0.829	6.12	4.97	3.12
A	90	2	0.311	0.885	3.36	9.39	3.04
A	90	3	0.653	0.737	4.34	7.62	3.04
B	3	1	0.277	0.133	19.15	1.18	10.50
B	3	2	0.219	0.067	20.52	0.58	10.28
B	3	3	0.678	0.357	20.16	1.19	10.64
B	28	1	0.355	0.368	16.60	1.11	10.19
B	28	2	0.243	0.239	18.24	1.34	10.05
B	28	3	0.397	0.413	17.34	1.46	10.76
B	90	1	0.400	0.660	14.62	1.31	8.76
B	90	2	0.382	0.746	15.66	1.25	8.83
B	90	3	0.315	0.700	15.33	1.53	9.26
C	3	1	0.590	0.437	16.04	7.20	8.51
C	3	2	0.741	0.691	19.53	6.30	10.18
C	3	3	0.658	0.561	15.85	8.31	8.25
C	28	1	0.580	0.726	12.18	6.63	6.76
C	28	2	0.565	0.531	12.83	9.07	5.86
C	28	3	0.630	0.690	13.67	5.96	6.44
C	90	1	0.889	0.574	11.12	6.01	6.79
C	90	2	0.620	0.506	11.38	7.46	4.64
C	90	3	0.669	0.381	11.86	5.88	6.39
D	3	1	0.411	0.352	27.03	1.70	17.47
D	3	2	0.231	0.452	29.07	1.69	17.25
D	3	3	0.335	0.452	28.69	1.92	19.63
D	28	1	0.317	0.240	22.68	1.68	14.97
D	28	2	0.284	0.093	24.93	2.40	14.84
D	28	3	0.493	0.432	24.29	1.74	16.36
D	90	1	0.270	0.195	21.22	1.52	13.81
D	90	2	0.213	0.216	21.77	1.36	11.49
D	90	3	0.278	0.284	21.71	2.50	14.58

Column 1 : Pores in the range 170-10 μm from mercury intrusion (% of sample vol)
Column 2 : Pores in the range .15-10 μm from mercury intrusion (% of sample vol)
Column 3 : Pores in the range .01-.15 μm from mercury intrusion (% of sample vol)
Column 4 : Pores in the range .003-.01 μm from mercury intrusion (% of sample vol)
Column 5 : Recovery pore volume from mercury intrusion (% of sample vol)

TABLE A3.9b (data from chapter 9)

Data column			1	2	3	4
Mix	Test Age	Curing Condn.	Wt.loss Paste	Wt.loss Mortar	Wt.loss Concrete	1 Year Dry Den g/cc.
A	3	1	0.166	0.075	0.036	2.347
A	3	2	0.166	0.078	0.038	2.350
A	3	3	0.172	0.076	0.038	2.369
A	28	1	0.160	0.074	0.034	2.373
A	28	2	0.163	0.075	0.037	2.385
A	28	3	0.158	0.069	0.032	2.370
A	90	1	0.159	0.074	0.033	2.384
A	90	2	0.161	0.072	0.034	2.373
A	90	3	0.156	0.057	0.030	2.361
B	3	1	0.157	0.065	0.036	2.421
B	3	2	0.150	0.068	0.037	2.410
B	3	3	0.161	0.067	0.035	2.423
B	28	1	0.148	0.060	0.033	2.389
B	28	2	0.142	0.064	0.033	2.389
B	28	3	0.150	0.062	0.034	2.387
B	90	1	0.138	0.058	0.030	2.406
B	90	2	0.136	0.059	0.032	2.419
B	90	3	0.143	0.056	0.029	2.411
C	3	1	0.253	0.092	0.045	2.360
C	3	2	0.243	0.090	0.044	2.357
C	3	3	0.260	0.095	0.042	2.342
C	28	1	0.245	0.088	0.040	2.325
C	28	2	0.233	0.084	0.043	2.336
C	28	3	0.241	0.090	0.042	2.340
C	90	1	0.244	0.088	0.045	2.362
C	90	2	0.231	0.081	0.046	2.420
C	90	3	0.239	0.084	0.046	2.340
D	3	1	0.245	0.078	0.051	2.374
D	3	2	0.216	0.084	0.048	2.381
D	3	3	0.252	0.086	0.049	2.364
D	28	1	0.219	0.076	0.035	2.350
D	28	2	0.205	0.079	0.036	2.343
D	28	3	0.232	0.081	0.036	2.352
D	90	1	0.220	0.074	0.036	2.367
D	90	2	0.199	0.071	0.039	2.368
D	90	3	0.221	0.073	0.043	2.357

Column 1 : Fractional weight loss from paste
Column 2 : Fractional weight loss from mortar
Column 3 : Fractional weight loss from concrete
Column 4 : Dry density concrete after 1 year of storage

TABLE A3.10a (data from chapter 10)

Data column			1	2	3	4
Mix	Test Age	Curing Condn.	Dry den Paste g/cc.	Dry den Mortar g/cc.	Dry den Concrete g/cc	Fraction paste hydrated
A	3	1	1.676	2.074	2.355	0.372
A	3	2	1.694	2.068	2.359	0.376
A	3	3	1.659	2.080	2.348	0.338
A	28	1	1.721	2.077	2.396	0.409
A	28	2	1.699	2.068	2.378	0.391
A	28	3	1.684	2.101	2.378	0.418
A	90	1	1.696	2.078	2.370	0.414
A	90	2	1.697	2.083	2.381	0.399
A	90	3	1.690	2.090	2.378	0.431
B	3	1	1.851	2.119	2.399	0.423
B	3	2	1.816	2.112	2.388	0.459
B	3	3	1.839	2.119	2.374	0.401
B	28	1	1.866	2.132	2.373	0.471
B	28	2	1.820	2.118	2.361	0.501
B	28	3	1.847	2.139	2.419	0.458
B	90	1	1.894	2.154	2.418	0.523
B	90	2	1.830	2.131	2.413	0.536
B	90	3	1.867	2.121	2.409	0.499
C	3	1	1.354	2.056	2.334	0.388
C	3	2	1.403	2.084	2.338	0.451
C	3	3	1.339	2.043	2.350	0.342
C	28	1	1.342	2.066	2.354	0.440
C	28	2	1.406	2.088	2.341	0.511
C	28	3	1.376	2.048	2.349	0.461
C	90	1	1.352	2.061	2.361	0.444
C	90	2	1.406	2.071	2.352	0.520
C	90	3	1.391	2.054	2.339	0.474
D	3	1	1.634	2.128	2.358	0.436
D	3	2	1.634	2.115	2.353	0.607
D	3	3	1.625	2.098	2.341	0.395
D	28	1	1.691	2.126	2.350	0.591
D	28	2	1.627	2.132	2.338	0.667
D	28	3	1.646	2.108	2.344	0.512
D	90	1	1.691	2.121	2.363	0.586
D	90	2	1.643	2.113	2.364	0.700
D	90	3	1.683	2.113	2.366	0.579

Column 1 : Dry density of paste
Column 2 : Dry density of mortar
Column 3 : Dry density of concrete
Column 4 : Fraction of paste formed by hydrated cement

TABLE A3.10b (data from chapter 10)

Data column			1	2	3	4	5
Mix	Test Age	Curing Condn.	Calc. paste porosity	Calc. mortar porosity	Calc. concrete P (cups)	Calc. concrete P (set1)	Calc. concrete P (1 yr)
A	3	1	32.69	19.55	8.62	13.63	14.51
A	3	2	32.15	20.36	9.30	13.30	14.29
A	3	3	34.66	19.78	9.34	14.50	12.34
A	28	1	32.50	20.50	8.90	9.96	12.39
A	28	2	32.31	20.30	9.27	11.50	10.73
A	28	3	30.78	17.35	7.38	11.10	11.95
A	90	1	35.68	21.77	9.34	13.33	11.84
A	90	2	34.58	20.51	9.02	11.80	12.68
A	90	3	31.11	16.52	7.35	11.30	13.15
B	3	1	29.07	18.63	8.92	12.12	9.79
B	3	2	29.44	19.38	9.05	13.27	10.93
B	3	3	30.11	18.88	8.57	14.72	9.64
B	28	1	27.17	17.29	8.00	14.84	13.13
B	28	2	28.15	18.45	7.93	16.15	13.19
B	28	3	28.24	17.29	8.30	10.06	13.40
B	90	1	24.63	16.15	7.26	10.17	11.41
B	90	2	26.84	17.20	7.70	10.63	10.02
B	90	3	26.37	17.12	7.12	11.07	10.89
C	3	1	44.87	19.75	10.78	11.80	9.06
C	3	2	42.08	18.51	10.55	11.52	9.48
C	3	3	46.30	20.66	10.00	10.07	11.01
C	28	1	47.70	20.41	10.37	10.63	13.61
C	28	2	41.68	17.94	10.65	11.44	11.98
C	28	3	42.34	19.61	9.95	10.20	11.11
C	90	1	47.39	20.71	11.69	9.92	9.79
C	90	2	42.27	18.56	11.41	10.51	3.37
C	90	3	40.47	17.97	10.57	10.94	10.86
D	3	1	36.89	16.60	12.40	11.60	9.91
D	3	2	32.77	18.15	11.67	12.15	9.20
D	3	3	38.19	19.00	11.88	13.37	10.96
D	28	1	30.84	16.40	8.46	12.46	12.48
D	28	2	31.64	16.58	8.62	13.78	13.16
D	28	3	34.56	17.87	8.65	13.10	12.24
D	90	1	30.96	16.35	8.68	11.10	10.62
D	90	2	30.16	16.28	9.37	10.99	10.60
D	90	3	31.47	16.51	10.36	10.76	11.72

Column 1 : Paste porosity calculated from weight loss
Column 2 : Mortar porosity calculated from weight loss
Column 3 : Concrete porosity calculated from weight loss (specially cast samples)
Column 4 : Concrete porosity calculated from weight loss (set 1 concrete cubes)
Column 5 : Concrete porosity calculated from weight loss (1 year old concrete cubes)

TABLE A3.10c (data from chapter 10)
The results for the SF samples are calculated in chapter 13

Data column			1	2	3
Mix	Test Age	Curing Condn.	Water loss(TG) %of mass	Lime loss(TG) %of mass	Carbonat loss(TG) %of mass
A	3	1	6.38	1.060	2.880
A	3	2	9.19	1.032	3.271
A	3	3	8.35	1.248	3.027
A	28	1	8.32	0.608	1.821
A	28	2	6.42	0.939	2.264
A	28	3	8.56	1.469	3.366
A	90	1	14.68	0.033	0.716
A	90	2	12.84	0.714	1.670
A	90	3	13.50	1.232	2.268
B	3	1	9.75	1.935	2.068
B	3	2	9.43	1.569	3.586
B	3	3	9.30	1.590	4.053
B	28	1	7.20	2.178	2.451
B	28	2	13.59	1.944	2.322
B	28	3	13.54	2.209	2.481
B	90	1	11.14	2.277	2.593
B	90	2	11.79	2.618	2.874
B	90	3	12.02	1.980	2.165
C	3	1	9.31	1.464	4.276
C	3	2	11.86	1.169	4.209
C	3	3	9.18	1.493	3.784
C	28	1	17.15	0.810	2.261
C	28	2	15.05	0.892	2.079
C	28	3	15.40	1.641	2.661
C	90	1	16.05	0.003	0.479
C	90	2	14.04	0.603	1.986
C	90	3	12.92	1.726	2.942
D	3	1	15.96	2.351	3.401
D	3	2	11.44	2.040	4.034
D	3	3	11.33	2.123	3.287
D	28	1	12.21	3.175	3.362
D	28	2	16.78	2.494	1.230
D	28	3	17.37	2.804	0.576
D	90	1	16.68	2.530	0.630
D	90	2	19.90	2.899	0.791
D	90	3	13.98	2.000	1.180

Column 1 : Weight loss in water peak
Column 2 : Weight loss in calcium hydroxide peak
Column 3 : Weight loss in calcium carbonate peak

TABLE A3.11a (data from chapter 11)

Data column			1	2	3	4
Mix	Test Age	Curing Condn.	1yr innr TG lime %of mass	1yr innr TG carb %of mass	1yr outr TG lime %of mass	1yr outr TG carb %of mass
A	3	1	0.102	0.185	0.000	0.93
A	3	2	0.095	0.186	0.000	4.66
A	3	3	0.069	0.285	0.000	5.03
A	28	1	0.114	0.370	0.000	2.04
A	28	2	0.107	0.133	0.000	2.13
A	28	3	0.083	0.000	0.000	1.48
A	90	1	0.132	0.208	0.000	1.19
A	90	2	0.127	0.139	0.000	2.57
A	90	3	0.104	0.185	0.000	6.13
B	3	1	0.368	0.348	0.161	2.46
B	3	2	0.932	0.553	0.162	2.39
B	3	3	0.869	1.830	0.172	2.34
B	28	1	0.715	0.508	0.439	3.63
B	28	2	1.387	1.459	0.200	2.68
B	28	3	0.927	0.449	0.110	2.69
B	90	1	1.550	1.522	0.282	3.22
B	90	2	1.269	1.141	0.000	4.39
B	90	3	1.068	0.973	0.000	2.97
C	3	1	0.190	0.152	0.000	4.35
C	3	2	0.000	0.055	0.000	4.58
C	3	3	0.029	0.090	0.000	6.10
C	28	1	0.009	0.029	0.000	5.55
C	28	2	0.123	0.227	0.000	9.23
C	28	3	0.007	0.246	0.000	7.13
C	90	1	0.124	0.273	0.000	5.20
C	90	2	0.148	0.281	0.000	7.09
C	90	3	0.001	0.031	0.000	8.66
D	3	1	0.440	0.133	0.210	2.01
D	3	2	0.841	0.663	0.146	1.45
D	3	3	0.596	0.456	0.304	4.66
D	28	1	0.808	1.156	0.113	3.25
D	28	2	1.342	1.687	0.197	1.73
D	28	3	0.962	1.217	0.013	3.43
D	90	1	0.871	1.227	0.000	4.90
D	90	2	0.783	1.373	0.008	2.77
D	90	3	0.779	0.714	0.000	4.05

Column 1 : Weight loss in lime peak for inner sample from one year old cubes
Column 2 : Weight loss in carbonate peak for inner sample from one year old cubes
Column 3 : Weight loss in lime peak for outer sample from one year old cubes
Column 4 : Weight loss in lime carbonate for outer sample from one year old cubes

TABLE A3.11b (data from chapter 11)

Data column			1	2	3	4
Mix	Test Age	Curing Condn.	Cube Strength N/sq.mm.	1 Year Strength N/sq.mm.	Mod. of Rupture N/sq.mm.	Tensile Strength N/sq.mm.
A	3	1	69.3	137.6	8.00	4.676
A	3	2	72.9	126.9	5.92	4.633
A	3	3	60.6	131.8	8.10	4.400
A	28	1	113.2	141.4	11.58	5.206
A	28	2	96.8	142.4	10.09	5.822
A	28	3	91.9	132.7	9.06	4.867
A	90	1	130.2	144.2	12.50	5.228
A	90	2	112.0	135.0	10.04	5.553
A	90	3	110.0	148.9	9.58	6.027
B	3	1	71.1	101.3	7.82	4.202
B	3	2	69.6	98.5	6.20	4.626
B	3	3	66.9	101.0	8.21	4.442
B	28	1	80.4	101.0	8.90	4.994
B	28	2	74.6	101.2	8.12	5.157
B	28	3	74.7	102.3	8.98	4.966
B	90	1	101.6	114.5	9.88	5.730
B	90	2	90.6	112.3	9.44	5.581
B	90	3	91.8	115.7	8.69	5.412
C	3	1	41.0	98.2	5.29	2.838
C	3	2	42.5	91.2	4.36	2.823
C	3	3	33.5	95.8	4.62	2.368
C	28	1	88.4	113.6	8.14	4.733
C	28	2	70.9	112.6	6.60	4.039
C	28	3	68.3	117.3	6.22	4.152
C	90	1	109.9	122.9	8.58	5.426
C	90	2	83.6	113.1	7.04	5.023
C	90	3	83.3	113.2	7.16	4.817
D	3	1	38.4	63.0	3.41	2.191
D	3	2	41.1	62.5	2.12	2.233
D	3	3	34.2	64.1	1.86	1.854
D	28	1	55.4	64.7	4.66	2.787
D	28	2	48.9	63.7	4.21	2.763
D	28	3	49.4	67.3	4.26	2.610
D	90	1	55.3	71.5	4.34	3.096
D	90	2	54.8	67.7	4.20	2.787
D	90	3	53.2	65.9	4.30	2.869

Column 1 : Compressive strength after curing
Column 2 : Compressive strength after one year drying
Column 3 : Flexural strength
Column 4 : Tensile strength

TABLE A3.12a (data from chapter 12)

Data column			1	2	3	4
Mix	Test Age	Curing Condn.	Static Modulus GPa.	Dynamic Modulus GPa.	Poissons Ratio .	PUNDIT Velocity Km/s
A	3	1	46.03	48.39	0.203	4.685
A	3	2	41.47	48.16	0.194	4.642
A	3	3	39.29	47.21	0.179	4.626
A	28	1	45.92	53.56	0.177	4.852
A	28	2	44.59	52.36	0.200	4.861
A	28	3	43.55	52.57	0.201	4.873
A	90	1	47.37	53.88	0.182	4.903
A	90	2	44.48	52.75	0.198	4.852
A	90	3	47.09	53.00	0.193	4.856
B	3	1	41.94	50.81	0.190	4.682
B	3	2	41.50	51.04	0.159	4.716
B	3	3	38.19	50.12	0.200	4.716
B	28	1	41.79	52.50	0.175	4.819
B	28	2	43.62	51.10	0.183	4.785
B	28	3	41.05	51.32	0.180	4.778
B	90	1	47.24	55.29	0.208	5.020
B	90	2	47.08	53.73	0.199	4.903
B	90	3	45.12	54.26	0.190	4.921
C	3	1	35.95	43.64	0.229	4.561
C	3	2	32.36	43.29	0.213	4.484
C	3	3	29.20	42.00	0.243	4.507
C	28	1	42.69	49.99	0.197	4.764
C	28	2	37.90	47.96	0.206	4.695
C	28	3	38.13	48.28	0.200	4.692
C	90	1	43.40	52.18	0.198	4.868
C	90	2	40.85	49.96	0.210	4.796
C	90	3	41.23	50.86	0.231	4.922
D	3	1	28.62	42.20	0.207	4.491
D	3	2	27.80	41.95	0.223	4.445
D	3	3	22.74	40.34	0.233	4.346
D	28	1	34.42	46.97	0.217	4.692
D	28	2	33.41	45.28	0.228	4.682
D	28	3	32.12	45.91	0.241	4.708
D	90	1	36.34	49.35	0.221	4.789
D	90	2	33.69	49.15	0.225	4.794
D	90	3	34.43	48.92	0.242	4.861

Column 1 : Static modulus
Column 2 : Dynamic modulus
Column 3 : Poisson's ratio
Column 4 : PUNDIT velocity

TABLE A3.12b (data from chapter 12)

Data column			1	2	3	4	5
Mix	Test Age	Curing Condn.	Calc. paste porosity	Calc. mortar porosity	Calc. concrete P (cups)	Calc. concrete P (set1)	Calc. concrete P (1 yr)
A	3	1	32.69	19.55	8.62	13.63	14.51
A	3	2	32.15	20.36	9.30	13.30	14.29
A	3	3	34.66	19.78	9.34	14.50	12.34
A	28	1	32.50	20.50	8.90	9.96	12.39
A	28	2	32.31	20.30	9.27	11.50	10.73
A	28	3	30.78	17.35	7.38	11.10	11.95
A	90	1	35.68	21.77	9.34	13.33	11.84
A	90	2	34.58	20.51	9.02	11.80	12.68
A	90	3	31.11	16.52	7.35	11.30	13.15
B	3	1	29.07	18.63	8.92	12.12	9.79
B	3	2	29.44	19.38	9.05	13.27	10.93
B	3	3	30.11	18.88	8.57	14.72	9.64
B	28	1	27.17	17.29	8.00	14.84	13.13
B	28	2	28.15	18.45	7.93	16.15	13.19
B	28	3	28.24	17.29	8.30	10.06	13.40
B	90	1	24.63	16.15	7.26	10.17	11.41
B	90	2	26.84	17.20	7.70	10.63	10.02
B	90	3	26.37	17.12	7.12	11.07	10.89
C	3	1	44.87	19.75	10.78	11.80	9.06
C	3	2	42.08	18.51	10.55	11.52	9.48
C	3	3	46.30	20.66	10.00	10.07	11.01
C	28	1	47.70	20.41	10.37	10.63	13.61
C	28	2	41.68	17.94	10.65	11.44	11.98
C	28	3	42.34	19.61	9.95	10.20	11.11
C	90	1	47.39	20.71	11.69	9.92	9.79
C	90	2	42.27	18.56	11.41	10.51	3.37
C	90	3	40.47	17.97	10.57	10.94	10.86
D	3	1	36.89	16.60	12.40	11.60	9.91
D	3	2	32.77	18.15	11.67	12.15	9.20
D	3	3	38.19	19.00	11.88	13.37	10.96
D	28	1	30.84	16.40	8.46	12.46	12.48
D	28	2	31.64	16.58	8.62	13.78	13.16
D	28	3	34.56	17.87	8.65	13.10	12.24
D	90	1	30.96	16.35	8.68	11.10	10.62
D	90	2	30.16	16.28	9.37	10.99	10.60
D	90	3	31.47	16.51	10.36	10.76	11.72

Column 1 : Paste porosity calculated from weight loss
Column 2 : Mortar porosity calculated from weight loss
Column 3 : Concrete porosity calculated from weight loss of samples cast in cups
Column 4 : Concrete porosity calculated from cubes after curing
Column 5 : Concrete porosity calculated from cubes after one year of drying

TABLE A3.13a (data from chapter 13)

Data column			1	2	3
Mix	Test Age	Curing Condn.	Measured mortar porosity	Measured paste porosity	Measured concrete porosity
A	3	1	13.77	22.56	5.88
A	3	2	17.50	25.59	6.00
A	3	3	14.43	24.49	5.08
A	28	1	13.24	18.41	4.46
A	28	2	14.29	22.23	5.95
A	28	3	10.90	19.22	4.86
A	90	1	13.76	17.30	4.71
A	90	2	12.38	19.90	4.71
A	90	3	11.91	17.92	4.91
B	3	1	18.28	25.83	7.93
B	3	2	19.35	28.72	8.06
B	3	3	19.27	28.10	7.68
B	28	1	16.31	22.67	6.94
B	28	2	17.70	25.69	6.60
B	28	3	16.25	24.05	6.70
B	90	1	16.07	19.55	6.39
B	90	2	16.81	23.10	6.53
B	90	3	17.55	21.14	6.41
C	3	1	15.87	34.21	6.92
C	3	2	17.39	37.01	7.74
C	3	3	16.07	36.91	5.69
C	28	1	13.87	28.79	7.01
C	28	2	14.76	32.92	6.77
C	28	3	15.09	30.69	6.83
C	90	1	14.02	27.29	6.13
C	90	2	16.74	31.33	7.23
C	90	3	15.87	29.50	7.28
D	3	1	18.08	33.87	10.71
D	3	2	19.31	34.44	10.24
D	3	3	18.82	36.55	10.30
D	28	1	16.90	27.01	8.51
D	28	2	17.00	31.40	8.29
D	28	3	17.88	30.39	9.06
D	90	1	17.19	24.62	8.24
D	90	2	18.15	29.49	8.40
D	90	3	17.31	26.64	9.22

Column 1 : Porosity from mortar SG measured by helium intrusion
Column 2 : Porosity from paste SG measured by helium intrusion
Column 3 : Porosity from concrete SG measured by helium intrusion

TABLE A3.13b (data from chapter 13)

REFERENCES

ACI Committee 226 1987
Silica fume in concrete - a report
ACI Materials Journal, March-April, pp.158-166

Aitcin,P.C. 1983a
Influence of condensed silica fume on the properties of fresh and hardened concrete
Condensed Silica Fume, Aitcin,P.C.(editor), University of Sherbrooke Quebec Canada, pp.25-27

Aitcin,P.C. 1983b
Physico-chemical properties of condensed silica fume
Condensed Silica Fume, Aitcin,P.C.(editor), University of Sherbrooke Quebec Canada, pp.16-19

Aitcin,P.C. 1983c
Historical data on the use of condensed silica fume in concrete
Condensed Silica Fume, Aitcin,P.C.(editor), University of Sherbrooke Quebec Canada, pp.6-8

Aitcin,P.C. and Pigeon,M. 1986
Performance of condensed silica fume used in pavements and sidewalks
Durability of Building Materials, Vol. 3, pp.353-368

Aitcin,P.C. and Regourd,M. 1985
The use of condensed silica fume to control Alkali-Silica Reaction - A field case study.
Cement and Concrete Research, Vol.15, pp.711-719

Aitcin,P.C. and Vezina,D. 1984
Resistance to freezing and thawing of silica fume concrete
Cement Concrete and Aggregates CCAGDP, Vol.6, no.1, pp.38-42

Andrade,C. and Gonzalez,J.A. 1978
Quantitative measurements of corrosion rate of reinforcing steels embedded in concrete using polarisation resistance measurements.
Werkstoffe und Korrosion, Vol.29,pp.517-519

Anon 1983
Micro-silica adds to the mix
Civil Engineering, August, pp.43-45

Anon 1985c
M.F.I. Manual
C.I.L. Electronics Worthing Sussex

Anon 1986a
Corrocem anti corrosive additive for concrete.
Scancem Chemicals, Slemmestad, Norway.

Anon 1986b
Ready mix sells the Silica solution
New Civil Engineer, 24 April, p.22

Anon 1988
USA ahead in super high strength concrete stakes
Building, 20 May, p.75

Arup,H. 1983
The mechanisms of protection of steel by concrete.
Corrosion of reinforcement in concrete construction, A.P.Crane(editor), Ellis Horwood, pp.151-159

Asgeirsson,H. 1986
Silica fume in cement and Silane for counteracting of Alkali-Silica reactions in Iceland
Cement and Concrete Research, Vol.16, pp.423-428

Asgeirsson,H. and Gudmundsson,G. 1979
Pozzolanic activity of silica dust
Cement and Concrete Research, Vol.9, pp. 249-252

Bamforth,P.B. 1987
The relationship between permeability coefficients for concrete obtained using liquid and gas.
Magazine of Concrete Research, Vol.39, no.138, March, pp.3-11

Bazant,Z.P. and Najjar,L.J. 1972
Nonlinear water diffusion in nonsaturated concrete.
Materiaux et Constructions, Vol.5, no.25, pp.1-8

Beeby,A.W. 1985
Developement of a corrosion cell for the study of the influences of environment and concrete properties on corrosion.
Conference of the Institution of Engineers, Australia *"Concrete 85-The performance of Concrete and masonary structures"*

Bracher,G. 1983
Corrosion monitoring in the industrial-related research area.
Corrosion of reinforcement in concrete construction, A.P.Crane.(editor), Ellis Horwood, pp.255-263

Bradley-Williams,T.S. 1986
The production of microsilica
Concrete Magazine, Vol.20, no.8, pp.17-18

Browne,R.D., Geoghegan,M.P. and Baker,A.F. 1983
Analysis of structural condition from durability results.
Corrosion of reinforcement in concrete construction, A.P.Crane(editor), Ellis Horwood, pp.193-222

Buenfeld,N.R. and Newman,J.B. 1984
The permeability of concrete in a marine environment
Magazine of Concrete Research, Vol 36, no. 127, June, pp.67-80

Buil,M. and Acker,P. 1985
Creep of a silica fume concrete
Cement and Concrete Research, Vol.15, pp.463-466

Buil,M. and Delage,P. 1987
Some further evidence on a specific effect of silica fume on the pore structure of portland cement mortars
Cement and Concrete Research, Vol 17, pp.65-69

Burge,T.A. 1983a
High strength lightweight concrete with condensed silica fume
A.C.I. publication SP.79 *Proceedings of the CANMET/A.C.I. conference on silica fume slag and other minerals in concrete,* pp.731-746

Burge,T.A. 1983b

Densified silica-cement coating as an effective corrosion protection.

Corrosion of reinforcement in concrete construction, A.P.Crane(editor), Ellis Horwood, pp.333-342

Byfors,K 1987

Influence of silica fume and flyash on chloride diffusion and pH values in cement paste

Cement and Concrete Research, Vol 17, pp.115-130

Cabrera,J.G. 1985

The porosity of concrete

Concrete Research Seminar, Leeds

Cabrera,J.G. 1988

Design of concrete for minimum porosity

In publication

Cabrera,J.G. Cusens,A.R. and Ramezanianpour,A. 1985

The effect of curing conditions on the carbonation of mortars containing cement, P.F.A., silica fume and trass

Proc.First international conference on the deterioration and repair of concrete in the gulf. Bahrain, 26-29 Oct, Vol 2

Cabrera,J.G. and Lynsdale,C.J. 1988

A simple gas permeameter for the measurement of concrete permeability

Magazine of Concrete Research, (accepted for publication in 1988)

Carette,G.G. and Malhotra,V.M. 1983a

Mechanical properties, durability and drying shrinkage of portland cement concrete incorporating silica fume.

Cement Concrete and Aggregates CCAGDP, Vol.5, no.1, pp.3-13

Chatterji,S., Thaulow,N. and Christensen,P. 1982

Pozzolanic activity of byproduct silica-fume from ferro-silicon production.

Cement and Concrete Research, Vol.15, pp.781-784

Cheng-yi,H. and Feldman,R.F. 1985a

Influence of silica fume on the microstructural development in cement mortars

*Cement and Concrete Research,*Vol.15, pp.285-294

Cheng-yi,H. and Feldman,R.F. 1985b
Hydration reactions in portland cement-silica fume blends
Cement and Concrete Research, Vol.15, pp.585-592

Cheng-Yi,H. and Feldman,R.F. 1985c
Dependence of frost resistance on the pore structure of mortar containing silica fume
A.C.I. Journal, Sept-Oct, pp.740-743

Christensen,D.W. Sorensen,E.V. and Radjy,F.F. 1984
Rockbond : A new microsilica concrete brdge deck overlay
Proc. International Bridge Conference Pittsburgh Pensylvania U.S.A., June,
pp.151-159

Davies,G. and Oberholster,R.E. 1987
Use of the NBRI accelerated test to evaluate the effectiveness of mineral admixtures in
preventing the alkali silica reaction
Cement and Concrete Research, Vol 17, pp. 97-107

Dawson,J.L. 1983
Corrosion monitoring of steel in concrete
Corrosion of reinforcement in concrete construction, A.P.Crane(editor), Ellis
Horwood, pp.175-192

Dhir,R.K. Jones,M.R. and Munday,J.G.L. 1985
A practical approach to studying carbonation of concrete
Concrete Magazine, Oct, pp.32-34

Dingsoyr,E., Mosberg,T. and Young,J.F. 1985
Influence of aggregates on the strength and elastic modulus of high strength mortars
containing microsilica.
Materials Research Society Symposium Proceeding, Vol.42,

Dumbleton,B. 1987a
Minimum water for maximum strength
New Civil Engineer, 17 September, pp.33-36

Dumbleton,B. 1987b
Silica strengthens Toronto tower
New Civil Engineer, 5 November, pp.40-46

Feldman,R.F. 1986b

Influence of condenced silica fume and sand/cement ratio on pore structure and frost resistance of portland cement mortars

ACI publication SP91 *Proceedings of the second international CANMET/ACI conference on the use of Fly Ash, Silica Fume, Slag and Natural Pozzolanas in concrete Madrid,* pp.973-990

Feldman,R.F. and Cheng-Yi,H. 1985a

Resistance of mortars containing silica fume to attack by a solution containing chlorides

Cement and Concrete Research, Vol.15, pp.411-420

Feldman,R.F. and Cheng-yi,H. 1985b

Properties of portland cement-silica fume pastes: 1) Porosity and surface properties.

Cement and Concrete Research, Vol.15, pp.765-774

Fontana,M.G. and Greene,N.D. 1967

Corrosion Engineering

McGraw Hill

Gautefall,O. 1986

Effect of condensed silica fume on the diffusion of chlorides through hardened cement paste

ACI publication SP91 Proceedings of the second international CANMET/ACI conference on the use of Fly Ash, Silica Fume, Slag and Natural Pozzolanas in concrete Madrid, pp.991-998

Gautefall,O. and Vennesland,O. 1983

Effect of cracks on the corrosion of embedded steel in silica-concrete compared to ordinary concrete

Nordic Concrete Research Publication, no.2, Dec, pp.17-28

Gee,M.D. 1986

Microsilica Concrete

The Construction Specifier , Dec, pp.44-50

Gjorv,O.E. 1983

Durability of concrete containing condensed silica fume

A.C.I. publication SP.79 *Proceedings of the CANMET/A.C.I. conference on silica fume slag and other minerals in concrete,* pp.695-708

Gjorv,O.E. Vennesland,O. and El-Busaidy,A.H.S. 1976
Diffusion of dissolved oxygen through concrete
Corrosion 76 Conference Houston Texas National Association of Corrosion Engineers, pp.17/1-17/8

Gonzalez,J.A., Alonso,C. and Andrade,C. 1983
Corrosion rate of reinforcements during accelerated carbonation of mortar made with different types of cement
Corrosion of reinforcement in concrete construction, A.P.Crane (editor), Ellis Horwood, pp.159-174

Gonzalez,J.A., Vazquez,A.J. and Andrade,C. 1982
Les effets des cycles d'humidite sur la corrosion des armatures galvanisees dans les mortiers carbonates et non carbonates
Materiaux et Constructions, Vol.15, No.88, pp.271-278

Gonzalez,J.A.,Molina,A.,Escudero,M.L. and Andrade,C. 1985a
Errors in the electrochemical evaluation of very small corrosion rates 2.Other electrochemical techniques applied to corrosion of steel in concrete
Corrosion science, Vol.25, No.7, pp.519-530

Gonzalez,J.A.,Molina,A.,Escudero,M.L. and Andrade,C. 1985b
Errors in the electrochemical evaluation of very small corrosion rates 1.Polarisation resistance method applied to corrosion of steel in concrete
Corrosion science, Vol.25, No.10, pp.917-930

Grutzeck,M.W., Roy,D.M. and Wolfe-Confer,D. 1982
Mechanism of hydration of portland cement composites containing ferrosilicon dust
Proc. 4th International Conference on Cement Microscopy (International Cement Microscopy Association Duncanville Texas) , pp.193-202

Hammond,E. and Robson,T.D. 1955
Comparison of the electrical properties of various cements and concretes.
The Engineer, Jan, pp.78-80 and 114-115

Hansen,T.C. Jensen,H. and Johannesson,T. 1986
Chloride diffusion and corrosion initiation of steel reinforcement in fly ash concretes
Cement and Concrete Research, Vol.16, pp.782-784

Hansen,T.C., Jensen,H. and Johannesson,T. 1986
Chloride diffusion and corrosion initiation of steel reinforcement in fly ash concrete.
ACI publication SP91 *Proceedings of the second international CANMET/ACI conference on the use of Fly Ash, Silica Fume, Slag and Natural Pozzolanas in concrete Madrid,* supplementary vol. 3,

Hansson,C.M. 1984
Comments on electrochemical measurements of the rate of corrosion of steel in concrete
Cement and Concrete Research, Vol 14 ,pp.574-584

Hansson,C.M., Frolund,Th. and Markussen,J.B. 1985
The effect of chloride cation type on the corrosion of steel in concrete by chloride salts.
Cement and Concrete Research, Vol 15, pp. 65-73

Hansson,I.L.H. and Hansson,C.M. 1983
Electrical resistivity measurements of portland cement based materials
Cement and Concrete Research, Vol.13, pp.675-683

Hansson,I.L.H. and Hansson,C.M. 1985
Ion conduction in cement based materials
Cement and Concrete Research, Vol.15, pp.201-212

Helland,S. 1986
Silica fume in high strength concrete
Nordsk Betong, 1-2, pp.91-95

Henry,R.L. and Kurtz,G.K. 1963
Water vapour transmission of concrete and of aggregates
U.S. Naval Civil Engineering Laboratory, Port Hueneme, California, June

Hertz,K. 1984
Heat induced explosion of dense concretes
Technical University of Denmark, Institute of Building Design, Report no.166

Hester,W.T. 1986b
Silica fume concrete
The Construction Specifier, December, pp.52-56

Higginbotham,P.G. 1985
Microtab all purpose statistical package
Edward Arnold London

Hjorth,L. 1982
Microsilica in concrete
Nordic Concrete Research Publication, no.1 pp.9.1-9.18

Holland,T.C., Krysa,A., Luther,M.D. and Liu,C. 1986
Use of silica-fume concrete to repair abrasion-erosion damage in the Kinzua dam
stilling basin.
ACI publication SP91 *Proceedings of the second international CANMET/ACI
conference on the use of Fly Ash, Silica Fume, Slag and Natural Pozzolanas in
concrete Madrid*, pp.841-864

Hooton,R.D. 1986
Permeability and pore structure of cement pastes containing fly ash,slag and silica
fume
ASTM STP 897 Blended cements, pp.128-143

Hope,B.B. Page,J.A. and Ip,A.K.C. 1986
Corrosion rates of steel in concrete
Cement and Concrete Research, Vol 16, pp.771-781

Hughes,B.P., Soleit,A.K.O. and Brierly,R.W. 1985
New technique for determining the electrical resistivity of concrete.
Magazine of Concrete Research, Vol.37, no.133, Dec, pp.243-248

Hustad,T. and Loland,K.E. 1981
Silica in concrete section 4 : permeability
Cement and Concrete Research Institute Norway, unpublished report

Jahr,J. 1979
Possible health hazards of different types of amorphous silicas
Institute of Occupational Health Oslo, unpublished report

Jahr,J. 1983
Possible health hazards from different types of amorphous silica / suggested threshold
limit values
Condensed Silica Fume:, Aitcin,P.C.(editor), University of Sherbrooke Quebec
Canada, pp.28-33

Jahren,P. 1983
Use of silica fume in concrete
A.C.I. publication SP.79 *Proceedings of the CANMET/A.C.I. conference on silica fume slag and other minerals in concrete*, pp.625-642

Jahren,P.A. 1986
Performance of concrete incorporating condensed silica fume and superplasticisers
ACI publication SP91 *Proceedings of the second international CANMET/ACI conference on the use of Fly Ash, Silica Fume, Slag and Natural Pozzolanas in concrete Madrid*, pp.865-892

Johansen,R. 1981
Silica in concrete section 6: Long term effects.
Cement and Concrete Research Institute Norway, unpublished report

John,D.G. Searson,P.C. and Dawson,J.L. 1981
Use of ac impedance technique in studies on steel in concrete in immersed conditions
British Corrosion Journal, Vol.16, no.2, pp.102-106

John,D.G., Coote,A.T., Treadway,K.W.J. and Dawson.J.L. 1983
The repair of concrete - a laboratory and exposure site investigation.
Corrosion of reinforcement in concrete construction, A.P.Crane (editor), Ellis Horwood, pp.263-286

Kawamura,M., Takemoto,K. and Hasaba,S. 1986
Effect of silica fume on alkali-silica expansion in mortars.
ACI publication SP91 *Proceedings of the second international CANMET/ACI conference on the use of Fly Ash, Silica Fume, Slag and Natural Pozzolanas in concrete Madrid,* pp.999-1012

Kennedy,J.B. and Neville, A.M. 1986
Basic Statistical Methods for Engineers and Scientists, Harper and Row New York

Kohno,K. and Komatsu,H. 1986
Use of ground bottom ash and silica fume in mortar and concrete.
ACI publication SP91 *Proceedings of the second international CANMET/ACI conference on the use of Fly Ash, Silica Fume, Slag and Natural Pozzolanas in concrete Madrid,* pp.1279-1292

Kumar,A. and Roy,D.M. 1986
Retardation of Cs+ and Cl- diffusion using blended cement admixtures
Journal of the American Ceramic Society, 69(4), pp.356-360

Kumar,A., Komarneni,S. and Roy,D.M. 1987
Diffusion of Cs+ and Cl- through sealing materials
Cement and Concrete Research, Vol.17, pp.153-160

Lawrence,C.D. 1981
Durability of concrete: molecular transport processes and test methods
Cement and Concrete Association, Technical Report 544

Lawrence,C.D. 1984
Transport of oxygen through concrete
British Ceramic Society Proceedings, no.35, pp.277-293

Lawrence.C.D. 1986
Measurements of permeability
8th Congress of Cement, Brazil

Leeming,M.B. 1983
Corrosion of steel reinforcement in offshore concrete - experience from the Concrete-in-the-Oceans Programme
Corrosion of reinforcement in concrete construction., A.P.Crane(editor), Ellis Horwood, pp.59-78

Li,S. and Roy,D.M. 1986
Investigation of the relations between porosity, pore structure, and Cl- diffusion of fly ash and blended cement pastes
Cement and Concrete Research, Vol.16, pp.749-759

Loland,K.E. and Hustad,T. 1981b
Silica in concrete section 2: Mechanical properties
Cement and Concrete Research Institute, Norway, unpublished report

Lynsdale,C.J.C. 1987
PhD Thesis
In preparation at University of Leeds

Maage,M. 1984
Effect of microsilica on the durability of concrete structures
FCB SINTEF, Report STF65 A84019, 86pp.

Maage,M. 1986
Strength and heat developement in concrete: Influence of fly ash and condensed silica fume
ACI publication SP91 *Proceedings of the second international CANMET/ACI conference on the use of Fly Ash, Silica Fume, Slag and Natural Pozzolanas in concrete Madrid*, pp.923-940

Malhotra,V.M. 1986
Mechanical properties and freezing-and-thawing resistance of non-air-entrained and air-entrained condensed silica-fume concrete using ASTM test C 666 procedures A and B.
ACI publication SP91 *Proceedings of the second international CANMET/ACI conference on the use of Fly Ash, Silica Fume, Slag and Natural Pozzolanas in concrete Madrid*, pp.1069-1094

Markestad,S.A. 1986
A study of the combined influence of condensed silica fume and a water reducing admixture on water demand and strength of concrete
Materials and Structures, Vol.19, no.109, pp.39-47

Marusin,S.L. 1986
Chloride ion penetration in conventional concrete and concrete containing condensed silica fume.
ACI publication SP91 *Proceedings of the second international CANMET/ACI conference on the use of Fly Ash, Silica Fume, Slag and Natural Pozzolanas in concrete Madrid*, pp.1119-1134

Mather,K. 1980
Factors affecting the sulfate resistance of mortars
Proc. 7th International Conference on the Chemistry of Cements Paris, pp.580-585

McCarter,W.J., Forde,M.C. and Whittington,H.W. 1981
Resistivity characteristics of concrete
Proc. Inst. Civ. Engineers, Part 2, Vol 71, March, pp.107-117

Meland,I. 1983
Hydration of blended cements
Nordic Concrete Research Publication , no.2, Dec, pp.183-196

Mills,R.H. 1985
Mass transfer of water vapour through concrete
Cement and Concrete Research, Vol. 15, pp.74-82

Monfore,G.E. 1968
The Electrical Resistivity of Concrete
Journal of the P.C.A. Research and Development Labs, May, pp.35-48

Morrison,G.L., Gilliland,W.J., Bukovatz,J.E., Jayaprakash,G.P. and Seitz,R.D.
1979
An Evapo-Transmission method for determining relative permeability of concrete
Federal Highway Administration , Report FHWA-KS-79-1

Nagataki,S. and Ujike,I. 1986
Air permeability of concretes mixed with fly ash and condensed silica fume
ACI publication SP91 *Proceedings of the second international CANMET/ACI
conference on the use of Fly Ash, Silica Fume, Slag and Natural Pozzolanas in
concrete Madrid*, pp.1049-1068

Nebesar,B. and Carette,G.G. 1986
Variations in the chemical composition, specific surface area, fineness and pozzolanic
activity of a condensed silica fume.
Cement Concrete and Aggregates CCAGDP, Vol.8, no.1, pp.42-45

Neville,A.M. 1981
Properties of concrete , Pitman third edition

Oberholster,R.E. and Westra,W.B. 1981
The effectiveness of mineral admixtures in reducing expansion due to alkali-aggregate
reaction with Malmesbury group aggregates.
Conference on Alkali-Aggregate Reaction NBRI Cape Town South Africa, March 30 -
April 3, no.30, 11pp.

Opsahl,O.A. 1981
Silica in concrete, section 5 : frost resistance.
Cement and Concrete Research Institute Norway, unpublished report

Ost.B and Monfore,G.E. 1966
Penetration of chloride into concrete
Journal of the P.C.A. Research and Revelopment Laboratories, January, pp.46-52

Page,C.L. Short,N.R. and Holden,W.R. 1986
The influence of different cements on chloride-induced corrosion of reinforcing steel
Cement and Concrete Research, Vol 16, pp. 79-86

Page,C.L. and Havdahl,J. 1985
Electrochemical monitoring of corrosion of steel in microsilica cement pastes.
Materiaux et Constructions, Vol 18, no. 103, pp.41-47

Perez-Pena,M. Roy,D.M. Bhalla,A.S. and Cross,L.E. 1986
Dieletric properties of densified hardened cementitious materials
Cement and Concrete Research, Vol.16, pp.951-965

Perry,C. and Gillott,J.E. 1985
The feasibility of using silica fume to control concrete expansion due to Alkali-Aggregate Reactions
Durability of Building Materials, 3, pp.133-146

Pigeon,M., Pleau,R. and Aitcin,P.C. 1986
Freeze-thaw durability of concrete with and without silica fume in ASTM C666 (Procedure A) Test method: internal cracking versus scaling
Cement Concrete and Aggregates CCAGDP, Vol.8, no.2, pp.76-851

Pistilli,M.F., Wintersteen,R. and Cechner,R. 1984
The uniformity and influence of silica fume from a U.S. source on the properties of portland cement concrete
Cement Concrete and Aggregates CCAGDP, Vol.6, no.2, pp.120-124

Popvic,K, Ukraincik,V and Djurekovic,A 1984
Improvement of mortar and concrete durability by the use of condensed silica fume
Durability of Building Materials, 2, pp.171-186

Powers,T.C. 1960
Physical properties of cement paste and concrete.
Proceedings of the fourth symposium on the chemistry of cement Washington D.C., pp.577-613

Preece,C.M. 1983
Characterisation of Densit for the protection of steel reinforcement.
Danish corrosion centre, unpublished report

Preece,C.M. Arup,H. and Frolund,T. 1983
Electrochemical behaviour of steel in dense silica-cement mortar
A.C.I. publication SP.79 *Proceedings of the CANMET/A.C.I. conference on silica fume slag and other minerals in concrete*, pp.785-796

Preece,C.M.,Gronvold,F.O. and Frolund,T. 1983
The influence of cement type on the electrochemical behaviour of steel in concrete.
Corrosion of reinforcement in concrete construction, A.P.Crane(editor), Ellis Horwood, pp. 393-406

Radjy,F.F., Bogen,T., Sellevold,E.J. and Loeland,K.E. 1986
A review of experiences with condensed silica fume concretes and products.
ACI publication SP91 *Proceedings of the second international CANMET/ACI conference on the use of Fly Ash, Silica Fume, Slag and Natural Pozzolanas in concrete Madrid*, pp.1135-1154

Rath,G. 1983
The operation and design of electric reduction furnaces for the production of ferrosilicon and silicon metal
Condensed Silica Fume, Aitcin,P.C.(editor),University of Sherbrooke Quebec Canada, p.15

Rau,G. and Aitcin,P.C. 1983
Different types of condensed silica fume
Condensed Silica Fume, Aitcin,P.C.(editor),University of Sherbrooke Quebec Canada, pp.9-14

Regourd,M. 1983
Pozzolanic reactivity of condensed silica fume
Condensed Silica Fume, Aitcin,P.C.(editor),University of Sherbrooke Quebec Canada, pp.20-24

Reinhold,R.E., Richter,R.E., Buck,A.D., Mather,K, Mather,B. and McDonald,J.E. 1986
Variations in cementitious media
U.S. Army Engineer Waterways Experimental Station Vicksburg Mississippi, Report SL-86-10

Rose,D.A. 1965
Water movement in unsaturated porous materials
Rilem Bulletin, no.29, Dec, pp.119-124

Sellevold,E.J. and Nilsen,T. 1986
Condensed silica fume in concrete : a world review
Elkem a/s Chemicals Box 208, 4620 Vagsbygd, Norway, unpublished report

Sellevold,E.J. and Radjy,F.F. 1983
Condensed silica fume (microsilica) in concrete : water demand and strength
developement
A.C.I. publication SP.79 *Proceedings of the CANMET/A.C.I. conference on silica
fume slag and other minerals in concrete* , pp.677-694

Skjolsfold,O. 1986
Carbonation depths of concrete with and without silica fume
ACI publication SP91 *Proceedings of the second international CANMET/ACI
conference on the use of Fly Ash, Silica Fume, Slag and Natural Pozzolanas in
concrete Madrid,* pp.1031-1048

Skrastins,J.I. and Zoldners,N.G 1983
Ready Mixed Concrete incorporating condensed silica fume
A.C.I. publication SP.79 *Proceedings of the CANMET/A.C.I. conference on silica
fume slag and other minerals in concrete,* pp.813-830

Smith,D.G.E. and Evans,A.R. 1986
Purple concrete in a Middle East town
Concrete, February, pp.36-41

Sneck,T. and Oinonen,H. 1970
Measurements of pore size distribution of porous materials
The State Institute for Technical Research, Finland, unpublished report

Sorensen,E.V 1983
Freezing and thawing resistance of condensed silica fume (microsilica) concrete
exposed to de-icing chemicals.
A.C.I. publication SP.79 *Proceedings of the CANMET/A.C.I. conference on silica
fume slag and other minerals in concrete,* pp.979-998

Spooner,D.C. 1983
The practical relevance of mechanisms of water and water vapour transport in porous building materials
Autoclaved Aerated Concrete, Moisture and Properties, ed.Wittmann F.H. Elsevier Scientific Publishing, pp.27-41

Stern,M. and Geary,A.L. 1957
Electrochemical polarisation. Theoretical analysis of the shape of polarisation curves
Journal of the Electrochemical Society, January, pp.56-63

Stratfull,R.F. 1983
Criteria for the cathodic protection of bridge decks.
Corrosion of reinforcement in concrete construction, A.P.Crane(editor) Ellis Horwood, pp.287-332

Tazawa,E. and Yonekura,A. 1986
Drying shrinkage and creep of concrete with condensed silica fume.
ACI publication SP91 *Proceedings of the second international CANMET/ACI conference on the use of Fly Ash, Silica Fume, Slag and Natural Pozzolanas in concrete Madrid,* pp.903-922

Tenoutasse,N. and Marion,A.M. 1986
The influence of silica fume on the hydration and microstructure of OPC pastes.
ACI publication SP91 *Proceedings of the second international CANMET/ACI conference on the use of Fly Ash, Silica Fume, Slag and Natural Pozzolanas in concrete Madrid,* supplementary vol. 3

Traetteberg,A. 1980
Frost action in mortar of blended cement with silica dust
Durability of building materials and components, ASTM STP691,Sereda,P.J. (editor), pp.536-548

Vennesland,O. 1981
Silica in concrete section 3: Corrosion of reinforcements.
Cement and Concrete Research Institute, Norway, unpublished report

Vennesland,O. and Gjorv,O.E. 1983
Silica concrete-protection against corrosion of embedded steel
A.C.I. publication SP.79 *Proceedings of the CANMET/A.C.I. conference on silica fume slag and other minerals in concrete,* pp.719-730

Virtanen,J. 1983
Freeze-thaw resistance of concrete containing blast furnace slag, fly ash or condensed silica fume.
A.C.I. publication SP.79 *Proceedings of the CANMET/A.C.I. conference on silica fume slag and other minerals in concrete*, pp.923-942

Whiting,D. 1981
Rapid determination of the chloride permeability of concrete
Report No.FHWA/RD-81/119 to the FHWA Washington DC.

Whittington,H.W. McCarter,J and Forde,M.C. 1981
The conduction of electricity through concrete
Magazine of Concrete Research, Vol 33, no.114

Wierig,H.-J. 1965
Die Wasserdampfdurchlassigkeit von Zementmortel und Beton.
Zement-Kalk-Gips, 18, no.9, Sept, pp.471-482

Wilkins,N.J.M. and Lawrence,P.F. 1983
The corrosion of steel reinforcements in concrete immersed in sea water
Corrosion of reinforcement in concrete construction, A.P.Crane(editor), Ellis Horwood, pp.119-142

Wittmann,F.H. 1987
An unusual energy source
Cement and Concrete Research, Vol 17, pp.161-163

Wolsiefer,J. 1984
Ultra high-strength field placeable concrete with silica fume admixture.
Concrete International, April, pp.25-31

Woodside,W. 1959
Water vapour permeability of porous media.
Canadian Journal of Physics, Vol 37, pp.413-416

Yamato,T., Yukio,E. and Soeda,M. 1986
Strength and freezing-and-thawing resistance of concrete incorporating condensed silica fume
ACI publication SP91 *Proceedings of the second international CANMET/ACI conference on the use of Fly Ash, Silica Fume, Slag and Natural Pozzolanas in concrete Madrid*, pp.1095-1118